

Identification of factors involved in *Staphylococcus aureus*- induced host cell death



DISSERTATION

zur Erlangung des

naturwissenschaftlichen Doktorgrades

der Julius-Maximilians-Universität Würzburg

vorgelegt von

Kathrin Stelzner

aus Coburg

Würzburg, 2019

Eingereicht am:

Mitglieder der Prüfungskommission

Vorsitzender:

Erstgutachter: Prof. Dr. Thomas Rudel

Zweitgutachter: Dr. PD Knut Ohlsen

Tag des Promotionskolloquiums:

Doktorurkunde ausgehändigt am:

Table of contents

Summary.....	6
Zusammenfassung	7
1 Introduction.....	9
1.1 <i>Staphylococcus aureus</i>	9
1.1.1 Human colonization and carriage.....	9
1.1.2 <i>S. aureus</i> infection and disease	10
1.1.3 Antibiotic resistance and epidemiology.....	11
1.2 <i>S. aureus</i> virulence factors	12
1.2.1 Cell surface-associated factors.....	13
1.2.2 Membrane-damaging toxins.....	14
1.2.3 Extracellular proteases	15
1.2.4 Other virulence-associated extracellular enzymes and proteins of <i>S. aureus</i>	16
1.3 <i>S. aureus</i> intracellular infection	17
1.3.1 Invasion and intracellular survival	17
1.3.2 Phagosomal escape and intracellular replication in non-professional phagocytes.....	19
1.3.3 Induction of host cell death	20
1.4 Cell death mechanisms.....	22
1.4.1 Apoptosis	22
1.4.2 Necrotic cell death	24
1.4.3 Parthanatos.....	25
1.4.4 Other modes of cell death	26
1.4.5 Calcium and cell death.....	27
1.5 Haploid genetic screens	30
1.6 Aim of the study.....	33
2 Material and Methods	34
2.1 Material	34
2.1.1 Laboratory instruments	34
2.1.2 Consumables and glassware.....	35
2.1.3 Chemicals and enzymes	36
2.1.4 Kits.....	39
2.1.5 Media and antibiotics.....	39
2.1.6 Buffers and solutions	41
2.1.7 Antibodies	43
2.1.8 Cell lines	43
2.1.9 Bacterial strains.....	44
2.1.10 Plasmids	45
2.1.11 Oligonucleotides	46
2.1.12 Software	47

2.2 Methods.....	47
2.2.1 Bacterial culture techniques.....	47
2.2.1.1 Cultivation of bacteria.....	47
2.2.1.2 Preparation of bacteria for <i>in vitro</i> infection.....	47
2.2.1.3 Preparation of bacteria for mouse infection.....	48
2.2.1.4 <i>In vitro</i> growth curves.....	48
2.2.1.5 Collection of <i>S. aureus</i> supernatant.....	48
2.2.2 Cell culture techniques.....	48
2.2.2.1 Cell cultivation and passaging.....	48
2.2.2.2 Cryopreservation of cells.....	48
2.2.3 DNA methods.....	49
2.2.3.1 Plasmid isolation.....	49
2.2.3.2 Genomic DNA isolation.....	49
2.2.3.3 Polymerase chain reaction (PCR).....	49
2.2.3.4 Restriction and ligation.....	50
2.2.4 RNA methods.....	50
2.2.4.1 RNA isolation and DNA digestion.....	50
2.2.4.2 Generation of cDNA by reverse transcription.....	50
2.2.4.3 Quantitative real-time PCR.....	50
2.2.5 Genetic manipulation of bacteria.....	51
2.2.5.1 Transformation of chemically competent <i>E. coli</i>	51
2.2.5.2 Preparation of electrocompetent <i>S. aureus</i>	51
2.2.5.3 Electroporation of <i>S. aureus</i>	51
2.2.5.4 Phage transduction of <i>S. aureus</i>	52
2.2.5.5 Site directed mutagenesis in <i>scpA</i>	52
2.2.5.6 Cloning of <i>S. aureus</i> mutants and fluorescent reporter strains.....	52
2.2.5.7 Cloning of plasmids.....	52
2.2.6 Genetic and transcriptional manipulation of human cells.....	53
2.2.6.1 siRNA transfection.....	53
2.2.6.2 Gene knock-out using CRISPR/Cas9.....	53
2.2.7 Protein biochemical methods.....	54
2.2.7.1 SDS-PAGE.....	54
2.2.7.2 Western blot.....	54
2.2.8 Cell infection protocols.....	55
2.2.8.1 Lysostaphin protection assay.....	55
2.2.8.2 Invasion assay.....	55
2.2.8.3 Phagosomal escape assay.....	55
2.2.8.4 Intracellular replication.....	56
2.2.8.5 Cytotoxicity assays.....	56
2.2.9 Microscopy.....	57

2.2.10 Murine infection model.....	58
2.2.11 HAP1 screen	58
2.2.12 Statistical analysis.....	59
3 Results	60
3.1 Intracellular <i>S. aureus</i> induces cell death in epithelial cells	60
3.2 Host cell factors involved in <i>S. aureus</i> -induced cytotoxicity	62
3.2.1 Haploid genetic screen to identify host cell factors involved in <i>S. aureus</i> -induced cytotoxicity.....	62
3.2.1.1 The intracellular lifestyle of <i>S. aureus</i> in HAP1 cells resembles that in HeLa cells	62
3.2.1.2 Optimization of screening conditions.....	64
3.2.1.3 Implementation of the haploid genetic screen.....	67
3.2.2 <i>S. aureus</i> -induced host cell death displays characteristics of apoptosis.....	71
3.2.2.1 Inhibition of caspases attenuates <i>S. aureus</i> -induced host cell death.....	71
3.2.2.2 Effector caspases are activated by intracellular <i>S. aureus</i>	74
3.2.2.3 <i>S. aureus</i> -infected cells display apoptotic morphology and Bid cleavage.....	76
3.2.3 A possible role of AIF in <i>S. aureus</i> -induced cell death	78
3.2.4 <i>S. aureus</i> -infected cells show features of necrotic cell death.....	78
3.2.5 Cellular H ₂ O ₂ is elevated during <i>S. aureus</i> intracellular infection.....	80
3.2.6 Intracellular <i>S. aureus</i> induces cellular Ca ²⁺ perturbations to promote host cell death.....	81
3.2.6.1 Intracellular <i>S. aureus</i> triggers cytosolic Ca ²⁺ rise	81
3.2.6.2 Changes in mitochondrial and ER Ca ²⁺ concentration induced by intracellular <i>S. aureus</i>	82
3.2.6.3 Store-operated Ca ²⁺ entry is not implicated in <i>S. aureus</i> -induced host cell death....	86
3.2.6.4 <i>S. aureus</i> triggers Ca ²⁺ influx via the host plasma membrane.....	88
3.2.6.5 Effector caspase activation and plasma membrane permeabilization follow cytosolic Ca ²⁺ overload in <i>S. aureus</i> -infected cells.....	91
3.2.6.6 Cytosolic Ca ²⁺ overload is not a common feature of apoptosis.....	95
3.2.7 Calpains are not essential for induction of host cell death by intracellular <i>S. aureus</i>	96
3.2.7.1 Calpains are activated by intracellular <i>S. aureus</i>	96
3.2.7.2 Inactivation of calpains has no effect on <i>S. aureus</i> intracellular lifestyle	97
3.3 Bacterial factors involved in <i>S. aureus</i> -induced cytotoxicity	101
3.3.1 Rsp and α -hemolysin do not contribute to <i>S. aureus</i> induced cytosolic Ca ²⁺ rise.....	101
3.3.2 Intracellular cytotoxicity of different <i>S. aureus</i> mutants in epithelial cells	104
3.3.3 Staphopain A induces intracellular cytotoxicity of <i>S. aureus</i>	104
3.3.3.1 Loss of staphopain A function leads to reduced cytotoxicity of intracellular <i>S. aureus</i>	104
3.3.3.2 Staphopain A does not interfere with invasion, phagosomal escape and intracellular replication of <i>S. aureus</i>	107
3.3.3.3 Mutation of staphopain A does not abolish cytosolic Ca ²⁺ overload in <i>S. aureus</i> -infected host cells	108
3.3.3.4 Ectopic expression of staphopain A in a non-cytotoxic <i>S. aureus</i> strain induces host cell death after phagosomal escape.....	110

3.3.3.5	Staphopain A induces host cell death with characteristics of apoptosis.....	113
3.3.3.6	Staphopain A promotes <i>S. aureus</i> colonization in a pneumonia infection model ..	115
4	Discussion.....	116
4.1	The intracellular lifestyle of <i>S. aureus</i> in epithelial cells.....	116
4.2	Haploid genetic screen as a tool for identifying host genes involved in <i>S. aureus</i> intracellular cytotoxicity	117
4.2.1	Evaluation of haploid genetic screen performance	117
4.2.2	Validation of significantly enriched genes identified in the haploid genetic screen.....	118
4.2.3	Diversity of <i>S. aureus</i> intracellular lifestyle	121
4.3	Cell death pathways activated by intracellular <i>S. aureus</i>	122
4.3.1	The role of apoptosis and caspases in <i>S. aureus</i> -induced cell death.....	123
4.3.2	Parthanatos and necroptosis in <i>S. aureus</i> -mediated cytotoxicity	125
4.4	Oxidative stress in <i>S. aureus</i> -infected cells	126
4.5	Ca ²⁺ signaling and <i>S. aureus</i> -induced host cell death.....	127
4.5.1	<i>S. aureus</i> -mediated cytosolic and mitochondrial Ca ²⁺ elevation.....	127
4.5.2	The role of calpains in <i>S. aureus</i> -induced host cell death.....	129
4.5.3	Origin of <i>S. aureus</i> triggered Ca ²⁺ rise.....	130
4.5.4	<i>S. aureus</i> virulence factors and cytosolic Ca ²⁺ overload.....	132
4.6	Staphopains in <i>S. aureus</i> intracellular cytotoxicity.....	134
4.6.1	A novel function for staphopain A.....	134
4.6.2	The role of staphopain B in <i>S. aureus</i> cytotoxicity.....	135
4.6.3	Mechanism of staphopain A-induced cell death	136
4.6.4	<i>In vivo</i> effects of staphopain A.....	138
4.7	Summary and perspectives.....	139
5	References	142
6	Appendix.....	177
6.1	Electronical supplement.....	177
6.2	Abbreviations	179
6.3	List of Figures	181
6.4	List of Tables	183
6.5	List of Videos.....	184
	Danksagung.....	185
	Selbstständigkeitserklärung	186

Summary

Staphylococcus aureus is a Gram-positive commensal bacterium, that asymptotically colonizes human skin and mucosal surfaces. Upon opportune conditions, such as immunodeficiency or breached barriers of the host, it can cause a plethora of infections ranging from local, superficial infections to life-threatening diseases. Despite being regarded as an extracellular pathogen, *S. aureus* can invade and survive within non-phagocytic and phagocytic cells. Eventually, the pathogen escapes from the host cell resulting in killing of the host cell, which is associated with tissue destruction and spread of infection. However, the exact molecular mechanisms underlying *S. aureus*-induced host cell death remain to be elucidated.

In the present work, a genome-wide haploid genetic screen was performed to identify host cell genes crucial for *S. aureus* intracellular cytotoxicity. A mutant library of the haploid cell line HAP1 was infected with the pathogen and cells surviving the infection were selected. Twelve genes were identified, which were significantly enriched when compared to an infection with a non-cytotoxic *S. aureus* strain.

Additionally, characteristics of regulated cell death pathways and the role of Ca^{2+} signaling in *S. aureus*-infected cells were investigated. Live cell imaging of Ca^{2+} reporter cell lines was used to analyze single cells. *S. aureus*-induced host cell death exhibited morphological features of apoptosis and activation of caspases was detected. Cellular H_2O_2 levels were elevated during *S. aureus* intracellular infection. Further, intracellular *S. aureus* provoked cytosolic Ca^{2+} overload in epithelial cells. This resulted from Ca^{2+} release from endoplasmic reticulum and Ca^{2+} influx via the plasma membrane and led to mitochondrial Ca^{2+} overload. The final step of *S. aureus*-induced cell death was plasma membrane permeabilization, a typical feature of necrotic cell death.

In order to identify bacterial virulence factors implicated in *S. aureus*-induced host cell killing, the cytotoxicity of selected mutants was investigated. Intracellular *S. aureus* employs the bacterial cysteine protease staphopain A to activate an apoptosis-like cell death characterized by cell contraction and membrane bleb formation. Phagosomal escape represents a prerequisite staphopain A-induced cell death, whereas bacterial intracellular replication is dispensable. Moreover, staphopain A contributed to efficient colonization of the lung in a murine pneumonia model.

In conclusion, this work identified at least two independent cell death pathways activated by intracellular *S. aureus*. While initially staphopain A mediates *S. aureus*-induced host cell killing, cytosolic Ca^{2+} -overload follows later and leads to the final demise of the host cell.

Zusammenfassung

Staphylococcus aureus ist ein Gram-positives, kommensales Bakterium, welches menschliche Haut- und Schleimhautoberflächen asymptomatisch kolonisiert. Unter günstigen Bedingungen, wie z. B. Immunschwäche oder verletzten Barrieren des Wirtes, kann es eine Vielzahl von Infektionen verursachen, die von lokalen, oberflächlichen Infektionen bis hin zu lebensbedrohlichen Krankheiten reichen. Obwohl *S. aureus* als extrazellulärer Erreger angesehen wird, kann das Bakterium von nicht-phagozytischen und phagozytischen Zellen aufgenommen werden und dort überleben. Schließlich bricht das Pathogen aus der Wirtszelle aus und die damit einhergehende Tötung der Wirtszelle wird mit Gewebeerstörung und Ausbreitung der Infektion in Verbindung gebracht. Die genauen molekularen Mechanismen, die dem *S. aureus* induzierten Wirtszelltod zugrunde liegen, müssen jedoch noch geklärt werden.

In dieser Arbeit wurde ein genomweiter haploid genetischer Screen durchgeführt, um Wirtszellgene zu identifizieren, die für die intrazelluläre Zytotoxizität von *S. aureus* entscheidend sind. Eine Mutantenbibliothek der haploiden Zelllinie HAP1 wurde mit dem Erreger infiziert und die Zellen, die die Infektion überlebten, wurden selektiert. Dabei wurden zwölf Gene identifiziert, die signifikant angereichert waren gegenüber einer Infektion mit einem nicht-zytotoxischen *S. aureus* Stamm.

Des Weiteren wurden Eigenschaften regulierter Zelltod-Signalwege und die Rolle der Ca^{2+} -Signalübertragung in *S. aureus* infizierten Zellen untersucht. Lebendzellbildgebung von Ca^{2+} -Reporterzelllinien wurde zur Analyse von einzelnen Zellen eingesetzt. Der *S. aureus* induzierte Wirtszelltod wies morphologische Merkmale von Apoptose auf und die Aktivierung von Caspasen wurde nachgewiesen. Der zelluläre H_2O_2 -Spiegel wurde durch die intrazelluläre Infektion mit *S. aureus* erhöht. Zusätzlich rief der intrazelluläre *S. aureus* eine zytosolische Ca^{2+} -Überbelastung in Epithelzellen hervor. Dies resultierte aus der Ca^{2+} -Freisetzung vom endoplasmatischen Retikulum und dem Einstrom von Ca^{2+} über die Plasmamembran und führte zu einer mitochondrialen Ca^{2+} -Überbelastung. Der finale Schritt des durch *S. aureus* induzierten Zelltods war die Permeabilisierung der Plasmamembran, ein typisches Merkmal des nekrotischen Zelltods.

Um bakterielle Virulenzfaktoren zu identifizieren, die am *S. aureus*-induzierten Wirtszelltod beteiligt sind, wurde die Zytotoxizität von ausgewählten Mutanten untersucht. Der intrazelluläre *S. aureus* nutzt die bakterielle Cysteinprotease Staphopain A, um einen Apoptoseartigen Zelltod zu aktivieren, der durch Zellkontraktion und Blasenbildung der Membran

gekennzeichnet ist. Der phagosomale Ausbruch stellt eine Voraussetzung für den Staphopain A-induzierten Zelltod da, während die intrazelluläre Replikation der Bakterien nicht notwendig ist. Darüber hinaus trug Staphopain A zu einer effizienten Kolonisation der Lunge in einem murinen Pneumonie-Modell bei.

Zusammenfassend lässt sich sagen, dass diese Arbeit mindestens zwei unabhängige Zelltod-Signalwege identifiziert hat, die durch den intrazellulären *S. aureus* aktiviert werden. Während zunächst Staphopain A den Tod der Wirtszelle einleitet, folgt später die zytosolische Ca^{2+} -Überlastung und führt zum endgültigen Untergang der Wirtszelle.

1 Introduction

1.1 *Staphylococcus aureus*

Staphylococci are facultative anaerobic, non-motile, non-spore forming Gram-positive bacteria first described in 1881 by Sir Alexander Ogston. The Scottish surgeon isolated the bacterium from pus of patient's knee joint abscesses (Ogston, 1882). Characteristic and eponymous is the arrangement of the spherical bacteria (Greek: kókkos “grain”) in grape-like aggregates (Greek: staphylé “grape”) (Figure 1.1A). The genus *Staphylococcus* belongs to the family of Staphylococcaceae in the genus Bacillales. Staphylococci are natural colonizers of human and animal skin and mucosa and can be divided into coagulase-positive and coagulase-negative species based on their ability to clump plasma. The most prominent species is *Staphylococcus aureus* (*S. aureus*), which is classified as coagulase-positive Staphylococcus. The German physician Friedrich Julius Rosenbach first described this species in 1884 (Rosenbach, 1884). Colonies of *S. aureus* are characterized by their orange-yellow pigmentation, after which the species name (Latin: aureus “golden”) was given (Figure 1.1B). The size of the bacterium ranges typically between 0.8 and 1.2 μm .

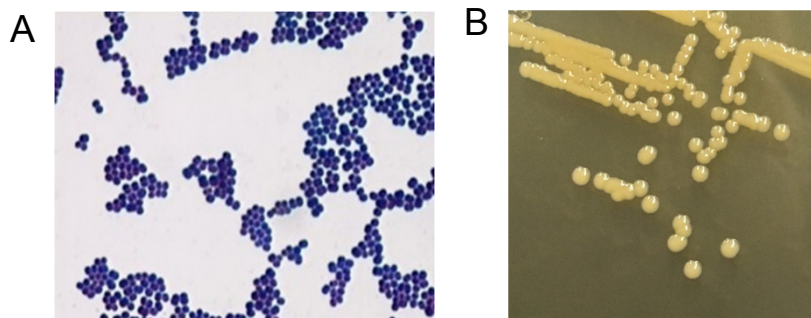


Figure 1.1: Microscopic and macroscopic characteristics of *S. aureus*.

(A) Gram staining of *S. aureus* illustrates the typical cocci shape and grape-like aggregates of staphylococci (Rajesh et al., 2017). (B) Colonies of *S. aureus* on Tryptic Soy Agar show the characteristic orange-yellow pigmentation.

1.1.1 Human colonization and carriage

About 20-30 % of the human population is asymptotically colonized by *S. aureus*. Originally, the anterior nares were regarded as primary colonization site of *S. aureus* (Williams, 1963), while more recently a similar or higher carriage rate was found at other body sites like throat and groin (Mertz et al., 2007; Ringberg et al., 2006; Senn et al., 2012). *S. aureus* can further be found on skin (axillae, chest, abdomen, perineum), vagina and in the gastrointestinal tract (Guinan et al., 1982; Williams, 1963). Three different types of *S. aureus* carriers were suggested: Whereas 20 % of the population persistently carry *S. aureus*, the majority of individuals (about 60 %) is only colonized for a certain period of time and classified as

intermittent carriers (Kluytmans et al., 1997; Williams, 1963). The rest of the population, about 20 %, are regarded as noncarriers. Persistent carriers have a higher bacterial load and increased anti-staphylococcal antibody titres compared to non- and intermittent carriers, which also show similar nasal elimination kinetics (van Belkum et al., 2009).

Determinants for *S. aureus* carriage are not fully understood. Environmental factors, such as geographic location, age and sex, influence the carriage rate as well as the use of oral contraceptives, smoking behaviour, diet, drug addiction, crowding, healthcare exposure and pre-existing diseases like diabetes, HIV or skin and soft tissue infections (Choi et al., 2006; Johannessen et al., 2012; Kluytmans et al., 1997; Olsen et al., 2012; Sollid et al., 2014). Host immune and genetic factors, such as polymorphisms in certain genes, were found to be associated with nasal carriage of *S. aureus* as well as natural competition with other bacterial species for the host niche impact *S. aureus* carriage (Bogaert et al., 2004; Emonts et al., 2008; Frank et al., 2010; Lina et al., 2003; Messaritakis et al., 2014; Uehara et al., 2000; van den Akker et al., 2006; Vuononvirta et al., 2011; Zipperer et al., 2016).

1.1.2 *S. aureus* infection and disease

S. aureus lives a double life as harmless commensal bacterium, that colonizes the human body and is transmitted without being recognized, and as notorious pathogen frequently causing serious infections with high morbidity, mortality and healthcare-associated costs (Schmidt et al., 2015). Infections of *S. aureus* are remarkably virulent given that the organism is a commensal. They are especially favoured by a weakened immune system of the colonized person, but altered microbiota, breached skin or mucosal barriers and presence of foreign material also facilitate invasive disease. Therefore, *S. aureus* represents a classical nosocomial pathogen, causing infections especially in hospital settings. However, by the end of the last century outbreaks in the community and later also infection of healthy individuals were reported (Centers for Disease and Prevention, 1999; Herold et al., 1998; Purcell and Fergie, 2005; Udo et al., 1993).

S. aureus can cause a wide variety of infections, which involve skin, soft-tissue, bone, joint, respiratory and endovascular system and may lead to severe, life-threatening diseases. Infection rates are higher in carriers of *S. aureus* than in non-carriers and disease is often caused by the endogenous strain carried by the patient (von Eiff et al., 2001; Wertheim et al., 2004). Most *S. aureus* infections are the result of the interaction of a variety of virulence factors. Only the expression of certain toxins, such as the toxic shock syndrome toxin (TSST), exfoliatins or enterotoxins, leads to clearly defined clinical pathologies such as toxic shock syndrome,

staphylococcal scalded skin syndrome and food poisoning (Bohach et al., 1990; Hennekinne et al., 2012; Mishra et al., 2016).

The pathogen represents a frequent cause of skin and soft tissue infections such as impetigo, folliculitis, cellulitis, wound infections, pyomyositis or necrotizing fasciitis. It is the most common pathogen isolated from surgical site infections (SSIs), cutaneous abscesses and purulent cellulitis (Tong et al., 2015). Persons suffering from atopic dermatitis are often colonized with *S. aureus*, which was found to exacerbate the disease (Leyden et al., 1974; Nakatsuji et al., 2016). Besides, *S. aureus* is the leading cause of bloodstream infections in most industrialized countries (Biedenbach et al., 2004; Lyytikainen et al., 2005; Martin et al., 2003). Once the pathogen penetrates the subcutaneous tissue and reaches the blood system, it can infect vital organs, which results in disseminated infections, such as infective endocarditis, septic arthritis or osteomyelitis, and descending urinary tract infections (Benfield et al., 2007; Fowler et al., 2003; Rieg et al., 2009). *S. aureus* is a common cause of ventilator-associated pneumonia (Hidron et al., 2008; Kollef et al., 2005) and also a frequent causative agent of secondary bacterial pneumonia following influenza A virus (IAV) infection (Randolph et al., 2011). Further, initial and early pulmonary infections in cystic fibrosis patients are associated with *S. aureus* (Kahl, 2010; Stone and Saiman, 2007). Although rare, *S. aureus* was reported to cause meningitis (Aguilar et al., 2010). Device-related infections caused by *S. aureus* are particularly problematic in nosocomial settings. Various implants, like artificial heart valves or prosthetic joints, and catheters can be colonized by *S. aureus* and subsequently covered with a biofilm. The formation of biofilms by *S. aureus* is recognized as major mediator of infection and associated with chronic and recalcitrant disease (Archer et al., 2011).

1.1.3 Antibiotic resistance and epidemiology

S. aureus is inherently sensitive to all antibiotics effective against Gram-positive bacteria, but the pathogen can quickly acquire resistance to a wide variety of antibiotics. All staphylococci possessing an additional penicillin binding protein (PBP2' or PBP2a) are called methicillin-resistant *S. aureus* (MRSA). Characteristic for MRSA is their multi-resistance, as they are also frequently resistant against other antibiotic classes besides β -lactamases, like tetracycline, aminoglycosides and macrolides. Only few reserve antibiotics are active against MRSA infections, but here also resistances have evolved, like vancomycin resistant *S. aureus* (VRSA) (Hiramatsu et al., 1997; Weigel et al., 2003).

In the late 1970s outbreaks of infections caused by MRSA strains were reported in hospitals in the United States (Crossley et al., 1979; Peacock et al., 1980). These strains spread over the

country and subsequently led to the worldwide pandemic of MRSA in hospitals, that continues to the present time (Hassoun et al., 2017; Stefani et al., 2012). By the end of the last century outbreaks in the community and later also infection of healthy individuals were reported (Centers for Disease and Prevention, 1999; Herold et al., 1998; Purcell and Fergie, 2005; Udo et al., 1993). This led to a dramatic increase of *S. aureus* infections, especially skin and soft tissue infections and unusually severe infections like necrotizing pneumonia, necrotizing fasciitis and myositis (Bradley, 2005; King et al., 2006; Miller et al., 2005; Pannaraj et al., 2006). There are also increasing reports of these community-acquired MRSA (CA-MRSA) strains isolated in hospitals (Maree et al., 2007).

CA-MRSA strains could be distinguished from hospital-acquired MRSA (HA-MRSA) strains by pulsed-field gel electrophoresis and by their sensitivity to most antibiotics except β -lactams. Compared to HA-MRSA, CA-MRSA harbored a novel, smaller variant of the methicillin-resistance locus (SCC*mec* IVa) (Baba et al., 2002). A further distinguishing feature is the presence of the Panton-Valentine leukocidin (PVL) locus (Vandenesch et al., 2003) and higher expression levels of some virulence factors, e.g. phenol-soluble modulins (PSMs) (Wang et al., 2007), which might explain their higher virulence (Voyich et al., 2005). The two clones MW2, pulsed-field type USA400 (sequence type 1), and LAC, pulsed-field type USA300 (sequence type 8), hereinafter referred to as USA400 and USA300, respectively, were particular widespread causative agents of CA-MRSA infections (Miller and Diep, 2008).

1.2 *S. aureus* virulence factors

Staphylococcus aureus possesses a huge armamentarium of virulence factors, which allows the bacterium to adapt to different host niches and to cause a plethora of diseases (Figure 1.2). The expression of virulence factors is regulated in complex signaling networks in response to extra- and intracellular signals and mainly mediated by two-component systems (TCS) and the Staphylococcal accessory regulator (Sar) A protein family (Cheung et al., 2004). The best-studied global gene regulator and TCS is the accessory gene regulator (Agr), which coordinates the expression of exoproteins and toxins via quorum sensing (Novick, 2003). As soon as a certain bacterial density, i.e. amount of autoinducer, is reached, Agr represses the expression of surface-associated adhesion molecules, while production of secreted proteins, such as toxins and enzymes, is induced. Thus, the pathogen can switch from a colonization phenotype, where proteins required for adhesion and immune evasion were found to be upregulated (Burian et al., 2010a; Burian et al., 2010b), to an invasive phenotype associated with tissue destruction, spread

of infection and protection against immune defense, which is mediated e.g. by toxins, proteases and superantigens.

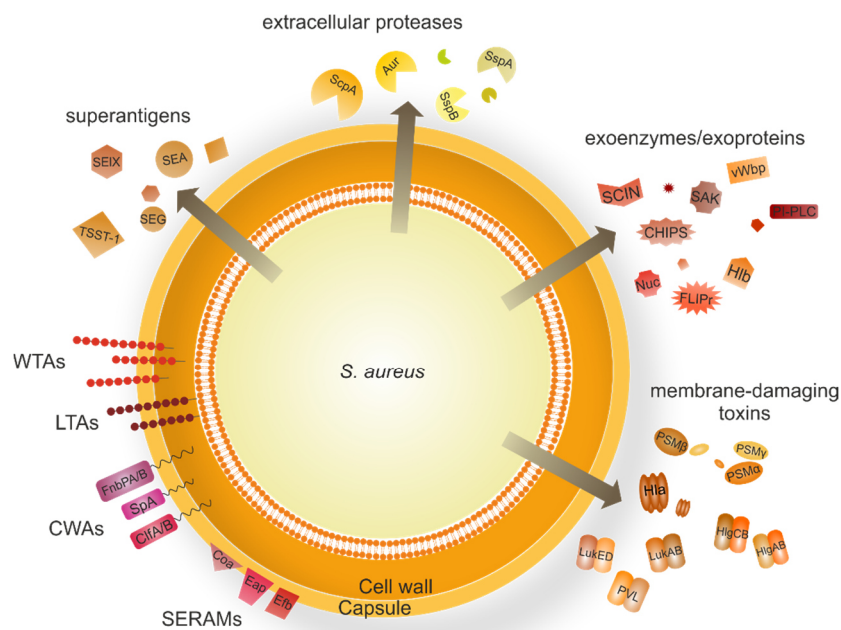


Figure 1.2: Overview of *S. aureus* major virulence factors.

Groups of the most prominent *S. aureus* virulence factors are depicted with representative factors. For details on individual components refer to section 1.2 (CWAs: cell wall-anchored proteins, SERAMs: secretable expanded repertoire adhesive molecules, LTAs: lipoteichoic acids, WTAs: wall teichoic acids; adapted from Sause et al. (2016)).

1.2.1 Cell surface-associated factors

The surface of *S. aureus* is decorated with proteins, that are covalently anchored to the cell wall peptidoglycan. These cell wall-anchored (CWA) proteins can be classified into four distinct groups, of which the heterogeneous family of microbial surface components recognizing adhesive matrix molecules (MSCRAMM) is the most prevalent group (Foster et al., 2014). *S. aureus* expresses up to 24 different CWA proteins, but the repertoire varies among strains and with environmental and growth conditions (Bischoff et al., 2004; Hammer and Skaar, 2011; McAleese et al., 2001; McCarthy and Lindsay, 2010). These surface proteins have numerous functions, including adhesion to and invasion of host cells and tissues, evasion of immune responses and biofilm formation (Foster et al., 2014). Staphylococcal protein A (SpA) is a well-known CWA protein, besides iron-regulated surface determinants (Isd) and the MSCRAMMs fibronectin-binding proteins (FnBPs), collagen adhesin (CnA) and clumping factors A/B (ClfA and ClfB).

In addition, non-covalently bound proteins, which are associated with the staphylococcal cell wall by ionic or hydrophobic interactions, can be found on the cell surface of *S. aureus*. Coagulase (Coa), the extracellular fibrinogen binding protein (Efb), the extracellular matrix

binding protein (Emp) or the extracellular adhesive protein (Eap) belong to this group, which is called secretable expanded repertoire adhesive molecules (SERAM). SERAMs are implicated in adhesion to host molecules, cells or tissue and in host defense mechanisms (Chavakis et al., 2005).

Non-proteinaceous macromolecules associated with the bacterial cell surface, such as Lipoteichoic acids (LTAs) and Wall teichoic acids (WTAs), were also shown to contribute to virulence by binding to host receptors and surfaces (Xia et al., 2010).

1.2.2 Membrane-damaging toxins

Besides surface-associated factors, secreted proteins, such as membrane-damaging exotoxins, comprise the second major group of *S. aureus* virulence factors. The main function of those cytolytic toxins is damage of host tissue and lysis of host cells, which may facilitate spread of infection. Membrane-damaging toxins form pores in the host plasma membrane and subsequently cause leakage and lysis of the cell. Here, either an initial interaction with a host receptor is necessary or interference with the membrane is less specific and no receptor interaction is required (Otto, 2014). The well-known *S. aureus* α -toxin, also named α -hemolysin (Hla), employs both of the described mechanisms in a concentration-dependent manner. At low α -toxin concentrations pore formation was shown to be dependent on the ADAM10 receptor and apoptosis was induced by selective release of monovalent ions and subsequent DNA fragmentation (Bantel et al., 2001; Inoshima et al., 2011; Jonas et al., 1994; Wilke and Bubeck-Wardenburg, 2010). However, at high doses α -toxin forms larger pores, which are also permissive for divalent ions like Ca^{2+} and massive necrosis is induced (Bantel et al., 2001). Hla is secreted as water-soluble monomers, which form heptameric β -barrel pores upon contact with a membrane (Gouaux et al., 1994; Song et al., 1996). Typically, α -toxin is known for its hemolytic properties, but the toxin also has been demonstrated to affect other human cell types, including epithelial cells, endothelial cells, T cells, monocytes and macrophages, and recent studies have shown that, besides its cytotoxic function, the toxin can interfere with cell signaling pathways regulating cell proliferation, inflammatory responses, cytokine secretion and cell-cell interactions (Oliveira et al., 2018).

S. aureus also produces a number of bi-component toxins, which are structurally similar to α -toxin and belong to the β -barrel pore-forming toxin family. These toxins consist of two different components, S- and F-subunit, which form hetero-oligomeric pores in the host membrane by binding to cellular receptors (Aman et al., 2010; Yamashita et al., 2011). *S. aureus* can express four of these leukotoxins, namely Pantan-Valentine leukotoxin (PVL/LukSF), leukotoxin ED

(LukED), leukotoxin AB/GH (LukAB/LukGH) and γ -toxin (γ -hemolysin/HlgAB and HlgBC), which share considerable sequence similarity. The toxins show slight differences in activity and target range suggesting that they are not redundant, but may have specialized functions in attacking and/or evading host defenses (Yoong and Torres, 2013). Whereas all leukotoxins can lyse neutrophils and other leukocytes, γ -toxin and LukED also target erythrocytes (Morinaga et al., 2003). Both LukAB and PVL preferentially target human neutrophils over rabbit and murine neutrophils (Loeffler et al., 2010; Malachowa et al., 2012). In contrast, LukED has been shown to lyse human, rabbit and mouse cells to equal extent (Alonzo et al., 2012; Alonzo et al., 2013). A group of small, amphipathic peptides called the phenol-soluble modulins (PSMs) also exert cytolytic activity (Wang et al., 2007). They attach in a non-specific way and thus integrate into the membrane forming an oligomeric pore, which is thought to be rather short-lived (Otto, 2014; Talbot et al., 2001). Initially discovered in *Staphylococcus epidermidis* (Mehlin et al., 1999) later two groups of PSMs, namely α -type (PSM α 1-4, δ -toxin/PSM γ) and β -type peptides (PSM β 1 and PSM β 2), were also found to be produced by most *S. aureus* strains (Li et al., 2009; Wang et al., 2007). In addition to cytolysis, which is only executed by α -type PSMs (Peschel and Otto, 2013), they can stimulate inflammatory responses and contribute to biofilm structuring and detachment (Kretschmer et al., 2010; Periasamy et al., 2012). However, the function of PSMs seems to be dependent on the concentration present (Peschel and Otto, 2013).

1.2.3 Extracellular proteases

S. aureus possesses ten major secreted proteolytic enzymes, which include a metalloprotease (aureolysin, Aur), two papain-like cysteine proteases (staphopain A (ScpA) and staphopain B (SspB)), a serine protease (V8, SspA) and six serine-like proteases (SplA-F) (Reed et al., 2001; Shaw et al., 2004). In contrast to the six Spl enzymes, which are active upon secretion, aureolysin, V8 protease, staphopain A and staphopain B are produced as zymogens. Whereas aureolysin and staphopain A zymogens auto-activate outside the cell (Nickerson et al., 2010; Nickerson et al., 2008), V8 protease and staphopain B activation is the result of a proteolytic cascade, in which aureolysin processes SspA and subsequently SspB is activated by SspA-mediated cleavage (Figure 1.3B) (Drapeau, 1978; Massimi et al., 2002). *S. aureus* extracellular proteases are organized in four distinct operons, *aur*, *sspABC*, *scpAB* and *splABCDEF*, where staphopain A and B are co-transcribed with their endogenous inhibitors, SspC and ScpB, respectively, to protect the bacteria from proteolytic degradation of cytoplasmic proteins (Figure 1.3A) (Filipek et al., 2003; Rzychon et al., 2003). Their expression is positively regulated by *agr* and negatively regulated by *sarA* (Shaw et al., 2004). The secreted extracellular

proteases have a broad substrate specificity and can degrade both "self" and "non-self" proteins. While initially thought to play a role in nutrient acquisition, they were shown to cleave host factors involved in virulence, like extracellular matrix (ECM) proteins, components of the innate immune system, plasma proteins and antimicrobial peptides, to promote *S. aureus* dissemination, tissue invasion and evasion of host immunity (Imamura et al., 2005; Laarman et al., 2012; Massimi et al., 2002; Ohbayashi et al., 2011; Paharik et al., 2016; Potempa et al., 1988; Sieprawska-Lupa et al., 2004). In addition, they modulate function or activity of *S. aureus* surface proteins and secreted toxins (Gonzalez et al., 2012; Karlsson et al., 2001; McAleese et al., 2001; McGavin et al., 1997; Zielinska et al., 2011). Besides, *S. aureus* secretes a series of other proteases. For instance, the serine proteases exfoliative toxins specifically cleave desmosomal cadherins of the superficial skin layers, leading to staphylococcal scalded skin syndrome (SSSS) (Bukowski et al., 2010). Further, *S. aureus* produces a serine protease, EpiP, which degrades collagen and casein (Kuhn et al., 2014).

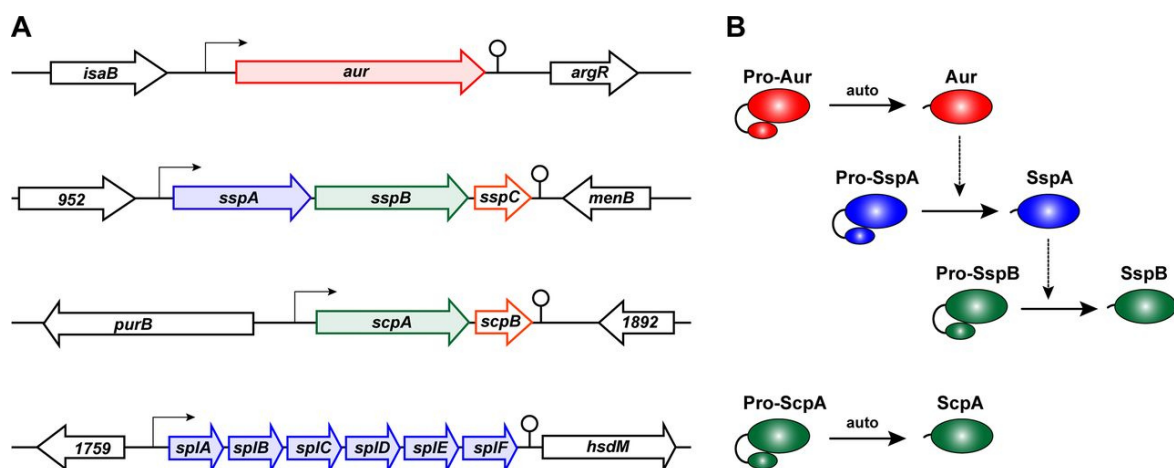


Figure 1.3: *S. aureus* extracellular protease genes and proteolytic activation.

(A) Genomic organization of extracellular protease operons based on the USA300 genome (red: metalloprotease, blue: serine proteases, green: cysteine proteases, orange: staphostatins). (B) *S. aureus* proteolytic activation cascade of Aur, SspA, and SspB is depicted. Pro-SspA is able to autoactivate (Mootz et al., 2013).

1.2.4 Other virulence-associated extracellular enzymes and proteins of *S. aureus*

Besides proteases, *S. aureus* also secretes a series of enzymes, which degrade host molecules or interfere with host metabolic or signaling cascades. The sphingomyelinase β -toxin (Hlb) degrades sphingomyelin on the surface of a variety of host cells and thus leads to cell lysis (Doery et al., 1963). However, in many *S. aureus* strains the *hlb* gene is disrupted by a pathogenicity island (Coleman et al., 1986; Winkler et al., 1965). Further, *S. aureus* produces two coagulases, staphylocoagulase (SC) and von Willebrand factor binding protein (vWbp), which inhibit phagocytosis by immune cells, cause abscess formation and promote adhesion of *S. aureus* to surfaces by the formation of fibrin clots (Cheng et al., 2010). In contrast,

staphylokinase (SAK) leads to degradation of fibrin clots facilitating bacterial penetration into tissue (Bokarewa et al., 2006). Moreover, it abolishes the bactericidal properties of alpha-defensins. The function of *S. aureus* lipases and nucleases in pathogenesis is only poorly understood. Nucleases may decrease the antibacterial activity of neutrophil extracellular traps (NETs), which consist of DNA released from lysed neutrophils (Brinkmann and Zychlinsky, 2012).

Further, *S. aureus* secretes specific proteins, which have strong impact on the host innate and adaptive immune system. The group of superantigens include the toxic shock syndrome toxin-1 (TSST-1), staphylococcal enterotoxins and superantigen-like toxins (SEL) (Holtfreter and Broker, 2005; Lina et al., 2004). Superantigens activate large subpopulations of T-lymphocytes simultaneously and thus cause a massive cytokine release, which is thought to be a defense mechanism of bacteria against the host immune system. Chemotaxis inhibitory protein of *S. aureus* (CHIPS), formyl peptide receptor-like-1 inhibitory protein (FLIPr) and FLIPR-like are *S. aureus* exotoxins, which interfere with leukocyte receptors to evade recognition and prevent subsequent activation of the immune system (de Haas et al., 2004; Prat et al., 2006; Prat et al., 2009). Staphylococcal complement inhibitor (SCIN) is a C3 convertase inhibitor, which blocks the ability of human neutrophils to phagocytose *S. aureus* (Rooijackers et al., 2005).

1.3 *S. aureus* intracellular infection

1.3.1 Invasion and intracellular survival

Although *S. aureus* is not considered a classical intracellular bacterium, it was shown that it can invade host cells and survive intracellularly for various periods of time. The pathogen is internalized by a variety of non-phagocytic cells, such as epithelial and endothelial cells, osteoblasts, fibroblasts and keratinocytes, and survives phagocytosis by neutrophils and macrophages (Figure 1.4) (Garzoni and Kelley, 2009; Strobel et al., 2016). Invasion of non-phagocytic cells by *S. aureus* is mediated by a zipper-type mechanism, in which bacterial adhesins interact with ECM proteins and/or specific host receptors. Here, the FnBPs, FnBPA and FNBPB, were identified as the major adhesins (Sinha et al., 2000). They indirectly bind to $\alpha_5\beta_1$ integrins on the host cell surface via the bridging molecule fibronectin, which induces endocytic uptake of the bacteria. Interestingly, $\alpha_5\beta_1$ integrins are rather expressed on the basolateral membranes of polarized tissue, indicating that only disrupted or damaged tissue may allow *S. aureus* invasion (Horn et al., 2018b). Additionally, other proteins, such as e.g. extracellular adherence protein (Eap) and staphylococcal autolysin (Atl), are involved in *S. aureus* invasion (Harraghy et al., 2003; Hirschhausen et al., 2010).

After invasion, *S. aureus* can survive inside host cells for extended periods of time, unlike most other extracellular bacteria (Hamill et al., 1986; Kubica et al., 2008b; Lowy et al., 1988; Tuchscher et al., 2011). The intracellular niche likely serves as a reservoir for chronic or relapsing staphylococcal infections and as a hideout from the host immune system and antibiotic treatment. Prolonged survival inside host phagosomes is associated with conversion to a slow growing persistent form called small colony variants (SCVs) (Proctor et al., 1994). SCVs possess a reduced metabolic activity and produce less virulence factors due to diminished expression of *agr* (Moisan et al., 2006). The trigger for phenotype switching is not fully clear, but SCVs seem to appear in a very dynamic manner and antibiotics, sub-lethal concentrations of hydrogen peroxide or the intracellular environment in general were shown to induce persistence of *S. aureus* (Krut et al., 2004; Painter et al., 2015; Tuchscher et al., 2011; Vesga et al., 1996). The alternative sigma factor σ_B , which is a transcription factor associated with stress responses, was identified to regulate formation of SCVs (Tuchscher et al., 2015).

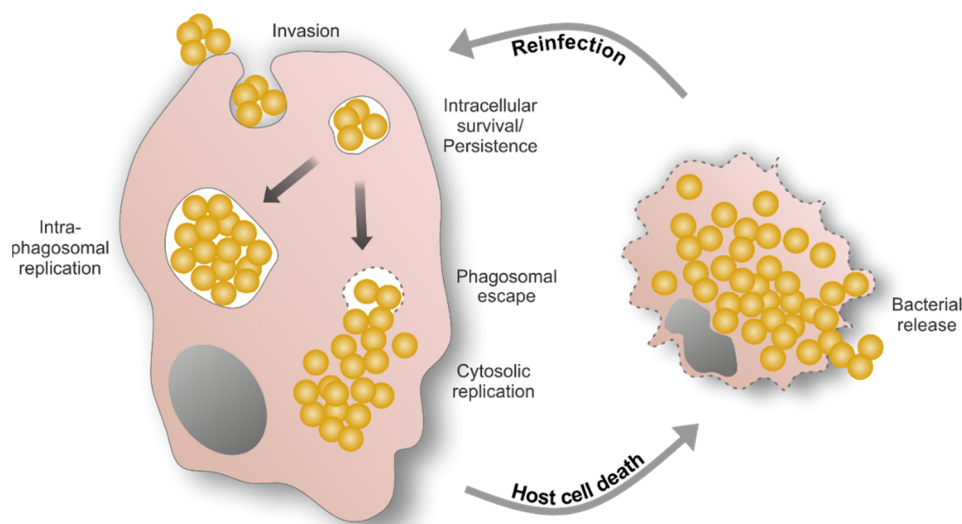


Figure 1.4: The intracellular lifestyle of *S. aureus*.

After internalization by receptor-mediated phagocytosis, *S. aureus* resides in an endophagosome, where it can survive for extended periods of time and/or transform to a persistent state. In professional phagocytes *S. aureus* replicates in the phagosomal lumen, whereas in non-professional phagocytes the pathogen escapes from the phagosome into the cytosol and subsequently replicates in the cytoplasm. In both cases, *S. aureus* kills the host cell from within, which results in bacterial release and secondary infection (adapted from Moldovan and Fraunholz (2018)).

Remarkably, intracellular *S. aureus* can withstand phagocyte-mediated killing and survive within macrophages for several days and up to 24 hours in neutrophils (Gresham et al., 2000; Kubica et al., 2008a; Melly et al., 1960; Rollin et al., 2017). The bacterium tolerates and may even require the acidic environment and antimicrobial effectors within the phagosome to mount an evasive response. The pathogen can travel hidden in these phagocytes to other sites of the body and thus lead to dissemination of infection (Gresham et al., 2000; Lehar et al., 2015;

Thwaites and Gant, 2011). However, the role of *S. aureus* intracellularity *in vivo* is not fully understood. Several studies demonstrate the existence of intracellular *S. aureus* in human *ex vivo* tissue cells. Intracellular bacteria were detected, for instance, in human tonsils, mast cells of nasal polyps and in epithelial cells within in the nasal mucosa and anterior nares of patients with recurrent sinusitis and healthy carriers (Clement et al., 2005; Hanssen et al., 2017; Hayes et al., 2015; Ou et al., 2016; Plouin-Gaudon et al., 2006; Zautner et al., 2010).

1.3.2 Phagosomal escape and intracellular replication in non-professional phagocytes

In contrast to phagocytic cells, where *S. aureus* replicates in the phagosome prior to induction of host cell death (Flannagan et al., 2016; Jubrail et al., 2016; Kobayashi et al., 2010; Tranchemontagne et al., 2016; Weinrick et al., 2004), phagosomal escape is required for intracellular replication and cytotoxicity of the pathogen in non-phagocytic cells (Figure 1.4) (Bayles et al., 1998; Horn et al., 2018b; Strobel et al., 2016). Phagosomal escape represents a strategy employed by intracellular bacteria, like *Listeria monocytogenes*, *Shigella flexneri* or *Francisella tularensis*, to avoid phagolysosomal killing. After the endocytic uptake, intracellular *S. aureus* readily translocates to the cytosol of host cells. Phagosomal escape of *S. aureus* is attributed to an *agr*-regulated factor, as mutants in *agr* or strains with a defect in *agr* expression are incapable of translocation into the cytoplasm (Blaettner et al., 2016; Jarry et al., 2008; Muenzenmayer et al., 2016; Shompole et al., 2003) and *agr* expression was found to be increased in phagolysosomes (Grosz et al., 2014; Qazi et al., 2001; Shompole et al., 2003). PSM α , whose expression is controlled by *agr*, was identified mediating of phagosomal escape in professional and non-professional phagocytes (Grosz et al., 2014; Muenzenmayer et al., 2016). The reduced escape rate of a mutant in the PSM-specific ABC transporter Pmt further corroborates this finding (Blaettner et al., 2016). However, PSM α alone is not sufficient for inducing phagosomal escape, because overexpression of PSM α in escape-deficient strains showed no effect (Giese et al., 2011; Grosz et al., 2014). The synergistic expression of PSM β , δ -toxin (PSM γ) and the sphingomyelinase β -toxin was shown to trigger phagosomal escape of *S. aureus*, but the cooperating factor(s) of PSM α -mediated phagosomal escape remain unknown (Giese et al., 2011). Additional phagosomal escape factors have been identified, including the non-ribosomal peptide synthetase (NRPS) complex AusAB (Blaettner et al., 2016). In keratinocytes, but not in epithelial cells, PVL was shown to contribute to *S. aureus* phagosomal escape (Blaettner et al., 2016; Chi et al., 2014; Grosz et al., 2014).

It has been reported that *S. aureus* is targeted by autophagy during intracellular residence in non-professional phagocytes. However, the pathogen is able to prevent acidification and

autophagosome-lysosome fusion and thus escapes the autophagic degradation (Mestre et al., 2010; Neumann et al., 2016; Schnaith et al., 2007). The *agr*-regulated virulence factor α -toxin is responsible for induction of autophagy (Maurer et al., 2015; Mauthe et al., 2012; Mestre et al., 2010; O'Keeffe et al., 2015). The toxin may perforate the membrane of *S. aureus*-containing endophagosomes, which is subsequently targeted by autophagy. By contrast, *S. aureus*-containing macrophage phagosomes showed no accumulation of autophagy-related proteins again indicating a different intracellular lifestyle of *S. aureus* in phagocytes when compared to other cell types (Flannagan et al., 2016).

S. aureus is capable of replicating inside different types of host cells (Flannagan et al., 2016; Kahl et al., 2000; Kubica et al., 2008b; Lowy et al., 1988; Qazi et al., 2001). In non-phagocytic host cells intracellular replication was observed in the cytosol after endo- or autophagosomal escape (Grosz et al., 2014; Horn et al., 2018b; Mestre et al., 2010; Neumann et al., 2016). Accordingly, proliferation of intracellular *S. aureus* is dependent on the expression of virulence factors required for translocation into the cytosol. Besides, intracellular *S. aureus* may subvert autophagy to promote its intracellular survival and replication (Bravo-Santano et al., 2018). Intracellular *S. aureus* severely depletes glucose and amino acid pools and glutaminolysis is highly activated in the host cell. This state of starvation might activate autophagy in the host cell to ensure energy generation and nutrient scavenging. This theory is further corroborated by the finding that chemical inhibition of autophagy impairs intracellular replication, whereas induction of autophagy leads to increased numbers of intracellular bacteria (Schnaith et al., 2007).

1.3.3 Induction of host cell death

Intracellular bacteria have evolved several strategies to promote their exit from the host cell, such as interference with host cell signaling to induce programmed cell death, the active breaching of host cell-derived membranes or deformation of the host membrane (Flieger et al., 2018). The former two mechanisms ultimately result in killing of the host cell. Induction of host cell death is associated with tissue and membrane barrier destruction, dissemination of infection, inflammation and pathogen transmission. Most intracellular pathogens induce exit of the host after intracellular replication and bacterial virulence factors implicated in this process are proteases, phospholipases and pore-forming toxins or cytolysins.

Several *S. aureus* virulence factors have been linked to induction of host cell death. Especially *S. aureus* membrane-damaging toxins can trigger cytolysis of a variety of different host cell types (Section 1.2.2). To what extent these effects can be attributed to cytotoxicity of

intracellular *S. aureus* must be investigated in more detail. In non-professional phagocytes α -toxin was identified as a key factor mediating intracellular cytotoxicity (Haslinger-Loeffler et al., 2005; Menzies and Kourteva, 2000), whereas the leukotoxin LukAB was shown to induce cell lysis after uptake of *S. aureus* by professional phagocytes (DuMont et al., 2013b; Melehani et al., 2015; Muenzenmayer et al., 2016; Ventura et al., 2010). LukAB-mediated intracellular cell death was also dependent on its host cell receptor CD11b, which is internalized upon phagocytosis (DuMont et al., 2013a; Muenzenmayer et al., 2016). Some reports connected PVL (Chi et al., 2014; Jin et al., 2013; Muenzenmayer et al., 2016) or PSMs (Rasigade et al., 2013; Surewaard et al., 2013) with host cell killing by intracellular *S. aureus*. Induction of host cell death is highly dependent on phagosomal escape and consequently on the expression of virulence factors mediating this process (Blaettner et al., 2016; Grosz et al., 2014; Lam et al., 2010). LukAB, PSMs and PVL were shown to also play a role in translocation of *S. aureus* from the phagosome into the host cell cytosol (Section 1.3.2) (Blaettner et al., 2016; Chi et al., 2014; Grosz et al., 2014).

Intracellular *S. aureus* has been shown to induce cell death in host cells ranging from epithelial and endothelial cells to osteoblasts and professional phagocytes like neutrophils and macrophages (Horn et al., 2018b). Reports on the molecular mechanisms underlying *S. aureus*-induced host cell killing are rather inconsistent concerning the mode of cell death involved. This likely arises from the diversity of *S. aureus* strains and types of host cells used in the studies. Most studies describe hallmarks of apoptosis in professional as well as non-professional phagocytes infected with *S. aureus*, such as DNA fragmentation, cell contraction and/or activation of caspases (Bayles et al., 1998; Kahl et al., 2000; Menzies and Kourteva, 1998; Nuzzo et al., 2000; Tucker et al., 2000). Activation of both the extrinsic or intrinsic pathway was observed in epithelial and endothelial cells, osteoblasts and primary human PBMCs (Alexander et al., 2001; Alexander et al., 2003; Baran et al., 1996; Esen et al., 2001; Haslinger-Loeffler et al., 2005; Jin et al., 2013; Weglarczyk et al., 2004; Wesson et al., 2000; Young et al., 2011). Besides, intracellular *S. aureus* was shown to induce a caspase-independent, autophagy-associated cell death in epithelial cells (Schnaith et al., 2007). Other studies observed characteristics of both apoptosis and necrosis in macrophages and mesothelial cells (Flannagan et al., 2016; Haslinger-Loeffler et al., 2006), whereas in primary human polymorphonuclear neutrophils (PMNs) intracellular *S. aureus* induced a necroptotic cell death (Greenlee-Wacker et al., 2014; Kobayashi et al., 2010).

1.4 Cell death mechanisms

Cell death is a critical process for organismal homeostasis in both physiological and pathological settings and is found in both multicellular as well as unicellular organisms. It can occur from perturbations of the intracellular or extracellular microenvironment or without any exogenous stimulus for physiological development or tissue turnover. In contrast to accidental cell death (ACD), which immediately results from severe physical, chemical or mechanical insults, regulated cell death (RCD) is executed by a stereotypical series of biochemical and morphological changes and usually confers a beneficial effect on the organism. A multitude of different cell death signaling pathways with diverse morphological, biochemical and functional characteristics have been identified in mammalian cells (Figure 1.5) (Galluzzi et al., 2018).

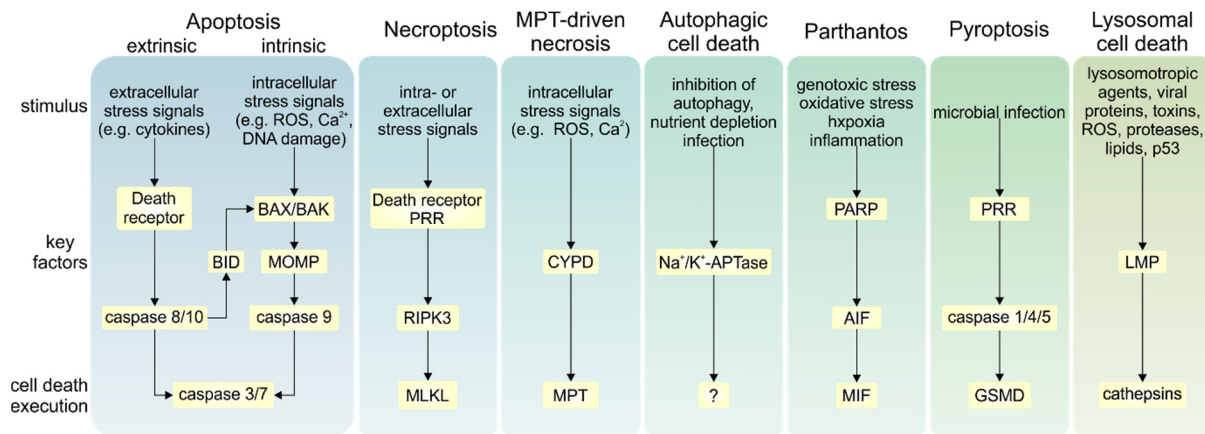


Figure 1.5: Major pathways of regulated cell death in mammalian cells.

Cells exposed to irreversible perturbations of the intracellular or extracellular microenvironment can activate several signal transduction pathways ultimately leading to their death. Dependent on the stimulus, the demise of the cell is executed by different molecular factors. For detailed description please refer to section 1.4 (adapted from Linkermann et al. (2014)).

1.4.1 Apoptosis

Apoptosis is the best-characterized and evolutionary most conserved form of programmed cell death. It displays distinctive morphological and biochemical hallmarks, like blebbing, cell shrinkage, nuclear fragmentation, chromatin condensation, chromosomal DNA fragmentation and plasma membrane changes. The main executioners of apoptosis are caspases, a family of protease enzymes, which - upon activation - cleave cellular components required for normal cellular function such as cytoskeletal and nuclear proteins. Apoptotic cells retain plasma membrane integrity and metabolic activity until the process is completed. End-stage apoptosis is characterized by the formation of small vesicles, known as apoptotic bodies, which allow for the rapid and immunologically silent clearance by macrophages or other cells with phagocytic activity in a process named efferocytosis (Green et al., 2016). *In vitro*, the absence of phagocytic

cells finally results in complete breakdown of the plasma membrane and the acquisition of a necrotic morphotype called secondary necrosis (Silva, 2010; Vanden Berghe et al., 2010). Apoptosis can be initiated through one of two distinct pathways. While the intrinsic apoptosis pathway leads to death mostly due to intracellular cell stress, the extrinsic pathway is activated upon perturbations of the extracellular microenvironment.

Factors like, for instance, hypoxia, genetic damage, high concentration of cytosolic Ca^{2+} , extreme oxidative stress or survival factor deprivation trigger the initiation of the intrinsic pathway. The crucial step for intrinsic apoptosis is irreversible and widespread mitochondrial outer membrane permeabilization (MOMP) (Galluzzi et al., 2016; Tait and Green, 2010), which is controlled by pro-apoptotic and anti-apoptotic members of the B-cell lymphoma 2 (BCL2) family. The activation of either BCL2-associated X protein (BAX) or BCL2 antagonist or killer (BAK) by BCL2 homology 3 (BH3)-only proteins is essential for MOMP. On activation, BAX and BAK undergo extensive conformational changes, leading to the mitochondrial targeting of BAX and the homo-oligomerization of BAK and BAX (Eskes et al., 2000; Hsu et al., 1997; Wei et al., 2000). These oligomers are believed to promote MOMP through the formation of proteinaceous channels or lipidic pores by destabilizing lipid membranes (Tait and Green, 2010). MOMP leads to the release of pro-apoptotic proteins, such as cytochrome c, second mitochondria-derived activator of caspase (SMAC) and Omi, from the mitochondrial intermembrane space. Cytochrome c binds apoptotic protease-activating factor 1 (APAF1), thus inducing its conformational change and oligomerization, which leads to the formation of the apoptosome, a caspase activation platform (Riedl and Salvesen, 2007). The apoptosome recruits, dimerizes and activates the initiator caspase 9, which, in turn, cleaves and activates the caspases 3 and 7. These effector caspases execute cell death by cleavage of various proteins. Additional steps ensure cell death, for instance, cytosolic SMAC and Omi block inhibitor of apoptosis proteins (IAPs), including X-linked inhibitor of apoptosis (XIAP), which are endogenous inhibitors of caspases (Du et al., 2000; Martins et al., 2002). A specific form of intrinsic apoptosis is termed anoikis, where the loss of integrin-dependent attachment to the extracellular matrix leads to cell death via MOMP and caspase 3 (Paoli et al., 2013).

The extrinsic apoptosis pathway is primarily mediated by signaling through membrane-bound death receptors, whose activation depends on the binding of their cognate ligand(s). Dependence receptors, which are activated when the levels of their specific ligand drop below a certain threshold, may also initiate extrinsic apoptosis (Gibert and Mehlen, 2015; Mehlen and Bredesen, 2011). Death ligands, such as Fas ligand (Fas-L), tumor necrosis factor (TNF) and TNF-related apoptosis-inducing ligand (TRAIL), bind to TNF family death receptors, which

allows the assembly of a dynamic multiprotein complex at the intracellular tail of the receptor, the so-called “death-inducing signaling complex” (DISC) (Aggarwal et al., 2012; Dickens et al., 2012; von Karstedt et al., 2017; Wajant, 2002). Procaspases 8 and 10 are activated by DISC and apoptosis is executed depending on the cell type (Barnhart et al., 2003). In so-called “type I cells”, e.g. thymocytes and mature lymphocytes, the proteolytic maturation of effector caspases 3 and 7 by caspase 8 is sufficient to induce cell death. Conversely, in “type II cells”, e.g., hepatocytes, pancreatic β cells and a majority of cancer cells, the intrinsic pathway is activated by caspase 8-dependent proteolytic cleavage of BH3 interacting-domain death agonist (BID) (Li et al., 1998; Luo et al., 1998). The truncated form of BID (tBID) activates and oligomerizes BAX and BAK leading to MOMP (Kim et al., 2009).

1.4.2 Necrotic cell death

The term necrosis is commonly used for non-apoptotic, accidental cell death. Originally, pathologists invented this term to designate the presence of dead tissue or cells irrespective of the pre-lethal processes (Majno and Joris, 1995). Cellular swelling (oncosis), swelling of organelles, plasma membrane rupture and subsequent loss of intracellular contents, which may cause an inflammatory response, represent typical characteristics of necrosis contrasting the features of apoptosis. However, there is no consensus on the biochemical changes, that characterize necrosis. Early plasma membrane permeabilization and the absence of hallmarks of other types of cell death are used to identify necrosis (Denecker et al., 2001; Kroemer et al., 2009). Thus, the term necrosis does not indicate a form of cell death, but rather refers to changes secondary to cell death by any mechanism.

A regulated form of cell death morphologically resembling necrosis has been identified, which shows a prominent role in multiple physiological and pathological settings (Vandenabeele et al., 2010). Perturbations of the intracellular or extracellular microenvironment, which are sensed by death receptors or pathogen recognition receptors (PRRs), such as toll-like receptors (TLRs) or cytosolic NOD-like receptors (NLRs), induce this type of cell death termed necroptosis. The most understood pathway of necroptosis is mediated by TNF receptor 1 (TNFR1). Upon stimulation, the death receptor induces the formation of a receptor interacting serine/threonine kinase 1 (RIPK1)- and RIPK3-containing amyloid-like signaling complex named as necrosome (Grootjans et al., 2017). First RIPK1 and then RIPK3 undergo a series of trans-phosphorylation or auto-phosphorylation events, which are required for necroptosis activation. RIPK3 is essential for TNF-induced necroptosis, whereas RIPK1 appears dispensable in some settings (Moujalled et al., 2013; Upton et al., 2010). Besides necroptosis,

RIPK1 also has a well-established role in mediating both TNF-dependent nuclear factor κ B (NF κ B) activation and apoptosis (Ofengeim and Yuan, 2013). The major executor of necroptosis is mixed lineage kinase domain like pseudokinase (MLKL), which is activated by phosphorylation by RIPK3 (Sun et al., 2012). Activated MLKL forms oligomers and translocates to organelle and plasma membranes, where it directly binds with phosphatidylinositol phosphates (PIPs) or cardiolipin (CL) and disrupts the membrane by pore formation (Zhang et al., 2016).

Another cell death mechanism, which manifests with a necrotic morphotype, is mitochondrial permeability transition (MPT)-driven necrosis (Izzo et al., 2016). The opening of the so-called “permeability transition pore complex” (PTPC), a supramolecular complex assembled at the junctions between the inner (IMM) and the outer mitochondrial membrane (OMM) results in the permeability of the IMM to small solutes, dissipation of the IMM potential ($\Delta\Psi_m$), osmotic breakdown of both mitochondrial membranes and subsequently to cell death. MPT-driven necrosis is initiated by intracellular perturbations, such as severe oxidative stress and cytosolic Ca^{2+} overload, which can be artificially imposed *in vitro* by potent oxidants, such as hydrogen peroxide, or ionophores, e.g. ionomycin. Ischemic insults cause MPT-driven necrosis *in vivo*. Cyclophilin D (CYPD), which is a crucial regulator of the MPT by promoting the opening of PTPC, is required for MPT-driven necrosis (Baines et al., 2005; Nakagawa et al., 2005).

1.4.3 Parthanatos

Severe and prolonged alkylating DNA damage as well as oxidative stress, hypoxia, hypoglycemia or inflammatory cues lead to the hyperactivation of a component of the DNA damage response (DDR) machinery named poly(ADP-ribose) polymerase 1 (PARP1), which results in a cell death called parthanatos (David et al., 2009; Fatokun et al., 2014; Virag et al., 2013). PARP1 hyperactivation causes NAD⁺ and ATP depletion, which ultimately results in a bioenergetic and redox collapse. Furthermore, it leads to the accumulation of poly(ADP-ribose) (PAR) polymers and poly(ADP-ribosyl)ated proteins at mitochondria causing $\Delta\Psi_m$ dissipation and MOMP. A key factor of parthanatos is the mitochondrial-associated apoptosis-inducing factor (AIF), which causes large-scale DNA fragmentation and chromatin condensation after the PAR polymer-induced translocation from the mitochondria to the nucleus (Wang et al., 2011; Yu et al., 2006). Macrophage migration inhibitory factor (MIF) was identified as the main nuclease, which is translocated to the nucleus by AIF to catalyze DNA cleavage and thus execute parthanatos (Wang et al., 2016).

1.4.4 Other modes of cell death

Pyroptosis is a caspase-dependent form of programmed cell death and part of the innate immunity, as it plays an important role in the defense against microbial infections. “Danger” signals, like pathogen-associated molecular patterns (PAMPs) or damage-associated molecular patterns (DAMPs), are sensed extra- or intracellularly by TLRs or NLRs resulting in the formation of large protein signaling complexes called inflammasomes. Activated inflammatory caspases (caspase 1, caspase 4 and caspase 5 or murine caspase 11) precipitate pyroptosis by catalyzing the proteolytic cleavage of gasdermin D (GSDMD) (Cookson and Brennan, 2001; Kayagaki et al., 2015; Shi et al., 2015). Cleaved GSDMD acts as the final and direct executor of pyroptotic cell death through selective targeting of the inner leaflet of the plasma membrane and subsequent pore-forming activity (Qiu et al., 2017). Initially, pyroptosis was thought to be relevant only for the demise of monocytes or macrophages, however, recent findings indicate that pyroptosis can also occur in cell types other than cells from the monocytic lineage, such as epithelial cells and keratinocytes (Shi et al., 2014).

The function of autophagy in cell death has been controversial, since autophagy generally exerts a cytoprotective function. Only blocking or defects in autophagy are associated with autophagy-dependent cell death (ACD) (Boya et al., 2005; Mroczek et al., 2015; Yousefi et al., 2006). Thus, cell death occurs only when macroautophagic responses fail, which are activated in response to stress as an ultimate attempt of the cell to preserve homeostasis (Galluzzi et al., 2015). Nevertheless, components of the machinery for macroautophagy or macroautophagic responses were shown to have a small impact on cell death (Denton et al., 2015; Masini et al., 2009; Saleh et al., 2016; Sharma et al., 2014).

Lysosomal membrane permeabilization (LMP), which results in the release of lysosomal contents, including proteolytic enzymes of the cathepsin family, to the cytoplasm, represents another mechanism of regulated cell death (Aits and Jaattela, 2013). Lysosomes generally serve as the cellular “recycling bins” filled with numerous hydrolases, but can cause cell and tissue autolysis upon rupture (de Duve, 1983). The molecular mechanisms operating upstream of LMP and lysosome-dependent cell death (LCD) are not fully elucidated. Lysosomotropic detergents, viral proteins, bacterial, fungal or snake toxins, reactive oxygen species, proteases, lipids and their metabolites, p53 and proapoptotic BCL2 family members were shown to contribute to LCD (Aits and Jaattela, 2013). However, possibly all cell death pathways eventually lead to LMP and the mechanisms underlying LMP are largely ambiguous (Vanden Berghe et al., 2010).

Other mechanisms of regulated cell death were described, such as ferroptosis, NETotic cell death, immunogenic cell death or entotic cell death (Galluzzi et al., 2018).

1.4.5 Calcium and cell death

In contrast to other cations, which solely contribute to enzyme activity, Ca^{2+} has an essential regulatory function in eukaryotic cells. Due to its low cytosolic concentration, the calcium ion is able to act as second messenger playing an important role in cell signaling and controlling diverse cellular functions. In excitable cells, these functions include muscle contraction or neurotransmitter release, whereas non-excitable cells Ca^{2+} regulates gene transcription, cell proliferation, cell cycle and also cell death (Berchtold et al., 2000; Bhosale et al., 2015; Dolmetsch et al., 1998; Kaeser and Regehr, 2014; Kuo and Ehrlich, 2015; Machaca, 2010). The regulation of so many processes is enabled by the versatility of the Ca^{2+} signaling mechanism in terms of speed, amplitude and spatiotemporal patterning and by various calcium-sensing effectors, that translate calcium signals (Clapham, 2007). Under resting conditions, the cytoplasmic Ca^{2+} concentration is 10^4 -fold lower (approx. 100 nM) than the Ca^{2+} concentration in the extracellular milieu (approx. 1 mM). Intracellular organelles, like endoplasmic reticulum (ER) and mitochondria, known as the internal Ca^{2+} -stores, accumulate Ca^{2+} and thus exhibit a higher Ca^{2+} concentration (100-500 μM) compared to the cytoplasm. The plasma membrane Ca^{2+} transport ATPase (PMCA) and $\text{Na}^+/\text{Ca}^{2+}$ exchanger (NCX), which transport calcium ions to the extracellular space, are responsible for maintaining the low cytoplasmic Ca^{2+} concentration in a resting cell (Figure 1.6). Upon cytosolic Ca^{2+} elevation, the sarcoendoplasmic reticulum Ca^{2+} -ATPase (SERCA) and, to a lower extent, the mitochondrial Ca^{2+} uniporter (mtCU) support this activity by filling the intracellular Ca^{2+} -stores.

Increases in cytosolic Ca^{2+} levels originate from uptake of extracellular calcium ions by plasma membrane Ca^{2+} channels, which is rather infrequent in many non-excitable cells, or by extrusion of Ca^{2+} from internal stores by the 1,4,5-triphosphate receptor (IP3R) and ryanodine receptor (RyR). The predominant Ca^{2+} entry mechanism in non-excitable cells is represented by store-operated calcium entry (SOCE), whereby Ca^{2+} influx across the plasma membrane is activated in response to a decrease in the ER Ca^{2+} content (Hogan and Rao, 2015). The main role of SOCE is to refill the internal Ca^{2+} stores for downstream Ca^{2+} signaling. An essential component of SOCE is stromal interaction molecule (STIM), a Ca^{2+} sensing ER transmembrane protein, which interacts with and thus activates the plasma membrane Ca^{2+} channel Orai-1 at ER-plasma membrane junctions (Park et al., 2009; Prakriya et al., 2006; Zhang et al., 2005). Release of Ca^{2+} from the ER by IP3R is mediated in response to receptor activation. G protein-

coupled receptors (GPCRs) and tyrosine-kinase receptors (TKR) activate phospholipase C (PLC), which in turn cleaves phosphatidylinositol 4,5 bisphosphate (PIP₂) into 1,4,5-inositol trisphosphate (IP₃) and diacylglycerol (DAG) (Taylor and Tovey, 2010). IP₃ binding to the IP₃R allows diffusion of Ca²⁺ from the ER to increase intracellular Ca²⁺ concentration and to activate SOCE (Taylor and Machaca, 2019).

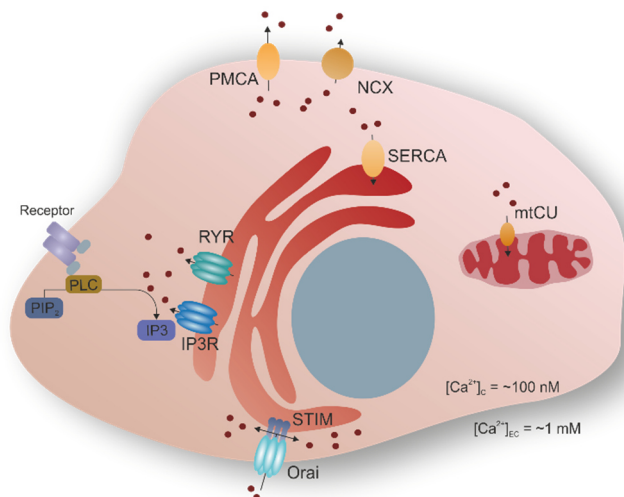


Figure 1.6: Calcium signaling in non-excitable cells.

Plasma and organelle membrane localized Ca²⁺ pumps, such as plasma membrane Ca²⁺ transport ATPase (PMCA), Na⁺/Ca²⁺ exchanger (NCX), sarcoendoplasmic reticulum Ca²⁺-ATPase (SERCA) and mitochondrial Ca²⁺ uniporter (mtCU) are responsible for extrusion of calcium ions from the cell to maintain a low cytosolic Ca²⁺ concentration. Cytosolic Ca²⁺ elevations are caused by release of calcium ions from the ER through 1,4,5-triphosphate receptor (IP₃R) and ryanodine receptor (RyR). Activation of cell receptors and subsequent phospholipase C (PLC)-mediated hydrolysis of phosphatidylinositol 4,5 bisphosphate (PIP₂) results in the production of 1,4,5-inositol trisphosphate (IP₃), which activates IP₃Rs. Low ER Ca²⁺ concentrations promote store-operated calcium entry (SOCE), whereby the interaction of stromal interaction molecule (STIM) and Orai at ER-PM junctions allows Ca²⁺ influx across the plasma membrane (adapted from Bonnet and Tran Van Nhieu (2016)).

The calcium ion possesses versatile functions in controlling cell survival and cell death in eukaryotic cells making it challenging to separate the different and multiple mechanisms (Figure 1.7). Ca²⁺ functions as second messenger activating or participating in cell death pathways, but also acts as executor of cell death (Cerella et al., 2010; Orrenius et al., 2015; Zhivotovsky and Orrenius, 2011). Regulated Ca²⁺ elevations serve as signaling events during the intrinsic apoptotic pathway. Local Ca²⁺ messages at the ER-mitochondria interface contribute to early apoptosis. Amplification loops between BAX activation and Ca²⁺ release from ER amplify cytochrome c release to a level sufficient for apoptosome nucleation and caspase activation. High local concentrations of Ca²⁺ favor the release of cytochrome c from mitochondria through BAX pores, whereas cytosolic cytochrome c in turn increases Ca²⁺ levels in the vicinity of IP₃R on the ER (Boehning et al., 2003; Nutt et al., 2002a; Pan et al., 2001). Interestingly, BAX activated via the extrinsic apoptosis pathway through tBid was not sensitive to Ca²⁺ modulation.

BAX and BAK also participate in Ca^{2+} release from the ER by either forming ion-permeable pores in the ER membrane or inducing IP3R channel opening (Nutt et al., 2002b; Zong et al., 2003). The anti-apoptotic protein BCL2 prevents Ca^{2+} leakage from the ER and subsequent activation of apoptosis by interaction with IP3R (Greenberg et al., 2014; Hanson et al., 2008; Lam et al., 1994).

A family of cysteine proteases called calpains is further involved in Ca^{2+} -induced apoptosis. The family comprises 15 members, of whom calpain 1, 2 and 4 are best characterized. Classical calpains are heterodimers consisting of a regulatory subunit (calpain 4) and a catalytic subunit (calpain 1/2). Their activation is triggered by autoproteolytic cleavage upon Ca^{2+} increase and is tightly regulated by the presence of the endogenous inhibitor protein calpastatin (Melloni et al., 1992; Suzuki and Sorimachi, 1998; Wingrave et al., 2003). Calpains cleave several members of the caspase and BCL2 family, such as BAX, Bid or BAK, to regulate apoptosis by either activating or inactivating these proteins (Bizat et al., 2003; Chen et al., 2001; Chua et al., 2000; Gafni et al., 2009; Gao and Dou, 2000; Mandic et al., 2002; Nakagawa and Yuan, 2000; Panaretakis et al., 2002; Wood et al., 1998). Besides, these cysteine proteases play a role in parthanatos by truncation and release of AIF from mitochondria (Ozaki et al., 2008, 2009).

When stress leads to Ca^{2+} overload, Ca^{2+} -produced damage may reach levels sufficient to cause necrotic cell death. Collapse of mitochondrial energy metabolism leads to a drastic drop in ATP levels, which stops Ca^{2+} -ATPases from pumping Ca^{2+} against a gradient from the cytosol to the ER or extracellular space. This results in ER Ca^{2+} depletion, cytosolic Ca^{2+} overload and subsequently to excess stimulation of Ca^{2+} -sensitive targets, like phospholipases, proteases and endonucleases in the cytosol (Caro and Cederbaum, 2007; McConkey et al., 1989; Tang et al., 1996). Under these conditions, coordination of the multiple Ca^{2+} -dependent pathways is lacking resulting in overlapping and superimposing effects leading to cell death.

Calcium ions also play a crucial role in MPT-driven necrosis induced by, for instance, oxidative stress, ischemia/reperfusion, ceramide and Ca^{2+} ionophores (Kristian and Siesjo, 1998; Lemasters et al., 1999; Szalai et al., 1999). Here, high concentration of mitochondrial Ca^{2+} activates CYPD, which promotes permeability transition pore (PTP) opening leading to MPT (Baines et al., 2005; Eliseev et al., 2007; Schinzel et al., 2005). In necroptosis, localization of MLKL to the plasma membrane leads to an influx of Ca^{2+} ions, which is mediated at least partly by a non-voltage sensitive, poorly selective cation channel of the plasma membrane named transient receptor potential cation channel subfamily M member 7 (TRPM7) (Cai et al., 2014; Gong et al., 2017). However, others detected a rapid intake of sodium, but not calcium ions or

Ca^{2+} oscillations due to Ca^{2+} release from endoplasmic reticulum during necroptosis (Chen et al., 2014; Ousingsawat et al., 2017).

Disruption of ER Ca^{2+} homeostasis leads ER stress, followed by, for instance, unfolded protein response (UPR) (Groenendyk et al., 2013; Krebs et al., 2011). During prolonged and severe activation of the UPR, cells are eliminated by intrinsic or extrinsic apoptosis (Iurlaro and Munoz-Pinedo, 2016; Urrea et al., 2013). In rodent cells, prolonged ER stress stimulates the activation of caspase 12, which acts on effector caspases to trigger apoptosis (Nakagawa et al., 2000).

However, the actual role of Ca^{2+} in cell death is still debated. It is clear that the signaling networks involved in cell death regulation are quite complex and that numerous opportunities for cross-talk between the different pathways exist. Figure 1.7 shows the different roles of Ca^{2+} alterations in survival or death of damaged cells.

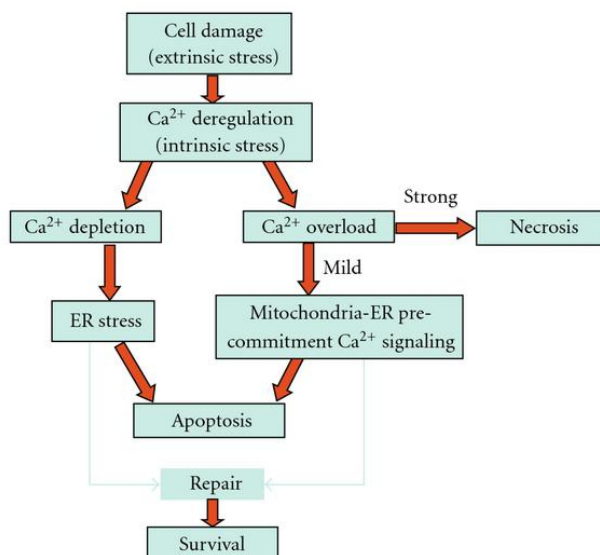


Figure 1.7: The role of Ca^{2+} signaling in cell survival and death upon cell damage.

Disturbance of the intracellular calcium homeostasis, such as Ca^{2+} depletion in the ER or mitochondrial or cytosolic Ca^{2+} overload, may either be repaired resulting in cell survival or results in different modes of cell death dependent on the type and intensity of the Ca^{2+} signal (Cerella et al., 2010).

1.5 Haploid genetic screens

Genetic screens are powerful tools to identify the molecular players in biological processes and diseases. While reverse genetics allow to study gene function by targeted mutation, forward genetic screens are employed to link a specific phenotype to a genotype. For the latter, genes need to be modified at a high scale and with high efficiency. In contrast to non-mammalian cells, genetic manipulation in human cells is complicated by the diploid nature of eukaryotic genomes. Introduction of homozygous genetic mutations in human cells is impacted by the low

efficiency of homologous recombination and the inability to combine mutant alleles using genetic crossings. Only with the discovery of RNA interference large scale screens were possible by knock-down of transcripts using small interfering RNAs (siRNAs) or short hairpin RNAs (shRNAs) (Moffat et al., 2006; Prahallad et al., 2012; Sun et al., 2014). However, this approach is limited, because it is prone to off-target effects and cannot completely inactivate gene function (Barrangou et al., 2015). An additional tool to manipulate eukaryotic genomes at a large scale was more recently discovered. The CRISPR/Cas9-System was successfully used for genome-wide screens in human cells (Shalem et al., 2014; Wang et al., 2014). Nevertheless, efficiency, off-target effects and scalability need to be optimized.

An alternative approach for forward genetic screens is haploid human genetics. Haploid cells carry only a single copy of their genes, which allows the investigation of recessive genetic phenotypes often masked in diploid cells. While most human somatic cells are diploid, some tumors harbor a sub-diploid to haploid genome (Leeb and Wutz, 2013). The human chronic myeloid leukemia cell line KMB-7 is haploid for all chromosomes except for chromosome 8 and a fragment of chromosome 5 (Andersson et al., 1995; Kotecki et al., 1999). An unsuccessful attempt at reprogramming KMB-7 into fully induced pluripotent stem cells resulted in the adherent cell line HAP1, which had lost its hematopoietic character and is lacking the second copy of chromosome 8 (Figure 1.8 A) (Carette et al., 2011b).

In order to perform genome-wide genetic screens with these haploid cell lines, cell libraries are generated by random insertional mutagenesis using a retroviral gene-trap vector, which contains a strong splice acceptor site, an efficient polyadenylation signal and a marker gene (Figure 1.8 B) (Carette et al., 2009). These elements ensure generation of loss-of-function alleles, when inserted in intronic regions in sense orientation relative to the gene or when inserted in exons irrespective of orientation. Although insertion by the retroviral gene trap vector is not completely random and has a bias for inserting around active promoters (LaFave et al., 2014), mutations leading to gene knockout in nearly all genes can be found (Carette et al., 2011a). Insertional mutagenesis allows identification of integration sites by the presence of a known DNA sequence at the site of integration. After mutagenesis, a selection can be applied to the pool of mutated cells in order to link genes to a phenotype. Viability or reporter gene expression can be used as read-out for positive selections. Successful positive selection screens are highly dependent on strong selection pressure, as few mutations leading to the desired phenotype need to be separated from millions of cells with wild type-like behavior. For screen analysis, selected cell clones are expanded to gain sufficient material for DNA isolation, amplification of insertion sites and DNA sequencing. Since the flanking genomic regions are amplified with the retroviral

sequences, insertion sites can be identified and mapped to the human genome after sequencing. Only sequence reads, that can be uniquely aligned, are considered for further analysis and additional reads are discarded, since a particular mutant in the population is not reliably represented by the number of sequence reads. Further filtering is performed by removing sequence reads, that align at multiple genomic regions, when allowing mismatch or in close proximity to one another. Subsequently, sequence reads can be assigned to genes and counted. By comparing the mutation density per gene to an unselected control dataset, genes with an enriched number of mutations can be identified and the significance of enrichment is calculated. This enables to control for background noise caused by potential retroviral integration hotspots.

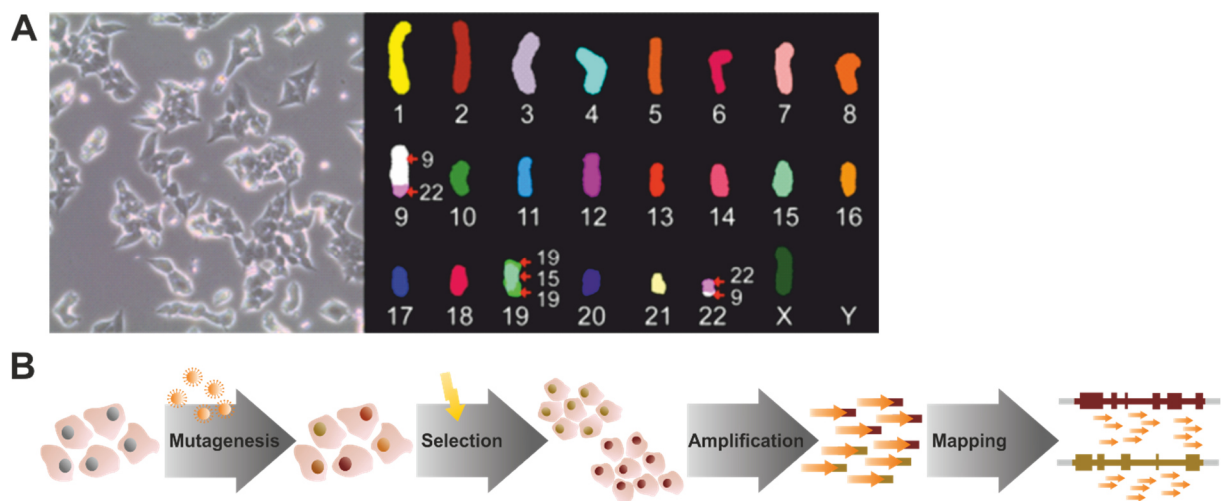


Figure 1.8: Genetic screens with human haploid cells.

(A) Light microscopic image (left) and spectral karyotyping (right) of HAP1 cell line (Essletzbichler et al., 2014). (B) Outline of a positive selection screen using haploid cells. A pool of haploid cells is mutagenized by a retroviral gene trap vector followed by selection for the anticipated phenotype. After expansion of selected cell clones, DNA is isolated and the retroviral gene trap vector sequences are amplified with the flanking genomic regions. DNA sequencing allows mapping of the vector insertion sites to the human genome. Unique mutations per gene are counted and compared to control dataset(s).

So far, haploid genetic screens have been successfully used to identify genes involved in anticancer drug action (Birsoy et al., 2013; Pettitt et al., 2013; Planells-Cases et al., 2015; Winter et al., 2014), cell death mechanisms (Cao et al., 2019; Dixon et al., 2015; Jacobson et al., 2013; Mandal et al., 2014), viral infection (e.g. Baggen et al., 2016; Hoffmann et al., 2017; Jae et al., 2014; Riblett et al., 2016; Staring et al., 2017) and resistance mechanisms against numerous bioactive small molecules (Elling et al., 2011; Reiling et al., 2013; Wijdeven et al., 2015) and against bacterial toxins (Carette et al., 2009; Carette et al., 2011a; Guimaraes et al., 2011; Papatheodorou et al., 2011). Host cell factors required for cytotoxicity of the *S. aureus* α -toxin were also investigated using a haploid genetic screen (Popov et al., 2015).

1.6 Aim of the study

Although not a professional intracellular pathogen, several *S. aureus* strains are capable of escaping from the phagosome, replicating in the host cell and inducing host cell death in many different cell types. Intracellular cytotoxicity of *S. aureus* is believed to contribute to tissue destruction and spread of infection *in vivo*. Whereas several factors mediating phagosomal escape of *S. aureus* have been identified, the molecular mechanisms underlying host cell death induced by the intracellular bacterium remain largely unknown.

The present study aims to identify host cell as well as bacterial factors involved in cell death mediated by intracellular *S. aureus*. A genome-wide screen in human haploid cells should be employed to identify host cell genes, whose loss of function renders the host cell resistant to *S. aureus* cytotoxicity. Besides, *S. aureus*-infected epithelial cells were to be tested for hallmarks of different cell death pathways, such as apoptosis, necrotic cell death or parthanatos. Live cell imaging allows to study the intracellular lifestyle of *S. aureus* at the single cell level. Using this method, the role of caspases and Ca^{2+} signaling in *S. aureus*-induced cell death was investigated. To study the contribution of bacterial virulence factors to *S. aureus* intracellular cytotoxicity selected single gene mutants should be tested for their ability to kill the infected host cell. Especially the role of the cysteine protease staphopain A in *S. aureus* infection and intracellular lifestyle was to be tested.

2 Material and Methods

2.1 Material

2.1.1 Laboratory instruments

Laboratory instruments used in this study are listed in Table 2.1.

Table 2.1: Laboratory instruments used in this study

Instrument	Model/Name	Manufacturer
Balances	EW 1500-2M	Kern, Germany
	ABS 80-4	
Electroporation system	MicroPulser™ Electroporator	Bio-Rad, USA
Cell incubator	Heracell 240i	Thermo Fisher Scientific, USA
	live-cell incubation chamber	Life Imaging Services, Switzerland
Centrifuges	Hitachi himac CT15RE	Hitachi-Koki, Japan
	Biofuge 15	Heraeus, Germany
	Mini Star silverline	VWR, USA
	Z 160 M	Hermle Labortechnik, Germany
	Megafuge 1.0 R	Heraeus, Germany
Chemiluminescence imager	ChemoStar, Cooled CCD Sensor	Intas, Germany
Electro blotter	PerfectBlue™ ‘Semi-Dry’ Blotter	VWR, USA
Electrophoresis system	PerfectBlue™ Dual Gel System	VWR, USA
FACS/flow cytometer	Aria III	Becton Dickinson, USA
Gel imager	Biostep Dark hood DH-40/50	Biostep GmbH, Germany
Microplate reader	Infinite® 200 Pro, Infinite® M Plex	Tecan, Switzerland
Microscopes	DMIL, DMR, TCS SP5	Leica, Germany
	Operetta	Perkin Elmer, USA
pH-meter	InoLab pH 720 with SenTix Electrode	WTW, Germany
See-saw rocker	SSL4	Stuart, UK
Spectrophotometer	Ultrospec™ 3100 pro	Amersham Bioscience, UK
Spectrophotometer (Micro)	NanoDrop 1000	Peqlab, Germany
RT-PCR system	StepOne Plus™	Applied Biosciences, USA
Thermocycler	Biometra T3 Thermocycler	Biometra, Germany
Thermo mixer	Thermomixer Comfort	Eppendorf, Germany
	Mixing block MB-102	Bioer, China

2.1.2 Consumables and glassware

Consumables and glassware used in this study are listed in Table 2.2.

Table 2.2: Consumables and glassware used in this study

Name	Specifications	Manufacturer
Cell culture dishes	100 x 20 mm, Standard growth surface for adherent cells, cell culture grade, sterile, Polystyrene	Sarstedt, Germany
Cell culture flasks	Corning [®] , sterile, cell culture grade (25 cm ² , 75 cm ² and 175 cm ²), Polystyrene	Corning, USA
Centrifuge tubes	Falcon [®] Centrifuge Tubes (15 ml, 50 ml), Polypropylene, Sterile, RNase-/DNase-free	Corning, USA
Chamber slides	μ-Slide 8 Well, Glass Bottom, sterile, for fluorescence microscopy	ibidi, Germany
Cryo Tubes	CryoPure Tube 1.6 ml, Polypropylene, sterile	Sarstedt, Germany
Cuvettes	Semi-micro cuvette 1.6 ml, Polystyrene	Sarstedt, Germany
Electroporation cuvettes	Cuvettes with 2 mm gap size, blue cap, polycarbonate, sterile	VWR, USA
Erlenmeyer flasks	Erlenmeyer flasks DURAN [®] narrow neck (2 l, 1 l, 100 ml)	Duran Group, Germany
Glass bottles	Duran [®] graduated glass bottles (1 l, 500 ml, 250 ml, 100 ml)	Duran Group, Germany
Inoculation loops	white (1 μl) and blue (10 μl), sterile, Polystyrene	Sarstedt, Germany
Microcentrifuge tubes	Micro tube (1.5 ml, 2 ml) with attached lid, Polypropylene	Sarstedt, Germany
	RNase-free Microfuge tubes (1.5 ml, 2 ml), Polypropylene, sterile	ThermoFisher Scientific, USA
Microtiter plates	Costar [®] (6, 12, 24, 48 and 96 well), cell culture grade, clear, TC-treated, sterile	Corning, USA
	μ-Plate 24 Well, black, sterile, for fluorescence microscopy	ibidi, Germany
Pasteur pipettes	made of glass, length 230 mm	Hartenstein, Germany
PCR tubes	PCR SoftTubes, 0.2 ml	Biozym, Germany
Petri Dishes	92x16 mm, with cams, Polystyrene	Sarstedt, Germany
Pipette tips	pipette tip (20 μl, 200 μl and 1000 μl), transparent, Polypropylene	Sarstedt, Germany
PVDF membrane	Polyvinylidene difluoride (PVDF) Western Blotting Membrane	Sigma Aldrich, USA
Round bottom tubes (for flow cytometry)	Falcon [®] Polystyrene Test Tube, with Snap Cap, sterile	Corning, USA
	Falcon [®] Polystyrene Test Tube, with Cell Strainer Snap Cap, sterile	Corning, USA
Serological Pipettes	CELLSTAR [®] , sterile, cell culture grade (1 ml, 5 ml, 10 ml and 25 ml), Polystyrene	Greiner Bio-One, Austria
Syringes	BD Plastipak [™] (1 ml, 5 ml, 10 ml and 50ml), luer-lock, sterile	Becton Dickinson, USA

Table 2.2 (continued)

Syringe filters	Filtropur (0.22 µm and 0.45 µm pore size), PES membrane, luer-lock, sterile	Sarstedt, Germany
Test tubes	clear soda lime glass, 8 ml, round bottom, with aluminum caps	Hartenstein, Germany
Whatman paper	Blotting paper, Thickness: ca. 0,76 mm, 330 g/m ² , high absorbency	Hartenstein, Germany

2.1.3 Chemicals and enzymes

Chemicals and enzymes used in this study are shown Table 2.3.

Table 2.3: Chemicals and enzymes used in this study

Chemical/enzyme	Specification	Manufacturer
Accumax TM		Sigma Aldrich, USA
Acetic acid	ROTIPURAN® 100 %, p.a.	Roth, Germany
Acetone		Roth, Germany
Agar	Agar-Agar, Kobe I (15 g/L)	Roth, Germany
Agarose	Agarose NEEO Ultra-Qualität	Roth, Germany
Alexa-Fluor 633 hydrazide		ThermoFisher Scientific, USA
Ammonium persulfate (APS)	for electrophoresis, ≥98%	Sigma Aldrich, USA
Ampicillin	Ampicillin sodium salt	Sigma Aldrich, USA
Anhydrotetracycline (AHT)	Anhydrotetracycline hydrochloride	ThermoFisher Scientific, USA
Annexin V-APC		Becton Dickinson, USA
BAPTA		Merck, Germany
BAPTA-AM		Merck, Germany
β-mercaptoethanol		Roth, Germany
Blasticidin	Blasticidine S hydrochloride	Sigma Aldrich, USA
Boc-Leu-Met-CMAC	t-BOC-L-Leucyl-L-Methionine amide, 7-Amino-4-Chloromethylcoumarin	ThermoFisher Scientific, USA
Bovine serum albumin (BSA)	Albumin Fraction V	Roth, Germany
Brain Heart Infusion Broth (BHI)		Sigma Aldrich, USA
Bromophenol blue		Roth, Germany
Calcium chloride (CaCl ₂)	Calcium chloride dihydrate	Roth, Germany
CellEvent TM Caspase-3/7 Green Detection Reagent		ThermoFisher Scientific, USA
Chloramphenicol		Serva, Germany
Coomassie R250		Serva, Germany
Cycloheximide (CHX)		Sigma Aldrich, USA
DMEM	DMEM, high glucose, no glutamine, no calcium	Gibco/ThermoFisher Scientific, USA

Table 2.3 (continued)

DNase I	RNase-free, 1 U/μl	ThermoFisher Scientific, USA
DNA loading dye	DNA Gel Loading Dye (6X)	ThermoFisher Scientific, USA
DNA ladder	GeneRuler 1 kb DNA Ladder GeneRuler 50 bp DNA Ladder	ThermoFisher Scientific, USA
DNA Polymerase	Taq DNA Polymerase E Phusion High-Fidelity DNA Polymerase	Genaxxon, Germany ThermoFisher Scientific, USA
dNTPs	dNTP-Set (Na salt) - 100mM	Genaxxon, Germany
DPBS	DPBS (1x) –CaCl ₂ –MgCl ₂	Gibco/ThermoFisher Scientific, USA
EDTA		AppliChem, USA
EGTA		Sigma Aldrich, USA
Erythromycin	BioReagent, suitable for cell culture	Sigma Aldrich, USA
Ethanol	puriss. p.a., absolute, ≥99.8% (GC)	Sigma Aldrich, USA
Ethanol denatured	≥ 99,8 %	Roth, Germany
E64		Merck Millipore, USA
Fetal bovine serum (FBS)		Sigma Aldrich, USA
Gentamicin	10 mg/ml	Gibco/ThermoFisher Scientific, USA
Glucose	D(+)-Glucose monohydrate	Roth, Germany
GlutaMAX™ Supplement		Gibco/ThermoFisher Scientific, USA
Glycerol	ROTIPURAN® ≥99,5 %, p.a., anhydrous	Roth, Germany
Glycine	ReagentPlus®, ≥99% (HPLC)	Sigma Aldrich, USA
HD Green	Intas HDGreen™ Plus	Intas, Germany
Hepes	1 M solution	Gibco/ThermoFisher Scientific, USA
HiPerFect Transfection Reagent		Qiagen, Germany
Hoechst 34580		ThermoFisher Scientific, USA
Hydrogen peroxide (H ₂ O ₂)	30 %, ROTIPURAN® p.a., ISO, stabilized	Roth, Germany
IMDM	IMDM (+L-Glutamine +HEPES)	Gibco/ThermoFisher Scientific, USA
Ionomycin	Ionomycin calcium salt from <i>Streptomyces globatus</i>	Sigma Aldrich, USA
Isopropanol	2-Propanol, ROTIPURAN® ≥99,8 %, p.a., ACS, ISO	Roth, Germany
Luminol		Roth, Germany
Lysostaphin		AMBI, USA
Magnesium Chloride Hexahydrate (MgCl ₂ •6 H ₂ O)		Roth, Germany

Table 2.3 (continued)

Magnesium Sulfate Heptahydrate (MgSO ₄ •7H ₂ O)		Roth, Germany
Methanol	≥99 %, for synthesis	Roth, Germany
NecroX-5		Cayman Chemicals/Biomol
N,N,N',N'- Tetramethylethylenediamine (TEMED)	BioReagent, suitable for electrophoresis, ~99%	Sigma Aldrich, USA
Nonfat Dried Milk Powder		AppliChem, USA
OptiMEM	Opti-MEM™, Reduced Serum Medium, GlutaMAX™ Supplement	Gibco/ThermoFisher Scientific, USA
Paraformaldehyd		Roth, Germany
p-coumaric acid		Sigma Aldrich, USA
Penicillin-Streptomycin	100x, 10,000 U/ml penicillin & 10,000 µg/ml streptomycin	Gibco/ThermoFisher Scientific, USA
Polyethylenimine (PEI)		Polysciences Inc., USA
Potassium chloride (KCl)		Merck, Germany
Protein ladder	PageRuler Prestained Protein ladder Spectra™ Multicolor Broad Range Protein Ladder	ThermoFisher Scientific, USA
Restriction enzymes		ThermoFisher Scientific, USA
Restore™ Plus Western Blot Stripping buffer		ThermoFisher Scientific, USA
Rifampicin	≥90 %, for biochemistry	Roth, Germany
RNase A		Roth, Germany
Rotiphorese® Gel 30	aqueous 30 % acrylamide and bisacrylamide stock solution at a ratio of 37,5:1	Roth, Germany
RPMI	RPMI 1640 Medium, GlutaMAX™ Supplement, HEPES RPMI 1640 Medium, no glutamine, no phenol red	Gibco/ThermoFisher Scientific, USA
Saccharose	D(+)-Saccharose	Roth, Germany
SDS	SDS Pellets	Roth, Germany
Sodium chloride (NaCl)		VWR, USA
Sodium pyruvate	100 mM (100x)	Gibco/ThermoFisher Scientific, USA
Staurosporine (STS)	Staurosporine from Streptomyces sp.	Sigma Aldrich, USA
SYBR Green	PerfeCTa® SYBR® Green FastMix™	Quantabio, USA
Thapsigargin		Sigma Aldrich, USA
TNFα		Cell signaling technology, USA
Trichloroacetic acid (TCA)		Roth, Germany

Table 2.3 (continued)

Tris	Trizma® base	Sigma Aldrich, USA
Trisodium citrate (Na ₃ C ₆ H ₅ O ₇)		Roth, Germany
Triton X 100		Roth, Germany
Trypsin	TrypLE™ Express Enzyme (1X), no phenol red	ThermoFisher Scientific, USA
Tryptic soy broth (TSB)		Sigma Aldrich, USA
Tryptone/Peptone ex casein		Roth, Germany
Tween20		Roth, Germany
T4 DNA ligase		ThermoFisher Scientific, USA
Yeast extract		Roth, Germany
Z-VAD-fmk		Invivogen, USA
2-APB		Sigma Aldrich, USA
7AAD		Becton Dickinson, USA

2.1.4 Kits

Kits used in this study are listed in Table 2.4.

Table 2.4: Kits used in this study

Kit	Manufacturer
PureLink® Quick Plasmid Miniprep kit	Invitrogen™, USA
NucleoSpin® Plasmid kit	Macherey-Nagel, Germany
NucleoSpin® Gel and PCR Clean-up kit	Macherey-Nagel, Germany
NucleoBond® PC 100 kit	Macherey-Nagel, Germany
QIAprep Spin Miniprep kit	QIAGEN, Germany
QIAamp DNA Mini kit	QIAGEN, Germany
QuikChange II Site-Directed Mutagenesis Kit	Agilent Technologies, USA
RNeasy Mini Kit	QIAGEN, Germany
TURBO DNA-free™ kit	Ambion, USA
RevertAid First Strand cDNA Synthesis kit	ThermoFisher Scientific, USA
Cytotoxicity detection kit ^{PLUS} (LDH)	Roche, Switzerland

2.1.5 Media and antibiotics

The composition of bacterial media can be found in Table 2.5.

Table 2.5: Composition of bacterial media

Name	Composition/Concentration
LB	10 g/l Tryptone/Peptone ex casein, 5 g/l Yeast extract, 5 g/l NaCl
TSB	30 g/l
BHI	37 g/l
SOC	20 g/l Tryptone/Peptone ex casein, 5 g/l Yeast extract, 0.6 g/l NaCl, 0.18 g/l KCl, 4.34 g/l MgCl ₂ •6 H ₂ O, 5.04 g/l MgSO ₄ •7H ₂ O, 20 mM Glucose

Media for liquid cultures and agar plates were autoclaved at 121 °C for 20 min. For preparation of agar plates 1.5 % (w/v) agar was added to the medium prior to autoclaving. Antibiotics were added after cooling the agar to 50 °C or to liquid culture media directly before use. The antibiotic stock solutions were stored at -20 °C. The stock solutions for rifampicin were always prepared freshly. The antibiotics used are listed in Table 2.6.

Table 2.6: Used antibiotics

Antibiotic	Stock solution (diluted in)	Final concentration
Ampicillin (Amp)	50 mg/ml (dH ₂ O)	100 µg/ml
Chloramphenicol (Cm)	10 mg/ml (EtOH)	10 µg/ml
Erythromycin (Erm)	10 mg/ml (EtOH)	5/10 µg/ml
Lysostaphin (Lyso)	1 mg/ml (dH ₂ O or DPBS)	2-20 µg/ml
Rifampicin (Rif)	1 mg/ml (methanol)	1 µg/ml
Anhydrotetracycline (AHT)	200 µg/ml (DMF)	200 ng/ml
Penicillin	10,000 U/ml	100 U/ml
Streptomycin	10,000 µg/ml	100 µg/ml
Gentamicin	10 mg/ml	100 µg/ml
Blasticidin	10 mg/ml (dH ₂ O)	30 µg/ml

All media and solutions used for cell culture and cell infection assays are listed in Table 2.7.

Table 2.7: Composition of cell culture media and solutions

Name	Composition
RPMI infection medium	RPMI 1640 Medium, GlutaMAX™ Supplement, HEPES 1 mM sodium pyruvate 10 % FBS
IMDM infection medium	IMDM 1 mM sodium pyruvate 10 % FBS
IMDM with antibiotics	IMDM infection medium 1x Penicillin-Streptomycin
RPMI imaging medium	RPMI 1640 Medium, no glutamine, no phenol red 1 mM sodium pyruvate 25 mM Hepes 1x GlutaMAX™ Supplement 10 % FBS
RPMI LDH medium/ FACS medium	RPMI 1640 Medium, no glutamine, no phenol red 1 mM sodium pyruvate 25 mM Hepes 1x GlutaMAX™ Supplement 1 % FBS 2 µg/ml lysostaphin
Annexin V staining buffer	RPMI FACS medium 10 µl/ml annexin V-APC 10 µl/ml 7AAD

Table 2.7 (continued)

DMEM without CaCl ₂	DMEM, high glucose, no glutamine, no calcium 1 mM sodium pyruvate 25 mM Hepes 1x GlutaMAX™ Supplement 10 % FBS
DMEM with CaCl ₂	DMEM, high glucose, no glutamine, no calcium 1 mM sodium pyruvate 25 mM Hepes 1x GlutaMAX™ Supplement 10 % FBS 1.8 mM CaCl ₂
Detachment solution	10 % TrypLE in DPBS
Cryo medium	infection medium 20 % FBS 10 % DMSO

2.1.6 Buffers and solutions

Buffers and solutions used can be found in Table 2.8. Distilled water (dH₂O) was used for all solutions, if not indicated otherwise. Buffers and solutions supplied by the manufacturer were used for enzyme reactions.

Table 2.8: Buffers and solutions used in this study

Buffer	Ingredients
<i>S. aureus</i> lysis buffer	200 µg/ml lysostaphin 20 mM Tris/HCl, pH 8 2 mM EDTA 20 µg/m RNase A 1.2 % Triton X 100
TAE buffer	40 mM Tris 20 mM acetic acid 1 mM EDTA
Electroporation buffer	0.5 M saccharose 10 % glycerol
Phage buffer	LB medium 5 mM CaCl ₂
Soft agar	LB medium 0.6 % agar 20 mM trisodium citrate
Laemmli buffer (2x)	100 mM Tris/HCl pH 6.8 4 % SDS 20 % glycerol 1.5 % β-mercaptoethanol 0.004 % bromophenol blue
SDS upper gel buffer	0.5 M Tris pH adjusted to 6.8 (HCl)
SDS lower gel buffer	1.5 M Tris pH adjusted to 8.8 (HCl)

Table 2.8 (continued)

SDS upper gel solution	125 mM Tris/HCl pH 6.8 (upper gel buffer) 5 % Rotiphorese® Gel 30 0.1 % SDS 0.1 % APS 0.08 % TEMED
SDS lower gel solution	375 mM Tris/HCl pH 8 (lower gel buffer) 7.5-12 % Rotiphorese® Gel 30 0.1 % SDS 0.1 % APS 0.08 % TEMED
10x SDS-PAGE running buffer	250 mM Tris 1.92 M glycine 1 % SDS
10x Semi Dry Transfer buffer	200 mM Tris 1.5 M glycine 0.2 % SDS
Semi Dry Transfer buffer	1x Semi Dry Transfer buffer 20 % methanol
10x Wet blot transfer buffer	250 mM Tris 1.92 mM Glycine
Wet blot transfer buffer	1x Wet blot transfer buffer 20 % methanol
10x TBS	500 mM Tris 1.5 M NaCl pH adjusted to 7.5
TBS-T	1x TBS 0.05 % Tween20
Blocking solution	5 % dry milk powder or BSA ad TBS-T
ECL solution 1	100 mM Tris/HCl pH 8.5 2.5 mM Luminol 0.4 mM p-coumaric acid
ECL solution 2	100 mM Tris/HCl pH 8.5 0.02 % H ₂ O ₂
Coomassie staining solution	0.25 % Coomassie R250 45 % ethanol 10 % acetic acid
Coomassie destaining solution	40 % ethanol 10 % acetic acid
Coomassie fixing solution	50 % methanol 10 % acetic acid

2.1.7 Antibodies

Primary and secondary antibodies used for western blot are listed in Table 2.9 and Table 2.10.

Table 2.9: Primary antibodies

Protein	Origin	Dilution	Manufacturer (Cat. No.)
AIF	mouse monoclonal IgG2b	1:200	Santa Cruz Biotechnology (sc-13116)
α -spectrin	mouse monoclonal IgG1	1:300	Santa Cruz Biotechnology (sc-48382)
α -toxin (<i>S. aureus</i>)	rabbit polyclonal	1:2000	Sigma Aldrich (S7531)
β -actin	mouse monoclonal IgG1	1:3000	Sigma Aldrich (A5441)
β -tubulin	mouse monoclonal IgG2b	1:1000	Merck Millipore (MAB3408)
Bid	rabbit polyclonal	1:1000	Cell signaling Technology (2002)
Calpain 1	rabbit polyclonal	1:1000	Cell signaling Technology (2556)
Calpain 4	mouse monoclonal IgG1	1:500	Merck Millipore (MAB3083)
Calpastatin	rabbit polyclonal	1:1000	Cell signaling Technology (4146)
cleaved caspase 3, large subunit	rabbit monoclonal IgG1	1:1000	Cell signaling Technology (9664)
GAPDH	rabbit polyclonal	1:1000	Santa Cruz Biotechnology (sc-25778)
MLKL	rabbit monoclonal IgG	1:1000	Cell signaling Technology (14993)
phospho-MLKL (Ser358)	rabbit monoclonal IgG	1:1000	Cell signaling Technology (91689)
PARP-1	rabbit polyclonal	1:500	Santa Cruz Biotechnology (sc-7150)
p53	mouse monoclonal IgG2a	1:500	Santa Cruz Biotechnology (sc-126)
Staphopain A (<i>S. aureus</i>)	rabbit polyclonal	1:500	antibodies-online (ABIN967004)

Table 2.10: Secondary antibodies

Antibody	Origin	Manufacturer (Cat. No.)
anti-mouse IgG-HRP	goat	Santa Cruz Biotechnology (sc-2005), Merck Millipore (12-349)
anti-rabbit IgG-HRP	goat	Santa Cruz Biotechnology (sc-2004), Biorad (170-6515), Dianova (111-175-144)

2.1.8 Cell lines

The cell lines used in this study are listed in Table 2.11.

Table 2.11: Used cell lines

Cell line	Source/Reference
HeLa 229	ATCC CCL-2.1
HeLa YFP-cwt	Grosz et al. (2014)
HeLa R-Geco	K. Paprotka
HeLa ER-LAR-Geco G-Geco	S. Vormittag, K. Paprotka
HeLa Mito-LAR-Geco G-Geco	S. Vormittag, K. Paprotka
HeLa HyPer-3	S. Vormittag, K. Paprotka
HAP1	L. Jae, Gene center Munich; Carette et al. (2011b)
HAP1 (mutagenized using gene trap vector)	L. Jae, Gene center Munich; Carette et al. (2011b)
HAP1 YFP-cwt	K. Paprotka

2.1.9 Bacterial strains

The bacterial strains used in this study are shown in Table 2.12.

Table 2.12: Bacterial strains used in this study

Strain	Description	Source/Reference
<i>E. coli</i>		
DH5 α	K-12 derivative, F ⁻ , <i>endA1</i> , <i>hsdR17</i> (<i>r_k</i> ⁻ , <i>m_k</i> ⁻), <i>supE44</i> , <i>thi-1</i> , <i>recA1</i> , <i>GyrA96</i> , <i>relA1</i> , λ , Δ (<i>lacZYA-argF</i>)U169, Φ 80 <i>dlacZ</i> Δ M15, <i>deoR</i> , <i>nupG</i>	BRL Life Technology
<i>S. aureus</i>		
RN4220	Restriction-deficient derivative of NCTC 8325-4 (cured of prophages Φ 11, Φ 12, Φ 13), β -toxin producer, no production of α -toxin or δ -toxin, phenotypically <i>agr</i> -negative	Kreiswirth et al. (1983)
RN4220 <i>phld-scpAB</i>	AHT-inducible expression of δ -toxin (<i>hld</i>), staphopain A (<i>scpA</i>), staphostatin A (<i>scpB</i>) and cerulean	This study
RN4220 <i>phld-scpA</i> _(C238A) B	AHT-inducible expression of δ -toxin (<i>hld</i>), staphopain A (<i>scpA</i>), staphostatin A (<i>scpB</i>) and cerulean with active site substitution C234A in <i>scpA</i>	This study
6850	Clinical osteomyelitis isolate, methicillin-sensitive, HGW	Vann and Proctor (1987)
6850 GFP	pJL74-SarAP1-GFP, expressing GFP as molecular marker	M. Grosz
6850 mRFP	pmRFPmars, expressing mRFP as molecular marker	K. Paprotka
6850 Cerulean	pSarAP1-Cerulean, expressing Cerulean as molecular marker	K. Paprotka
6850 <i>scpA::Bursa</i>	staphopain A transposon mutant, produced by phage transduction from NE1278 in 6850	This study
6850 <i>scpA::Bursa pscpAB</i>	<i>scpA</i> complementation in 6850 <i>scpA::Bursa</i>	This study
6850 Δ <i>hla</i>	<i>hla</i> deletion mutant	S. Das
6850 Δ <i>rsp</i>	<i>rsp</i> deletion mutant	S. Das
6850 Δ <i>hla</i> GFP	pJL74-SarAP1-GFP, expressing GFP as molecular marker	This study
6850 Δ <i>rsp</i> GFP	pJL74-SarAP1-GFP, expressing GFP as molecular marker	This study
Cowan I	NCTC 8530, isolated from septic arthritis, <i>agr</i> dysfunction, low expression of toxins and proteases	ATCC 12598
Cowan I GFP	pJL74-SarAP1-GFP, expressing GFP as molecular marker	A. Moldovan
Cowan I mRFP	pmRFPmars, expressing mRFP as molecular marker	This study
Cowan I Cerulean	pSarAP1-Cerulean, expressing Cerulean as molecular marker	This study
LAC	USA300 PFGE type, CA-MRSA	Maree et al. (2007)
LAC Δ <i>psma</i>	<i>psma</i> knockout of LAC, allelic replacement with a spectinomycin-resistance cassette	Wang et al. (2007)
LAC Δ <i>psm</i> β	<i>psm</i> β knockout of LAC, allelic replacement with a spectinomycin-resistance cassette	Wang et al. (2007)
LAC Δ <i>hld</i>	<i>hld</i> knockout of LAC; mutation in start codon abolished translation, while keeping RNAIII structure intact	Wang et al. (2007)
JE2	derivative of LAC, which was cured of three plasmids, USA300 PFGE type, CA-MRSA	Fey et al. (2013)
JE2 GFPsf	pGFPsf, JE2 expressing GFPsf as molecular marker	This study
JE2 mRFP	pmRFPmars, expressing mRFP as molecular marker	This study

Table 2.12 (continued)

JE2 mRFP	pmRFPmars, expressing mRFP as molecular marker	This study
JE2 NE1682	JE2 <i>hlgB::Bursa</i> , deficient in γ -toxin production	Fey et al. (2013)
JE2 NE934	JE2 <i>sspB::Bursa</i> , deficient in staphopain B production, SAUSA300_0950	Fey et al. (2013)
JE2 NE1278	JE2 <i>scpA::Bursa</i> , deficient in staphopain A production, SAUSA300_1890	Fey et al. (2013)
JE2 <i>scpA</i>	staphopain A transposon mutant, produced by phage transduction from NE1278 in JE2	This study
JE2 <i>scpA</i> GFPsf	JE2 <i>scpA::Bursa</i> , pGFPsf expressing GFP as molecular marker	This study
JE2 <i>scpA</i> mRFP	JE2 <i>scpA::Bursa</i> expressing mRFP as molecular marker	This study
JE2 <i>pscpAB</i>	<i>scpA</i> complementation in JE2 <i>scpA::Bursa</i>	This study
JE2 <i>pscpA</i> _(C238A) B	<i>scpA</i> complementation in JE2 <i>scpA::Bursa</i> with active site substitution C234A in <i>scpA</i>	This study

2.1.10 Plasmids

Plasmid used in this study are listed in Table 2.13.

Table 2.13: Plasmids used in this study

Plasmid	Description	Reference
p2085	derivate of pALC2084 (Bateman et al., 2001) with modified multiple-cloning site, shuttle vector with pC194 and pUC19 backbones, containing tetR and P _{xyl} /tet promoter driving GFPuvr expression, Cm ^R	Giese et al. (2009)
<i>pscpAB</i>	p2085- <i>scpAB</i> , native promotor of <i>scpAB</i>	This study
<i>pscpA</i> _(C238A) B	<i>pscpAB</i> with active site substitution C234A in <i>scpA</i>	This study
<i>phld-hlb</i> -cerulean	p2085- <i>hld-hlb</i> -cerulean, AHT-inducible expression	Giese et al. (2011)
<i>phld-scpAB</i>	p2085- <i>hld-hlb</i> -cerulean, AHT-inducible expression	This study
<i>phld-scpA</i> _(C238A) B	<i>phld-scpAB</i> -cerulean with active site substitution C234A in <i>scpA</i>	This study
pmRFPmars	p2085-SarAP1-mRFPmars, vector expressing mRFP in <i>S. aureus</i> under control of the constitutive sarAP1 promoter, Cm ^R	Paprotka et al. (2010)
pJL74	vector expressing GFP, Erm ^R	J. Liese, University Tübingen
pSarAP1-cerulean	p2085-SarAP1-cerulean, vector expressing cerulean in <i>S. aureus</i> under control of the constitutive sarAP1 promoter, Cm ^R	K. Paprotka
pGFPsf	pSK5632-SarAP1-GFPsf, low-copy vector expressing GFPsf in <i>S. aureus</i> under control of the constitutive sarAP1, Cm ^R	S. Das
pSpCas9 (BB)-2A-GFP	expressing Cas9 from <i>S. pyogenes</i> with 2A-EGFP, cloning backbone for sgRNA	Addgene (#48138)
pSpCas9 (BB)-2A-GFP-sgRNA CAPN1	expressing sgRNA for calpain 1	This study
pSpCas9 (BB)-2A-GFP-sgRNA CAPN4	expressing sgRNA for calpain 4	This study
pSc-TIA-CMV-BSR-TIA	sgRNA to zebrafish <i>TIA</i> gene, CMV sequence and blasticidin resistance flanked by two TIA target sites	L. Jae, Gene center Munich

2.1.11 Oligonucleotides

Oligonucleotides used in this study are listed in Table 2.14, Table 2.15 and Table 2.16. DNA and sgRNA oligonucleotides were purchased from Sigma Aldrich.

Table 2.14: DNA oligonucleotides used in this study

Name	Sequence (5'-3') ^a	Purpose
scpAB_prom_fwd _PstI	AAACTGCAGTATTCTATTGCATAGGTGTGG	Cloning of <i>pscpAB</i>
scpAB_TT_ rev_EcoRI	AAGAATTCCTATTTGAAGAGGAAAGGCTATTC	
MP_scpA1	CTCAAGGTAACAATGGTTGGgcgGCAGGCTATACGATGTCT	Cys>Ala active site substitution in <i>scpA</i> (Nickerson et al., 2010)
MP_scpA2	AGACATCGTATAGCCTGCcgcCCAACCATTGTTACCTTGAG	
scpAB_AvrII_fwd	GATCCCTAGGAGGTATAATAATGAAAAGAAACTTTCC	Cloning of <i>phld-</i> <i>scpAB</i>
scpAB_AvrII_rev	CATGGATCCTAGGTTATGACTTATGCTTAATGAAAG	
scpA rev	CATTATTGCCAGTAGGTATACTCTCAGTC	Sequencing of <i>pscpAB</i> and <i>phld-scpAB</i>
scpA fwd	GCAAACGCTGAGAGCAATTCAAATATCA	
MFpUCs1 (MF8)	GGGATGTGCTGCAAGGCG	
MF17pC194 (MF17)	GCATGTAACCTGGGCAGTGTC	
U6-fwd	GAGGGCCTATTTCCCATGATTCC	
RT-CAPN1 fwd	GAAGCGTCCCACGGAAGT	qRT-PCR for calpain 1
RT-CAPN1 rev	GTGCAGGAGGGTGTCTGTTG	
RT-CAPN2 fwd	CCCAACCTGTTCAAGATCATCC	qRT-PCR for calpain 2
RT-CAPN2 rev	AGGCTTCCGTTACTTTCAACC	
RT-CAPN4 fwd	ACCCACTCCGTAACCTC	qRT-PCR for calpain 4
RT-CAPN4 rev	GGGTAGCAACCGTGAA	
RT-GAPDH fwd	GAAATCCCATCACCATCTTCCAGG	qRT-PCR for GAPDH
RT-GAPDH rev	GACCCCAAGCCTTCCATG	

a: lower case letters mutated nucleotides

Table 2.15: siRNA oligonucleotides used in this study

Name	Function	Manufacturer (Cat. No.)
siCAPN1	functionally verified siRNA directed against human CAPN1	Qiagen (SI02225559)
siCAPN2	predesigned siRNA directed against human CAPN2	Qiagen (SI00338114)
siCAPN4	Predesigned siRNA directed against human CAPN4	Qiagen (SI00027664)
AllStars	thoroughly tested and validated nonsilencing siRNA with no homology to any known mammalian gene	Qiagen (SI03650318)

Table 2.16: sgRNA oligonucleotides used in this study

Gene	Splice variant	Exon	Sequence (5'-3') (top & bottom strand) ^a
CAPN1	CAPN1-004 ENST00000527323.5	1	caccGTCGGAGGAGATCATCACGC, aaacGCGTGATGATCTCCTCCGAC
CAPN4	CAPNS1-001 ENST00000246533.7	6	caccCATTGACACATGTCGCAGCA, aaacATGATAAACTGGGGGTCAGC

a: lower case letters BbsI restriction sites

2.1.12 Software

The following software was used in this study: ApE plasmid editor (M. Wayne Davis), Argus X1 gel documentation software (Biostep GmbH), BD FACSDiva™ Software (BD Biosciences), ChemoStar imaging software (Intas), CodonCode Aligner (CodonCode Corp.), Corel Draw X8 (Corel Corp.), Endnote X8 (Thomson Reuters), Fiji (Schindelin et al., 2012), GraphPad Prism 6 (GraphPad Software), i-control™ Microplate Reader software (Tecan), LAS AF software (Leica), Microsoft Office (Microsoft), Nanodrop ND-1000 software (PqLab), Operetta software Harmony (Perkin Elmer), StepOne™ software (Applied biosystems), VisiView® software (Visitron), Windows 7 (Microsoft).

2.2 Methods

2.2.1 Bacterial culture techniques

2.2.1.1 Cultivation of bacteria

Escherichia coli (*E. coli*) and *S. aureus* strains were grown overnight at 37 °C on LB or TSB agar plates, respectively, or in liquid medium. Media were supplemented with appropriate antibiotics, if required. Agar plates were stored at 4 °C until maximum time of 14 days. For bacterial overnight cultures, several colonies were inoculated in liquid medium and incubated at 37 °C and 180 rpm overnight, if not stated otherwise. For cryo-preservation bacterial overnight cultures were mixed with sterile glycerol to a final concentration of 25 % (v/v) and stored at -80 °C until use.

2.2.1.2 Preparation of bacteria for *in vitro* infection

Bacterial overnight cultures were diluted 1:20 in liquid medium and OD₆₀₀ was measured using a spectrophotometer. The infection preculture was inoculated to an OD₆₀₀ of 0.4 in 10 ml of TSB with appropriate antibiotics, if required, and incubated for 1 h at 37°C with agitation at 180 rpm to reach OD₆₀₀ of 0.6. Bacteria were harvested at 14,000 rpm, washed twice and resuspended in infection medium. A Thoma hemocytometer was used to determine bacterial cell numbers.

2.2.1.3 Preparation of bacteria for mouse infection

Overnight cultures of *S. aureus* strains in BHI medium were diluted to a final OD₆₀₀ of 0.05 in 50 ml fresh BHI medium and grown for 3.5 at 37 °C. All growth media for bacterial strains containing plasmids were supplemented with appropriate antibiotics. After centrifugation, the bacterial pellet was resuspended in BHI with 20 % glycerol, aliquoted and stored at -80 °C. For infection, aliquots were thawed, washed twice with DPBS and adjusted to the desired infection inoculum of 2x10⁸ CFU/20 µl. A sample was plated on TSB agar plates to confirm the correct bacterial concentration.

2.2.1.4 In vitro growth curves

Bacterial growth curves were measured using a TECAN plate reader. Bacterial cultures were inoculated in triplicates to an OD₆₀₀ of 0.1 in 400 µl TSB or infection medium and grown for intended periods at 37 °C in a 48 well microtiter plate. Absorbance was recorded every 10 min at 600 nm.

2.2.1.5 Collection of *S. aureus* supernatant

Bacteria were grown overnight in BHI medium supplemented with appropriate antibiotics and AHT, if necessary. Cultures were adjusted to an OD₆₀₀ of 10. Bacteria were collected by centrifugation and the supernatant was sterile filtered through a 0.22 µm membrane.

2.2.2 Cell culture techniques

2.2.2.1 Cell cultivation and passaging

Cell lines were propagated in appropriate medium supplemented with 10 % FBS and 1 mM sodium pyruvate (Table 2.7) in cell culture flasks and incubated at 37 °C and 5 % CO₂ in a humidified atmosphere. For passaging, cells were diluted 5-10 times to the next passage when they were 80-90% confluent, approximately every 2-3 days. Adherent cells were enzymatically detached in 10 % TrypLE in DPBS at 37 °C for 5 min after two washing steps with 1x DPBS. HeLa cells were grown in RPMI1640 and HAP1 cells in IMDM.

2.2.2.2 Cryopreservation of cells

Cells were grown up to 80-90 % confluency, detached by enzymatic digestion and pelleted at 1000 rpm for 10 min at room temperature. The pellet was carefully resuspended in 1 ml of appropriate cell culture medium containing 20 % FBS and 10 % DMSO and transferred to cryo-tubes, which were placed into isopropanol containers to allow slow cooling at -80 °C. For long term storage tubes were transferred to liquid nitrogen.

2.2.3 DNA methods

2.2.3.1 Plasmid isolation

For *E. coli* strains, plasmid DNA was isolated using PureLink[®] Quick Plasmid Miniprep kit or NucleoSpin[®] Plasmid Kit, according to manufacturer's instructions. *S. aureus* plasmid DNA was isolated using QIAprep Spin Miniprep kit according to manufacturer's instructions, with some modifications. The resuspension buffer (P1) was supplemented with 20 µg/ml lysostaphin and incubation was performed at 37 °C and 1000 rpm for 30 min to allow efficient lysis of *S. aureus*. For isolation of larger amounts of plasmid DNA the NucleoBond[®] PC 100 kit was used. Plasmid DNA was eluted with sterile water and stored at -20 °C.

2.2.3.2 Genomic DNA isolation

The QIAamp DNA Mini kit was used for isolation of genomic DNA according to manufacturer's instructions. Bacteria were harvested from overnight culture, washed and resuspended in *S. aureus* lysis buffer (Table 2.8). The mixtures were incubated at 37 °C and 1000 rpm for 30 min or until the mixture was clear and further processed as instructed. Isolation of genomic DNA from human cells was performed as described by the manufacturer's protocol. DNA quantity and quality were measured on a Nanodrop UV-Vis spectrophotometer. DNA was stored at -20°C.

2.2.3.3 Polymerase chain reaction (PCR)

For standard PCR, Taq polymerase with buffer E (with MgCl₂) was used according to the manufacturer's instructions. A final concentration of 200 µM of each dATP, dCTP, dGTP and dTT, 500 nM primer and 1.5 units polymerase were applied. After an initial denaturation step at 94 °C for 5 min, 30-35 cycles were conducted starting with denaturation at 94 °C for 1 min followed by annealing at approx. 5 °C below T_m of primers for 1 min and elongation for 1 min per kb at 72 °C. The final extension time was 10 min at 72 °C. For applications, where higher sequence accuracy was needed, Phusion polymerase was used with Phusion HF buffer. Initial denaturation was performed at 98 °C and the final extension time was 10 min at 72 °C. The cycling conditions were the following: 30-35 cycles of 5-10 sec denaturation at 98 °C, annealing for 15-30 sec at a T_m 3 °C above the lower primer T_m and elongation at 72 °C for 15-30 sec per kb. The optimal annealing temperature was determined by using the online tool T_m Calculator (www.thermofisher.com/tmcalculator). PCR products were mixed with loading dye, separated on 1-2 % agarose gels (1x TAE buffer) supplemented with 0.005 % HD Green by applying 80-120 V and visualized with UV light. If required, PCR products were purified using the NucleoSpin[®] Gel and PCR Clean-up kit.

2.2.3.4 Restriction and ligation

Amplified DNA fragments or vector DNA were digested using restriction endonucleases according to the manufacturer's instructions. If two restriction enzymes were used in the same reaction, buffer compatibility was checked using the online tool DoubleDigest Calculator (www.thermoscientific.com/doubledigest). Ligation of vector and insert was performed using T4 DNA ligase with the corresponding T4 DNA ligase buffer. The vector/insert molar ratios between 1:1 to 1:5 were tested. Required masses of insert and vector were calculated using the following formula: mass of insert (ng) = molar ratio of insert/vector x mass of vector (ng) x ratio of insert to vector lengths. For blunt-end ligation 5 % PEG 4000 solution was added to the reaction.

2.2.4 RNA methods

2.2.4.1 RNA isolation and DNA digestion

RNA from human cells was isolated using the RNeasy Mini Kit. Briefly, cell culture medium was completely removed and cells were quickly resuspended in RLT buffer containing 1 % β -mercaptoethanol. The lysate was homogenized by vortexing, RNA was precipitated using 70 % ethanol and purified using a silica membrane according to the manufacturer's instructions. RNA quantity and quality were measured on a Nanodrop UV-Vis spectrophotometer. The TURBO DNA-freeTM DNase kit was used to remove DNA contamination in RNA samples. Isolated RNA was mixed with DNase I in TURBO DNase buffer and incubated for 30 min at 37 °C followed by addition of a bead-based DNase inactivation reagent to stop the reaction. After 5 min incubation time the mixture was sedimented by centrifugation and the aqueous layer was collected. RNA was stored at -20 °C. DNA digestion was verified by PCR using qRT-primers against GAPDH (Table 2.14). Absence of PCR products confirmed successful DNA digestion.

2.2.4.2 Generation of cDNA by reverse transcription

Complementary DNA (cDNA) was generated by reverse transcription of messenger RNA using the RevertAid First Strand cDNA Synthesis kit. Briefly, 1000 ng RNA were mixed with random hexamer primers and incubated for 5 min at 65 °C. Reaction buffer, nucleotide mix, RNase inhibitor and reverse transcriptase were added and incubated for 5 min at 25 °C followed by 60 min at 42 °C and 5 min at 70 °C. Transcribed cDNA was stored at -20 °C.

2.2.4.3 Quantitative real-time PCR

Quantitative real-time PCR (qRT-PCR) was performed on a StepOne PlusTM PCR system in a 96 well plate format. The reaction mix was composed of SYBR Green master mix, 300 nM qRT-primers (Table 2.14) and 40 ng cDNA in a total volume of 20 μ l. Reactions were run for

40 cycles at 95 °C for 15 sec and 60 °C for 1 min after an initial holding stage of 10 min at 95 °C. At the end of each PCR run a melting curve was performed with 0.3 °C temperature increment. Analysis of relative gene expression was done according to the $2^{-\Delta\Delta C_T}$ method (Livak and Schmittgen, 2001). Gene expression was normalized to the expression levels of the house-keeping gene GAPDH. Non-template controls were run to verify the lack of contamination.

2.2.5 Genetic manipulation of bacteria

2.2.5.1 Transformation of chemically competent *E. coli*

Chemically competent *E. coli* were carefully mixed with plasmid DNA after thawing on ice. After 15 min incubation on ice samples were heat-shocked at 42 °C for 30 sec and subsequently chilled on ice for 5 min. 500 µl SOC medium was added and bacteria were incubated for 2.5 h at 37 °C and 180 rpm. Bacterial suspension was plated on selective LB agar plates and incubated at 37 °C until colonies appeared.

2.2.5.2 Preparation of electrocompetent *S. aureus*

An overnight culture of *S. aureus* was diluted to an OD₆₀₀ of 0.1 in 100 ml TSB medium and incubated until the culture reached OD₆₀₀ of 0.5-0.6. Bacteria were chilled on ice for 15 min, subsequently pelleted for 10 min at 4200 rpm and 4 °C in 50 ml centrifuge tubes and resuspended in 50 ml ice-cold, sterile dH₂O. This washing step was repeated twice with decreasing volumes of dH₂O (25 ml, 10 ml). Subsequent washing steps were performed with 10 ml, 5 ml and 0.35 ml sterile 10 % (v/v) glycerol at 4500 rpm and 4 °C for 15 min. Electrocompetent *S. aureus* were aliquoted in ice-cold microcentrifuge tubes and stored at - 80 °C.

2.2.5.3 Electroporation of *S. aureus*

Electrocompetent *S. aureus* were thawed on ice for 5 min with subsequent incubation for 15 min at room temperature. Heat-inactivation was performed at 56 °C for 2 min quickly followed by addition of 500 µl electroporation buffer. After centrifugation at 6000 rpm for 10 min the pellet was resuspended in 70 µl electroporation buffer (Table 2.8) and incubated for 5 min at room temperature. 1-5 µg plasmid DNA were added and carefully mixed. After 20 min incubation at room temperature the mixture was transferred to an electroporation cuvette and electroporation was performed at 1.8 kV for 2.5 msec in a MicroPulser™ electroporator. 1 ml TSB medium was immediately added. The mixture was then transferred to a 15 ml centrifuge tube and incubated for 1.5-2 h at 37 °C and 180 rpm. Bacteria were pelleted, resuspended in 100-200 µl TSB medium and plated on TSB agar plates containing the appropriate selective antibiotic. Plates were incubated for 24-48 h until colonies appeared.

2.2.5.4 Phage transduction of *S. aureus*

Phage lysate of the donor strain was prepared from an overnight culture in LB medium, which was diluted 1:100 and incubated at 37 °C and 180 rpm until OD₆₀₀ of 1 was reached. The bacterial culture was mixed with phage buffer (Table 2.8) and phage lysate at a ratio of 20:20:1 and incubated at 30 °C and 150 rpm until bacteria were lysed. After centrifugation at maximum speed the supernatant was sterile filtered and stored at 4 °C. The overnight culture of the recipient strain was treated with CaCl₂ at a final concentration of 5 mM and subsequently heat-shocked at 53 °C for 2 min. Phage lysate of the donor strain and bacterial culture of the recipient strain were mixed at ratio of 4:1 and incubated for 2.5-4 h at room temperature. Next, warm soft agar (55 °C) was added, mixed with the phage-bacteria solution and poured over LB agar plates containing an appropriate antibiotic. Plates were incubated at 37 °C until colonies appeared.

2.2.5.5 Site directed mutagenesis in *scpA*

Site directed mutagenesis for Cys238>Ala active site substitution in *scpA* was performed using oligonucleotides MP_scpA1 and MP_scpA2 (Nickerson et al., 2010) and QuikChange II Site-Directed Mutagenesis Kit according to the manufacturer's instructions. Mutation was verified by Sanger sequencing (SeqLab, Göttingen) using primer *scpA* fwd.

2.2.5.6 Cloning of *S. aureus* mutants and fluorescent reporter strains

The *S. aureus* insertional transposon mutant of staphopain A (NE1278) from the Nebraska transposon mutant library was transduced via phage ϕ 11 into the genetic background of wild type *S. aureus* JE2 and 6850 in order to avoid secondary site mutations. Clones were tested by PCR for presence of the transposon. To generate fluorescent reporter strains plasmids pmRFPmars, pJL74, pSarAP1-cerulean or pGFPsf were either electroporated or transduced into the respective strains (Table 2.12) using phage ϕ 11.

2.2.5.7 Cloning of plasmids

For complementation of staphopain A the *scpAB* operon including the native promotor region, 361 bp upstream of start codon, and the transcription termination signal, 253 bp downstream of the stop codon, was amplified by PCR from genomic DNA of *S. aureus* JE2 using the primers *scpAB_prom_fwd_PstI* and *scpAB_TT_rev_EcoRI*. Primers contained restriction sites matching the vector backbone, which allowed insertion in the correct orientation. The generated insert replaced *gfpuvr* in plasmid p2085 using cloning sites PstI and EcoRI. For construction of

phld-scpAB and *phld-scpA*_(C238A)B¹ the *scpAB* operon was amplified from *pscpAB* or *pscpA*_(C238A)B, respectively, using primers *scpAB_AvrII_fwd* and *scpAB_AvrII_rev*. The resulting fragment was cloned into *phld-hlb-cerulean* by replacing *hlb* using *AvrII* restriction sites. All assembled vectors were transformed into chemically competent *E. coli* DH5 α . Correct orientation or mutations were checked via restriction digest, PCR and Sanger sequencing (SeqLab, Göttingen) using primers MFpUCs1, MF17pC194, *scpA fwd* and *scpA rev*. Subsequently, vectors were electroporated into *S. aureus* RN4220 and, if required, further transduced into *S. aureus* JE2 or 6580 using phage ϕ 11.

2.2.6 Genetic and transcriptional manipulation of human cells

2.2.6.1 siRNA transfection

Human cells were seeded in 12 well microtiter plates at density of 4×10^4 cells per well in cell culture medium and incubated at 37 °C and 5 % CO₂. Meanwhile, siRNA was diluted in cold, serum-free cell culture medium to a final concentration of 5 nM in 100 μ l. 6 μ l HiPerFect were added and the mixture was incubated for 10 min at room temperature. Then, complexes were carefully added dropwise onto the freshly seeded cells and cells were further incubated at 37 °C and 5 % CO₂. Medium was changed after 24 h of incubation. 48 h after transfection the cells were used for infection and RNA was isolated to determine the efficiency of the knock-down by qRT-PCR.

2.2.6.2 Gene knock-out using CRISPR/Cas9

For designing gene-specific sgRNAs the CRISPOR online tool (crispor.tefor.net) was used and gene sequences were retrieved from Ensemble (www.ensembl.org). Exons coding for essential function(s) of the protein were chosen for genetic manipulation. Synthesized sgRNA oligonucleotides (Table 2.16) were cloned into pSp-Cas9(BB)-2A-GFP according to the protocol from Ran et al. (2013). Briefly, sgRNA strands were phosphorylated, annealed and subsequently cloned into pSp-Cas9(BB)-2A-GFP via *BbsI* restriction sites. After exonuclease treatment the assembled plasmid was transformed into *E. coli* DH5 α and subsequently isolated from single clones. Insertion of the sgRNA was verified by Sanger sequencing (SeqLab, Göttingen) using primer U6-fwd.

For plasmid transfection, HAP1 cells with a low passage number were seeded into 6 well microtiter plates at a density of 5×10^5 cells/well in cell culture medium containing antibiotic

¹ Performed by Helene Mehling, Master F1 Practical

24 h before transfection. 3.6 µg pSp-Cas9(BB)-2A-GFP-sgRNA, 400 ng pSc-TIA-CMV-BSR-TIA and 12 µg PEI were mixed in a total volume of 200 µl with OptiMEM and incubated for 10-15 min at room temperature. Meanwhile cells were washed and medium was renewed. The DNA-PEI-OptiMEM-Mix was added dropwise onto the cells. After 24 h incubation at 37 °C and 5 % CO₂ cells were detached and seeded in cell culture dishes (100 x 20 mm) at a ratio of 1:10, 1:50 and 1:100. The next day selection was applied by treatment with 30 µg/ml blasticidin. The BSR gene, which is released from pSc-TIA-CMV-BSR-TIA by sgRNA-directed cleavage of TIA sequences, is randomly inserted at the genomic site of the CRISPR/Cas9-induced double strand break. Subsequently, cells were monitored over 2-3 weeks and, if necessary, cells were washed and medium was renewed. When cell colonies were large enough, they were transferred to a 12-well plate using trypsin-soaked, sterile Whatman paper. Gene knock-out was verified by western blot.

2.2.7 Protein biochemical methods

2.2.7.1 SDS-PAGE

Protein samples from human cells were prepared in 2x Laemmli buffer and denatured by boiling at 95°C for 10 min. For SDS-PAGE of bacterial secreted factors, proteins from sterile supernatant were precipitated overnight at -20 °C in 25 % TCA. After centrifugation at 4 °C for 30 min the pellet was washed twice with ice-cold acetone. The dried pellet was resuspended in 2x Laemmli buffer and immediately incubated at 95°C for 10 min for protein denaturation. Proteins were separated via gel electrophoresis under denaturing conditions (SDS-PAGE) on a 7.5-12 % polyacrylamide gel. For staining of proteins, the polyacrylamide gel was incubated in Coomassie staining solution overnight under agitation, subsequently destained with repeated buffer exchange until protein bands were visible and fixed using appropriate buffers (Table 2.8).

2.2.7.2 Western blot

Proteins separated by SDS-PAGE were transferred to a PVDF membrane using a semi-dry blotting system. The PVDF membrane was activated in methanol and Whatman paper was soaked in semi-dry buffer. Sandwiches of Whatman paper, PVDF membrane and polyacrylamide gel were prepared. Immunoblotting was performed for 2 h at 1 mA/cm² in semi-dry buffer. For transfer of high molecular weight proteins blotting was performed in a wet blot apparatus at 250 mA and 4 °C overnight in wet blot transfer buffer. Subsequently, PVDF membranes were incubated for 1 hour in blocking solution and overnight at 4 °C with the first antibody (diluted in blocking solution). Membranes were washed three times with TBS-T for

10 min and primary antibodies were detected with a horseradish peroxidase (HRP)-conjugated secondary antibody using enhanced chemiluminescence (ECL) and an Intas imaging system.

2.2.8 Cell infection protocols

2.2.8.1 Lysostaphin protection assay

HeLa or HAP1 cells were cultivated as described in section 2.2.2. For infection, cells were seeded into 12 well microtiter plates at a density of $0.8-1 \times 10^5$ cells per well 24 hours prior to infection. 1 hour prior to infection medium was renewed and, if required, antibiotics or inhibitors were applied. Cells were counted using a hemocytometer. Infection subcultures of *S. aureus* were prepared and bacteria were enumerated as described in section 2.2.1.2. Human cells were infected with a multiplicity of infection (MOI) of 50, if not stated otherwise. After 1 h co-cultivation at 37 °C and 5 % CO₂ extracellular bacteria were removed by 30 min treatment with 20 µg/ml lysostaphin followed by washing and further incubation in medium containing 2 µg/ml lysostaphin and, if required, inhibitors or antibiotics until the end of experiment.

2.2.8.2 Invasion assay

Human cells were infected with *S. aureus* strains expressing GFP or mRFP, as described in section 2.2.8.1. 1 h after infection cells were treated with 20 µg/ml lysostaphin for 10 min to remove extracellular bacteria, washed twice with DPBS and detached using trypsin. After centrifugation for 10 min at 800 rpm cells were resuspended in fresh FACS medium. For determining invasion, the percentage of GFP/mRFP-positive cells representing the number of infected cells was measured by flow cytometry. Forward and sideward scatter (FSC-A and SSC-A) were used to identify the cell population and doublet discrimination was performed via FSC-H vs. FSC-W and SSC-H vs. SSC-W gating strategy. GFP fluorescence was measured using a 488nm laser and a 530/30 nm band pass filter for detection, mRFP fluorescence was detected using a 610/20 nm band pass filter and a 561 nm laser for excitation. 10,000 events were recorded for each sample. Uninfected cells were used to determine autofluorescence of the cells and signals above this value were defined as infected.

2.2.8.3 Phagosomal escape assay

HeLa YFP-cwt cells were seeded at a density of 4×10^4 cells per well in a 24 well µ-plate and infected with mRFP-expressing bacterial strains at a MOI of 10, as described in section 2.2.8.1. Bacteria were prepared for infection as described in section 2.2.1.2. After synchronization of infection by centrifugation (10 min at 500 rpm), infected cells were incubated for 1 hour to allow bacterial invasion. Subsequently, a 30 minute-treatment with 20 µg/ml lysostaphin

removed extracellular bacteria. Cells were washed and medium with 2 µg/ml lysostaphin was added. At 3 h p.i. cells were washed, fixed with 4 % paraformaldehyde overnight at 4 °C and permeabilized with 0.1 % Triton X-100. Nuclei were stained with Hoechst 34580. 10 non-overlapping images were acquired using an Operetta automated microscopy system (20x objective, NA=0.45) and analyzed with Harmony Software.¹ Co-localization of YFP-cwt and mRFP signals indicated phagosomal escape.

2.2.8.4 Intracellular replication

Human cells were infected with *S. aureus* strains expressing GFP or mRFP, as described in section 2.2.8.1. At 1 and 3 h p.i. or 1, 3, 6 and 8 h p.i. infected cells were detached using trypsin and resuspended in FACS medium after centrifugation for 10 min at 800 rpm. GFP/mRFP fluorescence (AFU) of infected cells was directly measured by flow cytometry. Gating and analysis of flow cytometry data were performed as described in section 2.2.8.2. The mean fluorescence intensity of infected cells represents a relative amount of intracellular bacteria. Increasing fluorescence over the time course of infection indicates intracellular replication of bacteria. Cowan I-infected cells served as replication-negative control.

2.2.8.5 Cytotoxicity assays

The Cytotoxicity Detection Kit Plus was used according to manufacturer's instruction to measure release of lactate dehydrogenase (LDH). Human cells were infected as described in section 2.2.8.1 and 1.5 h p.i. medium was replaced by LDH medium. At indicated time points after infection culture medium was transferred to a microcentrifuge tube, shortly centrifuged and 100 µl of supernatant from each sample were transferred into the well of a 96 well microtiter plate in triplicates. 100 µl of the freshly prepared reaction mixture (dye solution with catalyst) were added to the wells and incubated for 15 min at RT and protected from light. The reaction was stopped by addition of 50 µl stop solution. Optical densities were measured in a multimode reader at 492 nm after shaking the plate for 10 sec. Uninfected cells served as low control and lysed cells served as high control. Percentage cytotoxicity was calculated according to the following formula:

$$\% \text{ cytotoxicity } [(\text{experimental value} - \text{low control}) / (\text{high control} - \text{low control}) * 100].$$

¹ Performed by Kerstin Paprotka, Sebastian Blättner, Ursula Eilers and the Core Unit Functional Genomics, University Würzburg

For LDH assay with sterile *S. aureus* supernatant, 1, 2 or 5 % dilutions were prepared in LDH medium and added to fresh HeLa cells. 24 h after treatment LDH release was measured as described above.

For staining with annexin V and 7AAD HeLa cells were infected as described in section 2.2.8.1. At the desired time points after infection medium was collected from the wells and adherent cells were detached. Adherent and suspension cells of each sample were pooled and after centrifugation for 5 min at 800 xg cells were carefully resuspended in annexin V staining buffer. For staining with only 7AAD, annexin V was omitted from the staining buffer. After 10 minutes incubation protected from light cells were kept in ice-cold water and immediately analyzed by flow cytometry. Forward and sideward scatter (FSC-A and SSC-A) were used to identify the cell population and doublet discrimination was performed via FSC-H vs. FSC-W and SSC-H vs. SSC-W gating strategy. APC or 7AAD fluorescence was measured using a 633 nm or 561nm laser for excitation and a 660/20 nm or 610/20 nm band pass filter for detection, respectively. 10,000 events were recorded for each sample. Uninfected or Cowan I-infected cells served as negative control to determine autofluorescence and gates were set accordingly.

2.2.9 Microscopy

Phase contrast and fluorescence microscopic images of live cells were acquired with a LEICA DMR microscope connected to a SPOT camera using a 10x (Leica HC PL FLUOTAR, NA=0.32) or 20x (Leica C Plan, NA=0.3) objective and VisiView[®] software.

For time-lapse imaging, human cells were seeded in 8 well chamber μ -slides 24 hours prior to infection. Infection with fluorescent protein-expressing bacterial strains was performed at a MOI of 5, as described in section 2.2.8.1. Time-lapse imaging of the samples was performed on a Leica TCS SP5 confocal microscope using a 20x objective (Leica HC PL APO, NA=0.7) or 40x (Leica HC PL APO, NA=1.3) or 63x (Leica HCX PL APO, NA=1.3-0.6) oil immersion objectives. Prior to imaging cell culture medium was substituted with imaging medium containing antibiotics, inhibitors, fluorogenic enzyme substrates and/or chemicals, if indicated. The μ -slides were transferred to a pre-warmed live-cell incubation chamber surrounding the confocal microscope and perfusion with 5 % CO₂ in a humidified atmosphere and a temperature of 37 °C were applied during imaging. LAS AF software was used for setting adjustment and image acquisition. All images were acquired at a resolution of 1024x1024 pixels and recorded in 8-bit mode at predefined time intervals. Z-stacks were imaged with a step size of 0.4 μ m. In certain cases, chemical treatment was performed during imaging *in situ* at the live-cell incubation chamber. All image-processing steps were performed using Fiji (Schindelin et al.,

2012). For quantification of fluorescence intensities raw imaging data was used. For single cell analysis one region of interest (ROI) was defined for all recorded time frames. Fluorescence intensities (mean of RFU) were measured, background was subtracted and data were normalized to time point zero (R_0) obtaining relative fluorescence values. Maximum amplitude was determined as highest relative fluorescence value measured and peak latency was defined as the time point of maximum amplitude.

2.2.10 Murine infection model

The mice were housed in individually ventilated cages under normal diet in groups of four to five throughout the experiment with ad libitum access to food and water. Female Balb/c mice (6 weeks, Janvier Labs, Le Genest-Saint-Isle, France) were intranasally instilled with the infection dose of 2×10^8 CFU/20 μ l.¹ Mice were scored twice a day and sacrificed after 48 hours of infection. In order to measure the bacterial burden in the individual organs, lungs were harvested, homogenized and plated in serial dilutions on TSB agar plates.

All animal studies were approved by the local government of Franconia, Germany (approval number 55.2 2532-2-155) and performed in strict accordance with the guidelines for animal care and experimentation of German Animal Protection Law and the DIRECTIVE 2010/63/EU of the EU.

2.2.11 HAP1 screen

1.7×10^8 mutagenized HAP1 cells (7×10^6 cells/175 cm² flask, 24 flasks) were seeded 24 h prior to infection with *S. aureus*. Infection was performed with a MOI of 100 according to the protocol described in section 2.2.8.1. 3×10^8 mutagenized HAP1 cells were infected with 6850 mRFP (21 flasks), whereas 0.4×10^8 cells were inoculated with Cowan I mRFP. At 6 h p.i. infected cells were washed twice with DPBS, detached using trypsin and transferred to round bottom tubes. After centrifugation for 5 min at 800 rpm cells were resuspended in sorting buffer 4 (Table 3.1) containing 2 μ g/ml lysostaphin. Cells were counted and immediately subjected to cell sorting at 4 °C using a FACS Aria III. FSC and SSC were used to identify the cell population. To exclude cell doublets a FSC-W vs. FSC-H and SSC-W vs. SSC-H gating strategy was applied. Infected cells, i.e. mRFP-positive cells, were detected using a 610/20 nm band pass filter and a 561 nm laser for excitation. Approximately 400-500 events per sec were sorted and positive cells were collected in cooled, FBS-coated 15 ml centrifuge tubes containing

¹ Performed by Tobias Hertlein, Institute for Molecular Infection Biology, Würzburg

infection medium with 30 % FBS and 100 µg/ml gentamicin to prevent contamination. Due to the high cell number and long sorting time infection and sorting of HAP1 cells was performed in 8 separate steps with 42×10^6 cells each on two consecutive days. Sorted cells were resuspended in fresh infection medium containing 100 µg/ml gentamicin, counted and seeded into fresh 175 cm² flasks at a low cell density. A small number of cells was used for purity analysis. At 24 h p.i. 1 µg/ml rifampicin was added to kill all intracellular bacteria. Subsequently, cells were monitored, cell colonies were counted and, if necessary, cells were washed and medium was renewed. Six days after infection 7×10^6 or 1×10^6 infection-surviving cells were seeded for re-infection with *S. aureus* 6850 mRFP or Cowan I mRFP, respectively. Re-infection and sorting were performed as described for the first infection. Cells surviving first or first and second infection were harvested after 6 days and cell pellets were frozen for DNA isolation. DNA was isolated as described in section 2.2.3.2. A simplified experimental setup of the HAP1 screen is depicted in Figure 3.6. Subsequently, insertion sites of the gene trap vector were amplified, DNA was sequenced and the results were analyzed bioinformatically¹. Sequence reads were aligned to the human genome, stringently filtered, assigned to genes and unique gene mutations were counted.

2.2.12 Statistical analysis

Data were analyzed using GraphPad Prism Software. If not indicated otherwise, three biological replicates were performed and all data are presented as means with standard deviation (SD). Pairwise comparisons were assessed using unpaired Student's t-test. Analysis of variance (ANOVA) was performed to determine whether a group of means was significantly different from each other. ANOVA was performed with Tukey's post-hoc analysis for defining individual differences and Dunn's multiple comparison test was applied for Kruskal-Wallis test. P-values ≤ 0.05 were considered significant.

¹ Performed by Lucas Jae, Gene center Munich

3 Results

3.1 Intracellular *S. aureus* induces cell death in epithelial cells

It is well known that *S. aureus*, although being an extracellular pathogen, can invade cells and trigger host cell death in a variety of different cell types (Horn et al., 2018b). To investigate the intracellular lifestyle of *S. aureus* in epithelial cells, HeLa cells expressing a fluorescent marker for phagosomal escape (YFP-cwt) (Grosz et al., 2014) were infected with *S. aureus* 6850. After invasion extracellular bacteria were removed by lysostaphin treatment. Live-cell imaging revealed that intracellular *S. aureus* escaped from the phagosome into the cytosol of the host cell, depicted by the formation of fluorescent rings around the bacterial cells, and only thereafter bacterial replication and host cell death were observed (Figure 3.1 gray arrow, Video 1). Intracellular replication and cytotoxicity of *S. aureus* was not detected, when the bacteria were not able to translocate into the cytoplasm of the host cell (Figure 3.1 black arrows). Morphological characteristics of *S. aureus*-induced host cell death were cell contraction, retraction of pseudopodia and rounding of the cell, followed by cell lysis, indicated by the loss of fluorescence, and the formation of huge membrane blebs.

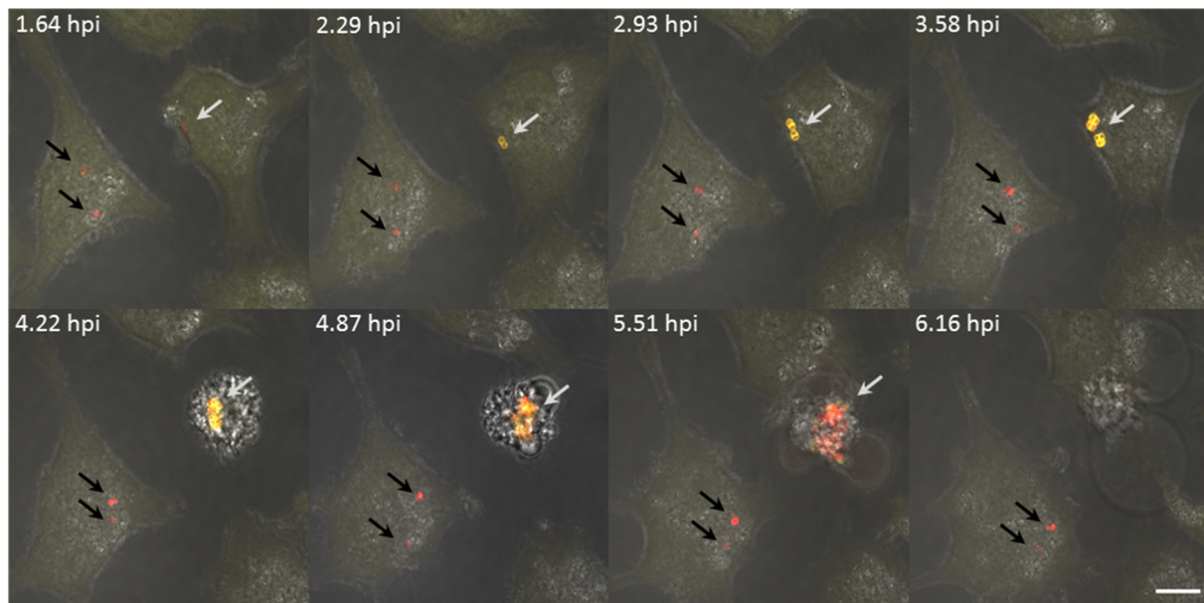


Figure 3.1: Intracellular lifestyle of *S. aureus* in epithelial cells.

HeLa YFP-cwt cells were infected with *S. aureus* 6850 mRFP and time-lapse imaging was performed. Intracellular *S. aureus* escaped into the cytoplasm of the host cell and subsequently replicated and induced host cell death (gray arrow) or resided in the phagosome (black arrows) (gray: BF, yellow: YFP-cwt, red: *S. aureus*, scale bar: 10 μ m).

Besides the MSSA strain 6850, infection of HeLa cells with the MRSA strain JE2 resulted in rounding of the host cell and intracellular bacterial replication was observed (Figure 3.2A). Quantification of cell lysis, measured by LDH release, demonstrated that both strains induced host cell death within hours after infection (Figure 3.2B). Host cell lysis caused by intracellular *S. aureus* began between 3 and 4.5 h p.i. and reached its maximum between 6 and 24 h p.i.. The

S. aureus strain Cowan I did not induce host cell death during the time course of the measurement (Figure 3.2A and B).

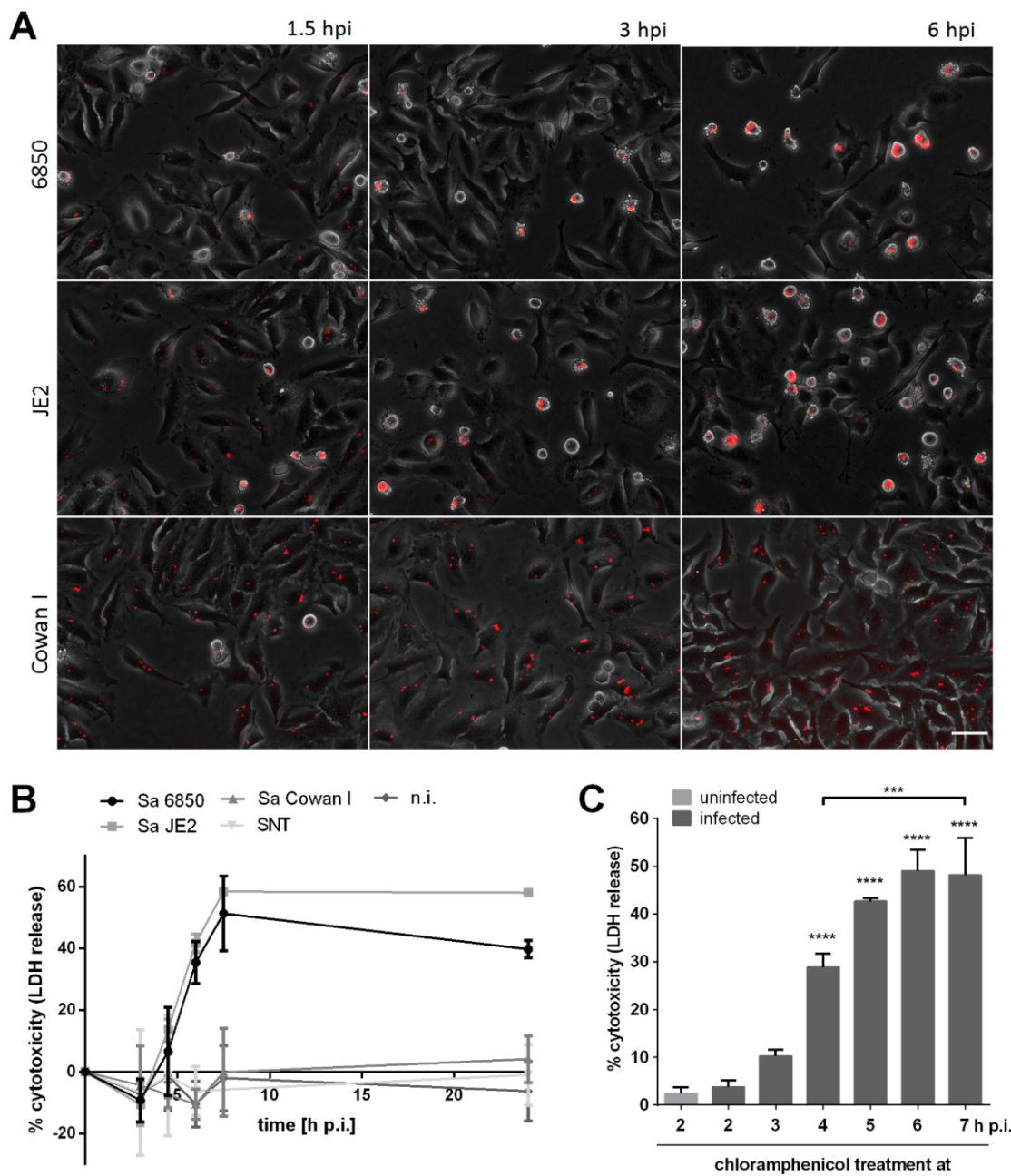


Figure 3.2: Kinetics of intracellular cytotoxicity of *S. aureus*.

(A) Microscopical analysis of HeLa cells infected with *S. aureus* 6850, JE2 or Cowan I expressing mRFP at 1.5, 3 and 6 h p.i. (red: *S. aureus*, gray: phase contrast, scale bar: 50 μ m). (B) HeLa cells were infected with *S. aureus* 6850, JE2 or Cowan I and LDH release was measured at several time points after infection (3, 4.5, 6, 7.5 and 24 h p.i.). Cells were treated with sterile supernatant of infected cells (SNT) or left uninfected and untreated (n.i.) ($n=2$). (C) LDH release of *S. aureus* 6850 infected HeLa cells was determined at 7 h.p.i.. Infected cells were treated with 60 μ g/ml chloramphenicol at time points 2, 3, 4, 5, 6 or 7 h p.i. and compared to uninfected, chloramphenicol-treated cells. One-way ANOVA was applied to determine statistical significance (***) $P<0.001$, **** $P<0.0001$).

The onset of *S. aureus*-induced host cell death was further specified using a translation inhibition assay. Infected HeLa cells were treated with 60 μ g/ml chloramphenicol at several

time points of infection to inhibit bacterial protein biosynthesis (Figure 3.2C). Chloramphenicol treatment at 2 and 3 h p.i. could prevent cell lysis induced by *S. aureus* 6850, while LDH release was partially inhibited by addition of the antibiotic at 4 h p.i.. Cytotoxicity of *S. aureus* 6850 was not significantly affected by chloramphenicol treatment at 5 and 6 h p.i.. Therefore, *S. aureus* induction of host cell death required synthesis of a proteinaceous factor between 3 and 5 h p.i.. To exclude secreted bacterial components, such as the cytotoxic α -hemolysin, to contribute to host cell death induced by intracellular *S. aureus*, medium from infected cells (SNT) 1 h p.i. was sterilized with 20 $\mu\text{g/ml}$ lysostaphin and overlaid on uninfected cells. LDH release was quantified over the course of the treatment, but no cell lysis was observed when compared to uninfected, untreated cells (n.i.) (Figure 3.2B), pointing to a host cell death induced exclusively by intracellular bacteria under the experimental conditions used.

3.2 Host cell factors involved in *S. aureus*-induced cytotoxicity

3.2.1 Haploid genetic screen to identify host cell factors involved in *S. aureus*-induced cytotoxicity

3.2.1.1 The intracellular lifestyle of *S. aureus* in HAP1 cells resembles that in HeLa cells

A genome-wide loss-of-function screening approach in human haploid cells was employed to characterize the molecular mechanisms underlying *S. aureus*-induced host cell death. Haploid genetic screens have already been successfully used to identify host factors of bacterial toxins (e.g. Guimaraes et al., 2011; Popov et al., 2015) or viable bacteria (Rosmarin et al., 2012) and genes involved in cell death mechanisms (e.g. Dovey et al., 2018; Mandal et al., 2014). Haploid genetic screens are limited to the usage of haploid cell lines. Therefore, the intracellular lifestyle of *S. aureus* in the adherent, haploid cell line HAP1 was initially investigated (Carette et al., 2011b).

It was detected that *S. aureus* 6850 invades and escapes from the phagosome in HAP1 cells (Figure 3.3A and B). Additionally, intracellular replication and induction of host cell death by *S. aureus* 6850 were observed in this cell line (Figure 3.3C and D). By comparison with HeLa cells, *S. aureus* 6850 exhibited the same rates of invasion, phagosomal escape, replication and cytotoxicity (Figure 3.3A-D). HAP1 and HeLa cells infected with *S. aureus* 6850 also showed similar morphological changes during infection (Figure 3.3E). Infected cells contracted and rounded up at later time points of infection, i.e. 4 h p.i., characteristic of cell death. Increasing numbers of intracellular bacteria were observed over the course of infection. Hence, the

microscopic analysis further illustrated the findings that *S. aureus* can invade, replicate and induce cell death in the haploid cell line HAP1 similarly to HeLa cells.

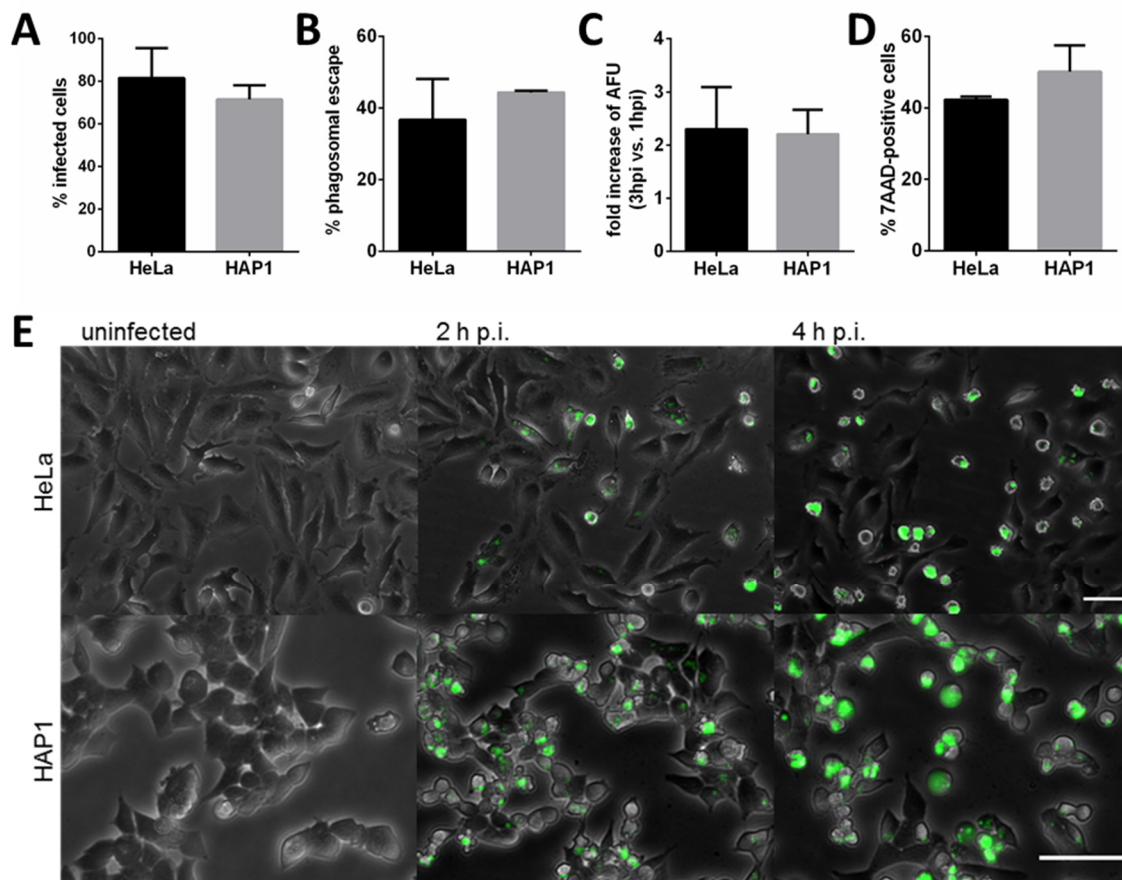


Figure 3.3: *S. aureus* intracellular lifestyle in HAP1 and HeLa cells.

(A) HeLa and HAP1 cells were infected with *S. aureus* 6850 GFP and invasion was determined at 1 h p.i. by flow cytometry as percentage of infected (i.e. GFP-positive) cells. (B) For detection of phagosomal escape HeLa YFP-cwt and HAP1 YFP-cwt cells were infected with *S. aureus* 6850 mRFP. At 3 h p.i. phagosomal escape was determined by means of co-localization of mRFP and YFP signals. (C) For determination of intracellular replication of *S. aureus* 6850 GFP in HeLa and HAP1 cells the mean GFP fluorescence (AFU), which represents the bacterial load, was measured by flow cytometry. The ratio of GFP fluorescence at 3 h p.i. to 1 h p.i. was calculated. (D) HeLa and HAP1 cells infected with *S. aureus* 6850 were stained with the cell-impermeable dye 7AAD at 5 h p.i. and analyzed by flow cytometry. (E) Microscopic images of uninfected and *S. aureus* 6850 GFP-infected HeLa and HAP1 cells 2 and 4 h p.i. (gray: phase contrast, green: *S. aureus*, scale bar: 50 μ m). Statistical significance was assayed using unpaired t-test.

Microscopical analysis also revealed that kinetics of host cell death in HAP1 cells were similar to HeLa cells (Figure 3.3E). To investigate the timing of *S. aureus* intracellular cytotoxicity in HAP1 more precisely, LDH release was determined at several time points during infection (Figure 3.4). Permeabilization of the plasma membrane induced by *S. aureus* was maximal at 24 h p.i., but this did not significantly differ from cell death rates at 6 and 7 h p.i.. Host cell lysis started at 4 h p.i.. At this time point cytotoxicity of *S. aureus* was significantly higher when compared to uninfected and Cowan I-infected HAP1 cells. Thus, *S. aureus* 6850-induced cell lysis of HAP1 cells was initiated between 4 and 6 h p.i.. These observations were in line with

the timing of cell death induced by *S. aureus* in HeLa cells (Figure 3.2B). *S. aureus* 6850 killed HeLa within hours, which was dependent on invasion and phagosomal escape (Section 3.1).

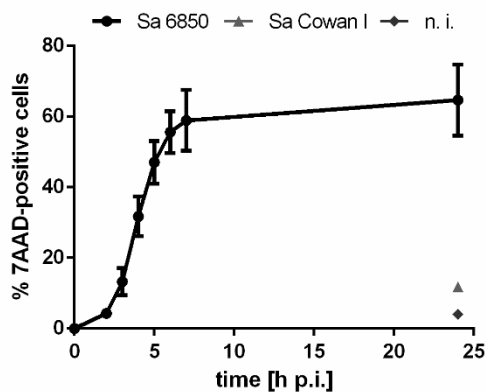


Figure 3.4: Timing of *S. aureus* 6850 induced cell death in HAP1 cells.

S. aureus 6850 cytotoxicity was determined by flow cytometrical analysis of 7AAD-stained, infected HAP1 cells at 2, 3, 4, 5, 6, 7 and 24 h p.i.. The percentage of 7AAD-positive cells was not significantly different at 6 and 7 h p.i. compared to 24 h p.i., but differed at 2 (****), 3 (****), 4 (****) and 5 h p.i. (*) significantly from the value determined at 24 h p.i.. Besides, cytotoxicity of *S. aureus* 6850 was significantly higher at 4 h p.i. compared to Cowan I-infected (**) or uninfected cells (***) at 24 h p.i. Statistical analysis was performed with one-way ANOVA (* $P < 0.05$, ** $P < 0.01$, *** $P < 0.001$, **** $P < 0.0001$).

3.2.1.2 Optimization of screening conditions

Ahead of performing the genome-wide screen with haploid human cells, optimization of screening conditions was required, since no protocol existed for *S. aureus* infection. First, the number of infected cells was optimized by testing different MOIs. As viability is the read-out for the screen, a high number of uninfected cells, i.e. cells, that survive the infection, would lead to a high background noise masking true hits. Therefore, the aim was to achieve the highest possible number of infected cells. HAP1 cells were infected with increasing MOIs of *S. aureus* 6850 mRFP and the number of infected cells was determined after an invasion time of 1 h (Figure 3.5A). Invasion efficiency of the pathogen was enhanced with increasing numbers of bacteria per cell, but infection with MOI 50 and higher did not significantly increase the number of infected cells compared to the highest MOI used (MOI 160). Infection with MOI 160 led to 69.0 % \pm 4.6 infected HAP1 cells and 64 % \pm 8.4 cells were infected using a MOI of 50. MOI 5, 10 and 20 resulted in significantly less infected cells compared to MOI 160.

Additionally, the relative number of intracellular bacteria was determined (Figure 3.5B). The highest amount of intracellular bacteria was detected using a MOI of 100 (10466 AFU \pm 1469). Again, infection with MOI of 50, 60 or 80 did not significantly decrease the number of intracellular bacteria when compared to MOI 100. Instead, using a MOI 10 or 20 led to significantly less intracellular bacteria compared to MOI 100. These results indicate that 50 bacteria per cell were sufficient for maximal infection of HAP1 cells.

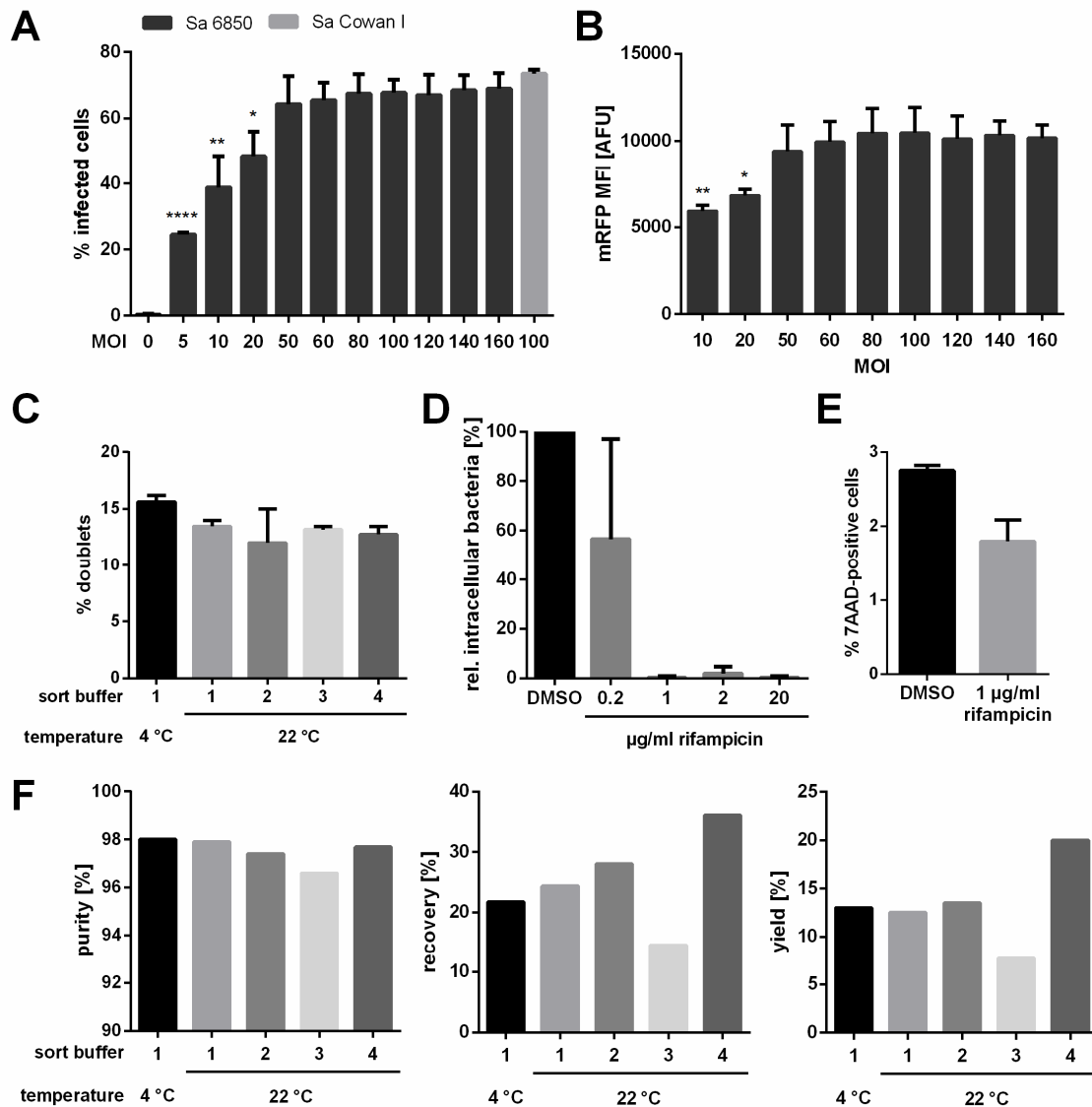


Figure 3.5: Optimization of screening conditions.

(A) HAP1 cells were infected with *S. aureus* 6850 mRFP using increasing MOIs or with Cowan I mRFP at a MOI of 100. At 1 h p.i. the number of infected cells, i.e. mRFP-positive cells, was determined by flow cytometry. For statistical analysis samples were compared to the highest value (MOI 160). (B) HAP1 were infected with *S. aureus* 6850 mRFP as described in (A) and the number of intracellular bacteria, i.e. mRFP mean fluorescence intensity (MFI), was quantified at 1 h p.i. by flow cytometry. For statistical analysis the maximum value (MOI 100) was used. (C) HAP1 cells were infected with *S. aureus* Cowan I mRFP and 5 h p.i. cells were resuspended in four different sort buffers (see Table 3.1). Infected cells were sorted by FACS at 22 °C or 4 °C. Cell doublets were detected by FSC-H vs. FSC-W and SSC-H vs. SSC-W. (D) HAP1 cells were infected with *S. aureus* 6850 and at 6 h p.i. 0.2, 1, 2 or 20 µg/ml rifampicin were added to kill intracellular bacteria. 48 h after rifampicin treatment cells were lysed and plated on TBS-Agar to determine numbers of intracellular bacteria. The relative number of intracellular bacteria was determined by comparison with DMSO treated samples (n=2). (E) 48 h after treatment with 1 µg/ml rifampicin or DMSO as solvent control, HAP1 cells were stained with 7AAD and cytotoxicity was measured by flow cytometry (n=2). (F) Experiment was performed as described in (C) and sort performance was analyzed by calculating purity, recovery and yield (n=1). Statistical analysis was performed using one-way ANOVA (* $P < 0.05$, ** $P < 0.01$, **** $P < 0.0001$).

Yet, infection of all cells could not be achieved and about one third of cells remained uninfected. Thus, fluorescence-activated cell sorting (FACS) was applied to exclude uninfected cells. HAP1 cells were infected with *S. aureus* 6850 and infected cells were selected by FACS. Four

different sort buffers (Table 3.1) were tested to identify the conditions, which favor low amount of cell doublets, accurate sorting and minimal cell loss. Infection with the non-cytotoxic strain Cowan I was employed for these experiments to prevent interference of *S. aureus*-induced cytotoxicity. None of tested sort buffers led to significantly less formation of cell doublets and aggregates (Figure 3.5C). The amount of cell doublets ranged from 12 % \pm 3.0 (sort buffer 2) to 13.5 % \pm 0.5 (sort buffer 1). Cooling of the sample to 4 °C also had no impact on cell aggregation, the percentage of cell doublets was slightly, but no significantly higher (15.6 % \pm 0.6). Re-analysis of the sorted cells revealed that purity, i.e. the number of infected cells in relation to all sorted cells, was high under all tested conditions, ranging from 96.6 % to 98 % (Figure 3.5F). No major impact of sorting temperature and buffer on sort purity was detected. The sort performance was further tested by determining recovery and yield. Recovery, which estimates the cell loss due to sort aborts, was best when using sort buffer 4 (36.1 %), while resuspension of cells in sort buffer 3 resulted in the lowest rate of recovery (14.5 %). The same applied for the yield, which accounts for any cell loss during the entire process of sorting. Here, sorting of cells in buffer 4 caused the highest yield (20 %) and was lowest using sort buffer 3 (7.7 %). In conclusion, sort buffer 4 revealed the best results. As sorting at 4 °C had no major negative effects, this temperature was chosen to slow down *S. aureus* infection during the sorting process.

Table 3.1: Composition of tested sort buffers

no.	Composition
1	IMDM + L-Glutamine, 25mM Hepes, 10% FBS
2	1x DPBS, 25 mM Hepes, 1 % FBS, 5 mM EDTA
3	1x DPBS, 25 mM Hepes, 1 % FBS, 1 mM EGTA, 100 μ g/ml DNaseI, 5 mM MgCl ₂
4	50 % IMDM + L-Glutamine, 50 % Accumax™, 25 mM Hepes, 5 % FBS

After sorting, the infected cells were cleared of intracellular bacteria to avoid further effects of the pathogen on the host cells and to ensure unrestricted growth of the surviving cells. For this purpose, the cell-permeable antibiotic rifampicin was chosen. Treatment of *S. aureus* 6850-infected HAP1 cells at 6 h p.i. with rifampicin led to a concentration dependent reduction of intracellular bacteria after 48 h of treatment compared to treatment with DMSO (Figure 3.5D). 1 μ g/ml rifampicin and higher concentrations were sufficient to kill nearly all intracellular bacteria. Treatment of HAP1 cells with 1 μ g/ml rifampicin did not affect the viability of the cells over a time period of 48 h (Figure 3.5E).

A crucial step of the haploid genetic screen is a stringent selection. An empirical value of 0.1 to 0.01 % surviving genotypes (Lucas Jae, personal communication) is favorable for this

purpose. Thus, the number of cell clones surviving infection with intracellular *S. aureus* 6850 was determined. Wild type HAP1 cells were used for this experiment, as due to spontaneous mutations results can be compared to infection of the mutagenized HAP1 cell library. Uninfected HAP1 cells were excluded by FACS under the optimized conditions determined before and the infected and surviving cells were sparsely re-seeded for counting cell colonies of single clones after a few days. An amount of 0.43 % surviving cell clones in relation to the number of infected cells was determined (Table 3.2). Taking into account that around 80 % of cells are lost during sorting (compare Figure 3.5F yield), a percentage of 2.14 % genotypes would survive the infection by intracellular *S. aureus* 6850. As these numbers were exceeding the amount of 0.1 to 0.01 % surviving genotypes and increase of MOI did not result in significantly higher bacterial numbers in HAP1 cells (compare Figure 3.5B), a second round of selection was performed. Therefore, cells, that survived the first infection with *S. aureus* 6850 were re-infected after seven days. Here, 0.72 % surviving cell clones were determined. Based on the results from the first and second infection, an overall survival rate of 0.0031 % was calculated. Considering 80 % of cell loss during sorting, 0.0768 % cells survived both infections. This was within the optimal range of 0.1 to 0.01 % surviving genotypes.

Table 3.2: Survival rates of HAP1 cells after infection with *S. aureus* 6850

	% surviving cells ^a	% surviving cells ^a (considering cell loss ^b)
1. infection	0.43	2.14
2. infection	0.72	3.59
both infections	0.0031	0.0768

^a in relation to the number of infected cells; ^b accounting for cell loss due to FACS (20 % yield)

3.2.1.3 Implementation of the haploid genetic screen

The results of the preliminary tests led to an adapted protocol for the HAP1 screen (Figure 3.6). Haploid genetic screens using HAP1 cells are usually performed with a starting cell number of 100 million mutagenized cells to account for sufficient complexity of the cell library (Blomen et al., 2015; Jae et al., 2013). As about one third of the cell population was not infected by *S. aureus* (Figure 3.5A), the output number of mutagenized HAP1 cell was increased to 150 million cells. As control, 21 million cells were seeded for infection with the non-cytotoxic strain *S. aureus* Cowan I. A MOI of 100 was chosen, since this number of bacteria per cell led to the second highest number of infected cells (67.7 % ± 4.0) and the highest number of intracellular bacteria (10466 AFU ± 1469) (Figure 3.5A and B). Infected cells were resuspended in sort buffer 4 (Table 3.1) and uninfected cells were excluded by FACS. Cell doublets and aggregates were excluded during cell sorting. 24 h p.i. 1 µg/ml rifampicin was added to the infected and

surviving cell clones to remove intracellular bacteria. After expansion of single cell clones for 5 to 6 days cells were harvested and 21 million or 170 thousand cells were seeded for re-infection with *S. aureus* 6850 or Cowan I, respectively. Here, the same infection and sorting protocol was applied.

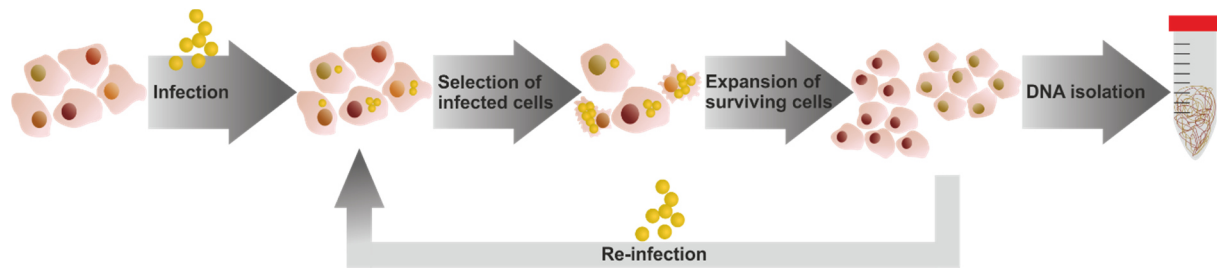


Figure 3.6: Simplified illustration of the experimental setup for the haploid genetic screen.

150 million mutagenized HAP1 cells were infected with *S. aureus* 6850 mRFP using a MOI of 100. Infected cells were selected by FACS and the cell clones surviving the infection were expanded to cell colonies over 5 to 6 days after removal of remaining intracellular bacteria by rifampicin treatment. The cells were harvested and genomic DNA was isolated, while 21 million cells were used for re-infection with *S. aureus* 6850. Infection with the non-cytotoxic strain *S. aureus* Cowan I was performed as control.

The performance of the sort was assessed by calculating purity, recovery and yield (Table 3.3) and similar results compared to the preliminary tests were obtained (compare Figure 3.5A and B). Colonies of cell clones surviving the infection were quantified to determine the stringency of the selection (Table 3.3). 0.41 % of cell clones survived the first infection with *S. aureus* 6850, while 0.43 % surviving cells was determined after the second infection. This resulted in an overall survival rate of 0.0018 %, which lies below the anticipated number of surviving genotypes of 0.1 to 0.01 %. However, cell loss was not considered. Since infection with *S. aureus* Cowan I does not induce host cell death, the survival rate of these cells, which were treated identically to those infected with *S. aureus* 6850, represents a good measure for comparison. Doing so, the survival rate of *S. aureus* 6850-infected, mutagenized HAP1 cells was 0.0914 % after two rounds of infection, which lies within the optimal range.

Genomic DNA of the surviving cells was isolated after the first and second round of infection with *S. aureus* 6850 or Cowan I. Subsequently, insertion sites of the gene trap vector were amplified, DNA was sequenced and the results were analyzed bioinformatically¹. Sequence reads were aligned to the human genome, stringently filtered, assigned to genes and unique gene mutations were counted. The number of mutations in each gene after infection with *S. aureus* 6850 was compared to those after infection with *S. aureus* Cowan I (Table 3.4, Table 6.1).

¹ Performed by Lucas Jae, Gene center Munich

Table 3.3: Sort performance and selection stringency of the HAP1 screen

Bacterial strain		% Purity	% Recovery	% Yield	% surviving cells ^a
Sa 6850	1. infection	94.7	37.7	14.0	0.41
	2. infection	95.7	42.1	21.0	0.43
	both infections				0.0018
Sa Cowan I	1. infection	94.8	36.9	15.4	11.37
	2. infection	95.4	35.6	21.0	17.33
	both infections				1.97
Sa 6850 vs. Sa Cowan I ^b	1. infection				3.61
	2. infection				2.48
	both infections				0.0914

^a in relation to the number of infected cells; ^b Infection with *S. aureus* 6850 in relation to infection with *S. aureus* Cowan I

In comparison to other haploid genetic screens (e.g. Carette et al., 2011b; Jae et al., 2013) the number of significantly enriched genes was small and enrichment was not very strong. After the first infection with *S. aureus* 6850 only one gene was significantly enriched, while mutations in 12 genes were significantly more abundant after two infections with *S. aureus* 6850 in comparison to Cowan I. Additionally, gene mutations, which might favor cell proliferation or hotspots of retroviral integration, were among the hits. TANC2, the top hit of the screen, had the highest number of unique mutations per gene (Table 6.1). These results suggest that the selection for genotypes, that survive infection with intracellular *S. aureus*, was not stringent enough and that hits cannot easily be identified due to background noise.

Table 3.4: Significantly enriched genes in mutagenized HAP1 cells surviving infection by intracellular *S. aureus* 6850 in comparison with infection by *S. aureus* Cowan I

number of infections	gene	infection with Sa 6850		infection with Sa Cowan I		p-value ^c	fdr-corrected p-value ^d
		mutations/gene ^a	total mutations ^b	mutations/gene ^a	total mutations ^b		
1x	TANC2	4045	1103762	3202	1068592	8,61E-18	1,43E-13
2x	TANC2	1861	425375	1711	560835	3,87E-27	6,17E-23
2x	WDR20	540	426696	417	562129	1,17E-16	9,31E-13
2x	KIAA1671	206	427030	149	562397	1,29E-08	6,85E-05
2x	TBCK	210	427026	169	562377	1,10E-06	0,00439381
2x	PAWR	184	427052	146	562400	2,86E-06	0,00797902
2x	DIP2B	410	426826	392	562154	3,50E-06	0,00797902
2x	KIF3B	320	426916	292	562254	3,51E-06	0,00797902
2x	MAP4K4	102	427134	67	562479	5,18E-06	0,01030673
2x	MAML1	40	427196	16	562530	1,76E-05	0,02782652
2x	TAOK1	188	427048	158	562388	1,91E-05	0,02782652
2x	MYH9	62	427174	34	562512	1,92E-05	0,02782652
2x	PHLPP1	178	427058	149	562397	2,72E-05	0,0360546

^a number of unique gene trap vector insertions in the respective gene; ^b number of all other unique gene trap vector insertions; ^c Statistical significance was determined by Fisher's exact-test. ^d fdr-corrected p-values ≤ 0.05 were considered significant.

Studying the function of the significantly enriched genes, involvement in wide variety of cellular processes were identified, ranging from intracellular signaling pathways to DNA methylation, transcriptional co-activation and intracellular organelle transport (Table 3.5).

Table 3.5: Function of significantly enriched genes in mutagenized HAP1 cells surviving infection by intracellular *S. aureus* 6850

gene	name	function	references
TANC2	Tetratricopeptide Repeat, Ankyrin Repeat And Coiled-Coil Containing 2	postsynaptic scaffold protein influencing synaptic spines and excitatory synapse strength, driver gene regulating the proliferation/survival of clonogenic breast cancer cells	Han et al. (2010); Mahmood et al. (2014)
WDR20	WD Repeat Domain 20	co-factor of ubiquitin-specific proteases USP12 and USP46	Dahlberg and Juo (2014); Kee et al. (2010)
KIAA1671		unknown function	
TBCK	TBC domain-containing protein kinase-like protein	putative GTPase-activating protein (GAP) for small GTPases of the Rab family, thought to play a role in actin organization, cell growth and cell proliferation by regulating the mammalian target of the rapamycin (mTOR) signaling pathway	Chong et al. (2016); Liu et al. (2013); Wu et al. (2014a)
PAWR	Pro-Apoptotic WT1 Regulator	tumor suppressor protein, selectively induces apoptosis in cancer cells	Hebbar et al. (2012)
DIP2B	Disco Interacting Protein 2 Homolog B	may participate in DNA methylation	Winnepenninckx et al. (2007)
KIF3B	Kinesin Family Member 3B	acts as a heterodimer with KIF3A to aid in membrane organelle transport, role in cell proliferation	Huang et al. (2014); Shen et al. (2019); Yamazaki et al. (1995)
MAP4K4	Mitogen-Activated Protein Kinase Kinase Kinase 4	expression is modulated by TNF-alpha and p53, activator of JNK signaling pathway	Bouzakri et al. (2009); Tesz et al. (2007); Yao et al. (1999) Miled et al. (2005)
MAML1	Mastermind Like Transcriptional Coactivator 1	functions as a transcriptional co-activator in the Notch signaling pathway	Oyama et al. (2011)
TAOK1	Thousand And One Amino Acid Protein Kinase 1	regulates various MAPK signaling pathways such as JNK and p38 MAPKs, involved in cytoskeleton stability and apoptosis	Hutchison et al. (1998); Mitsopoulos et al. (2003); Moore et al. (2000); Zihni et al. (2007)
MYH9	Myosin Heavy Chain 9	non-muscle myosin, involved in several important functions, including cytokinesis, cell motility and maintenance of cell shape	Pecci et al. (2018)
PHLPP1	PH Domain And Leucine Rich Repeat Protein Phosphatase 1	involved in regulation of Akt and PKC signaling, act as tumor suppressor and inhibits cell proliferation	Gao et al. (2008); Gao et al. (2005); Liu et al. (2009)

Roles in tumor development, cell proliferation, cell shape and cell death could be assigned more frequently to the enriched genes. These features, as indicated above, might be advantageous for

improved cell survival and therefore contribute to background noise in a positive selection screen using viability as a read-out. Protein interaction analysis revealed only one interaction of significantly enriched genes from the haploid genetic screen (Figure 3.7). The expression of PHLPP1, which leads to decreased cell proliferation and tumorigenesis through inhibition of Akt, is stabilized by the deubiquitinase USP46, whose activity is stimulated by WDR20 (Kee et al., 2010; Li et al., 2013).

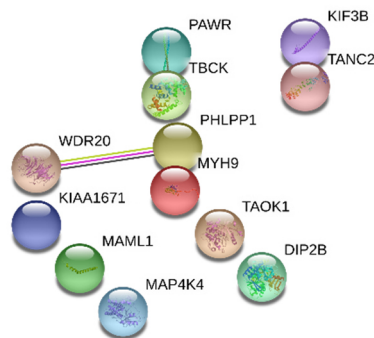


Figure 3.7: Protein-protein interaction analysis of significantly enriched genes in the haploid genetic screen using STRING. (Szkłarczyk et al., 2015)

The function of some of the significantly enriched genes could be remotely linked with existing information on cell death and *S. aureus* intracellular infection. TAOK1 regulates the p38 and JNK signaling pathways (Hutchison et al., 1998; Moore et al., 2000), which have been shown to play a role in *S. aureus* infection. Intracellular *S. aureus* can evade autophagy by a p38 α /MAPK14-mediated mechanism (Neumann et al., 2016). TBCK, another hit gene of the HAP1 screen, might be involved in autophagy, too, as it regulates the mammalian target of the rapamycin (mTOR) signaling pathway (Liu et al., 2013), which inhibits autophagy under nutrient starvation (Noda and Ohsumi, 1998). Schnaith et al. (2007) showed that intracellular *S. aureus* can exploit autophagy to promote replication and induction of host cell death. Furthermore, the tumor suppressor protein PAWR is associated with cell death induction in tumor cells (Hebbar et al., 2012). Therefore, the role of the genes TAOK1, TBCK, PAWR and TANC2 in host cell death induced by *S. aureus* were subsequently investigated in a Master thesis (Matsch, 2018) under my supervision (Section 4.2.2).

3.2.2 *S. aureus*-induced host cell death displays characteristics of apoptosis

3.2.2.1 Inhibition of caspases attenuates *S. aureus*-induced host cell death

The morphology of *S. aureus*-induced cell death is reminiscent of an apoptotic mode of cell death, in that infected cells showed retraction of pseudopodia, shrinkage, formation of membrane blebs and detachment from the substratum (Figure 3.1 and Figure 3.2A) (Kroemer et al., 2009). Therefore, a possible role of apoptosis in *S. aureus*-induced cytotoxicity was investigated. Apoptosis is largely executed by a family of cysteine proteases, the caspases (Earnshaw et al., 1999). Inhibition of caspases with the pan-caspase inhibitor Z-VAD-fmk led

to reduced cytotoxicity of *S. aureus* 6850 (Figure 3.8). LDH release of 6850-infected HeLa cells was decreased by 63 % (Figure 3.8A), while the number of annexin V- and 7AAD-positive cells was reduced by 57 % when pre-treated with the caspase inhibitor (Figure 3.8B and C). No difference in the number of annexin V-positive and 7AAD-negative cells and annexin V-negative and 7AAD-positive cells was observed when the cells were pre-treated with DMSO or 80 μ M Z-VAD-fmk. In contrast to Cowan I-infected cells, infection of HeLa cells with 6850 led to an increase in annexin V-negative and 7AAD-positive cells independent of treatment. Inhibition of caspases in Cowan I-infected cells did not induce cell death.

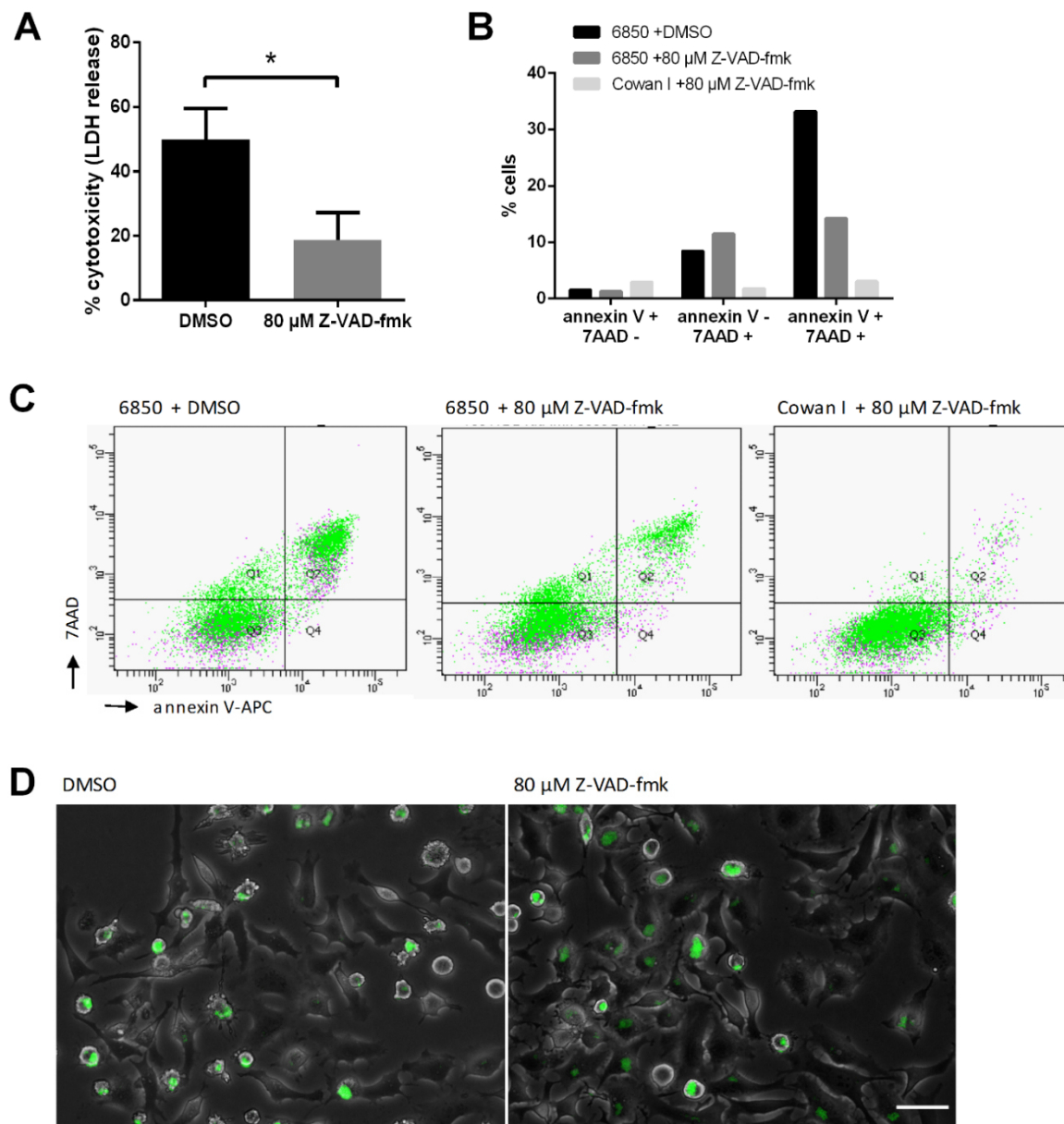


Figure 3.8: Inhibition of caspases reduces *S. aureus* induced host cell death.

HeLa cells were treated with 80 μ M Z-VAD-fmk or DMSO as solvent control 1 h prior to infection with *S. aureus* 6850 or Cowan I. (A) Bacterial cytotoxicity was determined 6 h p.i. by LDH assay. (B, C) Infected cells were stained with annexin V-APC and 7AAD 6 h p.i. to analyze cell death. Bar graph of quantified cell populations (B) and representative dot plots (C) are shown (n=1). (D) Less cell contraction of *S. aureus* 6850 GFP infected HeLa cells was observed at 6 h p.i. when cells were pre-treated with Z-VAD-fmk (gray: phase contrast, green: *S. aureus*, scale bar: 50 μ m). Statistical analysis was performed by unpaired t-test (* P <0.05).

Inhibition of caspases had no effect on bacterial invasion of epithelial cells. Pre-treatment of HeLa cells with 80 μM Z-VAD-fmk or DMSO and subsequent infection with *S. aureus* 6850 resulted in similar numbers of infected cells (Figure 3.9A). Besides, phagosomal escape of *S. aureus* 6850 in HeLa cells was detected independent of treatment with 80 μM Z-VAD-fmk or DMSO (Figure 3.9B, Video 2).

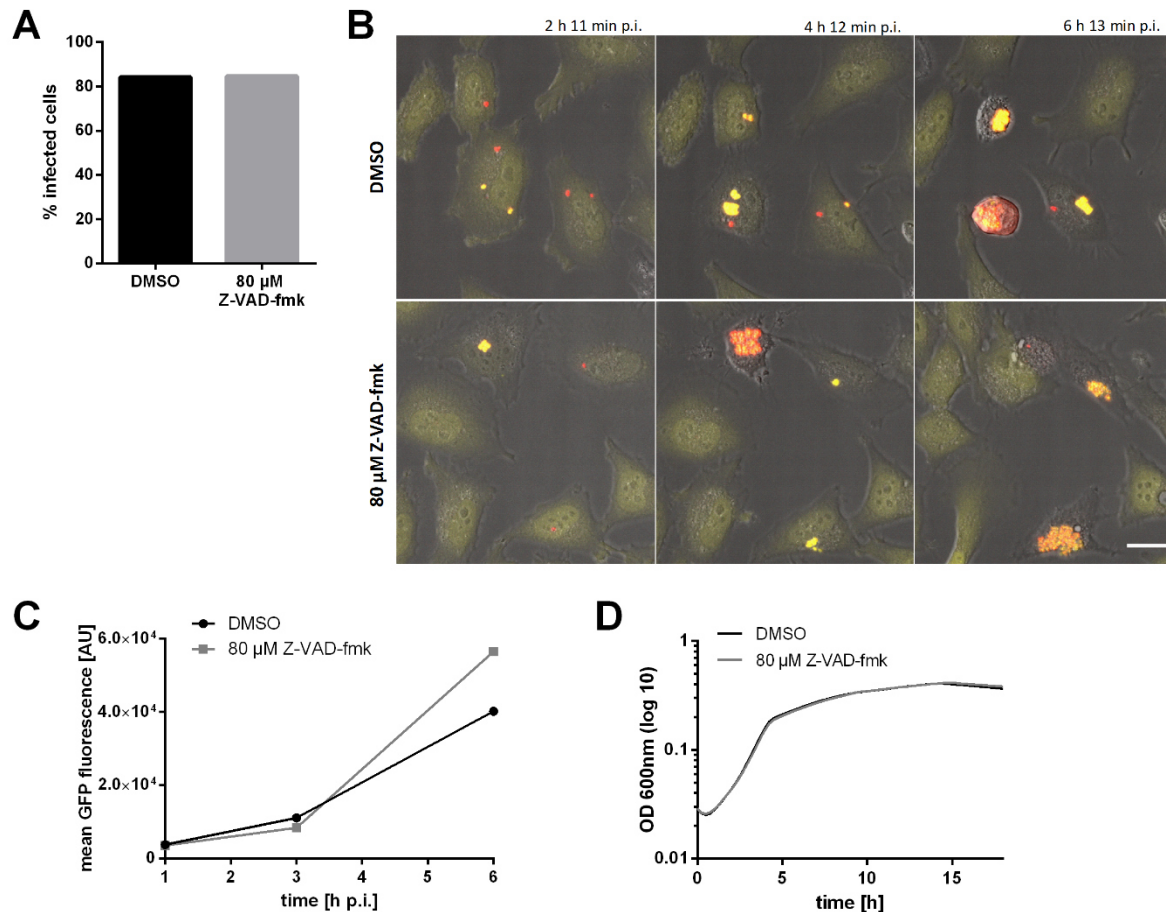


Figure 3.9: Invasion, phagosomal escape and replication of *S. aureus* 6850 upon caspase inhibition.

(A) Pre-treatment of HeLa cells with 80 μM Z-VAD-fmk did not influence the number of 6850 GFP-infected cells ($n=1$). (B) HeLa YFP-cwt cells were infected with *S. aureus* 6850 mRFP after 1 h pre-treatment with 80 μM Z-VAD-fmk or DMSO as solvent control. Live cell imaging revealed that 6850 was able to escape into the phagosome independent of treatment (red: *S. aureus*, yellow: YFP-cwt, gray: BF, scale bar: 20 μm). (C) Intracellular replication was determined by measurement of GFP fluorescence of 6850 GFP-infected HeLa cells at 1, 3, and 6 h p.i. ($n=1$). (D) Optical density (OD) at 600 nm of *S. aureus* 6850 treated with 80 μM Z-VAD-fmk or DMSO in RPMI medium without FBS was determined for 18 h at 10 min-intervals.

Intracellular replication was also observed under both conditions (Figure 3.9C). While at early time points of infection (1 and 3 h p.i.) similar amounts of intracellular bacteria were detected after treatment with 80 μM Z-VAD-fmk or DMSO, *S. aureus* 6850 was more abundant at 6 h p.i. in Z-VAD-fmk-treated HeLa cells when compared to DMSO treatment. No differential growth of *S. aureus* 6850 was observed, when the pathogen was cultured with 80 μM Z-VAD-fmk or DMSO *in vitro* (Figure 3.9D). Thus, inhibition of caspases had no effect on bacterial

invasion and phagosomal escape, but allowed increased intracellular replication of *S. aureus* 6850.

The morphology of *S. aureus* 6850-infected HeLa cells pre-treated with Z-VAD-fmk showed only minor differences when compared to DMSO treatment (Figure 3.8D), but on closer inspection cell shrinkage was more abundant in DMSO-treated cells in contrast to Z-VAD-fmk-treated cells. Treatment with DMSO and infection with *S. aureus* 6850 led to cell contraction after phagosomal escape of the bacteria, whereas Z-VAD-fmk treatment attenuated shrinkage of some infected cells (Video 2 and 3). Also, the number of intracellular bacteria seemed to be higher, which was consistent with the quantitative data (Figure 3.9C).

3.2.2.2 Effector caspases are activated by intracellular *S. aureus*

As inhibition of caspases reduced *S. aureus*-induced host cell death, the presence of activated caspases in *S. aureus*-infected cells was investigated. For activation, effector caspases 3 and 7, which are the executioners of apoptosis, are cleaved by initiator caspases of the intrinsic or extrinsic apoptotic pathway. HeLa cells were infected with *S. aureus* 6850 and an immunoblot was performed to investigate cleavage of caspase 3 (Figure 3.10A). At 4.5 h p.i. the large subunit p20 of caspase 3 was detected in *S. aureus*-infected cells, while later (6 h p.i.) both large subunits, p20 and p17, of caspase 3 were present. Infection with *S. aureus* Cowan I did not result in detection of cleaved caspase 3 at 4.5 h p.i.. A further biochemical marker of apoptosis is cleavage and inactivation of the DNA damage repair enzyme PARP-1, whose hyperactivation, by contrast, is implicated in parthanatos. Cleavage of PARP-1 by caspase 3 results in a 89 kDa-large fragment (Tewari et al., 1995). Immunoblot analyses were performed to study this protein (Figure 3.10B). During infection of HeLa cells with *S. aureus* 6850 the 89 kDa fragment of PARP-1 was detected at 4.5 h p.i., whereas infection with Cowan I showed no cleavage of PARP-1. The appearance of the PARP-1 cleavage fragment coincided with activation of caspase 3, which also occurred initially at 4.5 h p.i. (Figure 3.10B). However, both PARP-1 and caspase 3 cleavage were not very prominent.

The activation of effector caspases in *S. aureus* 6850-infected HeLa cells was further visualized by live cell imaging using a fluorogenic caspase 3/7 substrate (CellEvent™ Caspase-3/7 Green Detection Reagent) (Figure 3.10C). The fluorogenic substrate was cleaved, allowing fluorescence of the dye by binding to DNA, when infected cells were strongly contracted and tightly packed with intracellular bacteria. Activation of effector caspases occurred around 4.5 to 7 h p.i., depending on the MOI used. Infection with Cowan I did not result in increased

fluorescence of the fluorogenic caspase 3/7 substrate. These results indicate an activation of effector caspases by cytotoxic *S. aureus* 6850.

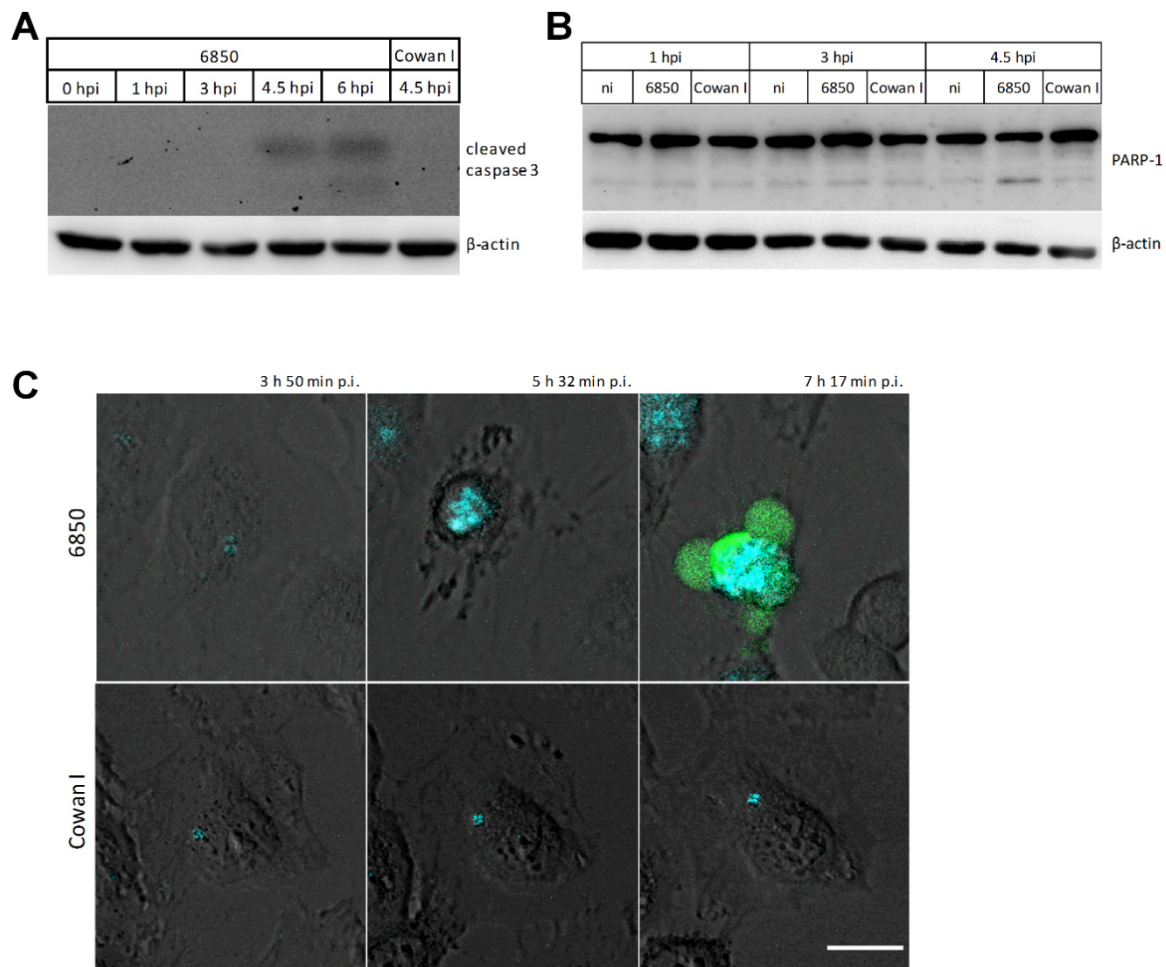


Figure 3.10: Caspase activation by intracellular *S. aureus*.

(A, B) Cell lysates of uninfected or *S. aureus* 6850- or Cowan I-infected HeLa cells were taken at 0, 1, 3, 4.5 and 6 h p.i and immunoblot analysis was performed. (A) To investigate caspase 3 cleavage anti-cleaved caspase 3 antibody (large subunits p17 and p20) and anti-β-actin antibody as loading control were used. (B) Anti-PARP-1 antibody was used to study PARP-1 (116 kDa) cleavage by caspase 3 resulting in an 89 kDa-fragment. (C) Live cell imaging of HeLa cells infected with *S. aureus* 6850 Cerulean or Cowan I Cerulean revealed activation of effector caspases in cells infected with cytotoxic *S. aureus*. CellEvent™ Caspase-3/7 Green Detection Reagent was added immediately before imaging (3 h p.i.) (cyan: *S. aureus*, green: CellEvent™ Caspase-3/7 Green Detection Reagent, gray: BF, scale bar: 20μm).

However, inhibition of caspases with Z-VAD-fmk did not abolish the activation of effector caspases (Figure 3.11, Video 3). Treatment with 80 μM Z-VAD-fmk prior to infection with *S. aureus* 6850 still led to an increase in fluorescence of the fluorogenic caspase 3/7 substrate (Figure 3.11A). Quantification of the relative CellEvent Caspase 3/7 Detection reagent fluorescence of single infected cells revealed that the amplitude of the caspase 3/7 activation signal was not affected by inhibition of caspases, but the time point of maximal fluorescence was delayed (Figure 3.11B-D). Activation of effector caspases happened approximately 1-2 h later, when *S. aureus*-infected cells were treated with Z-VAD-fmk.

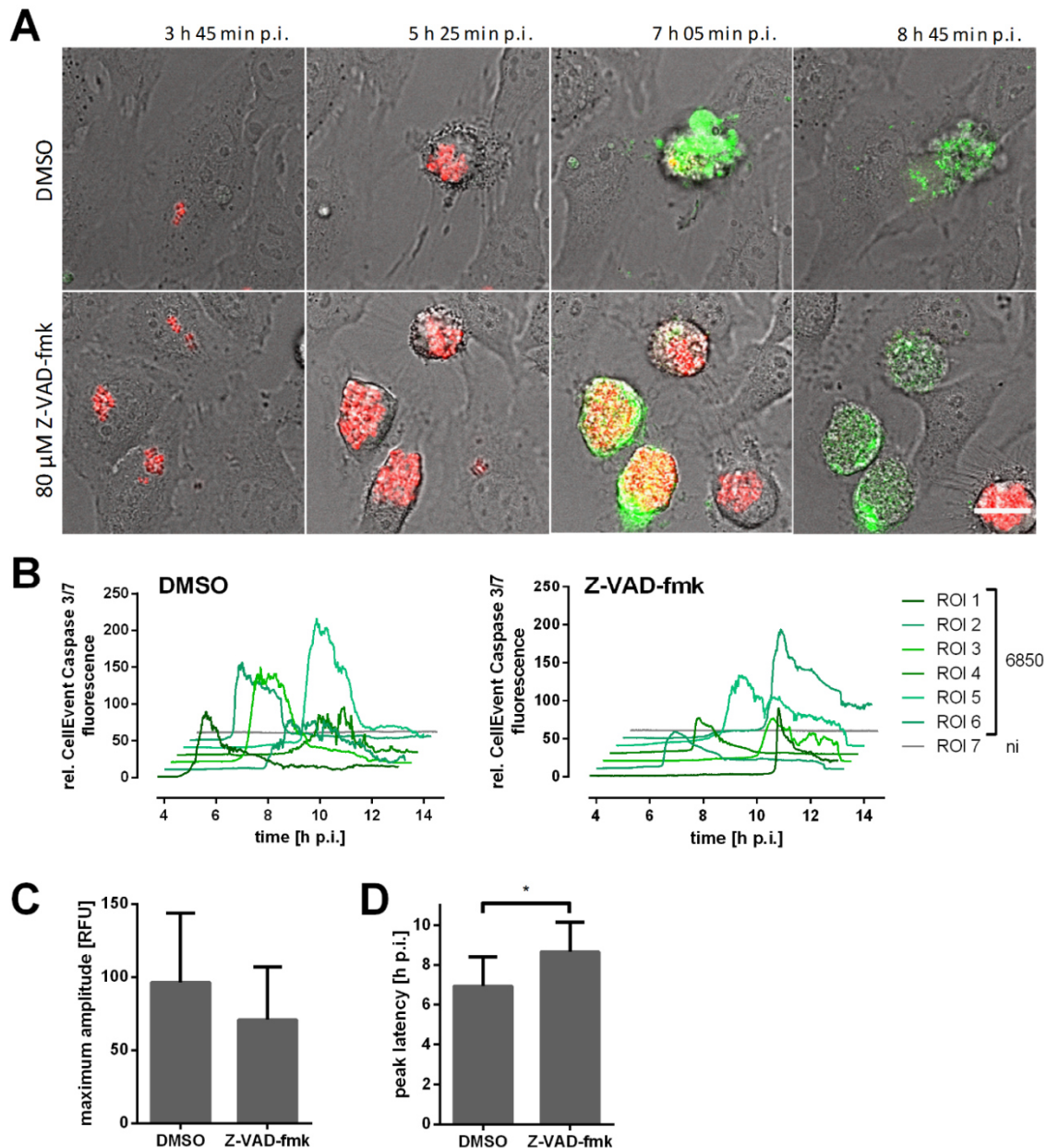


Figure 3.11: Effector caspase activation in *S. aureus* infected cells cannot be inhibited with Z-VAD-fmk.

HeLa cells were pre-treated with 80 μ M Z-VAD-fmk or DMSO 1 h prior to infection with *S. aureus* 6850 mRFP and CellEvent™ Caspase-3/7 Green Detection Reagent was added immediately before live cell imaging. (A) Representative stills of time-lapse fluorescence microscopy of *S. aureus* 6850 infected cells pre-treated with DMSO or Z-VAD-fmk (red: *S. aureus*, green: CellEvent™ Caspase-3/7 Green Detection Reagent, gray: BF, scale bar: 20 μ m). (B) Relative CellEvent Caspase 3/7 fluorescence was quantified over the time period of infection in single infected cells after DMSO (left) or Z-VAD-fmk (right) treatment. (C) The maximum amplitude of the relative CellEvent Caspase 3/7 fluorescence of 7 to 8 single infected cells was determined after DMSO or Z-VAD-fmk treatment. (D) The latency of the relative CellEvent Caspase 3/7 fluorescence maximum after *S. aureus* intracellular infection was determined upon DMSO or Z-VAD-fmk in 7 to 8 single cells. Statistical analysis was performed by unpaired t-test ($*P < 0.05$).

3.2.2.3 *S. aureus*-infected cells display apoptotic morphology and Bid cleavage

Other morphological indicators of apoptosis, besides the observed cellular shrinkage and blebbing of the plasma membrane (Figure 3.1 and Figure 3.2A), are nuclear fragmentation, chromatin condensation and the formation of membrane-enclosed fragments, called apoptotic

bodies. The fluorogenic caspase 3/7 substrate, CellEvent Caspase 3/7 Detection reagent, is conjugated to a dye, which only fluoresces upon release by cleavage of effector caspases and subsequent binding to DNA. Thus, localization of DNA is possible in cells, which were stained with the fluorogenic substrate and where effector caspases are activated. In HeLa cells infected with *S. aureus* 6850 fluorescence of CellEvent Caspase 3/7 Detection reagent was detected (Figure 3.10C) and revealed nuclear condensation and fragmentation of the DNA and nucleus (Figure 3.12, Video 3). Some cells also partly broke up into extracellular vesicles containing DNA and those apoptotic bodies were phagocytosed by neighboring cells (Video 3).

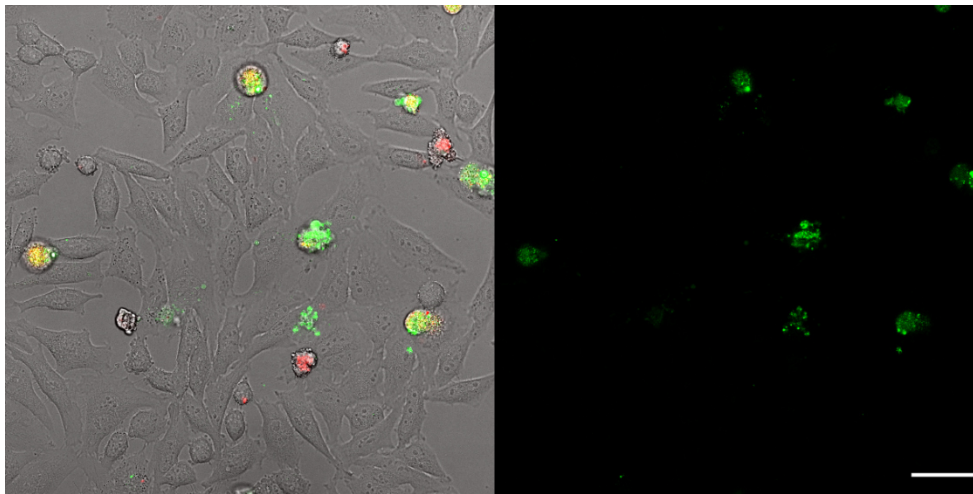


Figure 3.12: Nuclear fragmentation in *S. aureus* 6850 infected cells.

HeLa cells were infected with *S. aureus* 6850 mRFP and CellEvent™ Caspase-3/7 Green Detection Reagent was added immediately before live cell imaging. Stills from 7 h 9 min p.i. are shown (left: merge, right: CellEvent™ Caspase-3/7 Green Detection Reagent) (red: *S. aureus*, green: CellEvent™ Caspase-3/7 Green Detection Reagent, gray: BF, scale bar: 50 μ m). DNA fragmentation was observed, as the fluorogenic Caspase-3/7 substrate binds to DNA upon cleavage.

To further characterize *S. aureus*-induced apoptosis, the pro-apoptotic BCL2 family member Bid was investigated. Bid connects the extrinsic apoptotic pathway with the intrinsic, mitochondria-dependent pathway of apoptosis (Li et al., 1998), which is required in type II cells, such as HeLa cells (Mandal et al., 1996; Yasuhara et al., 1997). The protein is activated by caspase 8-mediated cleavage, which results in a 15 kDa-large protein termed truncated Bid (tBid) localized to mitochondria. No presence of tBid in *S. aureus*-infected HeLa cells was observed (Figure 3.13A). However, the amount of full-length Bid was decreased in HeLa cells after 4.5 and 6 h p.i. with *S. aureus* 6850, while a band slightly smaller compared to full-length Bid at approximately 21 to 19 kDa appeared. Besides, the tumor suppressor p53 is implicated in apoptosis, regulating, for instance, Bid expression (Mandal et al., 2008; Sax et al., 2002) or assisting in translocation of Bid from the nucleus to mitochondria (Song et al., 2009). Infection with *S. aureus* did not alter the protein levels of p53 in HeLa cells (Figure 3.13B).

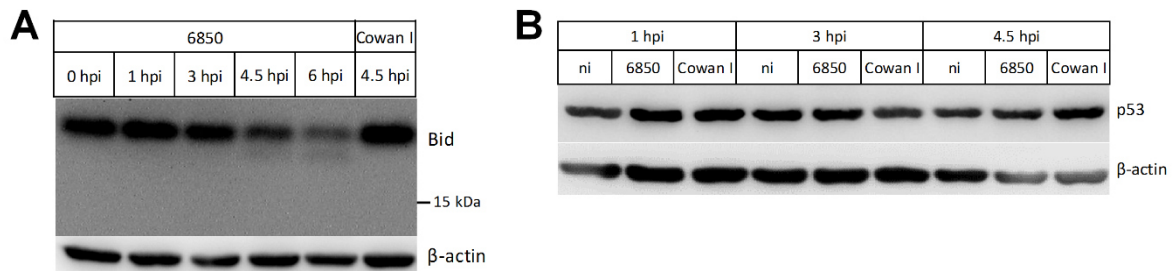


Figure 3.13: Immunoblot analyses of apoptosis-related proteins during infection with *S. aureus*.

HeLa cells were infected with *S. aureus* 6850, Cowan I or left uninfected and cell lysates for immunoblot analysis were taken at 1, 3, 4.5 or 6 h p.i.. Proteins were separated via SDS-PAGE and transferred onto a PVDF membrane. β-actin was detected as loading control. (A) Detection of Bid (22 kDa) cleavage resulting in tBid (15 kDa) after infection with *S. aureus* using anti-Bid antibody. (B) Protein levels of p53 were investigated using anti-p53 antibody after infection with *S. aureus* 6850 in comparison to uninfected or Cowan I-infected cells.

3.2.3 A possible role of AIF in *S. aureus*-induced cell death

One of the key processes of parthanatos is the binding of PAR polymers to AIF (Loeffler et al., 2001). This promotes the cleavage and release of AIF from the mitochondrial periphery to the cytosol, where it translocates to the nucleus eventually causing DNA fragmentation and chromatin condensation (Susin et al., 1999). The presence of the truncated, cytosolic form of AIF (57 kDa) was only very faintly observed in *S. aureus*-infected HeLa cells at 5 and 6 h p.i. (Figure 3.14). A slight decrease of the mature, mitochondrial form of AIF (62 kDa) at 6 h p.i. was noted in contrast to the loading control, which indicated no overall protein reduction. Staining with the anti-AIF antibody resulted in unspecific bands, which complicated the identification of the band representing truncated AIF.



Figure 3.14: Immunoblot analyses of AIF truncation during HeLa infection with *S. aureus*.

HeLa cells were infected with *S. aureus* 6850 or Cowan I and cell lysates for immunoblot analysis were taken at 1, 3, 4, 5 or 6 h p.i.. Proteins were separated via SDS-PAGE and transferred onto a PVDF membrane. GAPDH was detected as loading control. Anti-AIF antibody was used to detect the mature, mitochondrial form (62 kDa) and the truncated, cytosolic form (57 kDa) of AIF.

3.2.4 *S. aureus*-infected cells show features of necrotic cell death

Infection of epithelial cells with *S. aureus* 6850 ultimately resulted in cell lysis, which is associated with necrotic cell death. After phagosomal escape, intracellular replication of *S. aureus* and host cell shrinkage, bacteria lysed, indicated by loss of fluorescence. This was presumably due to the breakdown of the host cell plasma membrane, which in turn led to influx of tissue culture medium containing the staphylolytic protease lysostaphin (Figure 3.1, Video

1). Host cells expressing the fluorescent escape marker YFP-cwt also showed decreasing fluorescence indicating loss of membrane integrity accompanied by the formation of huge membrane blebs. Lysis of *S. aureus* 6850-infected cells was further proven, as release of the cytoplasmic enzyme LDH (Figure 3.2B) and staining with the membrane-impermeable dye 7AAD (Figure 3.3D) was detected. The timing of *S. aureus*-induced host cell lysis was visualized using the membrane-impermeant, small fluorescent dye Alexa Fluor 633 hydrazide (AF633) (Figure 3.15A and B, Video 4). Accumulation of the fluorescent dye in the infected cell coincided with the formation of huge membrane blebs, after host cell contraction and bacterial replication occurred. Uninfected or Cowan I-infected cells were not stained with Alexa Fluor 633 hydrazide.

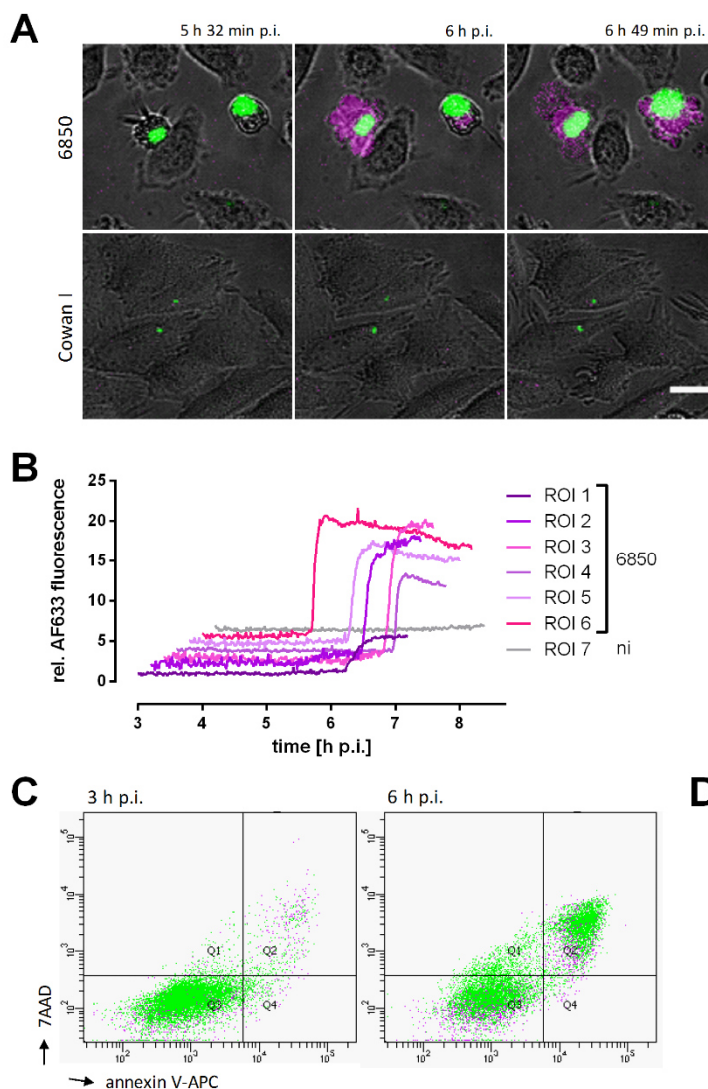


Figure 3.15: Cytotoxic *S. aureus* induces host cell lysis.

(A, B) Live cell imaging of HeLa cells infected with *S. aureus* 6850 GFP or Cowan I GFP after addition of Alexa Fluor 633 hydrazide (AF633) showed permeabilization of the host cell plasma membrane by cytotoxic *S. aureus* 6850. Stills of representative cells (A, green: *S. aureus*, magenta: AF633, gray: BF, scale bar: 20 μ m) and quantification of the relative AF633 fluorescence over the time period of infection in single, uninfected (ni) and infected cells (6850) (B) are shown. (C) HeLa cells infected with *S. aureus* 6850 were stained with annexin V-APC and 7AAD at 3 and 6 h p.i.. Scatter plots of flow cytometric analysis are shown. (D) Immunoblot analysis of *S. aureus* 6850- or Cowan I-infected HeLa cells to detect phosphorylation of MLKL. Anti-MLKL, anti-pMLKL (Ser358) and anti-GAPDH (loading control) antibodies were used.

Implementation of an apoptosis detection assay by staining of cells with annexin V and 7AAD revealed no typical apoptotic behavior of *S. aureus* 6850-infected cells (Figure 3.15C, Figure 3.8B and C). Rather, a simultaneous staining of infected cells with both markers was observed,

instead of initial acquisition of annexin V followed by 7AAD-staining. A form of regulated necrosis, called necroptosis (Linkermann and Green, 2014), is executed by MLKL, which inserts into cell membranes upon its phosphorylation leading to cell lysis. However, in *S. aureus*-infected cells no clear phosphorylation of MLKL was detected (Figure 3.15). The protein concentration of MLKL was decreased at 6 h p.i. in *S. aureus* 6850-infected cells compared to Cowan I-infected cells, whereas the loading control (GAPDH) indicated no reduction of the total protein concentration.

3.2.5 Cellular H₂O₂ is elevated during *S. aureus* intracellular infection

Reactive oxygen species (ROS) may also play a role in *S. aureus*-induced host cell death. Aside from antimicrobial defence, ROS were shown to participate in intrinsic apoptosis, parthanatos or MPT-driven necrosis (Redza-Dutordoir and Averill-Bates, 2016). In *S. aureus*-infected HeLa cells an increase in cellular H₂O₂ was detected using a cell line expressing a genetically encoded fluorescent indicator for intracellular H₂O₂ (Figure 3.16A and B, Video 5)¹ (Bilan et al., 2013).

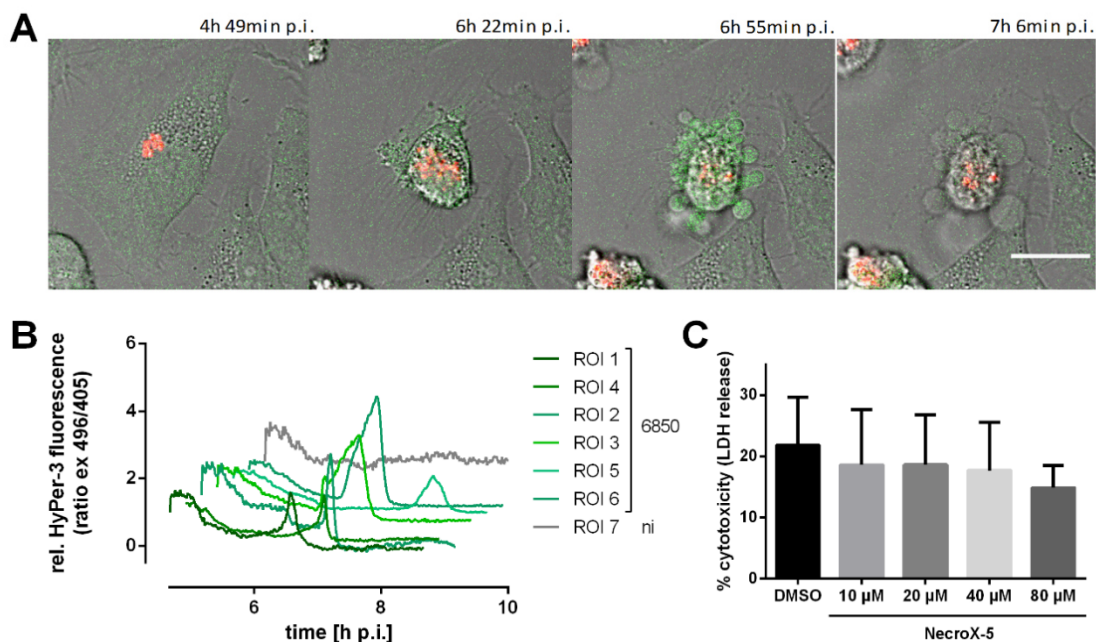


Figure 3.16: Intracellular *S. aureus* induces production of reactive oxygen species.

(A, B) HeLa HyPer-3 cells were infected with *S. aureus* 6850 mRFP and subjected to live cell imaging. The relative amount of intracellular H₂O₂ was determined by calculating the ratio of 496 nm to 405 nm excitation of HyPer-3. Stills from time-lapse imaging are shown (A, red: *S. aureus*, green: HyPer-3 (ratio ex. 496/405 nm), gray: BF, scale bar: 20 μm) and quantification of rel. HyPer-3 fluorescence (ratio ex. 496/405 nm) of single, infected or uninfected cells (ROI) as a function of time was performed (B). (C) LDH release was determined after treatment of HeLa cells with increasing concentrations of NecroX-5 (10, 20, 40 and 80 μM) or DMSO as solvent control prior to infection with *S. aureus* 6850 (n=2).

¹ Performed in cooperation with Simone Vormittag, Master student

The rise in ROS occurred between 6 and 8 h p.i. with *S. aureus* 6850, after host cell contraction and intracellular replication of the pathogen. The timing was reminiscent of activation of effector caspases (Figure 3.10C, Video 3) and host cell lysis (Figure 3.15A, Video 4). Uninfected cells did not show an increase in H₂O₂. Treatment of *S. aureus* 6850-infected HeLa cells with NecroX-5, an inhibitor of mitochondrial oxidative stress (Thu et al., 2012), led to a concentration-dependent reduction of host cell death, but could only partially inhibit cell death (Figure 3.16C). The highest concentration of NecroX-5 applied (80 μM) led to a decrease of *S. aureus*-induced cytotoxicity by 32 %, although this was not statistically significant.

3.2.6 Intracellular *S. aureus* induces cellular Ca²⁺ perturbations to promote host cell death

3.2.6.1 Intracellular *S. aureus* triggers cytosolic Ca²⁺ rise

A genome-wide shRNA screen to identify host cell factors involved in *S. aureus*-induced cell death revealed a possible role of Ca²⁺ (Winkler, 2015). It was therefore interesting to investigate, whether intracellular *S. aureus* induces Ca²⁺ fluxes in the host cell and thus activates signaling pathways and Ca²⁺-sensing proteins implicated in cell death mechanisms. To measure changes in cellular Ca²⁺ concentration an indicator cell line, HeLa R-Geco, was utilized, which changes fluorescence intensity upon elevation or reduction of cytosolic Ca²⁺. Infection of this cell line with *S. aureus* 6850 and subsequent live cell imaging showed a massive increase in cytosolic Ca²⁺ (Figure 3.17A, Video 6). The cytosolic Ca²⁺ rise occurred after the onset of bacterial intracellular replication and after host cell shrinkage, but was followed by the formation of huge membrane blebs and loss of bacterial and cellular fluorescence. Analysis of single cells allowed relative quantification of the cytosolic Ca²⁺ concentration and revealed a roughly two- to six-fold increment of R-Geco fluorescence in infected cells between 5 and 7 h p.i. (Figure 3.17B). The high cytosolic Ca²⁺ level was sustained for approximately several minutes up to one hour. Uninfected cells did not exhibit any major changes in cellular Ca²⁺ concentration.

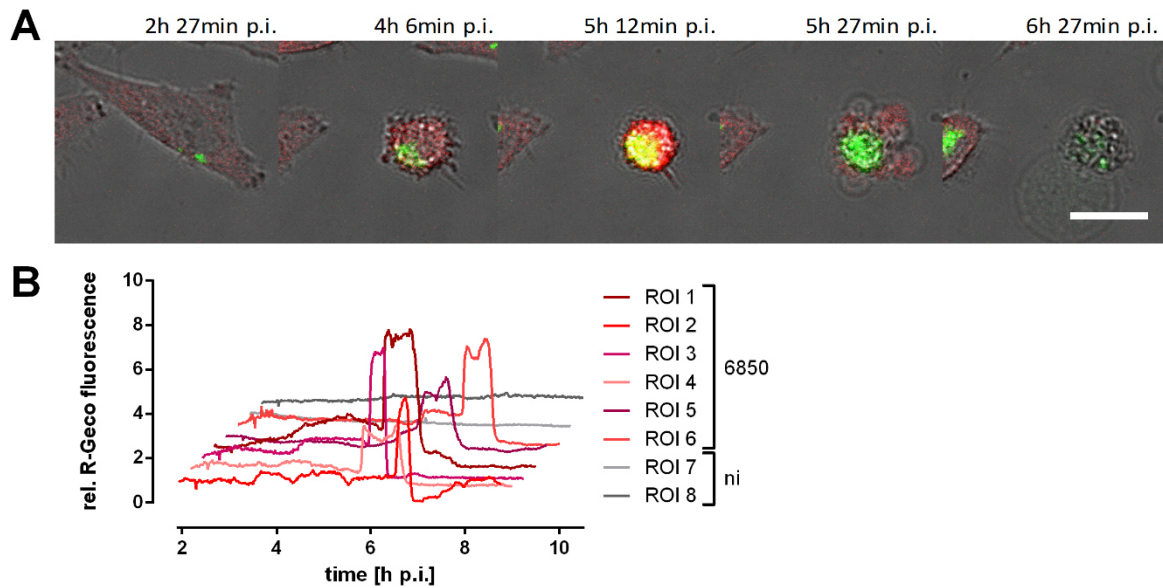


Figure 3.17: Infection with *S. aureus* leads to a massive cytosolic Ca^{2+} increase in epithelial cells. HeLa R-Geco cells were infected with *S. aureus* 6850 GFP and infection was visualized by live cell imaging. (A) Stills from time-lapse imaging are shown (green: *S. aureus*, red: R-Geco, gray: BF, scale: 25 μm). (B) Quantification of relative R-Geco fluorescence of single cells (ROI) infected with *S. aureus* 6850 or not infected (ni) was performed over the course of infection.

3.2.6.2 Changes in mitochondrial and ER Ca^{2+} concentration induced by intracellular *S. aureus*

The rise in cytosolic Ca^{2+} in *S. aureus*-infected cells (Figure 3.17) could result from an influx of Ca^{2+} ions through permeable pores in the plasma membrane or a release of Ca^{2+} from intracellular stores of the host cell. In order to investigate alterations in Ca^{2+} concentration of the intracellular Ca^{2+} -storing organelles during infection with *S. aureus*, reporter cell lines expressing a red-fluorescent mitochondrial- or ER-targeted fluorescent Ca^{2+} sensor (ER-LAR-Geco and Mito-LAR-Geco) in addition to a green-fluorescent cytosolic Ca^{2+} indicator (G-Geco) were employed. The localization of both ER-LAR-Geco and Mito-LAR-Geco was compartment specific with a typical distribution of the fluorophores for ER and mitochondria, respectively (Figure 3.20C and D). HeLa Mito-LAR-Geco G-Geco were infected with *S. aureus* 6850 and fluorescence was monitored over the time course of infection (Figure 3.18). A fluorescence increase upon infection with *S. aureus* was observed for both the cytosolic (G-Geco) as well as the mitochondrial Ca^{2+} indicator (Mito-LAR-Geco) (Figure 3.18A, Video 7). Quantification of single cell fluorescence uncovered that the increment in cytosolic Ca^{2+} in *S. aureus*-infected cells was followed by an increase of mitochondrial Ca^{2+} concentration within minutes (Figure 3.18B). Interestingly, Mito-LAR-Geco fluorescence did not reach basal levels after the rise in contrast to G-Geco fluorescence. No or only a partial decline of mitochondrial Ca^{2+} concentration was detected after the initial rise.

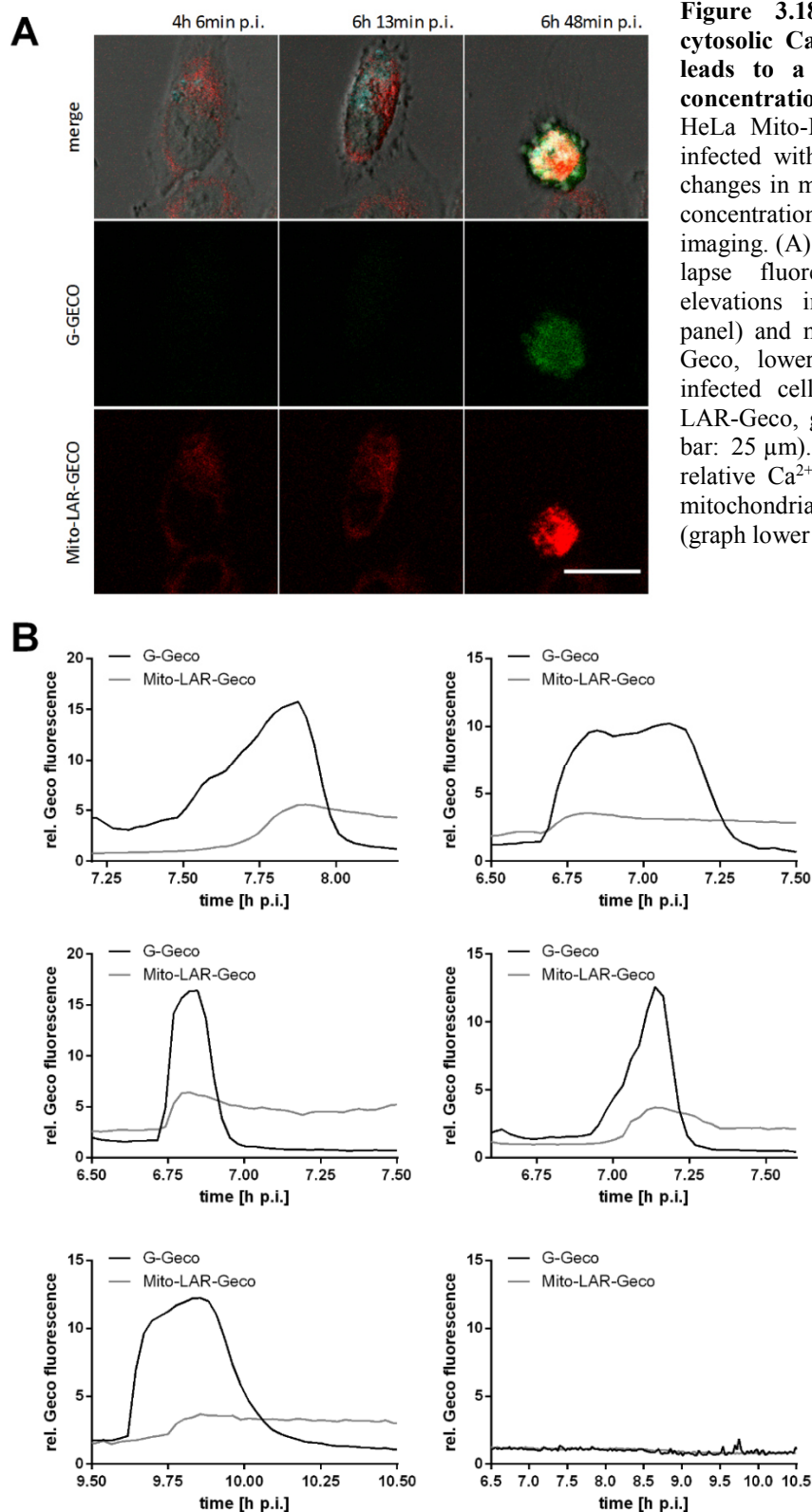


Figure 3.18: The *S. aureus* triggered cytosolic Ca^{2+} increase in epithelial cells leads to a rise of mitochondrial Ca^{2+} concentration.

HeLa Mito-LAR-Geco G-Geco cells were infected with *S. aureus* 6850 Cerulean and changes in mitochondrial and cytosolic Ca^{2+} concentration were monitored by live cell imaging. (A) Representative stills from time-lapse fluorescence microscopy showed elevations in cytosolic (G-Geco, middle panel) and mitochondrial Ca^{2+} (Mito-LAR-Geco, lower panel) in a *S. aureus* 6850 infected cell (cyan: *S. aureus*, red: Mito-LAR-Geco, green: G-Geco, gray: BF, scale bar: 25 μm). (B) Relative quantification of relative Ca^{2+} concentrations in cytosol and mitochondria of single, infected or uninfected (graph lower row right) cells.

The second major intracellular Ca^{2+} store is the endoplasmic reticulum (ER). Similar to mitochondrial Ca^{2+} concentration, changes in ER Ca^{2+} amount in *S. aureus*-infected HeLa cells were detected using ER-LAR-Geco, a red fluorescent ER-targeted Ca^{2+} indicator, in combination with green fluorescent cytosolic Ca^{2+} sensor (G-Geco) (Figure 3.19).

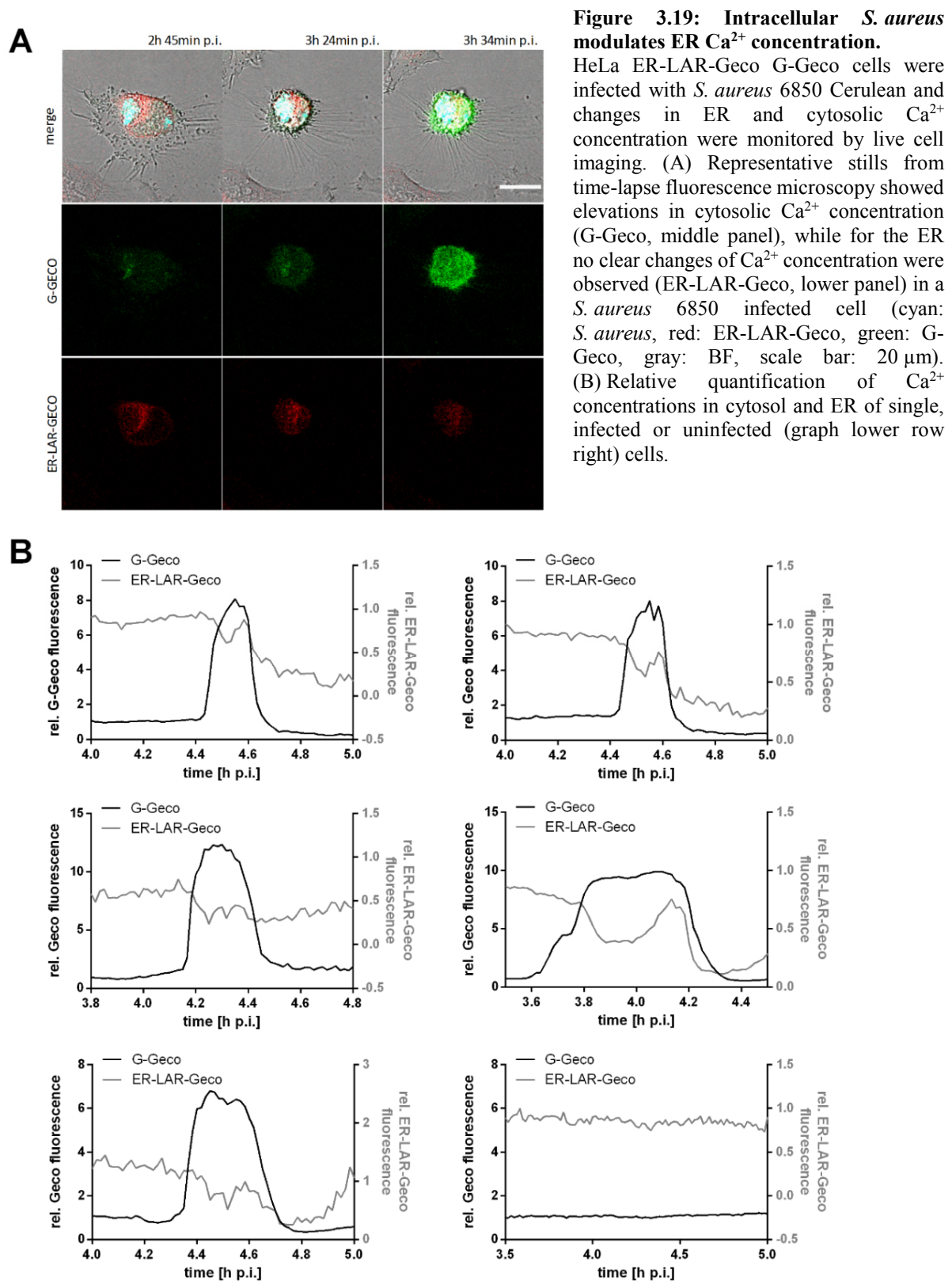


Figure 3.19: Intracellular *S. aureus* modulates ER Ca^{2+} concentration.

HeLa ER-LAR-Geco G-Geco cells were infected with *S. aureus* 6850 Cerulean and changes in ER and cytosolic Ca^{2+} concentration were monitored by live cell imaging. (A) Representative stills from time-lapse fluorescence microscopy showed elevations in cytosolic Ca^{2+} concentration (G-Geco, middle panel), while for the ER no clear changes of Ca^{2+} concentration were observed (ER-LAR-Geco, lower panel) in a *S. aureus* 6850 infected cell (cyan: *S. aureus*, red: ER-LAR-Geco, green: G-Geco, gray: BF, scale bar: 20 μm). (B) Relative quantification of Ca^{2+} concentrations in cytosol and ER of single, infected or uninfected (graph lower row right) cells.

HeLa cells expressing these Ca^{2+} indicators were infected with *S. aureus* 6850 and fluorescence was monitored over time. In contrast to mitochondria, no clear changes in ER Ca^{2+} concentration were observed in infected host cells, while the cytosolic Ca^{2+} concentration increased (Figure 3.19A, Video 8). However, quantification of ER-LAR-Geco fluorescence

disclosed small changes coinciding with the huge increase in cytosolic Ca^{2+} (Figure 3.19B). Concomitant with the onset of cytosolic Ca^{2+} rise, a decrease in ER Ca^{2+} concentration was observed, while ER-LAR-Geco fluorescence increased minutes later to then drop again with the decline of G-Geco fluorescence. Compared to the changes in cytosolic and mitochondrial Ca^{2+} concentration, the shift of the ER-LAR Geco fluorescence was rather small.

To determine, whether intracellular *S. aureus* induces only minor changes in ER Ca^{2+} concentration or if the dynamic range of the ER Ca^{2+} indicator is reduced, HeLa ER-LAR-Geco G-Geco cells were treated with Ca^{2+} perturbing agents (Figure 3.20). Ionomycin, an ionophore produced by *Streptococcus conglobatus*, led to a quick and high increase of cytosolic Ca^{2+} , while the amount of Ca^{2+} in the ER dropped (Figure 3.20A). Similarly, addition of the SERCA inhibitor thapsigargin resulted in a transient rise of Ca^{2+} concentration in the cytosol and depletion of Ca^{2+} from the ER (Figure 3.20B). However, both substances induced only small changes in ER-LAR-Geco fluorescence when compared to G-Geco. The results indicate that the ER Ca^{2+} indicator was functional and that even high concentrations of Ca^{2+} perturbing agents did not trigger a stronger shift of ER-LAR-Geco fluorescence when compared to *S. aureus* infection.

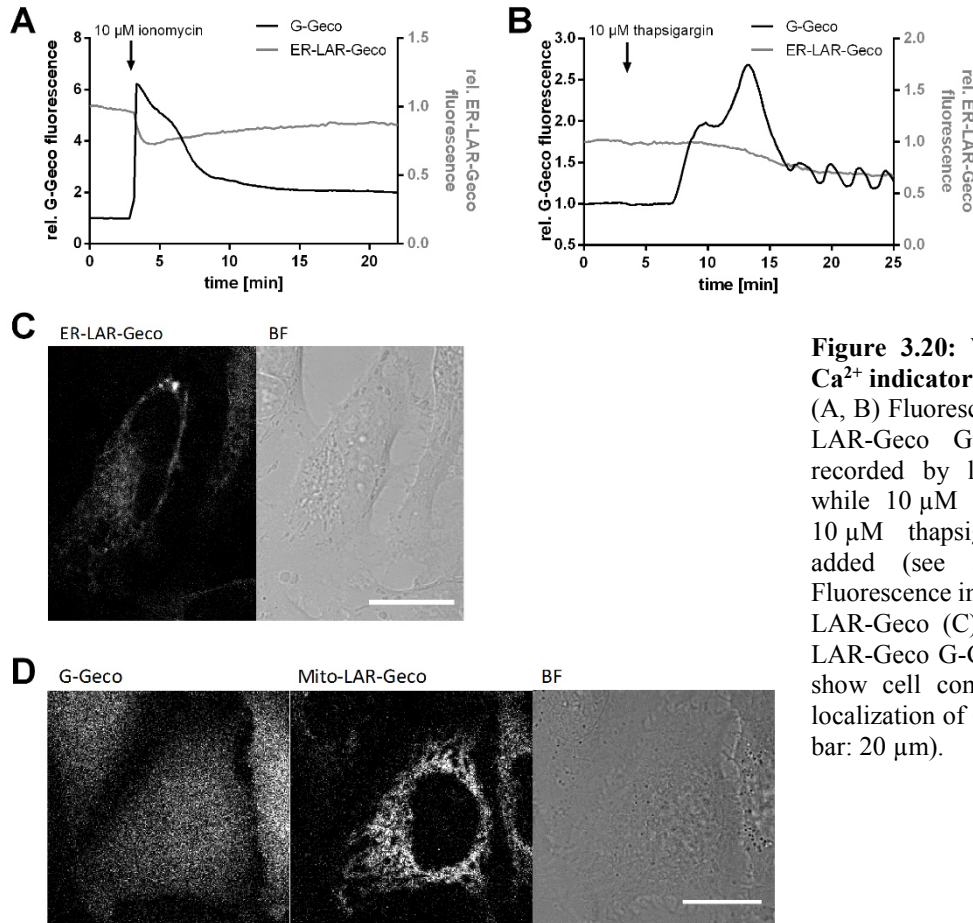


Figure 3.20: Validation of the Ca^{2+} indicator cell lines.

(A, B) Fluorescence of HeLa ER-LAR-Geco G-Geco cells was recorded by live cell imaging, while 10 μM ionomycin (A) or 10 μM thapsigargin (B) were added (see arrows). (C, D) Fluorescence images of HeLa ER-LAR-Geco (C) and HeLa Mito-LAR-Geco G-Geco (D) cell lines show cell compartment specific localization of Ca^{2+} sensors (scale bar: 20 μm).

3.2.6.3 Store-operated Ca^{2+} entry is not implicated in *S. aureus*-induced host cell death

As a decrease in ER Ca^{2+} concentrations was observed in *S. aureus*-infected cells, which occurred rather simultaneously with the cytosolic Ca^{2+} increase (Figure 3.19B), it is conceivable that store-operated Ca^{2+} entry (SOCE) is implicated in *S. aureus*-induced cell death. Here, Ca^{2+} depletion from the ER activates Ca^{2+} entry across the plasma membrane. To test this, the inhibitor 2-aminoethyl diphenylborinate (2-APB) was used, which blocks SOCE activity at high concentrations. HeLa cells were pre-treated for 1 h with 30 μM 2-APB and subsequently infected with *S. aureus* 6850. Staining of infected cells with 7AAD revealed that 2-APB treatment significantly reduced cytotoxicity of *S. aureus* by 83 % when compared to DMSO-treated cells (Figure 3.21A).

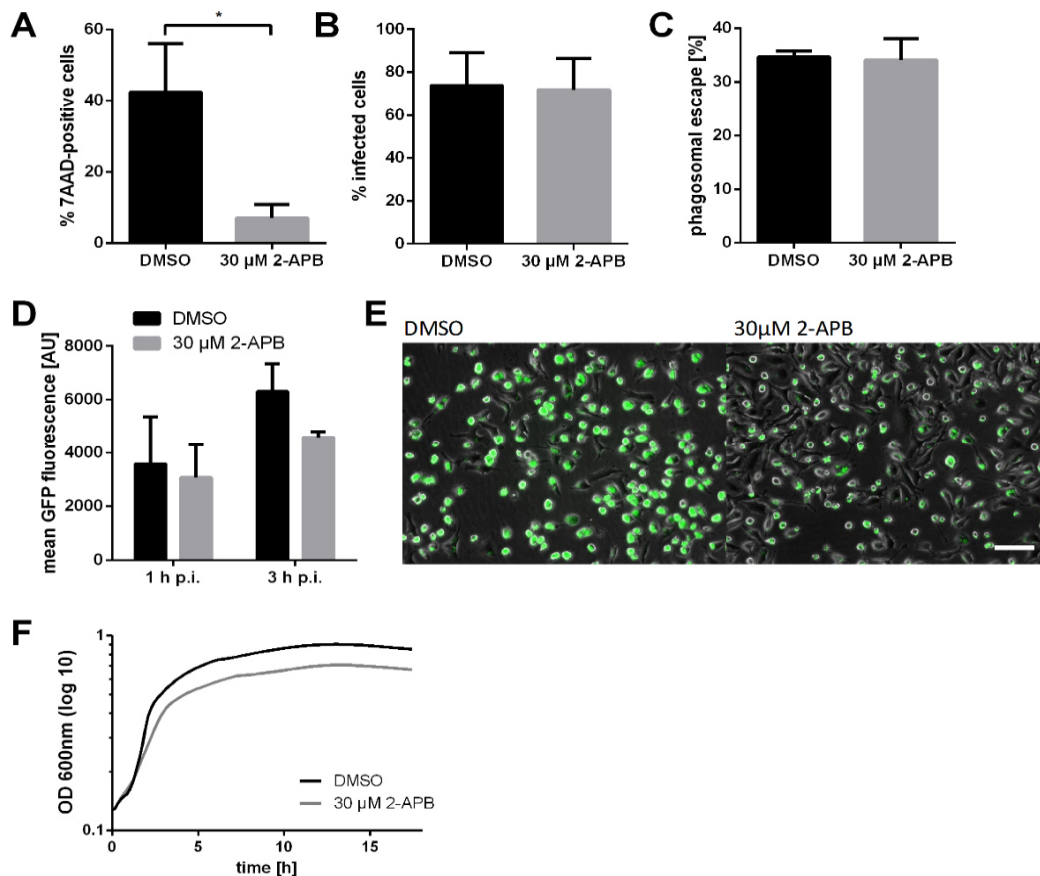


Figure 3.21: 2-APB reduces *S. aureus* induced cytotoxicity, but also attenuates bacterial replication.

(A-E) HeLa or HeLa YFP-CWT (D) cells were treated with 30 μM 2-APB or DMSO as solvent control 1 h prior to infection with *S. aureus* 6850 (A), 6850 GFP (B, C, E) or 6850 mRFP (D). (A) Cytotoxicity was determined at 6 h p.i. by 7AAD staining. (B) Number of infected host cells, i.e. GFP-positive cells, was measured at 1 h p.i.. (C) Translocation of bacteria into the host cell cytosol was determined by quantification of co-localization of intracellular bacteria and the cytosolic escape marker YFP-CWT at 4 h p.i. ($n=2$). (D) The relative number of intracellular bacteria was identified by measuring the mean fluorescence intensity of infected cells at 1 and 3 h p.i. ($n=2$). (E) Fluorescence microscopy revealed less contracted host cells and intracellular bacteria after treatment with 2-APB in contrast to DMSO at 6 h p.i. (green: *S. aureus*, gray: phase contrast, scale bar: 100 μm). (F) Optical density (OD) at 600 nm of *S. aureus* 6850 treated with 30 μM 2-APB or DMSO in RPMI medium without FBS was determined for 17.5 h at 10 min-intervals. Statistical analysis was performed by unpaired t-test ($*P<0.05$).

Invasion and phagosomal escape of *S. aureus* 6850 were not affected by 2-APB treatment (Figure 3.21B and C). Nevertheless, a lower number of intracellular bacteria was detected at 3 h p.i. in 2-APB-treated cells in comparison to the DMSO control, although the difference was not significant (Figure 3.21D). There was a distinct difference in the number of intracellular bacteria when comparing 2-APB treatment ($4586 \text{ AFU} \pm 209$) and DMSO control ($6305 \text{ AFU} \pm 1041$). This result was also obtained at 6 h p.i., when HeLa cells pre-treated with 2-APB contained considerably less intracellular bacteria compared to cells treated with DMSO (Figure 3.21E). However, *S. aureus* showed impaired growth in medium the presence of $30 \mu\text{M}$ 2-APB when compared to the solvent control (DMSO) (Figure 3.21F).

Ca^{2+} signaling was studied in *S. aureus*-infected HeLa R-Geco cells treated with 2-APB, however the inhibitor was only added at approximately 3 h p.i. in order to avoid effects on bacterial replication (Figure 3.22, Video 9). Time-lapse imaging showed that intracellular *S. aureus* was replicating despite 2-APB treatment (Figure 3.22A). Still, addition of the inhibitor did not abolish *S. aureus* triggered cytosolic Ca^{2+} increase. Quantification of R-Geco fluorescence showed no major impact on Ca^{2+} signals of single infected cells upon 2-APB treatment when compared to DMSO treatment (Figure 3.22B). For comparison purposes, the Ca^{2+} response of each measured cell was characterized by the maximal amplitude of relative R-Geco fluorescence and the latency from the time point of infection to this maximum amplitude. Both amplitude and latency of the cytosolic Ca^{2+} increase were not significantly affected by 2-APB treatment (Figure 3.22C and D).

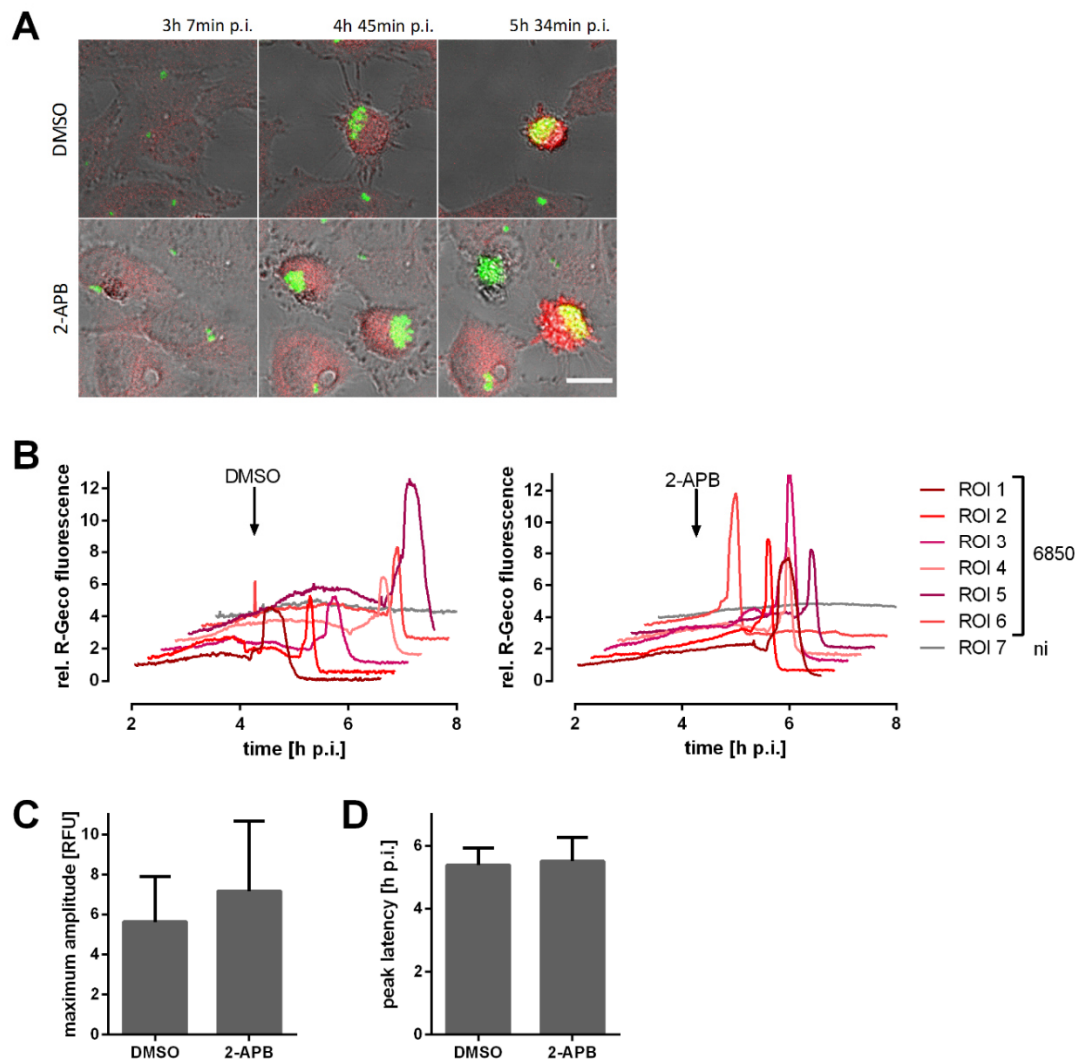


Figure 3.22: 2-APB treatment does not abolish *S. aureus* induced cytosolic Ca^{2+} increase.

HeLa R-Geco cells were infected with *S. aureus* 6850 GFP and cytosolic Ca^{2+} , i.e. R-Geco fluorescence, was measured by time-lapse imaging. At 3 h 7 min p.i. DMSO or 30 μM 2-APB were added. (A) Representative stills from time-lapse fluorescence microscopy showed elevations in cytosolic Ca^{2+} concentration independent of treatment, while intracellular bacteria replicated (green: *S. aureus*, red: R-Geco, gray: BF, scale bar: 20 μm). (B) Relative quantification of cytosolic Ca^{2+} concentrations of single infected (6850) or uninfected (ni) cells after DMSO (left) or 2-APB (right) treatment. (C) The peak amplitude of the relative R-Geco fluorescence of 7 to 11 single infected cells was quantified after DMSO or 30 μM 2-APB treatment. (D) The latency of the relative R-Geco fluorescence peak after *S. aureus* intracellular infection was determined and the mean value of 7 to 11 cells was calculated. Statistical analysis was performed by unpaired t-test.

3.2.6.4 *S. aureus* triggers Ca^{2+} influx via the host plasma membrane

In order to test, if the observed increase in cytoplasmic Ca^{2+} originated from the extracellular space, HeLa R-Geco cells were cultivated in Ca^{2+} -free cell culture medium. The cells were tested for Ca^{2+} concentration changes induced by ionomycin in presence and absence of Ca^{2+} and 0.2 mM of the selective Ca^{2+} chelator BAPTA (Figure 3.23A). The combination of Ca^{2+} -withdrawal and chelation with BAPTA resulted in a strong reduction of R-Geco fluorescence. Therefore, HeLa R-Geco cells were infected with *S. aureus* 6850 and after bacterial invasion and phagosomal escape, 3 h p.i., medium was replaced and cells were monitored for Ca^{2+}

concentration changes in presence and absence of extracellular calcium ions (Figure 3.23B and C, Video 10).

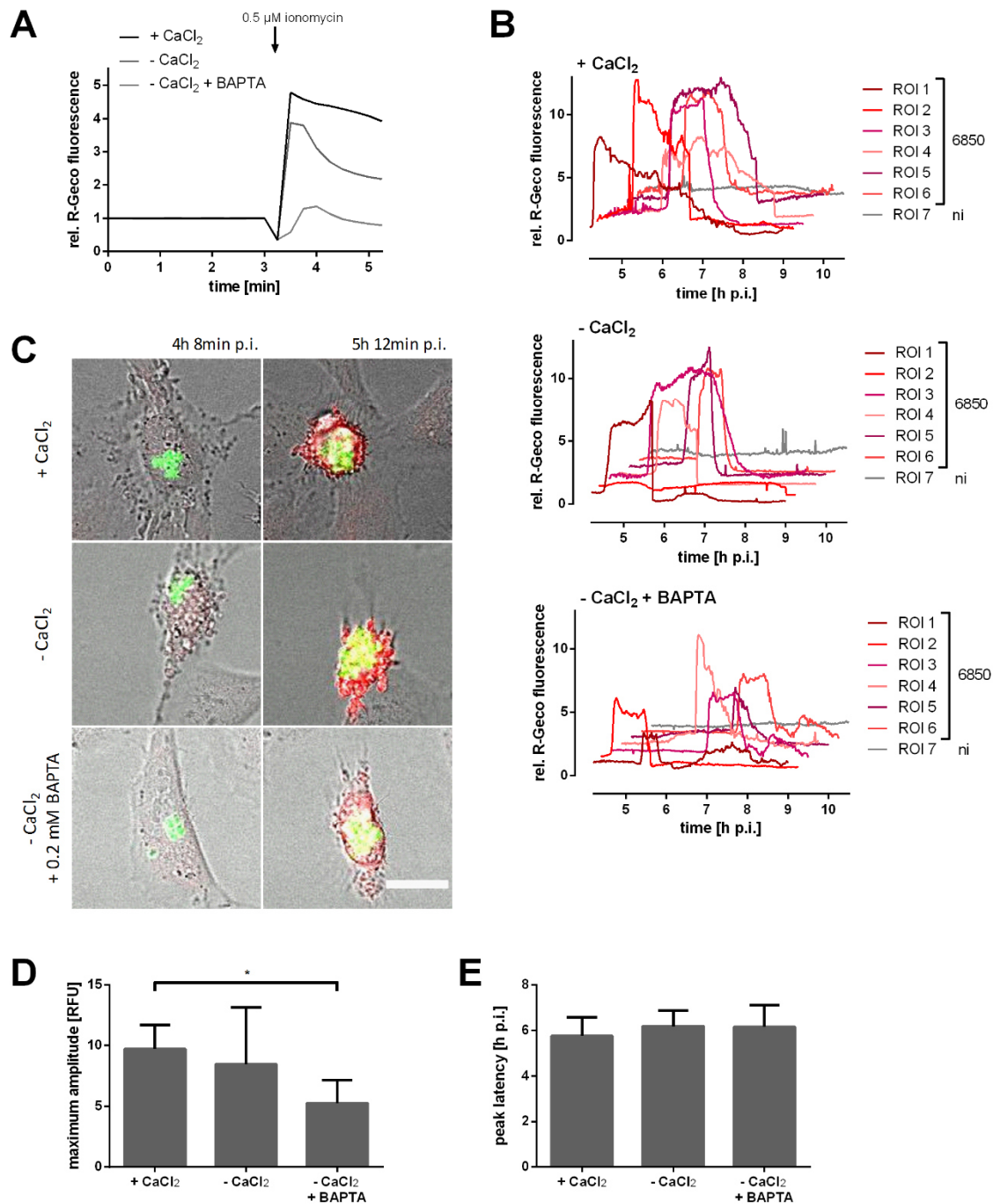


Figure 3.23: Removal of extracellular Ca²⁺ during *S. aureus* intracellular infection in epithelial cells.

(A) HeLa R-Geco cells were cultivated in medium with 1.8 mM CaCl₂, without CaCl₂ or without CaCl₂ and 0.2 mM BAPTA and 0.5 μM ionomycin were added while recording of R-Geco fluorescence. (B-E) HeLa R-Geco cells were infected with *S. aureus* 6850 GFP and 3 h p.i. medium with 1.8 mM CaCl₂ (+ CaCl₂), without CaCl₂ (- CaCl₂) or without CaCl₂ and 0.2 mM BAPTA (- CaCl₂ + BAPTA) was added. Subsequently, R-Geco fluorescence was monitored by live cell imaging. (B) Relative R-Geco fluorescence of single infected (6850) or uninfected (ni) cells was quantified over the time course of infection under the different conditions. (C) Representative stills of infected HeLa R-Geco cells with or without extracellular Ca²⁺ (green: *S. aureus*, red: R-Geco, gray: BF, scale bar: 20 μm). (D) The maximal amplitude of the relative R-Geco fluorescence of 6 to 11 single infected cells under the different conditions was determined. (E) The latency of maximal relative R-Geco fluorescence peak after *S. aureus* intracellular infection was determined in 6 to 11 single infected cells. Statistical analysis was performed by ordinary one-way ANOVA (**P*<0.05).

S. aureus triggered elevations in cytosolic Ca^{2+} under all tested conditions. However, quantification of the relative R-Geco fluorescence showed reduced *S. aureus*-induced cytosolic Ca^{2+} increases in infected cells, when extracellular Ca^{2+} was omitted from the medium. Additional chelation of residual extracellular calcium ions with BAPTA reduced the cytosolic Ca^{2+} peak significantly, whereas no temporal changes of the cytosolic Ca^{2+} rise were detected upon removal of extracellular Ca^{2+} (Figure 3.23C and D). Morphological differences of infected cells were not detected under the all tested conditions (Video 10).

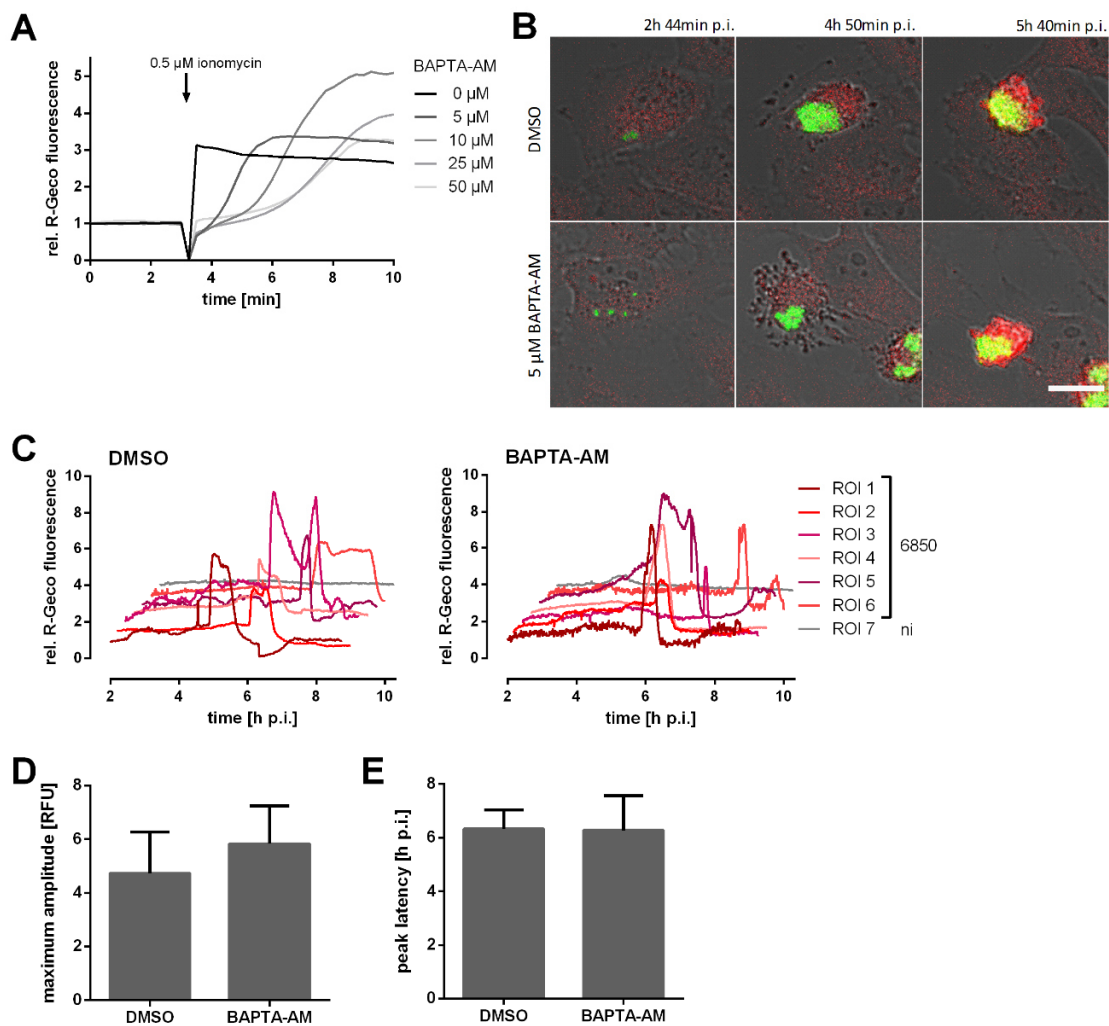


Figure 3.24: Chelation of intracellular Ca^{2+} during *S. aureus* infection of epithelial cells.

(A) HeLa R-Geco cells were treated with DMSO or 5, 10, 25 or 50 μM BAPTA-AM and while recording R-Geco fluorescence 0.5 μM ionomycin were added. (B-E) HeLa cells were infected with *S. aureus* 6850 GFP, 2 h p.i. DMSO or 5 μM BAPTA-AM were added and R-Geco fluorescence was monitored over time. (B) Stills of representative infected cells are depicted (green: *S. aureus*, red: R-Geco, gray: BF, scale bar: 20 μm). (C) Relative R-Geco fluorescence of single infected (6850) or uninfected (ni) cells was quantified over the time course of infection under the different conditions. (D) The maximum amplitude of the relative R-Geco fluorescence of 6 to 11 single infected cells under the different conditions was determined. (E) The latency of relative R-Geco fluorescence peak after *S. aureus* intracellular infection in 6 to 11 single infected cells was calculated. Statistical analysis was performed by unpaired t-test.

Next, intracellular Ca^{2+} ions were chelated using the cell-permeable BAPTA-AM. Increasing concentrations of BAPTA-AM delayed, but did not reduce ionomycin-induced cytosolic Ca^{2+} increase (Figure 3.24A). Rather higher values of relative R-Geco fluorescence were detected after addition of ionomycin in contrast to the control. Since concentrations of BAPTA-AM above 10 μM were cytotoxic to HeLa cells after several hours of incubation (data not shown), infected HeLa R-Geco cells were treated with 5 μM BAPTA-AM after 2 h of infection and R-Geco fluorescence was recorded over time. Differences between BAPTA-AM treated and DMSO treated cells were not observed (Figure 3.24B, Video 11). Infected host cells rounded and cytosolic Ca^{2+} increase was observed before formation of membrane blebs and cell lysis. Quantification of relative R-Geco fluorescence of single infected cells did not reveal a clear difference between DMSO and BAPTA-AM treatment (Figure 3.24C). The amplitude and latency of the maximal Ca^{2+} concentration measured was not significantly changed by BAPTA-AM treatment (Figure 3.24C and D).

3.2.6.5 Effector caspase activation and plasma membrane permeabilization follow cytosolic Ca^{2+} overload in *S. aureus*-infected cells

To elucidate the timing of effector caspase activation and its correlation to cytosolic Ca^{2+} increase during *S. aureus* intracellular residence, HeLa R-Geco cells were infected with *S. aureus* 6850 and CellEvent™ Caspase-3/7 Green Detection Reagent (CellEvent Caspase 3/7) was added to visualize activation of caspases 3 and 7 by live cell imaging (Figure 3.25, Video 12). First, an increase in R-Geco fluorescence was observed, which was superseded by an increase in CellEvent Caspase 3/7 fluorescence (Figure 3.25A). Quantification of the fluorescence of individual cells showed that CellEvent Caspase 3/7 fluorescence was activated when R-Geco fluorescence reached its maximum (Figure 3.25B). By contrast, fluorescence of CellEvent and R-Geco did not increase notably in non-infected cells.

Caspases were shown to cleave key components of the Ca^{2+} regulatory system (Hirota et al., 1999; Schwab et al., 2002). As inhibition of caspases attenuated *S. aureus*-induced cell death (Figure 3.8), HeLa G-Geco cells were treated with 80 μM of the caspase inhibitor Z-VAD-fmk prior to infection with *S. aureus* 6850. However, caspase inhibition did not abrogate bacteria-induced increases in cytosolic Ca^{2+} concentration (Figure 3.26, Video 13). Infected cells displayed elevations in G-Geco fluorescence (Figure 3.26A). Relative quantification of fluorescence failed to detect clear differences in cytosolic Ca^{2+} signals in infected HeLa cells after treatment with Z-VAD-fmk when compared to the DMSO control (Figure 3.26B). The

amplitude of the Ca^{2+} signal was not altered upon caspase inhibition, but the Ca^{2+} peak was delayed (Figure 3.26C and D).

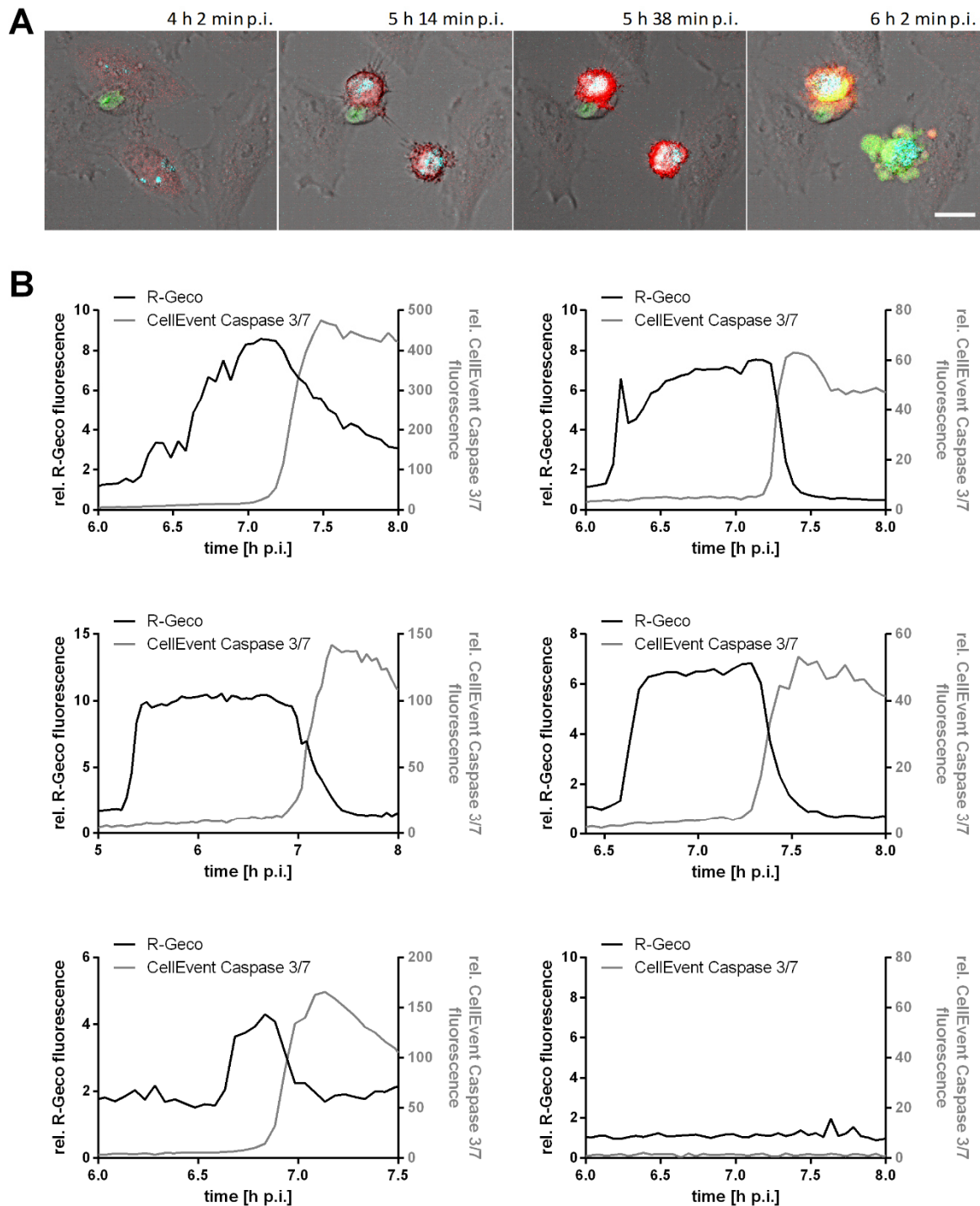
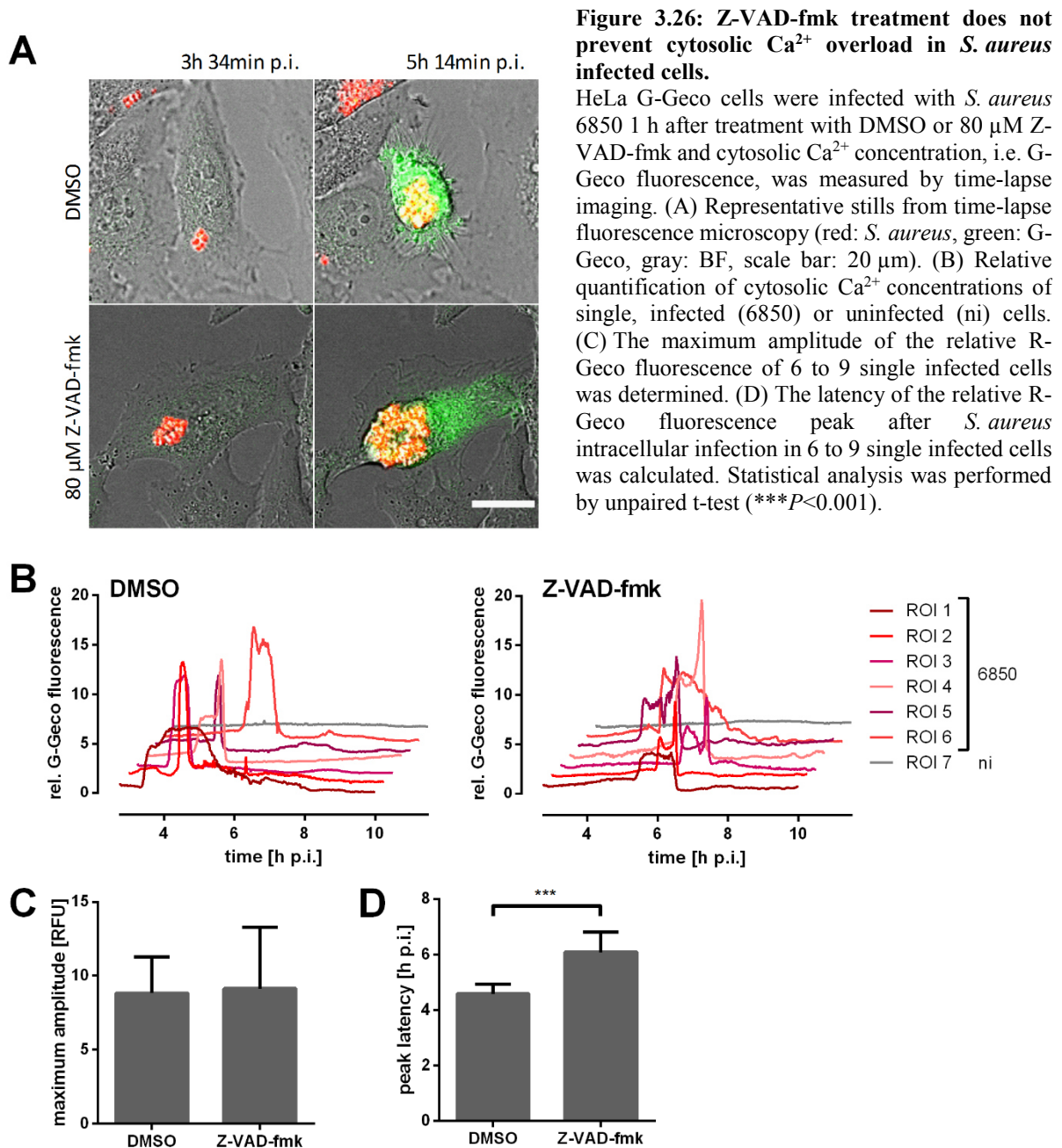


Figure 3.25: Activation of effector caspase follows cytosolic Ca^{2+} increase in *S. aureus* infected cells.

HeLa R-Geco cells were infected with *S. aureus* 6850 Cerulean and CellEvent™ Caspase-3/7 Green Detection Reagent (CellEvent Caspase 3/7) was added prior to live cell imaging. (A) Representative stills from time-lapse imaging are shown (cyan: *S. aureus*, red: R-Geco, green: CellEvent Caspase 3/7, gray: BF, scale bar: 20 μm). (B) The relative R-Geco and CellEvent Caspase 3/7 fluorescence of single uninfected (graph lower row right) or *S. aureus* 6850-infected cells was quantified over time.



Based on morphological observations of the infected host cells, the cytosolic Ca²⁺ increase occurred prior to cell lysis. The host cell completely lost R-Geco fluorescence only after the Ca²⁺ concentration had risen (Figure 3.17). Additionally, lysis of intracellular bacteria due to presence of lysostaphin in the culture medium was observed after the Ca²⁺ increase. This confirms the assumption about the chronological sequence of events, in which the Ca²⁺ concentration first increases in *S. aureus*-infected cells and then the cell lyses. Staining of *S. aureus*-infected HeLa R-Geco cells with small and membrane-impermeant fluorophore Alexa Fluor 633 hydrazide (AF633) could prove this theory (Figure 3.27, Video 14). Accumulation of the fluorescent dye in the infected host cell ensued the cytosolic Ca²⁺ rise (Figure 3.27A). Quantification of the relative fluorescence of single, *S. aureus* 6850-infected

cells revealed that AF633 fluorescence started to increase when the R-Geco fluorescence reached its maximum (Figure 3.27B). In uninfected cells increases in fluorescence were not observed. Thus, the activation of effector caspases in *S. aureus* 6850-infected epithelial cells thus coincides with cell lysis, whereas the increase in cytosolic Ca^{2+} precedes both events.

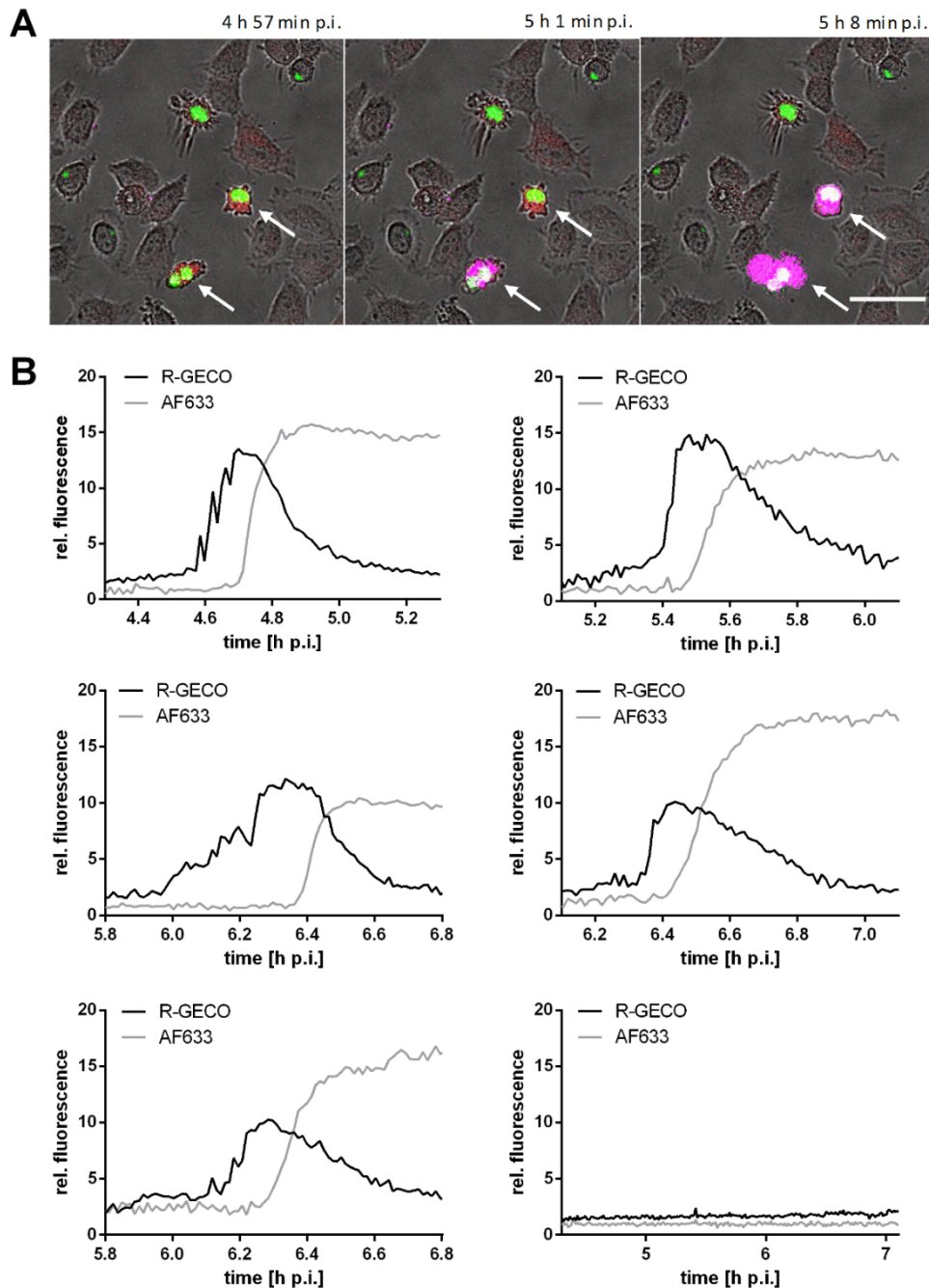


Figure 3.27: The cytosolic Ca^{2+} increase in *S. aureus* infected cells is followed by cell lysis.

HeLa R-Geco cells were infected with *S. aureus* 6850 GFP and live cell imaging was performed after addition of the fluorescent dye Alexa Fluor 633 hydrazide. (A) Stills from time-lapse imaging showed increase in R-Geco fluorescence preceding accumulation of AF633 in infected host cells (see arrows; green: *S. aureus*, red: R-Geco, magenta: AF633, gray: BF, scale: 50 μm). (B) Relative fluorescence of single cells infected with *S. aureus* 6850 or single uninfected cells (graph lower row right) was quantified over the course of infection.

3.2.6.6 Cytosolic Ca^{2+} overload is not a common feature of apoptosis

To test, if the cytosolic Ca^{2+} increase in *S. aureus*-infected cells is a common phenomenon in dying cells, HeLa cells were treated with different cytotoxic agents and R-Geco fluorescence of single cells was monitored (Figure 3.28, Video 15).

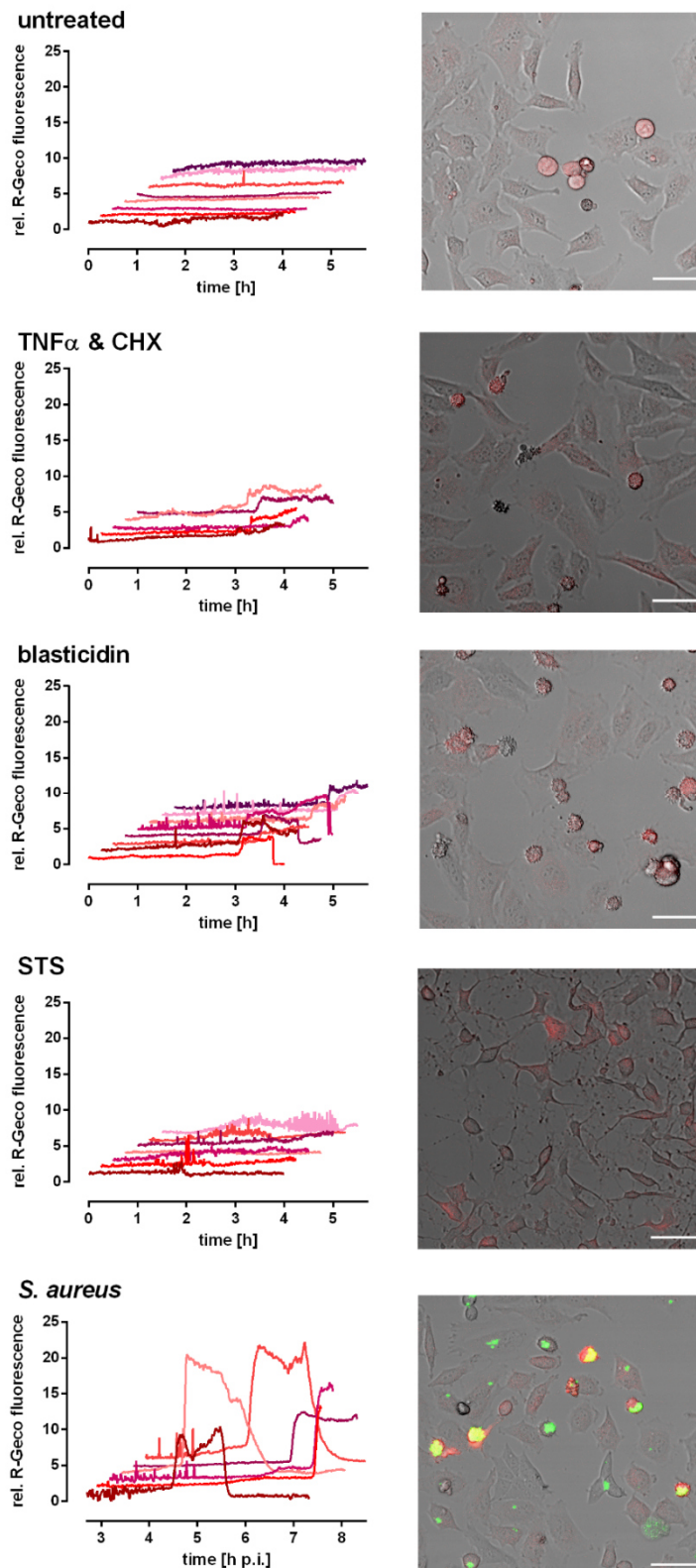


Figure 3.28: Ca^{2+} signaling in different types of cell death.

HeLa R-Geco cells remained untreated, were treated with 5 $\mu\text{g/ml}$ CHX and 5 ng/ml TNF α , 50 $\mu\text{g/ml}$ blasticidin or 10 μM staurosporine (STS) or infected with *S. aureus* 6850 GFP. Live cell imaging was performed and the R-Geco fluorescence of single cells with cell death morphology was measured over the period of imaging (left). Representative images of differently treated cells are shown (right, red: R-Geco, green: *S. aureus*, gray: BF, scale bar: 50 μm).

In contrast to the strong increase in cytosolic Ca^{2+} induced by intracellular *S. aureus*, only small Ca^{2+} elevations or oscillations were observed in HeLa cells treated with either 5 ng/ml $\text{TNF}\alpha$ and 5 $\mu\text{g}/\text{ml}$ cycloheximide (CHX), 50 $\mu\text{g}/\text{ml}$ blasticidin or 10 μM staurosporine (STS). $\text{TNF}\alpha/\text{CHX}$ and blasticidin treatment induced cell shrinkage and rounding of cells reminiscent of *S. aureus*-induced cell death, but resulted only in small cytosolic Ca^{2+} elevations, whereas a more necrotic phenotype was observed for STS-treated cells, which was accompanied by only minor Ca^{2+} oscillations. This shows that only infection with *S. aureus* results in cytosolic Ca^{2+} overload when compared to the cytotoxic agents used in the present study.

3.2.7 Calpains are not essential for induction of host cell death by intracellular *S. aureus*

3.2.7.1 Calpains are activated by intracellular *S. aureus*

A family of Ca^{2+} -activated cysteine proteases, the calpains, is implicated in cell death processes, such as apoptosis (Lopatniuk and Witkowski, 2011). The Ca^{2+} overload triggered by intracellular *S. aureus* could mediate host cell death by the activation of calpains. An indication for activation of calpains is the presence of autocatalytically cleaved forms of this protease (Melloni et al., 1992). The molecular mass of calpain 1 (80 kDa) is reduced to 78 kDa and then to 76 kDa, while autolysis of the small subunit calpain 4 results in an 18 kDa-fragment after a series of three processing steps. In *S. aureus* 6850-infected HeLa cells autolysed calpains were detected after 4.5 h p.i. by immunoblot analysis (Figure 3.29A). Uninfected cells, infection with the non-cytotoxic *S. aureus* Cowan I or infections at earlier time points (1 and 3 h p.i.) did not result in accumulation calpain autolysis products. Further, protein levels of the endogenous calpain-specific inhibitor calpastatin were reduced 4.5 h p.i. in cells infected with *S. aureus* 6850. The calpain-specific cleavage of the 280 kDa-large cytoskeletal protein α -spectrin can also be used as a biomarker for calpain activation (Zhang et al., 2009). In *S. aureus* 6850-infected HeLa cells the calpain-specific 150 kDa- and 145 kDa-large breakdown products of α -spectrin were detected at 5 and 6 h p.i. (Figure 3.29B). A weak band was also observed at a size below 130 kDa at those time points, which likely represents the caspase-specific 120 kDa-large breakdown product of α -spectrin (Figure 3.29B). Infection with Cowan I did not induce cleavage of α -spectrin in HeLa cells. Next, the presence of activated calpains in *S. aureus*-infected host cells was determined by applying a fluorogenic calpain substrate (Boc-Leu-Met-CMAC). *S. aureus* 6850- or Cowan I-infected cells were loaded with Boc-Leu-Met-CMAC and increased fluorescence was specifically observed in cells infected with the cytotoxic strain 6850 (Figure 3.29C). Taken together, these results suggest that intracellular *S. aureus* 6850 triggers activation of calpains.

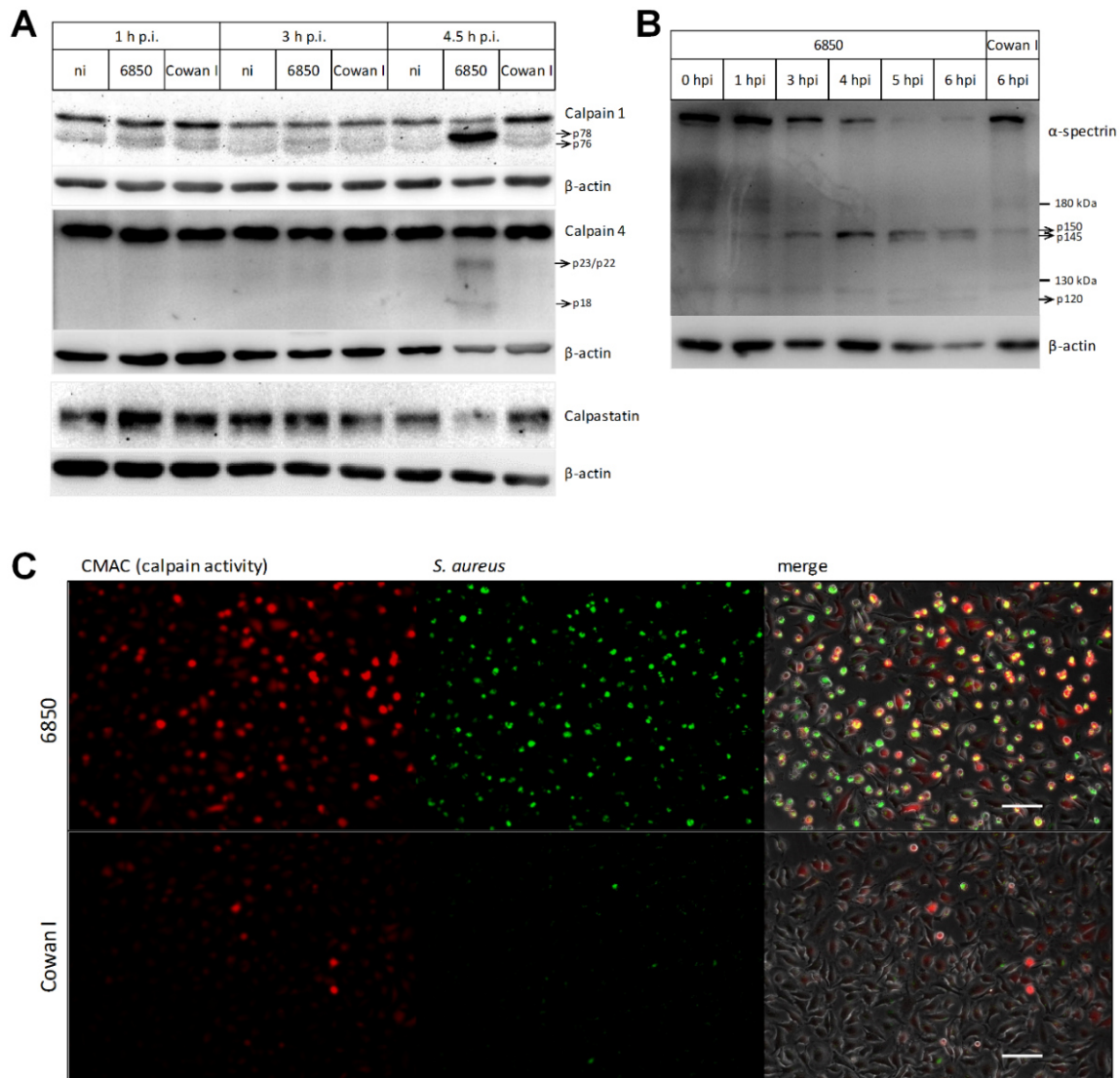


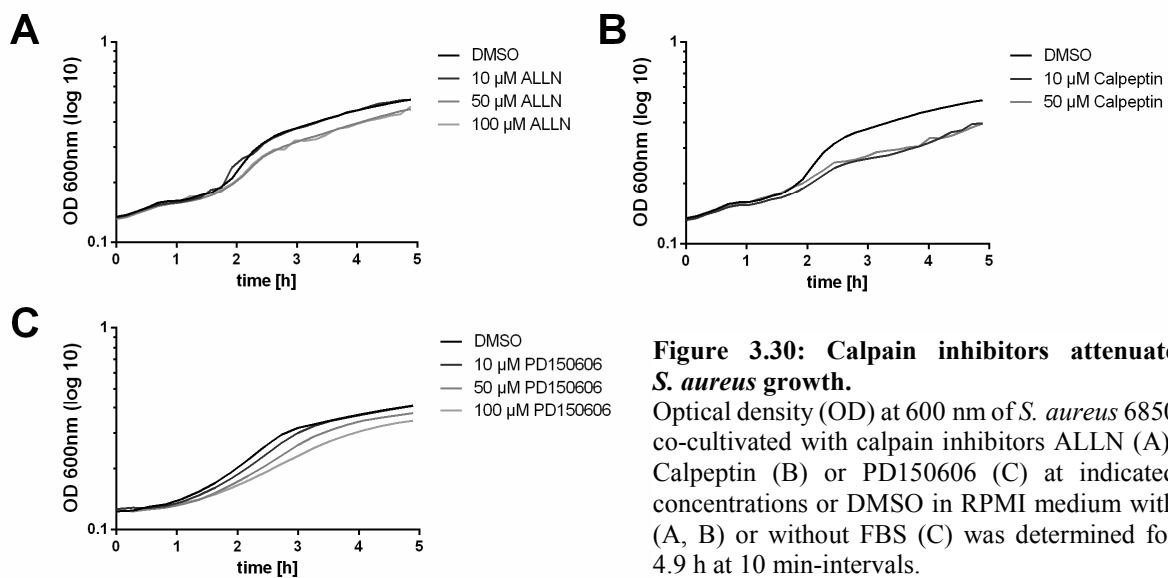
Figure 3.29: Calpain activation in *S. aureus* infected cells.

(A) HeLa cells were infected with *S. aureus* 6850 or Cowan I or remained uninfected (ni) and cell lysates were prepared at 1, 3 and 4.5 h p.i.. Proteins were separated by SDS-PAGE and transferred onto a PVDF membrane. Protein abundance and/or cleavage of calpain 1, calpain 4, calpastatin and β-actin as loading control was detected using the specific antibodies. (B) Immunoblot assay was performed as described for (A). *S. aureus* 6850- or Cowan I-infected cells were lysed at 0, 1, 3, 4, 5 and 6 h p.i.. Calpain-specific cleavage of α-spectrin (150 and 145 kDa) was observed by application of an anti-α-spectrin antibody with anti-β-actin antibody as loading control. (C) HeLa cells were loaded with a fluorogenic calpain substrate (10 μM Boc-Leu-Met-CMAC) after infection with *S. aureus* 6850 or Cowan I. The presence of activated calpains was detected in 6850-infected cells at 4.5 h p.i. by fluorescence microscopy (red: Boc-Leu-Met-CMAC, green: *S. aureus*, gray: phase contrast, scale bar: 100 μm).

3.2.7.2 Inactivation of calpains has no effect on *S. aureus* intracellular lifestyle

As inhibitors against calpains, such as ALLN, Calpeptin or PD150606, may have off-target effects (McDonald et al., 2001; Ono et al., 2016; Sasaki et al., 1990) and growth of *S. aureus* was attenuated when co-incubated with these inhibitors (Figure 3.30), siRNA-based knock-downs of the large subunits Calpain 1 and Calpain 2 and the small subunit Calpain 4 were performed to investigate their role in *S. aureus*-induced host cell death. Whereas knock-down of Calpain 1 led to an increased cell death of HeLa cells infected with *S. aureus* 6850 at 6 h p.i.

(38.1 ± 3.5 %), knock-down of Calpain 4 showed a reduction of 7AAD staining (20.6 ± 1.6 %) when compared to the control (29.2 ± 3.4 %) (Figure 3.31A). Transfection with Calpain 2-specific siRNA only slightly reduced *S. aureus*-induced host cell death (27.6 % \pm 0.4). However, 7AAD staining after knock-down of either Calpains 1, 2 or 4 was not significantly different in comparison to the siRNA negative control (AllStars Negative Control siRNA). Invasion of *S. aureus* into HeLa cells (Figure 3.31B), phagosomal escape (Figure 3.31C and D) and intracellular replication of *S. aureus* 6850 (Figure 3.31E) were unchanged in the knock-down cells. Nevertheless, siRNA-mediated decrease in Calpain 1 expression showed increased numbers of escaped, cytosolic bacteria (12.1 ± 0.4 % phagosomal escape, 5003 ± 1957 AFU) at 3 h p.i. when compared to the control (7.9 ± 3.7 % phagosomal escape, 3850 ± 891 AFU). The expression of the targeted genes was successfully and efficiently decreased as determined by qRT-PCR (Figure 3.31F). Transfection of HeLa cells with siCAPN1 led to a knock-down of Calpain 1 by 96 %, while expression of Calpain 4 was increased in these cells. Expression of Calpain 2 was reduced by 85 % after transfection with siCAPN2, which also resulted in increased expression of Calpain 4. Transfection with siCAPN4 reduced the expression of Calpain 4 by 95 %, while the mRNAs levels of Calpain 2 were decreased in these cells.



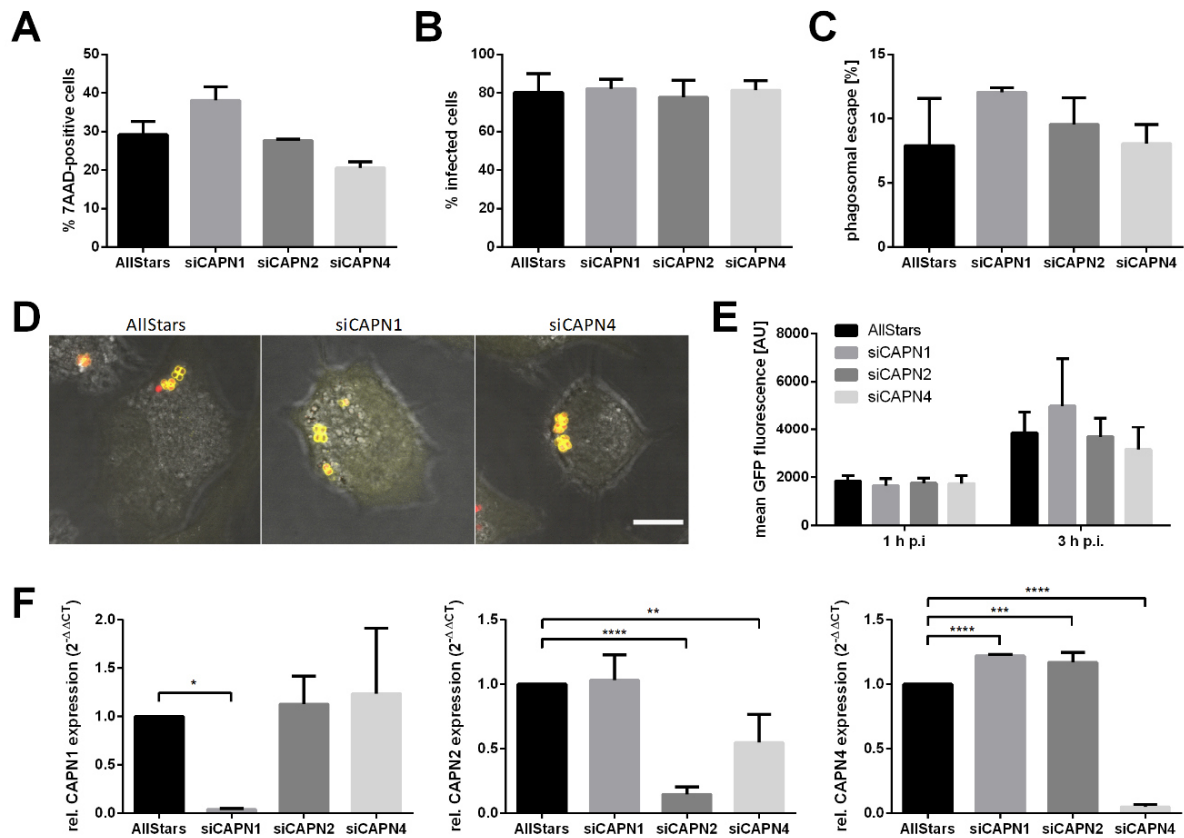


Figure 3.31: Knock-down of calpains 1, 2 or 4 has no significant effect on *S. aureus* intracellular lifestyle.

(A-E) HeLa cells were transfected with siRNA against Calpain 1 (siCAPN1), Calpain 2 (siCAPN2) or Calpain 4 (siCAPN4) mRNA or AllStars Negative Control siRNA (Allstar) and subsequently infected with *S. aureus* 6850 (A), 6850 GFP (B, E) or 6850 mRFP (C, D). (A) Cytotoxicity of *S. aureus* was determined at 6 h p.i. by staining of infected cells with 7AAD (n=2). (B) Invasion of *S. aureus* 6850 was measured as number of GFP-positive cells at 1 h p.i.. (C) Translocation of bacteria into the host cell cytosol was determined by quantification of colocalization of intracellular bacteria and the cytosolic escape marker YFP-cwt (n=2). (D) Live cell imaging of HeLa YFP-cwt cells infected with *S. aureus* 6850 revealed phagosomal escape of the pathogen after knock-down of Calpain 1 (siCAPN1) or Calpain 4 (siCAPN4) (red: *S. aureus*, yellow: YFP-cwt, gray: BF, scale bar: 10 μ m). (E) The relative number of intracellular bacteria was identified by measuring the mean fluorescence intensity of infected cells at 1 and 3 h p.i.. (F) RNA was isolated from HeLa cells transfected with siRNA against Calpain 1 (siCAPN1), Calpain 2 (siCAPN2) or Calpain 4 (siCAPN4) mRNA or AllStars Negative Control siRNA (Allstar) and transcribed into cDNA. qRT-PCR was performed with specific primers against the investigated genes (CAPN1: left graph, CAPN2: middle graph, CAPN4: right graph). Statistical analysis was performed by one-way ANOVA (* P <0.05, ** P <0.01, *** P <0.001, **** P <0.0001).

To rule out off target-effect of siRNAs and to generate a full knock-down of calpain expression, the CRISPR/Cas9-System was used to introduce mutations in CAPN4 and CAPN1 genes. The haploid cell line HAP1 was used for this purpose, because knock-out clones can be efficiently and relatively easy generated due to the presence of only one allele per gene. The intracellular lifestyle of *S. aureus* 6850 in HAP1 cells was shown to correspond to that in HeLa cells (Section 3.2.1.1) and activation of calpains in HAP1 cells was observed, too (Figure 3.32A). Calpain-specific cleavage of α -spectrin was detected 6 h p.i. in HAP1 cells infected with *S. aureus* 6850. CRISPR/Cas9-induced mutations in CAPN4 and CAPN1 led to gene knock-out as shown by the absence of protein detected by immunoblot (Figure 3.32B and C). Mutations in CAPN4 also

reduced or abolished protein levels of calpain 1 and calpain 2. However, knock-out of calpain 4 or calpain 1 did not reduce cytotoxicity of *S. aureus* 6850 in HAP1 cells at 6 h p.i. (Figure 3.32D and E). The LDH release of infected HAP1 *CAPN4* and *CAPN1* knock-out cells did not significantly differ from HAP1 wild type cells. In summary, these results indicate that calpains play no essential role in *S. aureus*-induced host cell death, although an activation of these proteases was observed.

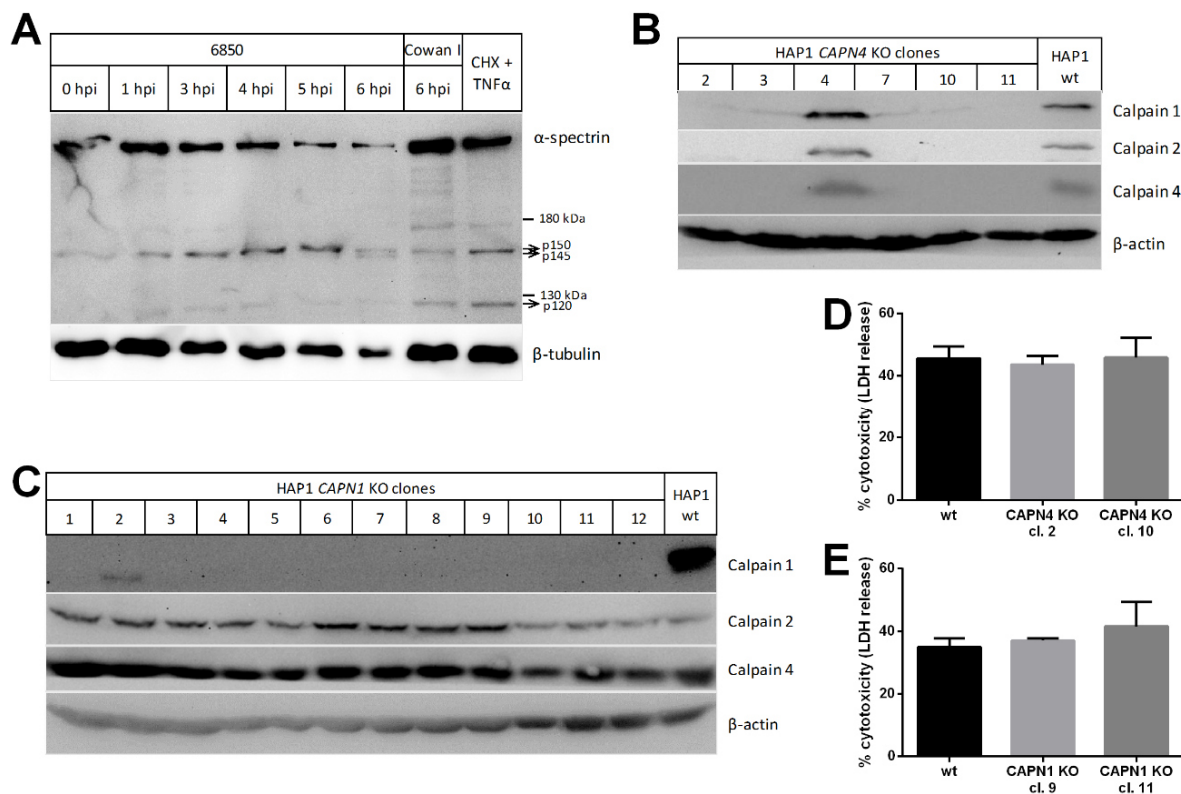


Figure 3.32: Knock-out of calpain 1 or 4 in HAP1 cells has no impact on *S. aureus*-induced cytotoxicity.

(A) *S. aureus* 6850- or Cowan I-infected HAP1 cells were lysed at 0, 1, 3, 4, 5 and 6 h p.i. and uninfected cells or cells treated with 10 μ g/ml cycloheximide (CHX) and 10 ng/ml TNF α for 7 h were used as control. Proteins were separated by SDS-PAGE and transferred onto a PVDF membrane. α -spectrin was detected using an anti- α -spectrin antibody and an anti- β -tubulin antibody served as loading control. Calpain-specific cleavage of α -spectrin (150 and 145 kDa) was observed at 6 h p.i. with *S. aureus* 6850, while CHX- and TNF α -treatment induced caspase-specific cleavage of α -spectrin (150 and 120 kDa). (B, C) Immunoblot analysis of HAP1 *CAPN4* KO (B) and *CAPN1* KO (C) clones generated using CRISPR/Cas9 was performed to check gene knock-out. Assay was performed as described for (A) and antibodies against Calpain 1, 2 and 4 and β -actin as loading control were used. (D, E) LDH release of HAP1 wild type (wt), *CAPN4* KO (clone 2 and 10, D) or *CAPN1* KO (clone 9 and 11, E) cells infected with *S. aureus* 6850 revealed no effect of calpains on *S. aureus* cytotoxicity at 6 h p.i. (n=2). Statistical analysis was performed by one-way ANOVA.

As it is known that calpains cleave caspases 3 and 7, which facilitates their activation (Blomgren et al., 2001; Ruiz-Vela et al., 1999; Waterhouse et al., 1998), and effector caspase activation was observed in *S. aureus* 6850-infected cells (Figure 3.10C, Video 3), it was interesting to investigate, if a knock-out of calpains abolished activation of caspase 3. Therefore, *CAPN4* knock-out cells, which were also negative for calpain 2 and had a very low expression of calpain

1 (Figure 3.32B), were infected with *S. aureus* 6850 and CellEvent™ Caspase-3/7 Green Detection Reagent was applied (Figure 3.33, Video 16). However, live cell imaging revealed that knock-out of calpain 4 did not eliminate caspase 3 and 7 activation when compared to wild type HAP1 cells.

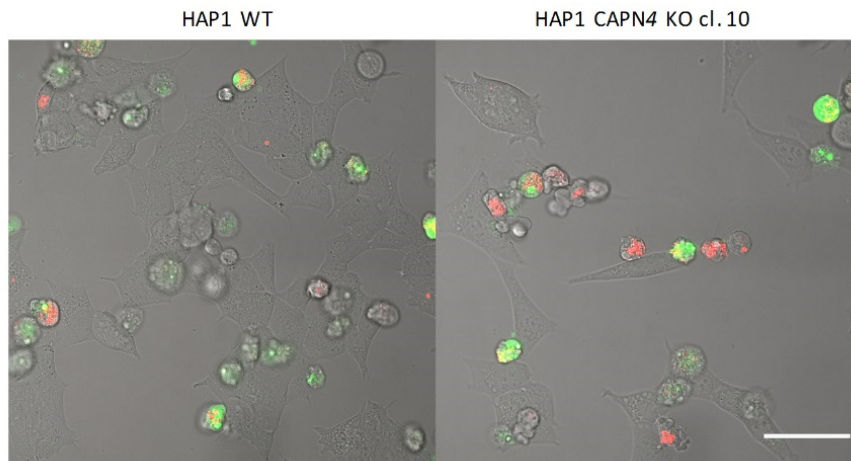


Figure 3.33: Effector caspase activation in *S. aureus* infected Calpain 4 knock-out cells.

HAP1 wild type (WT) or *CAPN4* KO (clone 10) cells were infected with *S. aureus* 6850 mRFP and effector caspase activation was determined by addition of CellEvent™ Caspase-3/7 Green Detection Reagent immediately before live cell imaging (red: *S. aureus*, green: CellEvent™ Caspase-3/7 Green Detection Reagent, gray: BF, scale bar: 50 μm).

3.3 Bacterial factors involved in *S. aureus*-induced cytotoxicity

3.3.1 Rsp and α -hemolysin do not contribute to *S. aureus* induced cytosolic Ca^{2+} rise

Since several *S. aureus* toxins are known to trigger Ca^{2+} fluxes in human cells (Bouillot et al., 2018), secreted virulence factors were tested for their ability to induce cytosolic Ca^{2+} overload. Treatment of HeLa R-Geco cells with 10 % sterilized supernatant of a *S. aureus* 6850 overnight culture led to high and frequent oscillations of cytosolic Ca^{2+} in most cells (Figure 3.34, Video 17). This was followed by a sustained Ca^{2+} increase, which occurred after cell contraction, but prior to the formation of one or more huge membrane blebs (Figure 3.34C). This succession of events is reminiscent of *S. aureus* intracellular infection (Figure 3.17A).

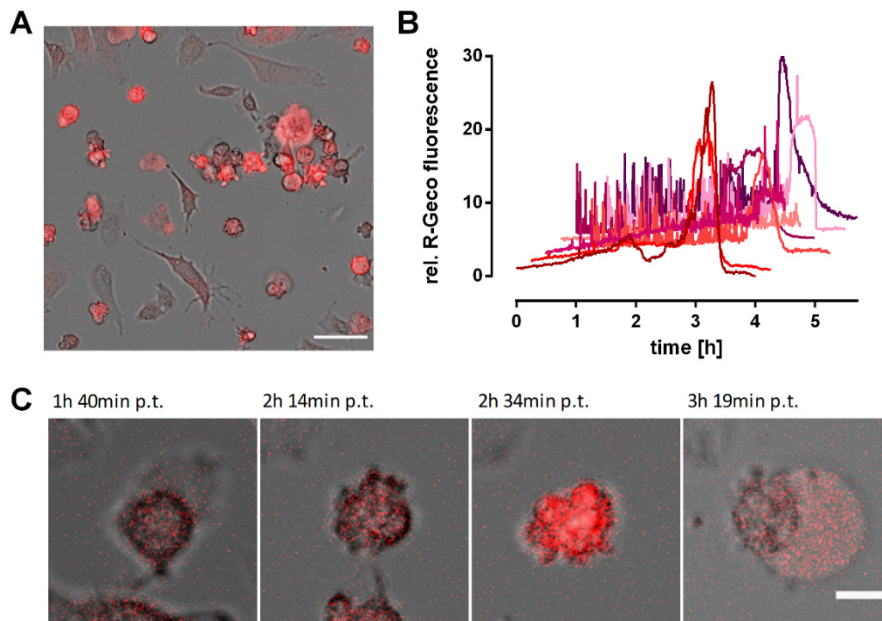


Figure 3.34: Effects of *S. aureus* secreted factors on cellular Ca^{2+} signaling.

HeLa R-Geco cells were treated with 10 % sterilized supernatant of a *S. aureus* 6850 overnight culture (SNT) and R-Geco fluorescence was monitored over time. (A) Representative still of imaged field of view is depicted (red: R-Geco, gray: BF, scale bar: 50 μm). (B) Relative R-Geco fluorescence of single cells was quantified upon SNT treatment. (C) Representative stills of one SNT-treated HeLa R-Geco cell (red: R-Geco, gray: BF, scale bar: 10 μm).

The well-studied pore-forming toxin α -hemolysin (*hla*) can form Ca^{2+} -permissive pores, which at high concentrations lead to Ca^{2+} elevations in the cell cytosol (Eichstaedt et al., 2009; Fink et al., 1989). α -hemolysin expression depends partly on the long ncRNA SSR42, which is the effector of the virulence regulator Rsp (Horn et al., 2018a). Mutants in *rsp* showed attenuated intracellular cytotoxicity and prolonged intracellular residence of *S. aureus* (Das et al., 2016). Therefore, *S. aureus* mutants in *hla* and *rsp* were investigated for their Ca^{2+} flux inducing properties. HeLa R-Geco cells were infected with *S. aureus* 6580, 6850 Δhla or 6850 Δrsp and relative R-Geco fluorescence was monitored by live cell imaging. Infection of HeLa R-Geco cells with isogenic *hla* or *rsp* mutants could not abolish the cytosolic Ca^{2+} increase (Figure 3.35A-E, Video 18). Elevations in R-Geco fluorescence were observed independent of the genetic phenotype of *S. aureus*. Measurements of relative cytosolic Ca^{2+} concentrations of single, 6850-infected cells revealed no major differences between infection with *S. aureus* 6850, 6580 Δhla or 6850 Δrsp . The amplitude as well as the latency of maximal R-Geco fluorescence was not significantly different in HeLa cells infected with 6580 Δhla or 6850 Δrsp compared to the wild type (Figure 3.35E and F). Investigation of cytotoxicity of *S. aureus* 6850 Δhla or 6850 Δrsp towards HeLa cells also showed no significant differences when compared to 6850 wild type (Figure 3.35G). Host cell death was determined by LDH release at 1, 3, 6 and

24 h p.i. in HeLa cells. Yet, at 6 h p.i. both mutants were attenuated in cytotoxicity in contrast to the wild type.

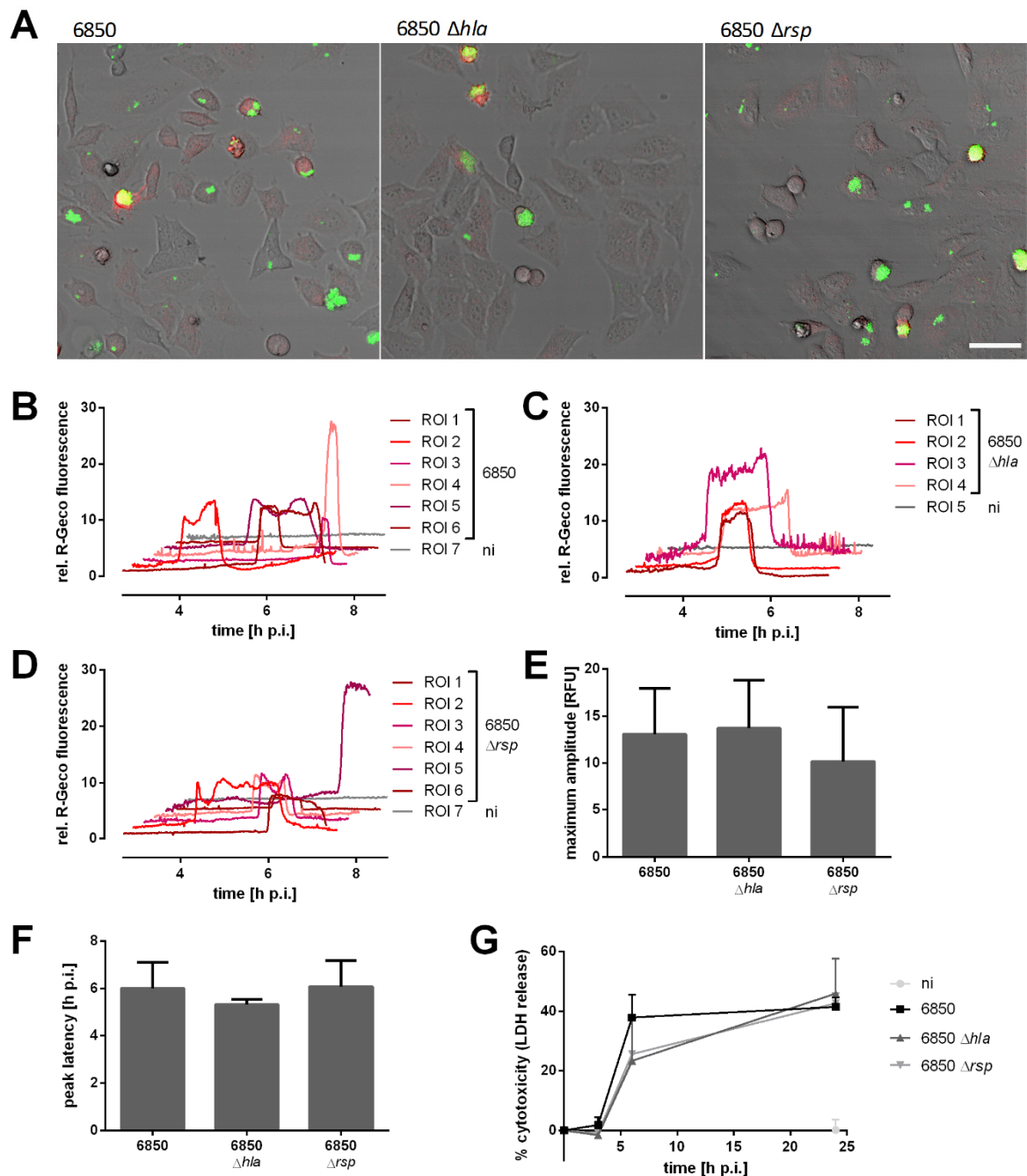


Figure 3.35: Ca^{2+} signaling and cytotoxicity in epithelial cells infected with *S. aureus* 6850 Δhla or 6850 Δrsp . (A-F) HeLa R-Geco cells were infected with *S. aureus* 6850 GFP, 6850 Δhla GFP or 6850 Δrsp GFP and R-Geco fluorescence was monitored over time by live cell imaging. (A) Stills of time-lapse imaging at 5 h 6 min p.i. are shown (green: *S. aureus*, red: R-Geco, gray: BF, scale: 50 μm). (B-D) Relative R-Geco fluorescence was quantified over the time period of infection in single cells infected with *S. aureus* 6850 (B), *S. aureus* 6850 Δhla (C) or 6850 Δrsp (D) or in single uninfected cells (ni). (E) The peak amplitude of the relative R-Geco fluorescence of 4 to 12 single infected cells was determined. (F) The latency of relative R-Geco fluorescence peak after *S. aureus* intracellular infection was calculated in 4 to 12 single cells. (G) Cytotoxicity of *S. aureus* 6850, 6850 Δhla or 6850 Δrsp in HeLa cells was determined by LDH assay at 1, 3, 6 and 24 h p.i.. Statistical analysis was performed by one-way ANOVA.

3.3.2 Intracellular cytotoxicity of different *S. aureus* mutants in epithelial cells

In order to investigate bacterial factors involved in induction of host cell death by intracellular *S. aureus*, bacterial mutants were tested for their cytotoxic behavior towards epithelial cells. Mutants of *S. aureus* virulence factors, which may be involved in the formation of Ca^{2+} -permeable pores and/or belong to a class of proteins associated with bacterial induced cell death, were chosen. Cell death of infected HeLa cells was determined by LDH release 6 h p.i. (Figure 3.36). Transposon mutants of the cysteine proteases staphopain A (ScpA) and staphopain B (SspB) and the pore-forming toxin subunit HlgB were tested for their cytotoxic ability (Figure 3.36A). Inactivation of SspB or HlgB led to a slight, but not significant decrease in host cell death, while mutation of ScpA showed a strong reduction in cytotoxicity of *S. aureus* JE2 when compared to infection with the wild type strain. Knock-out of the phenol-soluble modulins α (PSM α) also reduced the number of dead cells in *S. aureus* LAC (Figure 3.36B). The cytotoxicity of LAC $\Delta\text{psm}\beta$ was slightly decreased, whereas a mutant in δ -toxin showed no effect on induction of host cell death when compared to the wild type.

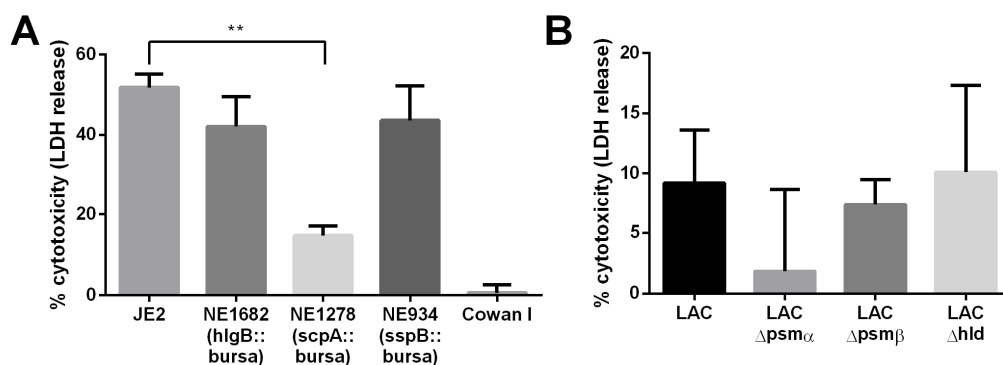


Figure 3.36: Cytotoxicity of different *S. aureus* mutants in epithelial cells.

HeLa cells were infected with *S. aureus* wild type or mutant strain and induction of host cell death was determined 6 h p.i. by LDH release. Cytotoxicity of *S. aureus* JE2, JE2 *hlgB::bursa* (NE1682), JE2 *scpA::bursa* (NE1278) and JE2 *sspB::bursa* (NE934) (A, n=2) and LAC, LAC $\Delta\text{psm}\alpha$, LAC $\Delta\text{psm}\beta$ and LAC Δhld (B, n=2) was investigated. Statistical analysis was performed by one-way ANOVA (** $P < 0.01$).

3.3.3 Staphopain A induces intracellular cytotoxicity of *S. aureus*

3.3.3.1 Loss of staphopain A function leads to reduced cytotoxicity of intracellular *S. aureus*

The role of the cysteine protease staphopain A in *S. aureus*-induced host cell death was further investigated. To exclude side effects of secondary site mutations, the *bursa aurealis* transposon (Fey et al., 2013) inserted in the *scpA* gene was freshly transduced into the JE2 wild type strain obtaining JE2 *scpA*. An apoptosis detection assay was performed by staining of infected cells with annexin V-APC and 7AAD. Results obtained with the LDH assay (Figure 3.36A) were confirmed, since the *scpA* mutant induced significantly fewer annexin V- and 7AAD-positive

cells in contrast to the wild type (Figure 3.37A and B). No significant differences in annexin V- and 7AAD-positive cells were observed between infection with JE2 *scpA* and Cowan I and the number of annexin V-positive and 7AAD-negative cells and annexin V-negative and 7AAD-positive cells did not significantly differ between JE2, JE2 *scpA* and Cowan I.

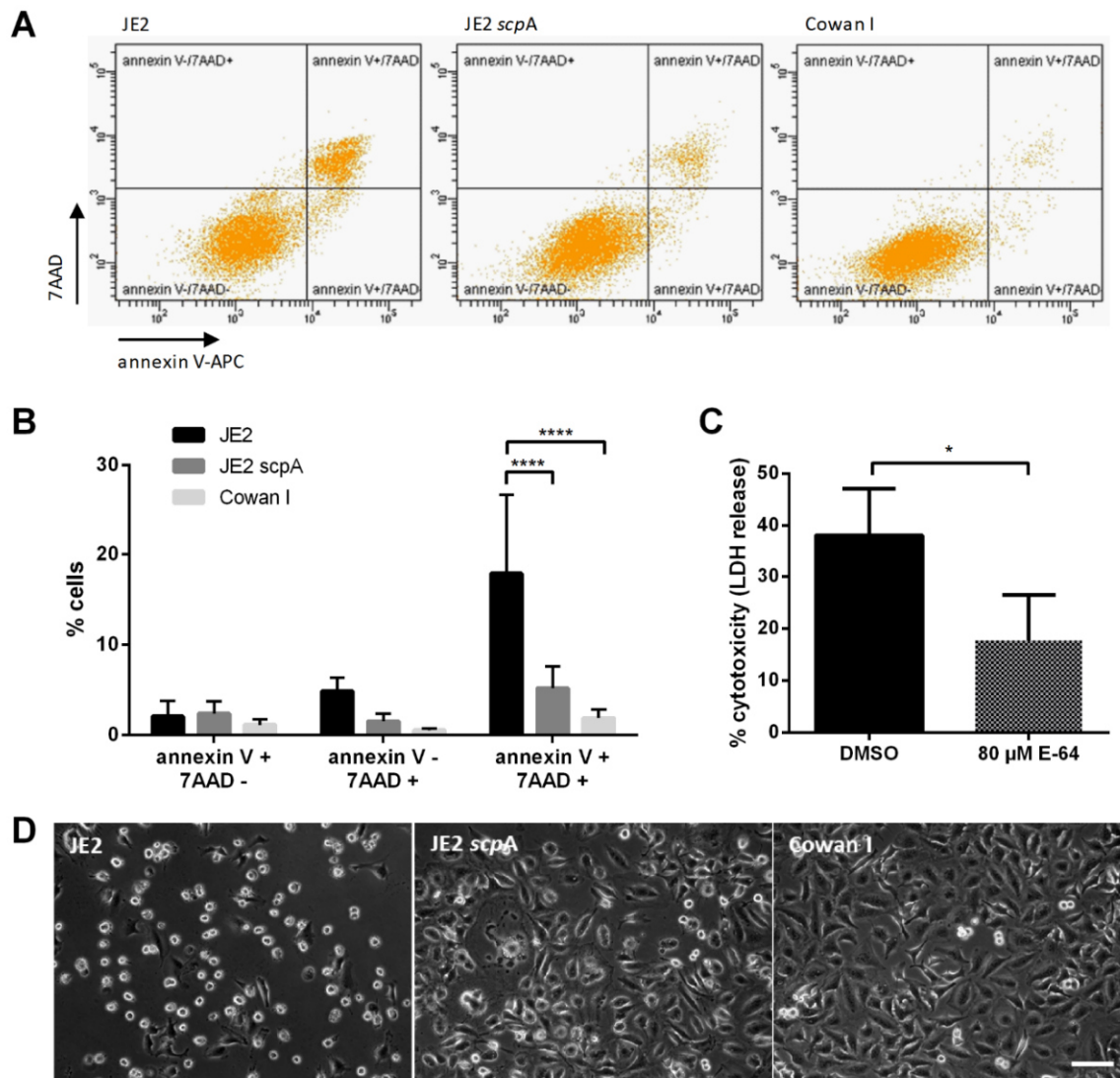


Figure 3.37: Inactivation or inhibition of staphopain A leads to less cell death induced by intracellular *S. aureus*.

(A, B) HeLa cells were infected with *S. aureus* JE2, JE2 *scpA* or Cowan I, stained with annexin V and 7AAD at 6 h p.i. and analyzed by flow cytometry. Representative scatter plots (A) and bar graph of quantified cell populations (B) are shown. (C) HeLa cells infected with *S. aureus* JE2 were treated with 80 μM E-64 or solvent control (DMSO) 1 h prior to infection and at 6 h p.i. LDH release was quantified. (D) Phase contrast images of *S. aureus* JE2, JE2 *scpA* or Cowan I-infected cells were taken at 6 h p.i. (scale bar: 100 μm). Statistical analysis was performed by two-way ANOVA (B) or unpaired t-test (C) (* $P < 0.05$, **** $P < 0.0001$) (Stelzner et al. (2019) submitted).

Inhibition of staphopain A with the cysteine protease inhibitor E-64 led to reduction of *S. aureus* cytotoxicity by 54 % (Figure 3.37C). Besides, the morphology of JE2 *scpA*-infected HeLa cells was reminiscent of infection with the non-cytotoxic strain Cowan I but not with the JE2 wild type (Figure 3.37D). While infection with JE2 showed typical signs of cell death like rounding, retraction of pseudopodia and detachment from the substratum (Kroemer et al.,

2009), HeLa cells infected with JE2 *scpA* mostly exhibited an adherent morphology, although cells appeared to be filled with granular particles.

To further verify the role of staphopain A in *S. aureus*-induced cytotoxicity, loss of ScpA function was complemented by plasmid with a functional *scpAB* transgene, containing the native promoter region and the transcription terminator of the operon. LDH release in HeLa cells induced by the complemented *scpA* mutant, JE2 *pscpAB*, was significantly increased over the *scpA* mutant at 6 h p.i. (Figure 3.38A and B). Cytotoxicity levels of JE2 *pscpAB* (40.6 % \pm 9.2) were higher when compared to the wild type (28.8 % \pm 2.9), but the increase was not significant.

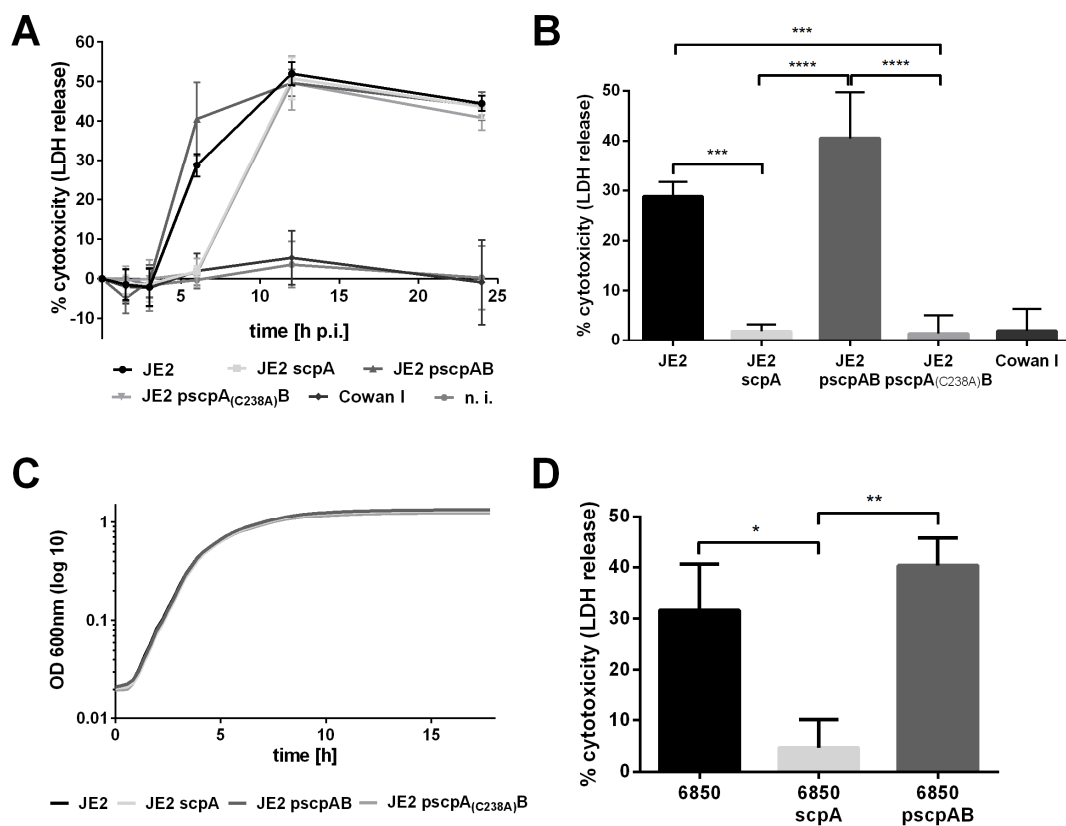


Figure 3.38: Complementation with *scpAB*, but not with *pscpA*(C238A)B, restores the cytotoxicity of the staphopain A mutant.

(A, B) Induction of host cell death was determined at 1.5, 3, 6, 12 and 24 h p.i. (A) or 6 h p.i. (B) in HeLa cells infected with JE2 wild type, *scpA* mutant (JE2 *scpA*), complemented mutant (JE2 *pscpAB*), complemented mutant with active mutation in *scpA* (JE2 *pscpA*(C238A)B) or Cowan I. (C) Optical density (OD) at 600 nm of bacterial strains in TSB was determined for 18 h at 10 min-intervals. (D) HeLa cells were infected with *S. aureus* 6850, 6850 *scpA* and 6850 *pscpAB* and LDH release was quantified at 6 h p.i.. Statistical analysis was determined by one-way ANOVA (* P <0.05, ** P <0.01, *** P <0.001, **** P <0.0001) (Stelzner et al. (2019) submitted).

Functional inactivation of the transgene *scpA* by active site mutation (C238A, JE2 *pscpA*(C238A)B) abolished the cell death induced by the complemented *scpA* mutant at 6 h p.i.. LDH release of JE2 *scpA* (1.9 % \pm 1.4) and JE2 *pscpA*(C238A)B (1.4 % \pm 3.6) was significantly reduced to levels of Cowan I-infected cells (2.0 % \pm 4.4) at 6 h p.i. when compared to JE2 wild

type or JE2 *pscpAB* (Figure 3.38A and B). However, at 12 and 24 h p.i. cytotoxicity of JE2 *scpA*- and JE2 *pscpA*_(C238A)B was consistent with the LDH release of JE2- or JE2 *pscpAB*-infected HeLa cells. This finding indicated a delayed cell death induced by the staphopain A mutant. The observed differences in cytotoxicity were not due to impaired or enhanced growth of the bacterial strains used (Figure 3.38C). Loss of staphopain A function also led to reduced cytotoxicity of the MSSA-strain 6850 ($4.7\% \pm 5.5$) in comparison to the 6850 wild type ($31.6\% \pm 9.0$), which was rescued by complementation with *pscpAB* ($40.4\% \pm 5.4$) (Figure 3.38D).

3.3.3.2 Staphopain A does not interfere with invasion, phagosomal escape and intracellular replication of *S. aureus*

In order to investigate a possible role of staphopain A in *S. aureus* invasion of epithelial cells, HeLa cells were infected with JE2 or JE2 *scpA* mutant and cell invasion was determined by quantification of infected cells at 1 h p.i. (Figure 3.39A). No significant differences in the number of infected cells was detected. Likewise, the *scpA* mutant was tested for phagosomal escape (Figure 3.39B and C, Video 19). Infection of HeLa YFP-cwt cells with JE2 or JE2 *scpA* revealed similar rates of phagosomal escape of both strains, while Cowan I did not or very rarely translocate into the cytoplasm of the host cell. Therefore, effects of staphopain A on invasion or phagosomal escape of *S. aureus* can be excluded.

Investigation of intracellular replication of the *scpA* mutant in epithelial cells showed that JE2 *scpA* grew to the same extent as the wild type until 6 h p.i. (Figure 3.39D and E, Video 20). While the amount of intracellular JE2 subsequently decreased, JE2 *scpA* continued replicating. The amount of intracellular JE2 *scpA* ($82971 \text{ AFU} \pm 6478$) was significantly higher at 8 h p.i. compared to the wild type ($45282 \text{ AFU} \pm 5230$). The non-cytotoxic strain Cowan I did not replicate intracellularly. A growth benefit of the staphopain A mutant was excluded, as no differential growth was detected *in vitro* (Figure 3.38C). The decline in intracellular replication of the wild type coincided with increased host cell death at 6 h p.i. (Figure 3.38A and B), whereas the *scpA* mutant did not induce cytotoxicity at this time point. Besides, morphological differences of the infected cells were detected, as described above (Figure 3.37D). Host cells infected with JE2 underwent major morphological changes, such as cell rounding and retraction of pseudopodia, whereas JE2 *scpA* induced only minor changes of cell shape (Figure 3.39E).

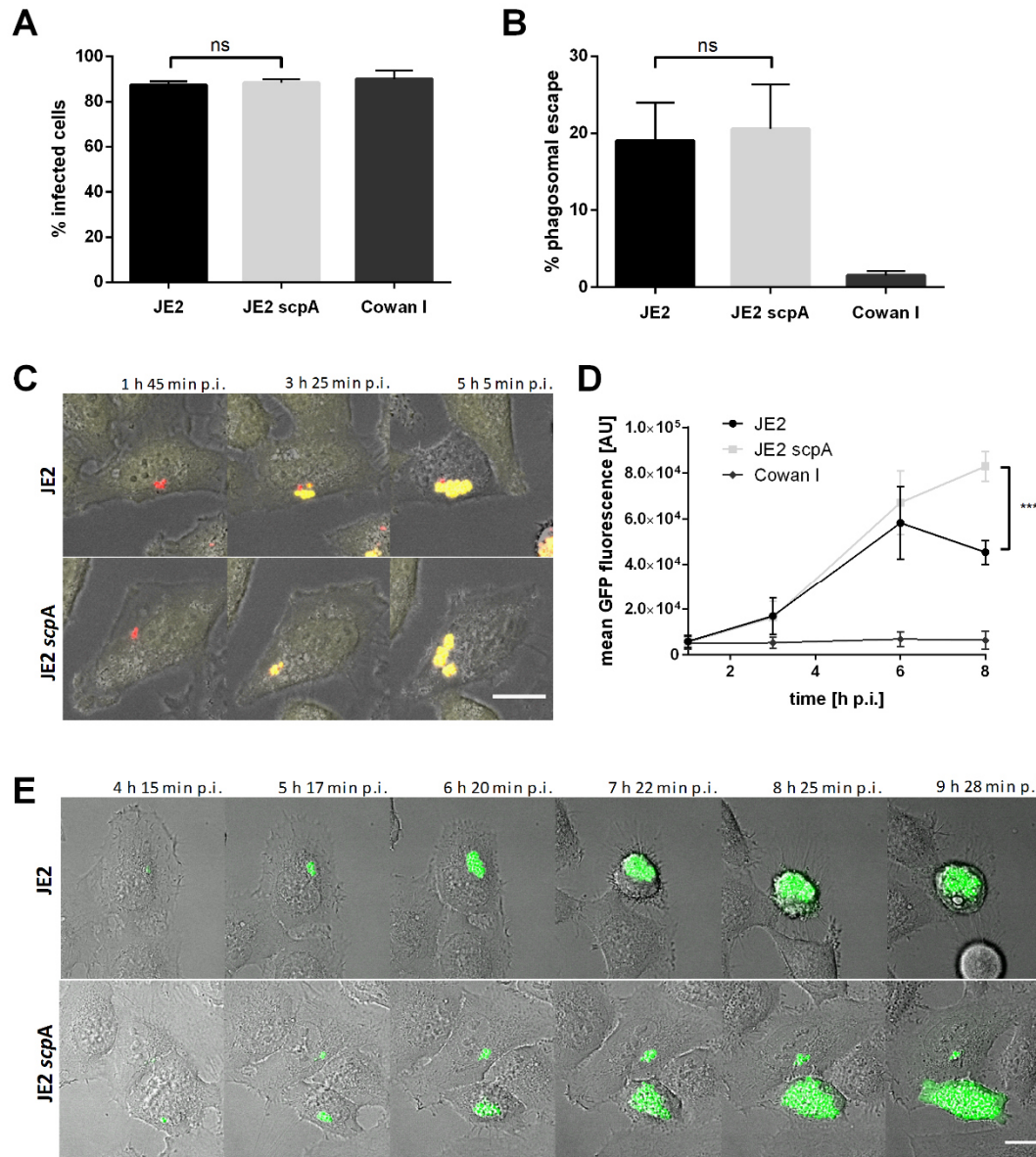


Figure 3.39: Loss of staphopain A function has no effect on *S. aureus* invasion or phagosomal escape, but leads to prolonged intracellular replication.

(A) HeLa cells were infected with *S. aureus* JE2, JE2 *scpA* or Cowan I expressing GFP and the number of GFP-positive cells, representing the infected cells, was determined at 1 h p.i.. (B) Phagosomal escape was determined by quantification of co-localization of intracellular bacteria and the cytosolic escape marker YFP-cwt at 3 h p.i. in HeLa YFP-cwt cells infected with *S. aureus* JE2 mRFP, JE2 *scpA* mRFP or Cowan I mRFP. (C) Live cell imaging of HeLa YFP-cwt cells infected with *S. aureus* JE2 mRFP (upper panels) or JE2 *scpA* mRFP (lower panels) revealed phagosomal escape of both strains (red: *S. aureus*, yellow: YFP-cwt, gray: BF, scale bar: 20µm). (D) HeLa cells were infected with JE2, JE2 *scpA* or Cowan I expressing GFP. At 1, 3, 6 and 8 h p.i. the mean GFP fluorescence, representing the relative number of intracellular bacteria, was quantified. (E) Live cell imaging was performed to study intracellular replication of JE2 (upper panels) and JE2 *scpA* (lower panels) in HeLa cells (green: *S. aureus*, gray: BF, scale bar: 20µm). Statistical significance was determined by one-way ANOVA (***) ($P < 0.001$) (Stelzner et al. (2019) submitted).

3.3.3.3 Mutation of staphopain A does not abolish cytosolic Ca²⁺ overload in *S. aureus*-infected host cells

As a cytosolic Ca²⁺ rise was observed in *S. aureus* 6850-infected HeLa cells followed by activation of effector caspases and host cell lysis (Section 3.2.6.1), Ca²⁺ signaling in *S. aureus*

JE2 *scpA*-infected cells was investigated to elucidate a possible role of staphopain A in inducing Ca^{2+} elevations. HeLa R-Geco cells were infected with *S. aureus* JE2 or JE2 *scpA* and time-lapse fluorescence microscopy was performed to quantify cytosolic Ca^{2+} concentration during intracellular infection of *S. aureus* (Figure 3.40, Video 21).

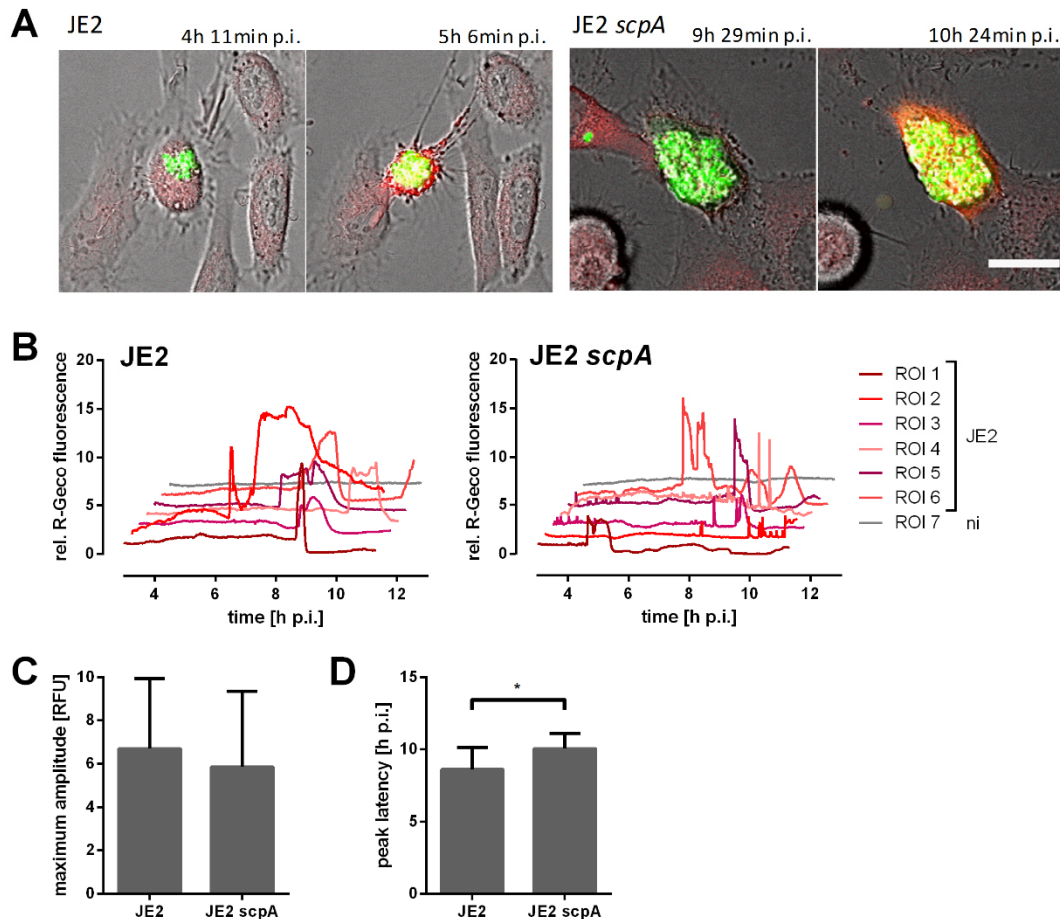


Figure 3.40: *S. aureus* JE2 *scpA* triggers cytosolic Ca^{2+} overload in epithelial cells.

HeLa R-Geco cells were infected with *S. aureus* JE2 GFP or JE2 *scpA* GFP and cytosolic Ca^{2+} concentration, i.e. R-Geco fluorescence, was measured by time-lapse imaging. (A) Representative stills from time-lapse fluorescence microscopy showed elevations in cytosolic Ca^{2+} concentration independent of the bacterial strain used for infection (green: *S. aureus*, red: R-Geco, gray: BF, scale bar: 20 μm). (B) Relative quantification of cytosolic Ca^{2+} concentrations of single, infected (JE2) or uninfected (ni) cells. (C) The maximum amplitude of relative R-Geco fluorescence of 10 single infected cells was determined. (D) The latency after infection until the maximum amplitude of relative R-Geco fluorescence was quantified in 10 single cells. Statistical significance was determined by unpaired t-test ($*P < 0.05$).

Similar to *S. aureus* 6850, intracellular *S. aureus* JE2 was capable of inducing cytosolic Ca^{2+} overload. However, loss of staphopain A function did not prevent cytosolic Ca^{2+} rise induced by intracellular *S. aureus* (Figure 3.40A). Increased R-Geco fluorescence was observed in *S. aureus* JE2- and JE2 *scpA*-infected HeLa cells. But while *S. aureus* JE2 wild type induced rather sustained Ca^{2+} elevations for hours to minutes, the duration of the cytosolic Ca^{2+} peaks induced by infection with *S. aureus* JE2 *scpA* seemed to be shorter (Figure 3.40B). However, the amplitude of the cytosolic Ca^{2+} rise did not differ, whereas the time point of maximal

amplitude was delayed in cells infected with *S. aureus* JE2 *scpA* when compared to the wild type (Figure 3.40C and D). Likewise, loss of staphopain A function did not abolish activation of effector caspases (Figure 3.41, Video 22). As described before, morphological differences between cells infected with *S. aureus* JE2 or JE2 *scpA* were evident, as infection with JE2 wild type led to host cell contraction, whereas JE2 *scpA*-infected cells showed only minor alterations of cell morphology.

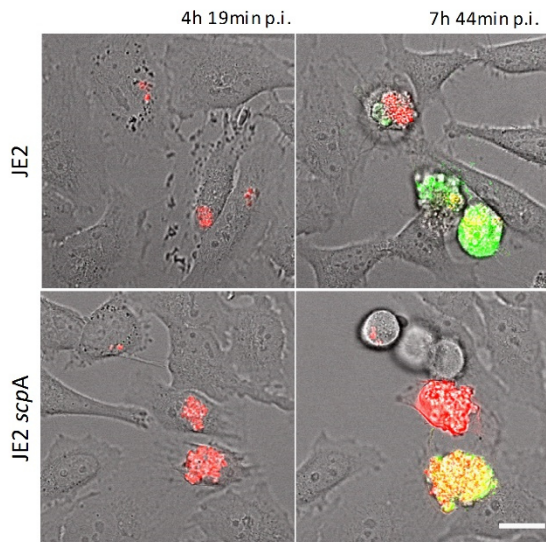


Figure 3.41: *S. aureus* JE2 *scpA* triggers activation of effector caspases.

HeLa cells were infected with *S. aureus* JE2 mRFP or JE2 *scpA* mRFP and CellEvent Caspase 3/7 detection reagent was added prior to time-lapse imaging. Representative stills from live cell fluorescence microscopy are depicted (red: *S. aureus*, green: CellEvent, gray: BF, scale bar: 20 μ m).

3.3.3.4 Ectopic expression of staphopain A in a non-cytotoxic *S. aureus* strain induces host cell death after phagosomal escape

To elucidate the role of staphopain A in the intracellular lifestyle of *S. aureus* further, it was investigated, if expression of *scpAB* in the non-cytotoxic laboratory strain RN4220 is sufficient to kill the host cell. *S. aureus* RN4220, just as Cowan I, is internalized by host cells, yet is not capable to escape from the phagosome. However, ectopic expression of *S. aureus* δ -toxin has been shown to permit translocation of this strain into the host cell cytosol, while the number of host cells was not reduced (Giese et al., 2011). This transgenic strain was employed for ectopic expression of staphopain A yielding *S. aureus* RN4220 *phld-scpAB*, which collinearly expresses δ -toxin (*hld*), staphopain A (*scpA*), staphostatin A (*scpB*) and the fluorescent protein cerulean under control of an AHT-inducible promoter. Secretion of the mature, proteolytically active form of staphopain A by this strain in the presence of AHT was proven (Figure 3.42A) (Nickerson et al., 2010). Mutation of the active site of staphopain A (*scpA*_(C238A)) prevented the formation of the mature ScpA, while the inactive precursor proScpA and other, so far unidentified forms of staphopain A accumulated.

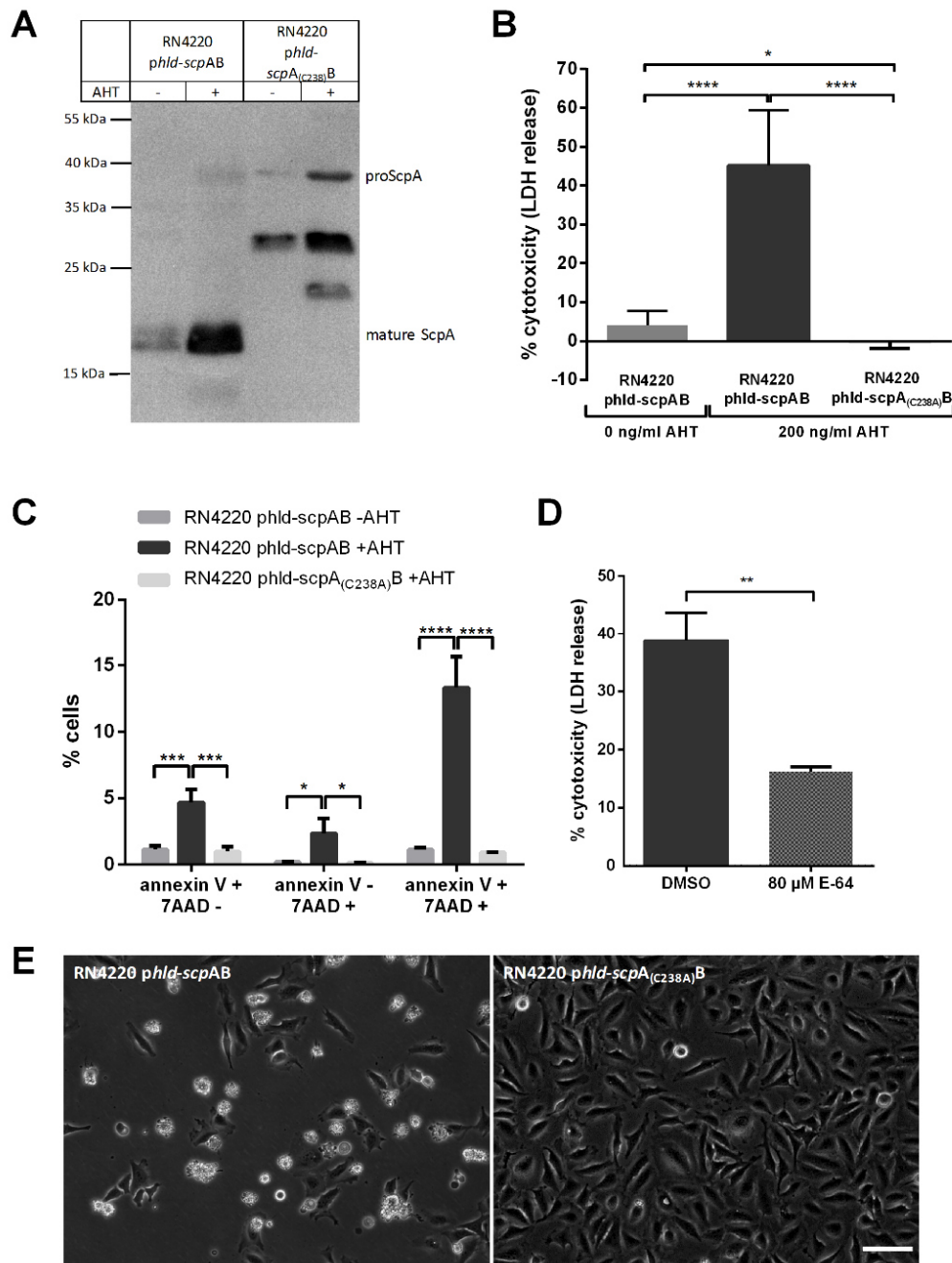


Figure 3.42: Ectopic expression of staphopain A in a non-cytotoxic *S. aureus* strain leads to host cell death. (A) Western blot for detection of staphopain A was performed with protein samples from supernatant of *S. aureus* RN4220 *phld-scpAB* or RN4220 *phld-scpA_(C238A)B* cultures grown overnight with or without addition of 200 ng/ml AHT. Expression of functional ScpA allowed the detection of the mature protein (17 to 20 kDa), while expression of an active site-mutated staphopain A led to accumulation of proScpA (ca. 40 kDa) (Nickerson et al., 2010). (B, C) HeLa cells were infected with *S. aureus* RN4220 *phld-scpAB* or RN4220 *phld-scpA_(C238A)B* with or without 200 ng/ml AHT and cytotoxicity was determined by LDH assay at 6 h p.i. (B, n=6) or annexin V-APC and 7AAD staining at 4.5 h p.i. (C). (D) HeLa cells were treated with 80 μM E-64 or solvent control (DMSO) and 200 ng/ml AHT 1 h prior to infection with *S. aureus* RN4220 *phld-scpAB*. 6 h p.i. LDH release was quantified. (E) Phase contrast images of HeLa cells infected with *S. aureus* RN4220 *phld-scpAB* or RN4220 *phld-scpA_(C238A)B* in the presence of 200 ng/ml AHT (scale bar: 100 μm). Statistical significance was determined by one-way (B) or two-way ANOVA (C) or unpaired t-test (D) (* $P < 0.05$, ** $P < 0.01$, *** $P < 0.001$, **** $P < 0.0001$) (Stelzner et al. (2019) submitted).

Infection of HeLa cells with these transgenic strains, RN4220 *phld-scpAB* and RN4220 *phld-scpA*_(C238)B, in the presence of AHT led to host cell death, when the functional, mature form of ScpA was expressed (Figure 3.42B and C). LDH release of HeLa cells was significantly increased after 6 h p.i. with RN4220 *phld-scpAB* ($45.1\% \pm 14.3$) in contrast to infection with RN4220 *phld-scpA*_(C238)B ($-0.2\% \pm 1.6$), where no cytotoxicity was detected (Figure 3.42B). Infection with RN4220 *phld-scpAB* omitting AHT-treatment resulted in very low level of cytotoxicity ($4.0\% \pm 3.6$). Similar results were obtained by staining of infected cells at 4.5 h p.i. with annexin V-APC and 7AAD (Figure 3.42C). The number of annexin V-positive and 7AAD-negative cells, annexin V-negative and 7AAD-positive cells and annexin V-positive and 7AAD-positive cells was significantly increased after infection with RN4220 *phld-scpAB* in the presence of AHT when compared to infection with RN4220 *phld-scpA*_(C238)B under AHT-treatment or RN4220 *phld-scpAB* without AHT. Pre-treatment of host cells with the cysteine protease inhibitor E-64 also decreased the cytotoxicity of RN4220 *phld-scpAB* by 58 % (Figure 3.42D). Phase contrast microscopy of HeLa cells infected with RN4220 *phld-scpAB* or RN4220 *phld-scpA*_(C238)B further illustrated the cytotoxicity of staphopain A (Figure 3.42E). While expression of the functional *scpA* induced cell rounding and detachment from the substratum, viable, adherent cells were observed after expression of inactive *scpA*_(C238A).

Both transgenic strains, *S. aureus* RN4220 *phld-scpAB* and RN4220 *phld-scpA*_(C238)B, were able to translocate from the phagosome to the cytoplasm of the host cell (Figure 3.43A arrows, Video 23). However, only RN4220 *phld-scpAB* induced cell contraction after phagosomal escape. The morphological changes triggered by RN4220 *phld-scpAB* occurred within seconds after permeabilization of the phagosomal membrane. In contrast to results obtained for *S. aureus* 6850 (Figure 3.3C) or JE2 (Figure 3.39D and E, Video 20), intracellular replication of RN4220 *phld-scpAB* or RN4220 *phld-scpA*_(C238)B was not observed (Video 23).

To exclude a cytotoxic effect of extracellular staphopain A, epithelial cells were treated with supernatant from RN4220 *phld-scpAB* and RN4220 *phld-scpA*_(C238)B overnight cultures (Figure 3.43C). Induction of expression with AHT led to high amounts of the mature, proteolytically active form of staphopain A, while RN4220 *phld-scpA*_(C238)B secretes only the inactive precursor of ScpA (Figure 3.43B, Figure 3.42A). Treatment of HeLa cells with increasing amounts of these supernatants showed a concentration-dependent increase in LDH release 24 h after treatment (Figure 3.43C). However, supernatant of RN4220 *phld-scpAB* did not induce more cell death when compared to RN4220 *phld-scpA*_(C238)B.

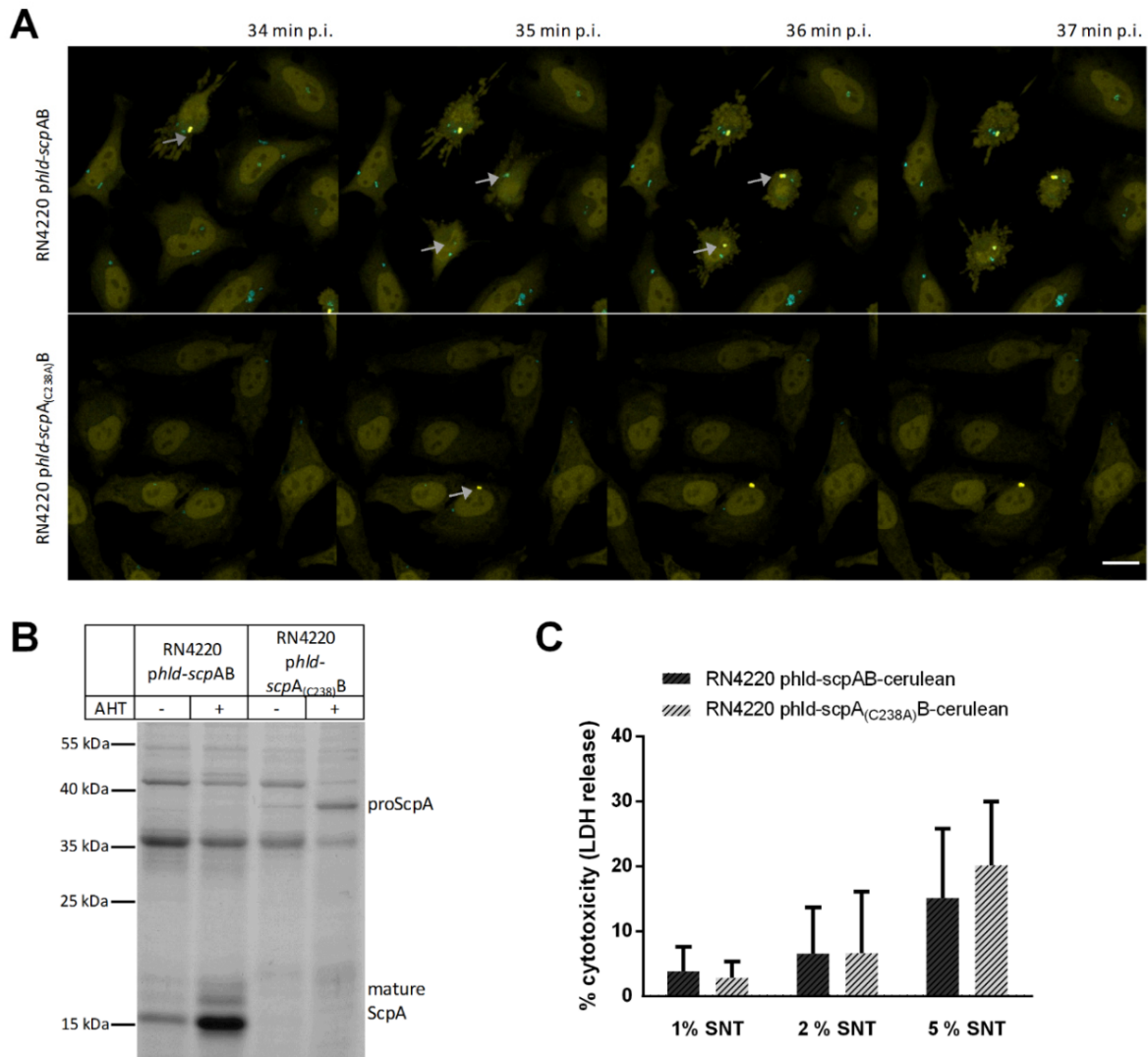


Figure 3.43: Staphopain A leads to cell death after phagosomal escape.

(A) HeLa YFP-cwt cells were infected with *S. aureus* RN4220 *phld-scpAB* (upper panels) or RN4220 *phld-scpA_(C238A)B* (lower panels) in the presence of 200 ng/ml AHT and live-cell imaging was performed (cyan: *S. aureus*, yellow: YFP-cwt, scale bar: 20 μ m). (B) SDS-PAGE and Coomassie staining was performed to study proteins secreted by *S. aureus* RN4220 *phld-scpAB* or RN4220 *phld-scpA_(C238A)B* with or without supplementation of 200 ng/ml AHT. (C) HeLa cells were treated with 1, 2 or 5 % of sterile culture supernatant (SNT) of AHT-treated *S. aureus* RN4220 *phld-scpAB* or RN4220 *phld-scpA_(C238A)B*. LDH release was determined 24 h after treatment and normalized to treatment with BHI medium used for bacterial cultures. Statistical significance was determined by two-way ANOVA (Stelzner et al. (2019) submitted).

3.3.3.5 Staphopain A induces host cell death with characteristics of apoptosis

The morphology of *S. aureus* RN4220 *phld-scpAB*-infected cells was reminiscent of apoptotic cells, since cell rounding and contraction, retraction of pseudopodia and plasma membrane blebbing were observed (Figure 3.42E and Figure 3.43A) (Kroemer et al., 2009). Therefore, the staphopain A-induced cell death was investigated for molecular markers of apoptosis. Staining with annexin V-APC and 7AAD revealed a typical apoptotic behaviour of RN4220 *phld-scpAB*-infected HeLa cells, in that the cells first acquired annexin V followed by staining with 7AAD (Figure 3.44A). At 1 h p.i. similar amounts of infected cells were annexin V-positive

and 7AAD-negative and annexin V- and 7AAD- positive, while 4.5 h p.i. most cells were annexin V- and 7AAD- positive (Figure 3.44B). Inhibition of caspases with Z-VAD-fmk led to a significant reduction RN4220 *phld-scpAB*-induced cytotoxicity by 27 % (Figure 3.44C). Additionally, activated effector caspases were detected in extracellular vesicles originating from HeLa cells infected with RN4220 *phld-scpAB* (Figure 3.44D, Video 24). Increased CellEvent fluorescence was observed in those vesicles, which appeared at later time points of infection after cell contraction and the formation of membrane blebs. An increase in cytosolic Ca^{2+} of the infected host cell was not detected (Figure 3.44D, Video 24).

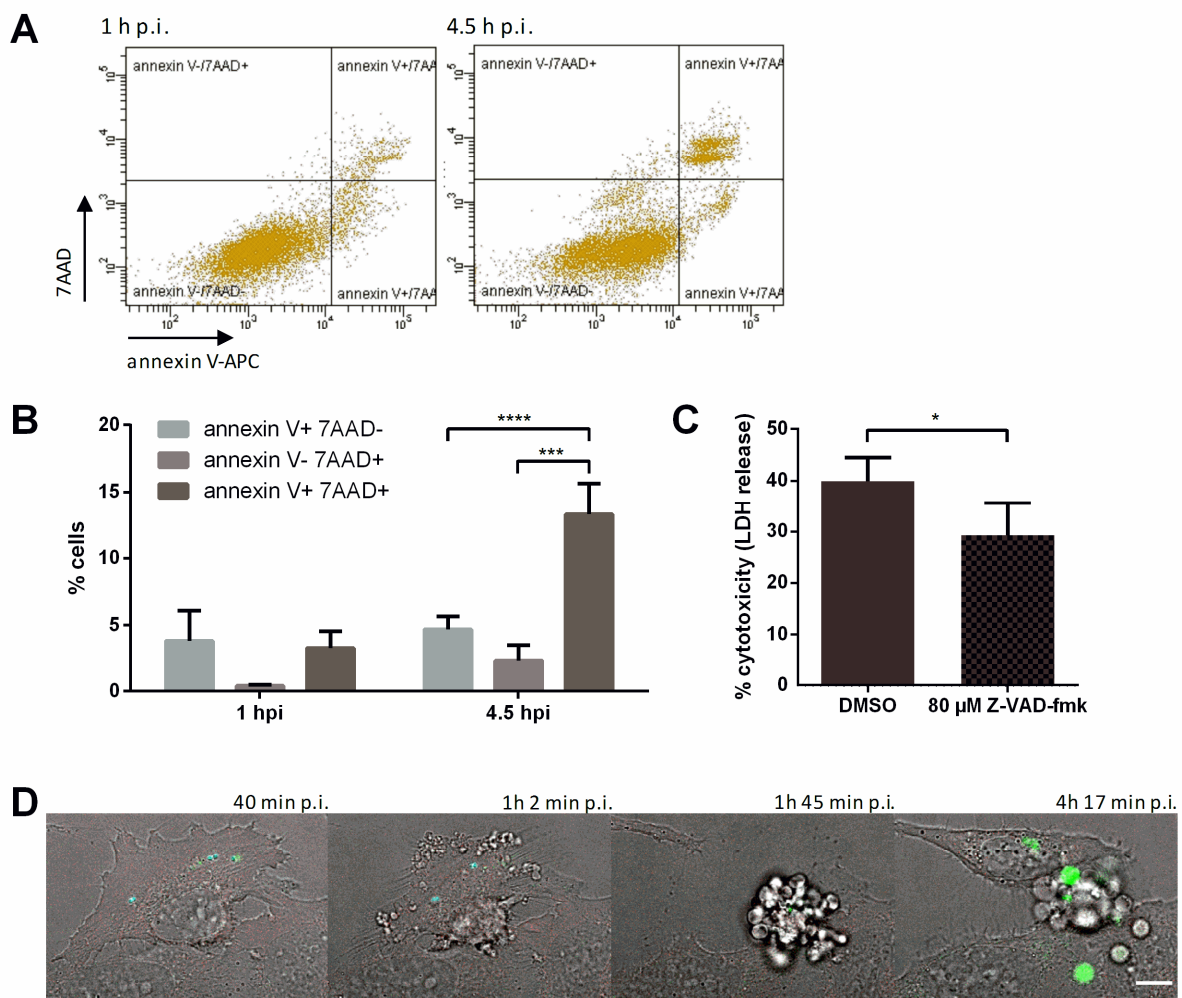


Figure 3.44: Staphopain A-induced cell death shows features of apoptosis.

(A, B) HeLa cells were infected with *S. aureus* RN4220 *phld-scpAB* in the presence of 200 ng/ml AHT and stained with annexin V-APC and 7AAD at 1 and 4.5 h p.i.. Representative scatter plots (A) and bar graph of quantified cell populations (B) are shown. (C) Pretreatment of HeLa cells with 80 μM Z-VAD-fmk and 200 ng/ml AHT led to reduction of RN4220 *phld-scpAB*-induced cell death when compared to treatment with solvent control (DMSO). (D) HeLa R-Geco cells were infected with *S. aureus* RN4220 *phld-scpAB* in the presence of 200 ng/ml AHT and prior to live cell imaging CellEvent™ Caspase3/7-substrate was added. Representative stills are shown (cyan: *S. aureus*, red: R-Geco, green: CellEvent™ Caspase3/7 substrate, gray: BF, scale bar: 10 μm). Statistical significance was determined by two-way ANOVA (B) and unpaired t-test (C) (* $P < 0.05$, *** $P < 0.001$, **** $P < 0.0001$) (Stelzner et al. (2019) submitted).

3.3.3.6 Staphopain A promotes *S. aureus* colonization in a pneumonia infection model

To investigate, if staphopain A also plays a role in *S. aureus* virulence *in vivo*, mice were intranasally administered with JE2 wild type, *scpA* mutant or complemented mutant. 48 h p.i. the bacterial burden in the lung of the animals was determined by plating of the tissue lysates¹ (Figure 3.45). Loss of staphopain A function led to significantly decreased numbers of bacteria in the mouse lung tissue in contrast to infection with the wild type. By complementation of the staphopain A mutant, the decrease in the bacterial numbers in the lung was reversed. The bacterial load in the lung tissue of JE2 *scpA* and JE2 *pscpAB*-infected mice was close to significance. Infection with JE2 wild type and complemented mutant led to the same bacterial load in the murine lung.

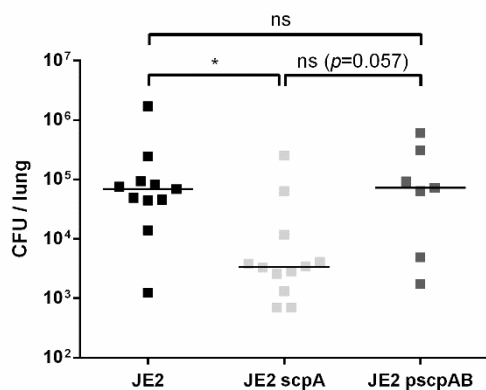


Figure 3.45: Staphopain A promotes *S. aureus* colonization of the lung.

CFUs from lung tissue of Balb/c mice, which were intranasally infected with *S. aureus* JE2, JE2 *scpA* or JE2 *pscpAB*, were recovered 48 h p.i.. Statistical significance was determined by Kruskal-Wallis test (* $P < 0.05$) (Stelzner et al. (2019) submitted).

¹ Performed by Tobias Hertlein, Institute for Molecular Infection Biology, Würzburg

4 Discussion

4.1 The intracellular lifestyle of *S. aureus* in epithelial cells

Although *S. aureus* is not regarded as a typical intracellular bacterium, it is able to invade epithelial and endothelial cells, osteoblasts, fibroblasts and keratinocytes and survives within professional phagocytes for extended periods (Horn et al., 2018b). In non-professional phagocytic cells, the pathogen escapes from the phagosome, replicates intracellularly and induces host cell death. Time-lapse imaging performed in the present study reveals direct evidence from live cells and bacteria that cytotoxic *S. aureus* only multiplies after its translocation into the cytosol followed by induction of host cell death in HeLa cells (Figure 3.1, Video 1). Thereby, the microscopy performed in the present study corroborates previous findings, which demonstrate the dependence of intracellular replication on phagosomal escape and the potential cytoplasmic location of this event (Grosz et al., 2014; Jarry et al., 2008).

The timing of *S. aureus*-induced host cell death in epithelial cells was characterized revealing initiation of cell death between 3 and 5 h p.i. by a proteinaceous factor, since only at earlier time points during infection chloramphenicol treatment was capable of suppressing LDH release (Figure 3.2C). Likewise, the onset of host cell lysis triggered by intracellular *S. aureus* lies between 3 and 4.5 h p.i. (Figure 3.2B). Thus, induction of host cell death required *de novo* synthesis of a protein, which may mediate cell lysis directly or after a time lag of up to 90 min. Since *S. aureus*-induced cytotoxicity is highly dependent on phagosomal escape (Blaettner et al., 2016; Grosz et al., 2014; Lam et al., 2010), inhibition of factor(s) inducing phagosomal escape, such as PSM α , is conceivable to also impair host cell death. Therefore, it cannot clearly be concluded that a protein is triggering *S. aureus*-induced cell death independently of phagosomal escape. However, phagosomal escape of cytotoxic *S. aureus* strains commenced approx. 2.5 h p.i. in epithelial cells (Grosz et al., 2014), which is prior to the starting time point of host cell death determined here (3-5 h p.i.).

The present study was conducted to identify factors promoting *S. aureus* cytotoxicity, but having no effect on phagosomal escape. Besides the dependence of *S. aureus* cytotoxicity on phagosomal escape, the molecular pathways and factors underlying *S. aureus*-mediated cell death remain largely unclear. Inconsistent and to some extent contradicting findings were reported, which were often only specific for the cell type or bacterial strain used (reviewed in Horn et al., 2018b).

4.2 Haploid genetic screen as a tool for identifying host genes involved in *S. aureus* intracellular cytotoxicity

4.2.1 Evaluation of haploid genetic screen performance

A loss-of-function genetic screen in human haploid cells was performed to identify genes mediating *S. aureus*-induced host cell death. This approach avoids potential off-target effects and incomplete knockdowns of RNA interference-based screens and is advantageous over chemical mutagenesis screens, since it causes only a limited number of disrupted genes per cell, which can be readily identified (Carette et al., 2009). Nevertheless, haploid genetics is restricted to certain few cell lines such as HAP1, whose susceptibility to infection by intracellular *S. aureus* had previously not been investigated. The present study showed that the adherent haploid cell line HAP1 is infected and killed by intracellular *S. aureus* (Section 3.1). The extent of invasion, phagosomal escape, intracellular replication and cytotoxicity of *S. aureus* 6850 as well as the timing of intracellular infection in HAP1 cells were comparable to infection of HeLa cells suggesting similar pathways of pathogen-induced host cell death in both cell types.

In order to identify host factors involved in these pathways, a previously established HAP1 mutant cell library was used (Carette et al., 2011b). This library had been successfully employed to identify host cell factors involved in viral infection (e.g. Baggen et al., 2016; Hoffmann et al., 2017; Jae et al., 2014; Riblett et al., 2016; Staring et al., 2017). Whereas during viral infections host cell infection rates close to 100 % can be titrated, *S. aureus* 6850 infects not all HAP1 host cells (71 ± 7 %; Figure 3.3A, Figure 3.5A). This incomplete infection was not dependent on the cell line or bacterial strain used, since *S. aureus* 6850 infection of HeLa cells also led to 82 ± 14 % infected cells and infection of HAP1 cells with highly cell invasive *S. aureus* strain Cowan I resulted in 74 ± 1 % of infected cells (Figure 3.3A, Figure 3.5A). The reason for this is unclear. Differential expression of bacterial adhesion factors, such as fibronectin-binding proteins, or host cell receptors promoting *S. aureus* invasion may explain why not all host cell are infected. Expression of invasion-relevant factors may be influenced by the cell cycle/growth phase of the bacterial or host cell. It is well known that *S. aureus* surface proteins, such as adhesins, are primarily expressed during exponential growth phase (Gordon and Lowy, 2008; Lowy, 1998). However, bacterial cells were harvested for infection from this growth phase (Section 2.2.1.2).

A critical step for a successful screen is a high selective pressure and a selection stringency of 0.1 to 0.01 % surviving genotypes has proven to be favorable for haploid genetic screens (Lucas Jae, personal communication). Therefore, preliminary tests were performed to determine the number of surviving cell clones after infection with cytotoxic *S. aureus* 6850 (Table 3.2). HAP1

wild type cells were infected with *S. aureus* 6850, extracellular bacteria were removed and infected cells were selected by FACS. The loss of the cells during the sorting process as well as while preparing the cells for sorting and during seeding after sorting posed a difficulty. During sorting around 80 % of the HAP1 cells were lost (Figure 3.5F). However, considering this cell loss, two repeated infections of HAP1 cells with *S. aureus* 6850 were sufficient for the anticipated selective pressure in the preliminary tests (0.0768 %).

For the HAP1 screen, mutagenized cells were infected with *S. aureus* 6850, 6 h p.i. uninfected cells were excluded by FACS and infection-surviving cell clones were expanded for several days (Figure 3.6). Part of the cells was used for re-infection. DNA was prepared from the cells, transposon insertion sites were amplified and sequenced, reads were aligned to the human genome and unique gene mutations were counted (Table 6.1). Mutagenized cells were also infected with *S. aureus* Cowan I as negative control. Due to the lack of cytotoxicity of this strain, cell loss can be determined independently of the bacterial infection in contrast to *S. aureus* 6850. Infection of the mutagenized HAP1 cells with Cowan I led to 83 to 89 % of HAP1 cells irrecoverable after sorting and re-seeding (Table 3.3). Taking these numbers into account, the selection stringency calculated for the HAP1 screen (0.0914 %) is sufficient to enrich for target genes. Results from the HAP1 screen also revealed that the complexity of the mutagenized HAP1 cell library was not affected by the cell loss (Table 6.1).

However, only 12 genes were significantly enriched (Table 3.4) and enrichment was not very strong in contrast to other haploid genetic screens (compare e.g. Carette et al., 2011b; Jae et al., 2014; Staring et al., 2017). Significantly enriched were mutants in genes, which are involved in processes such as cell proliferation (TANC2, TBCK, KIF3B, PHLPP1) cell shape (TAOK1, MYH9) and cell death (PAWR), which might be advantageous for survival of those cell clones over others (Table 3.5). TANC2 demonstrated the highest total number of unique mutations suggesting that this gene represents a hot spot for retroviral integration (Table 6.1). Insertion by the retroviral gene trap vector is not completely random and has a bias for inserting around active promoters (LaFave et al., 2014). Taken together, these observations suggest a too low selective pressure in the haploid genetic screen, which complicates the identification of hits over the background noise.

4.2.2 Validation of significantly enriched genes identified in the haploid genetic screen

Extensive literature research revealed only few connections between the genes identified in the HAP1 screen and factors reported in the literature to play a role in bacterial or specifically *S. aureus* infection of host cells. Most interesting was the regulatory role of the kinase TAOK1

with the p38 MAPK and JNK signaling pathways (Hutchison et al., 1998; Moore et al., 2000), which have been previously shown to play a role in *S. aureus* infection. The JNK signaling pathway is involved in *S. aureus*-mediated killing of endothelial cells (Esen et al., 2001), whereas intracellular *S. aureus* exploits a p38 α -mediated mechanism to escape autophagy (Neumann et al., 2016). Autophagy is triggered after invasion of non-professional phagocytes by the *agr*-dependently expressed α -toxin (Mauthe et al., 2012; Mestre et al., 2010; O'Keeffe et al., 2015). *S. aureus* induces activation of p38 α , which localizes at the bacteria-containing autophagosomes. Knock-out of p38 α led to increased co-localization of *S. aureus* with autophagosomes and to decreased survival of intracellular bacteria (Neumann et al., 2016). Thus, knock-out of TAOK1 may result in reduced activation of p38 and JNK signaling pathways and therefore prevent *S. aureus* escape from xenophagy and bacteria-induced host cell death. TAOK1 itself may be activated by α -toxin or, as it was shown that TAOK1 regulates p38 in response to genotoxic stimuli (Raman et al., 2007), by DNA damage caused by the pathogen. *S. aureus* induces DNA double strand breaks during infection (Deplanche et al., 2019).

Subsequent investigation confirmed that p38 is phosphorylated and activated in HAP1 cells during infection with *S. aureus* 6850 (Figure 4.1) (Matsch, 2018). Knock-out of TAOK1 in HAP1 cells prevented the co-localization of phosphorylated p38 and intracellular *S. aureus* (Figure 4.1B), but did not reduce *S. aureus*-induced cell death in HAP1 cells (Figure 4.2). Interestingly, TAOK1 was also identified in a genome-wide CRISPR/Cas9 screen as factor contributing to *S. aureus* infection-induced deoxyadenosine (dAdo) intoxication of phagocytes (Winstel et al., 2018). Disruption of the TAOK1 pathway by p38 inhibition led to increased survival of dAdo-treated macrophages at high concentrations of the inhibitor, but could not fully restore viability of the macrophages.

Further, TBCK was knocked-out in HAP1 cells to determine its role in *S. aureus*-induced host cell death (Matsch, 2018). TBCK regulates the mTor signaling pathway (Liu et al., 2013), which, among other pathways, controls autophagy (Noda and Ohsumi, 1998). As described above, *S. aureus* infection induces autophagy in response to α -toxin. Induction of autophagy has been implicated in promotion of *S. aureus* intracellular replication and induction of host cell death (Schnaith et al., 2007), since bacteria did not replicate within and mediate killing of autophagy-deficient atg5^{-/-} mouse embryonic fibroblasts. Autophagy induction by rapamycin restored both replication and cytotoxicity of non-cytotoxic *S. aureus* strains. TBCK therefore may trigger autophagy via mTor signaling in response to α -toxin exposure and thus enable replication and induction of host cell death of intracellular *S. aureus*. However, loss of TBCK

function did not lead to reduced cell death of mutant HAP1 cells infected with *S. aureus* 6850 when compared to the wild type (Figure 4.2B).

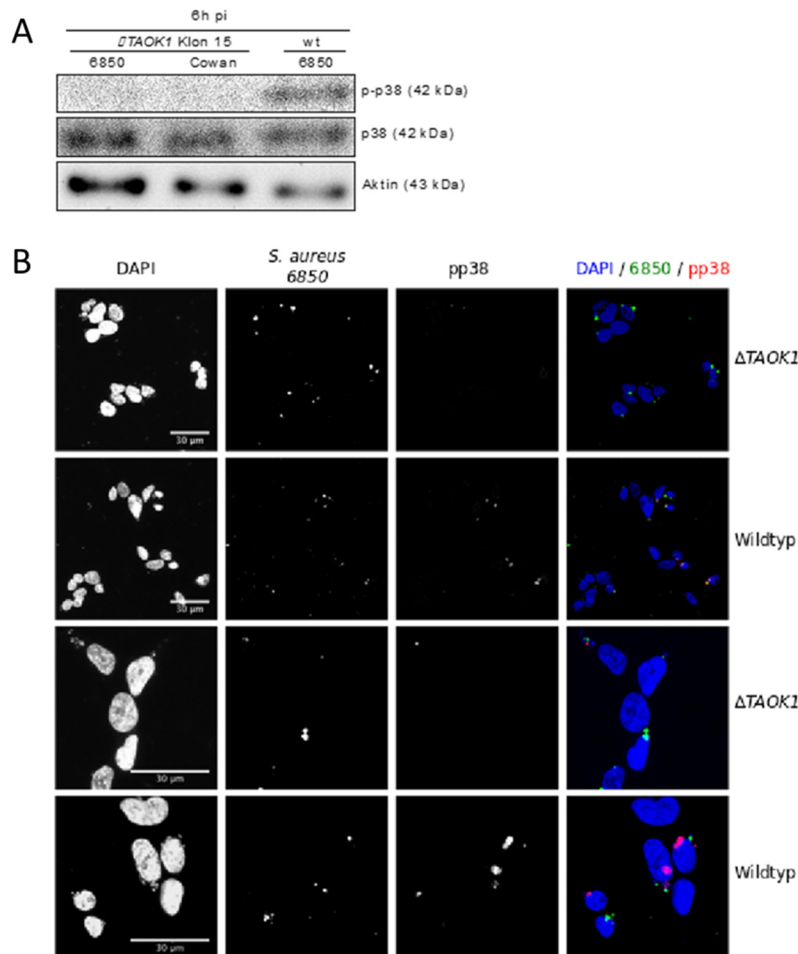


Figure 4.1: Activation of p38 during *S. aureus* infection is dependent on TAOK1.

(A) Immunoblot blot of SDS-PAGE-separated cell lysates from *S. aureus* 6850 or Cowan I infected HAP1 wild type cells (wt) or HAP1 Δ TAOK1 clone 15. Protein levels of phospho-p38 (p-p38) and p38 were detected. Detection of actin served as loading control. (B) Immunofluorescence staining of phospho-p38 (pp38) in HAP1 wild type or Δ TAOK1 cells infected with *S. aureus* 6850 expressing GFP. DNA was stained with DAPI (Matsch, 2018).

Induction of cancer cell apoptosis by PAWR has been previously described (Hebbar et al., 2012) suggesting an involvement in pathogen-induced host cell death, too. The ability of PAWR to selectively cause apoptosis in cancer cells has been attributed to the difference in protein kinase A (PKA) levels between normal and cancer cells (Gurumurthy et al., 2005). However, in a study using quantitative proteomics protein levels of PKA were not altered in *S. aureus*-infected human bronchial epithelial cells compared to uninfected cells, but phosphorylation of other proteins by PKA was important for *S. aureus* intracellular infection (Richter et al., 2016). Further, the knockout of PAWR did not demonstrate changes in host cell death after infection with *S. aureus* (Figure 4.2C) (Matsch, 2018).

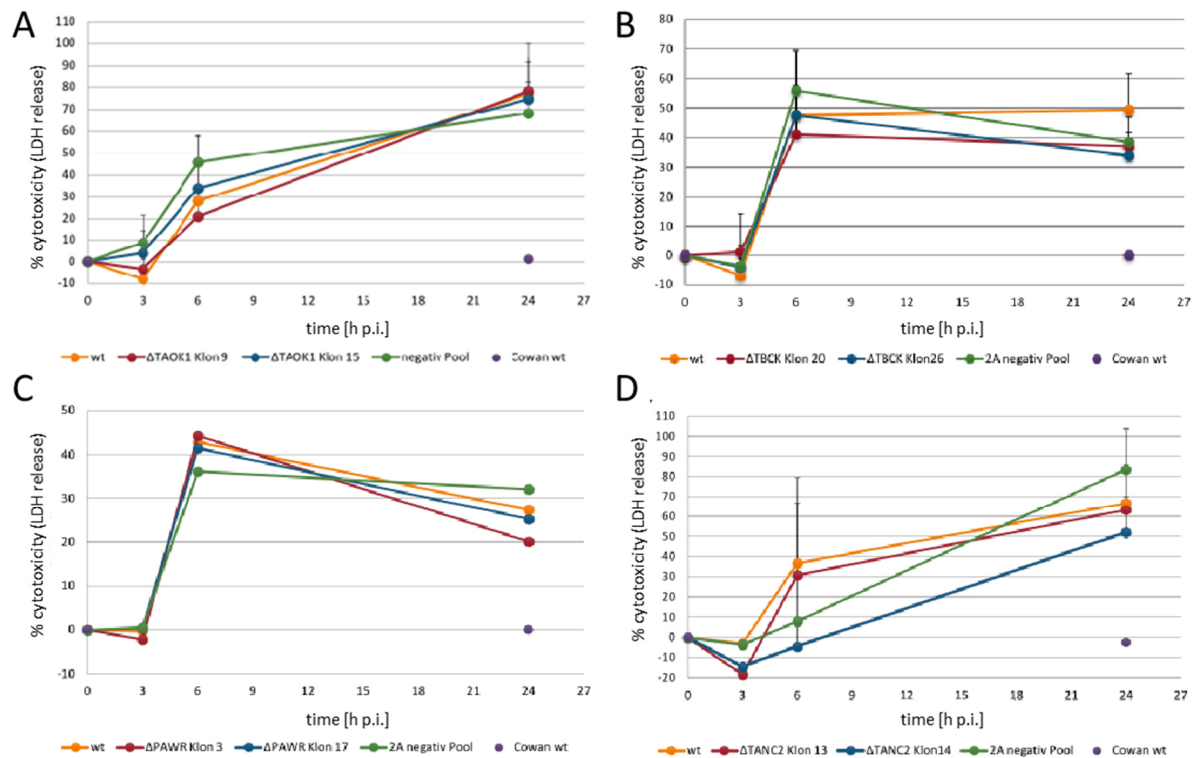


Figure 4.2: The role of TAOK1, TBCK, PAWR and TANC2 in *S. aureus* cytotoxicity.

The genes TAOK1 (A), TBCK (B), PAWR (C) and TANC2 (D) were knocked out in HAP1 cells using CRISPR/Cas9. LDH release was determined at 3, 6 and 24 h p.i. of HAP1 wild type cells (wt, yellow), first HAP1 knock-out clone (red), second HAP1 knock-out clone (blue) and HAP1 negative pool (green) with *S. aureus* 6850. Infection of wild type HAP1 cells with *S. aureus* Cowan I served as non-cytotoxic control (purple) (Matsch, 2018).

Similarly, the CRISPR/Cas9-derived knock-out of TANC2 in HAP1 did not alter host cell death during intracellular *S. aureus* infection, although mutations in TANC2 were highly enriched in cells surviving *S. aureus* infection (Figure 4.2 D) (Matsch, 2018).

4.2.3 Diversity of *S. aureus* intracellular lifestyle

Investigation of the four genes TAOK1, TBCK, PAWR and TANC2, whose mutants were significantly enriched in the haploid screen, did not reveal a role of those genes in host cell death triggered by intracellular *S. aureus*. This further proves, as discussed above that the selective pressure by *S. aureus*-mediated cytotoxicity on HAP1 host cells was insufficient during the haploid genetic screen, although the selection stringency calculated for the HAP1 screen was within the anticipated range when accounting for cell loss (Table 3.3).

One explanation for this may be redundant pathways exploited by *S. aureus* to escape from the host cell. For instance, both apoptotic and necrotic features of cell death have been described for *S. aureus*-induced cytotoxicity (Section 3.2.2 and 3.2.4, Table 4.1) (Horn et al., 2018b), which may indicate that independent processes are activated by intracellular *S. aureus* to kill the host cell. However, the haploid screen cannot identify genes that contribute redundantly to *S. aureus*-induced cell death, because insertional mutagenesis using the retroviral gene trap

vector was titrated to obtain only one mutation per cell (Carette et al., 2009) and insertion sites only from the cell pool, but not from single cells, were mapped.

The high background noise in the HAP1 screen could also be caused by impure sorting of the infected cells. Incorrect sorting of uninfected cells leads to false-positive results. Purity of the sort determined by re-analysis of the sorted cells ranged between 95-96 % (Table 3.3). In comparison to the anticipated selection stringency of 0.1 to 0.01 % a value of 5 to 6 % false-positives caused by impure sorting is very high. Re-infection, however, decreased the total number of false-positives due to impure sorting to 0.18 % for *S. aureus* 6850-infected cells and 0.24 % for *S. aureus* Cowan I-infected cells. Besides, the purity values were very likely reduced by dead cells, which typically occur after sorting due to e.g. mechanical or thermal stress. Therefore, a dead cell exclusion dye should be used when re-analyzing sorted cells.

Another reason for the difficulties in identifying host cell factors involved in *S. aureus*-induced host cell death in the HAP1 screen is heterogeneity in the intracellular infection of *S. aureus*. It was observed that only part of the intracellular bacteria escaped from the phagosome and subsequently killed the host cells (Figure 3.1, Video 1), which was reported by other studies, too (Palma Medina et al., 2019; Rollin et al., 2017). It is known that *S. aureus* can switch to an intracellular persistent state (Proctor et al., 1994), which is mediated by the alternative sigma factor σ^B (Tuchscherer et al., 2015). This small colony variant (SCV) phenotype is associated with reduced intracellular cytotoxicity (Krut et al., 2003) likely resulting from low expression of *agr* (Moisan et al., 2006). The mechanism of the phenotypic switch is not yet understood, but the intracellular milieu of a host cell is sufficient for induction of persistence (Vesga et al., 1996). Phenotypic switching from fully virulent bacteria to SCVs and back seems to be a highly dynamic and rapid process (Tuchscherer et al., 2011). About one quarter of the initial inoculum used for infection is able to induce persistence. Besides, genetic instability of the *agr* locus during laboratory cultivation is well known and was also described to occur *in vivo* (McNamara and Iandolo, 1998; Somerville et al., 2002; Traber and Novick, 2006; Traber et al., 2008). However, a functional *agr* system is essential for phagosomal escape and subsequent cytotoxicity of *S. aureus* (Blaettner et al., 2016; Jarry et al., 2008; Muenzenmayer et al., 2016; Shompole et al., 2003). Therefore, it is conceivable that during the HAP1 screen not all intracellular bacteria were cytotoxic, although a high multiplicity of infection was used.

4.3 Cell death pathways activated by intracellular *S. aureus*

Originally, scientists differentiated between programmed, apoptotic and accidental, necrotic cell death. By now, several pathways of regulated cell death have been described (Section 1.4)

(Galluzzi et al., 2018). Still, all molecular mechanisms are not always fully understood and pathways may be activated simultaneously and overlap. Intracellular bacteria exploit these mechanisms and either prevent premature cell death to preserve their protected replicative niche or promote their exit from the host cell by induction of cell death (Boehme and Rudel, 2009; Flieger et al., 2018). Intracellular *S. aureus* has been shown to induce apoptosis in several types of host cells, autophagy-dependent cell death in epithelial cells and fibroblasts, necroptosis in neutrophils or necrosis-like cell death in endothelial cells (Horn et al., 2018b). Additionally, several studies could not clearly identify the involvement of a particular cell death mechanism or found features of more than one cell death pathway (Flannagan et al., 2016; Greenlee-Wacker et al., 2014; Haslinger-Loeffler et al., 2006; Melehani et al., 2015). In the present study, also characteristics of multiple cell death mechanisms were detected in *S. aureus*-infected cells (Table 4.1).

Table 4.1: Morphological and biochemical changes of different modes of cell death detected in *S. aureus*-infected epithelial cells

Type of cell death	Morphological characteristics	Biochemical characteristics	Reference
Apoptosis	cell contraction	caspase 3/7 activation	Section 3.2.2
	membrane blebs	involvement of caspases (Z-VAD-fmk)	
	nuclear fragmentation	PARP-1 cleavage	
	apoptotic bodies	cytosolic Ca ²⁺ overload	Section 3.2.6.1
		increased cellular H ₂ O ₂	Section 3.2.5
(Secondary) necrosis	cell lysis	no PS exposure	Figure 3.15C
MPT-driven necrosis	cell lysis	cytosolic and mitochondrial Ca ²⁺ overload	Section 3.2.6.1, 3.2.6.2
		increased cellular H ₂ O ₂	Section 3.2.5
Parthantos	cell lysis	AIF cleavage ^a	Section 3.2.3
Necroptosis	cell lysis	MLKL phosphorylation ^a	Figure 3.15D

^a only weak evidence, further prove is required

4.3.1 The role of apoptosis and caspases in *S. aureus*-induced cell death

Morphological features of apoptosis were detected in *S. aureus*-infected cells, such as cell contraction, membrane blebs, nuclear fragmentation and the formation of apoptotic bodies (Figure 3.1, Figure 3.2A and Figure 3.12, Video 3). This observation is in line with other studies, where osteoblasts, epithelial and endothelial cells were infected with *S. aureus* (Chi et al., 2014; Kahl et al., 2000; Menzies and Kourteva, 1998; Tucker et al., 2000). In professional phagocytes membrane blebbing, lamellipodium retraction and nuclear condensation upon infection with *S. aureus* was reported (Flannagan et al., 2016; Kobayashi et al., 2010). The

involvement of caspases, the major executors of apoptosis, in *S. aureus*-induced cell death is controversial. Some studies report a role of caspases in *S. aureus*-infected cells (Flannagan et al., 2016; Haslinger-Loeffler et al., 2005; Jin et al., 2013; Weglarczyk et al., 2004; Wesson et al., 2000), while others describe a caspase-independent cell death mechanism (Kobayashi et al., 2010; Muenzenmayer et al., 2016; Schnaith et al., 2007).

In the present study, a potential role of caspases in *S. aureus*-induced cytotoxicity was detected. Inhibition of caspases led to a strong reduction of *S. aureus* cytotoxicity without affecting bacterial invasion and phagosomal escape (Figure 3.8 and Figure 3.9, Video 2). Intracellular replication may even be enhanced upon Z-VAD-fmk treatment. Morphologically, inhibition of caspases with Z-VAD-fmk attenuated cell contraction of pathogen-infected cells (Video 3). These findings were highly reminiscent of host cell death induced by the *scpA* mutant (Sections 3.3.3.1 and 3.3.3.2). Loss of staphopain A also strongly reduced *S. aureus* intracellular cytotoxicity, while enhancing intracellular replication of the pathogen and preventing host cell contraction. These apparent similarities suggest nonspecific effects of Z-VAD-fmk on staphopain A. Indeed, Z-VAD-fmk has been shown to inhibit the activity of cathepsins, calpains, papain, picornaviral 2A proteinases and peptide N-glycanase (Deszcz et al., 2004; Misaghi et al., 2006; Misaghi et al., 2004; Rozman-Pungercar et al., 2003; Schotte et al., 1999; Wolf et al., 1999). Thus, the results obtained by the use of Z-VAD-fmk have to be carefully evaluated.

Moreover, in the present study activation of effector caspases 3/7 was documented in *S. aureus*-infected cells by a fluorogenic caspase substrate (Figure 3.10, Video 3). Increased fluorescence of the effector caspase substrate occurred at rather late time points of infection, which is after cell contraction and cytosolic Ca^{2+} overload of *S. aureus*-infected cells and approximately at the same time as cell lysis (Figure 3.10 and Figure 3.15A, Video 4 and Video 12). The presence of active caspase 3 subunits and cleavage of PARP-1, which is a substrate of caspases 3/7, further corroborate this observation (Chaitanya et al., 2010). Both plasma membrane permeabilization and effector caspase activation were initiated at the maximum amplitude of cytosolic Ca^{2+} concentration (Figure 3.25, Figure 3.27). It can be speculated that apoptosis, executed by caspases 3/7, and a necrotic cell death, as indicated by permeabilization of the plasma membrane, are triggered in parallel by *S. aureus*-induced cytosolic Ca^{2+} overload. Alternatively, apoptosis and activation of effector caspases may be rapidly followed by secondary necrosis, which occurs in the absence of efferocytosis (Silva, 2010).

Interestingly, *S. aureus*-infected macrophages are also killed through a pathway characterized by membrane blebbing and activation of caspase 3 followed by cell lysis (Flannagan et al., 2016). In this study, plasma membrane permeabilization occurred 12 to 18 min after caspase 3 activation. The authors therefore suggest an apoptotic mode of cell death, which readily transits to a necrotic state and which is likely mediated by *S. aureus* cytolytic toxins.

Besides the potential side effects of Z-VAD-fmk, the inhibitor also did neither attenuate nor abolish caspase 3/7 activation in *S. aureus*-infected cells (Figure 3.11, Video 3). Upon inhibitor treatment, only a delay of caspase 3/7 activation was observed, whereas the amplitude of effector caspase substrate fluorescence was not reduced. Likewise, in *S. aureus*-infected macrophages caspase 3 activation was not completely blocked by Z-VAD-fmk treatment (Flannagan et al., 2016). Caspase 3 activation was found delayed, too, with only a slightly reduced number of caspase 3-positive cells. The identical fluorogenic caspase 3/7 activity reporter was used in both studies, while the concentration of Z-VAD-fmk differed marginally (100 μ M vs. 80 μ M in the present study). It is therefore conceivable that effector caspases are massively activated in pathogen-infected cells and the inhibitor concentrations used were not sufficient to block this process, although rather high amounts of Z-VAD-fmk were applied. Alternatively, cleavage of the fluorogenic caspase substrate might non-specifically be mediated by other proteases, which are activated during *S. aureus* intracellular infection. For instance, other families of human and bacterial cysteine proteases, i.e. calpains and staphopain A, are active during intracellular infection of *S. aureus* and could account for caspase substrate cleavage. However, neither knock-out of calpain 4 nor mutation of staphopain A did abolish effector caspase activation (Figure 3.33 and Figure 3.41, Video 16 and Video 22). The fluorogenic caspase substrate may also be redundantly cleaved by several proteases.

Thus, an involvement of caspases in *S. aureus*-induced cytotoxicity cannot be clearly shown. These findings may also explain the controversial results on the role of caspases by other studies (reviewed in Horn et al., 2018b), as described above.

4.3.2 Parthanatos and necroptosis in *S. aureus*-mediated cytotoxicity

Since contribution of apoptosis in *S. aureus*-induced host cell death was not evident and *S. aureus* cytotoxicity culminated in permeabilization of the host cell membrane (Figure 3.2B, Figure 3.15A-C, Video 4), a possible role of other cell death mechanisms was investigated. Parthanatos, also formerly known as a caspase-independent apoptosis mechanism, is activated, for instance, upon oxidative stress and severe DNA damage. During *S. aureus* infection an increased production of cellular H₂O₂ was observed (Figure 3.16) and DNA damage is induced

(Deplanche et al., 2019). A key factor of parthanatos is AIF, which normally resides within mitochondria, but translocates to the nucleus upon proteolytic activation (Wang et al., 2011; Yu et al., 2006). The truncated form of AIF, and thus activation of parthanatos, can be detected by Western blot. In *S. aureus*-infected HeLa cells only faint bands were detected, which potentially represent truncated AIF (Figure 3.14).

Similarly, necroptosis of *S. aureus*-infected host cells could not be clearly demonstrated. Activation of MLKL upon phosphorylation by RIPK3 triggers this cell death pathway, which culminates in rupture of the cellular membranes and release of intracellular components (Vandenabeele et al., 2010). In the present study, only very weak phosphorylation of MLKL was detected in epithelial cells infected with *S. aureus* (Figure 3.15D). Other studies found an opposing role of MLKL and necroptosis during *S. aureus* infection. *S. aureus*-induced killing of human PMNs partially required the activity of RIPK3, but was independent of MLKL and RIPK1 (Greenlee-Wacker et al., 2017). Likewise, knockout of RIPK3 improved the outcome of mice infected with *S. aureus* in skin, sepsis and pneumonia models, whereas RIPK1 and MLKL were implicated in bacterial clearance (Kitur et al., 2015; Kitur et al., 2016). The authors conclude that the host cell triggers necroptosis executed by RIPK1 and MLKL to limit pathological inflammation, while *S. aureus* exploits apoptosis activated by RIPK3 to induce host cell death.

In conclusion, implication of MLKL and AIF and the respective regulated cell death pathways in cytotoxicity induced by *S. aureus* requires further investigation. Results on AIF cleavage and MLKL phosphorylation need to be further validated by repetition of the experiments with positive controls and evidence of other characteristics of these cell death pathways.

4.4 Oxidative stress in *S. aureus*-infected cells

High levels of intracellular ROS represent an intracellular stress signal that is implicated as stimulus of several types of regulated cell death, for instance intrinsic apoptosis, MPT-driven necrosis, parthanatos or lysosomal cell death (Redza-Dutordoir and Averill-Bates, 2016). Oxidative stress can cause damage to proteins, nucleic acids, lipids, membranes and organelles such as mitochondria (Halliwell, 2011). The present study detected an increase of intracellular H₂O₂ in *S. aureus*-infected cells (Figure 3.16A and B, Video 5). The timing of H₂O₂ increase was reminiscent of plasma membrane permeabilization and activation of caspases 3/7, as it occurred after cell contraction but with the formation of membrane blebs. Due to leakage from the respiratory electron transport chain most intracellular ROS is produced in the mitochondria (Murphy, 2009). NecroX-5 can effectively inhibit mitochondrial H₂O₂ and ONOO⁻ generation

and thus protect the cell from death by caspase-, RIPK1- and PI3K-independent mechanisms such as MPT-driven necrosis or parthanatos (Kim et al., 2010). In *S. aureus*-infected macrophages NecroX-5 treatment reduced bacteria-induced mitochondrial H₂O₂ elevations (Abuaita et al., 2018). *S. aureus*-induced cell death was attenuated by NecroX-5, however no significant decrease was noted (Figure 3.16C). These results indicate an additional source of H₂O₂, besides mitochondria, in *S. aureus*-infected cells. ROS can also be produced by NADPH oxidases (Nox) and their dual oxidase relatives (Duox) localized at various cellular membranes (Dickinson and Chang, 2011). Nox proteins are classically known as important ROS producers implicated in phagocytic killing of pathogens, but Nox and Duox isoforms were also found to be expressed in virtually every cell type and Nox activation is associated with cell death (Bedard and Krause, 2007).

H₂O₂ may also be produced by the host cell to contain bacterial infection. Although non-phagocytic cells produce ROS at lower rates when compared to immune cells, they can kill intracellular pathogens by the same mechanism (Battistoni et al., 2004). *S. aureus* was killed inside osteoblasts via induction of oxidative stress (Mohamed et al., 2016). Besides, the pathogen possesses several strategies to resist oxidative killing by host cells (Clauditz et al., 2006; Cosgrove et al., 2007; Karavolos et al., 2003). Reduced *S. aureus* cytotoxicity upon NecroX-5 treatment rather supports a positive effect of ROS for the pathogen. It is also interesting to note that treatment of *S. aureus* with sublethal doses of H₂O₂ increases expression of virulence factors associated with cytotoxicity such as staphopain A (Das et al., 2016). Therefore, the cellular increase in H₂O₂ may promote *S. aureus* cytotoxicity by enhanced expression of the protease staphopain A. Yet, to what extent the host cell and the bacteria benefit or suffer from intracellular oxidative stress needs further investigation.

4.5 Ca²⁺ signaling and *S. aureus*-induced host cell death

4.5.1 *S. aureus*-mediated cytosolic and mitochondrial Ca²⁺ elevation

As a genome-wide shRNA screen to identify host cell factors involved in *S. aureus*-induced cell death revealed a possible role of Ca²⁺ (Winkler, 2015) and upregulation of transcripts involved in regulation of calcium homeostasis were reported in neutrophils after phagocytosis of CA-MRSA strains (Kobayashi et al., 2010), alterations in intracellular Ca²⁺ levels during *S. aureus* intracellular infection were investigated in the present study. Intriguingly, intracellular *S. aureus* induced a massive overload of cytosolic Ca²⁺ levels after the onset of bacterial intracellular replication and cell contraction (Figure 3.17, Video 6). This was followed by the formation of membrane blebs, cell lysis and the subsequent decrease of cytosolic Ca²⁺

concentration. These observations indicate that the perturbation of intracellular Ca^{2+} homeostasis by *S. aureus* infection may result in cell lysis. Results from later experiments could support the hypothesis that prolonged high cytosolic Ca^{2+} concentrations culminate in cell lysis (Figure 3.27). Thus, a high and sustained concentration of cytosolic Ca^{2+} induced by intracellular *S. aureus* may induce a necrotic cell death by excess stimulation of Ca^{2+} -sensitive targets, such as phospholipases, proteases and endonucleases in the cytosol (Caro and Cederbaum, 2007; McConkey et al., 1989; Tang et al., 1996).

The rise in cytosolic Ca^{2+} was succeeded by Ca^{2+} elevation in mitochondria (Figure 3.18, Video 7). Mitochondria are involved in Ca^{2+} compartmentalization and are able to buffer cytosolic Ca^{2+} to a certain extent. A Ca^{2+} rise in the cytosol is typically paralleled by a cycle of mitochondrial Ca^{2+} uptake and subsequent release (Celsi et al., 2009). The affinity of the mitochondrial uniporter for Ca^{2+} is rather low and the size of the mitochondrial Ca^{2+} pool is small under physiological conditions, but upon high cytosolic Ca^{2+} concentrations larger amounts of Ca^{2+} can accumulate in the mitochondria (Thor et al., 1984). Excessive Ca^{2+} uptake by mitochondria activates PTP via CYPD leading to MPT-driven necrosis (Baines et al., 2005; Basso et al., 2005). Abrupt loss of permeability to small solutes of the inner mitochondrial membrane leads to $\Delta\Psi_m$ dissipation and an osmotic imbalance eventually resulting in the structural breakdown of the organelle. MPT-driven necrosis induced mitochondrial swelling and mitochondrial outer membrane rupture. Accordingly, the cytosolic Ca^{2+} rise induced by intracellular *S. aureus* may lead to cell death by subsequent mitochondrial Ca^{2+} overload and MPT-driven necrosis. The detection of mitochondrial morphological alterations in *S. aureus*-infected cells based on Mito-LAR-Geco fluorescence was impeded by host cell contraction and may require higher magnification imaging. The generation of cellular H_2O_2 in *S. aureus*-infected cells (Figure 3.16) may further point towards a role of MPT-driven necrosis, because MPT can result from or generate ROS (Izzo et al., 2016; Kinnally et al., 2011). Besides, as discussed above, intracellular *S. aureus* induces plasma membrane permeabilization, which is the final step of this cell death pathway.

Interestingly, the facultative intracellular pathogen *Shigella* was shown to induce MPT-driven necrotic cell death (Carneiro et al., 2009; Dupont et al., 2009). This cell death pathway was induced as a result of an altered ratio of the two BCL2 family members Bnip3 and BCL2 leading to loss of mitochondrial inner membrane potential, mitochondrial damage and CYPD activation. It is speculated that a sustained cytosolic Ca^{2+} increase due to plasma membrane permeabilization induces mitochondrial Ca^{2+} overload and thus MPT-driven necrosis (Bonnet and Tran Van Nhieu, 2016). So far, only during host cell invasion of *Shigella* local and global

Ca²⁺ responses were noted, which are regulated by a bacterial type III effector (Sun et al., 2017; Tran Van Nhieu et al., 2003; Tran Van Nhieu et al., 2013).

Ca²⁺ signaling is implicated in several cell death pathways and mechanisms (Section 1.4.5). However, the amplitude and duration of the cytosolic, ER and mitochondrial Ca²⁺ signal in these processes are only poorly characterized. Thus, the cytosolic Ca²⁺ increase induced by intracellular *S. aureus* was directly compared to Ca²⁺ signal in cells dying by different apoptotic mechanisms (Figure 3.28). Cell death was induced by TNF α and CHX treatment (Pajak et al., 2005), staurosporine (Kabir et al., 2002) and the translation inhibitor blasticidin (Lindqvist et al., 2012). Morphologically, cell death induced by TNF α /CHX and blasticidin resembled that of intracellular *S. aureus*, whereas cell death induced by staurosporine, which was reported to also induce necroptosis (Dunai et al., 2012; Simenc and Lipnik-Stangelj, 2012), appeared more necrotic. However, none of the treatments induced cytosolic Ca²⁺ elevations to a similar extent when compared to intracellular *S. aureus*. This observation suggests that a high cytosolic Ca²⁺ increase is not characteristic to all cell death mechanisms and may rather be unique for *S. aureus*-mediated cell death.

4.5.2 The role of calpains in *S. aureus*-induced host cell death

Ca²⁺ can also induce apoptosis via the Ca²⁺-activated cysteine proteases calpains. During infection with *S. aureus*, the activation of effector caspases 3/7 followed after the increase in cytosolic Ca²⁺ (Figure 3.25) suggesting an involvement of an apoptotic mode of cell death in *S. aureus*-infected cells. Indeed, calpains were activated almost simultaneously with the cytosolic Ca²⁺ rise (Figure 3.29). However, knock-down and knock-out of calpains 1, 2 and 4 could not abolish or reduce *S. aureus*-induced host cell death (Figure 3.31 and Figure 3.32). Additionally, activation of effector caspases was not affected by calpain 4 gene inactivation (Figure 3.33). Therefore, activation of calpains 1, 2 and 4 plays no essential role in *S. aureus*-induced host cell death. Apart from these most studied calpain isoforms, other members of the calpain family might be implicated in *S. aureus*-induced host cell death. So far, fifteen mammalian calpain isoforms have been identified, out of which some show only tissue specific expression (Ono and Sorimachi, 2012). Calpain 10, which is ubiquitously expressed, was shown to be targeted to mitochondria as well as calpain 1, 2 and 4 and calpastatin (Kar et al., 2007; Ozaki et al., 2009; Tavares and Duque-Magalhaes, 1991). Mitochondrial calpains are associated with apoptosis by cleaving the mitochondrial Na⁺/Ca²⁺ exchanger, which may lead to mitochondrial Ca²⁺ overload and release of proapoptotic proteins, such as cytochrome C (Kar et al., 2009). Mitochondrial calpains were also shown to cleave AIF upon an intracellular Ca²⁺

increase leading to parthanatos (Chen et al., 2011; Norberg et al., 2008; Ozaki et al., 2009; Polster et al., 2005). However, AIF cleavage was only weak in *S. aureus*-infected cells (Figure 3.14). Interestingly, overexpression of mitochondrial calpain 10 led to mitochondrial fragmentation and swelling, which was blocked with the MPT inhibitor cyclosporine A (Arrington et al., 2006). This observation is in line with earlier findings that a mitochondrial calpain-like activity regulated MPT (Aguilar et al., 1996; Gores et al., 1998).

Shigella flexneri also activated calpains, which ultimately leads to necrotic cell death (Bergounioux et al., 2012). Calpains, which are activated by Ca^{2+} release from intracellular stores and calpastatin degradation by the bacterial virulence factor VirA, prevent rapid apoptotic cell death by degradation of p53. At the same time, calpains likely act as executioners for MPT-driven necrosis. Despite similarities such as activation of calpain 4, p53 degradation was not observed in *S. aureus*-infected cells (Figure 3.13) and knock-out and knock-down of calpain 4 did not abrogate bacterial induction of cell death (Figure 3.33).

4.5.3 Origin of *S. aureus* triggered Ca^{2+} rise

The endoplasmic reticulum is the major compartment for Ca^{2+} storage and signaling and thus usually the source of increases of cytosolic Ca^{2+} concentration. In non-excitabile cells, such as epithelial cells, perturbations of the cellular Ca^{2+} homeostasis may arise from Ca^{2+} leakage from the ER or, less frequently, the extracellular space. In the present study, a cytosolic Ca^{2+} overload was detected after infection of reporter cells with *S. aureus* (Figure 3.17, Video 6). If this Ca^{2+} originated from the ER, an earlier decrease in the ER Ca^{2+} concentration should be measurable. Indeed, a decline in the ER Ca^{2+} level was detected after *S. aureus* infection of epithelial cells, which coincided with the cytosolic Ca^{2+} rise (Figure 3.19). However, it was difficult to resolve the temporal correlation between cytosolic and ER Ca^{2+} signals during *S. aureus* infection. The dynamic range of the ER Ca^{2+} sensor (ER-LAR-Geco) is rather small (Figure 3.20A and B) (Wu et al., 2014b) requiring exact measurements to detect the small changes in its fluorescence. However, live cell imaging over longer time periods often does not allow for high spatiotemporal accuracy. Since the live cells move laterally but also in z-direction, imaging of whole cells and even more their intracellular organelles is impeded, for instance, by a shift in focus or migration of the cell or cellular structure under investigation.

Automated cell segmentation for every time frame would be desirable to identify single cells, but the fluorescent signal of the Ca^{2+} sensors was too weak for this purpose. Other ER Ca^{2+} sensors could be tested, which may exhibit a higher dynamic range, although very few ER Ca^{2+} sensors have been developed until now (Henderson et al., 2015; Suzuki et al., 2014; Zhuo et

al., 2015). Brightfield images have been used for cell segmentation, but this requires deep learning models with individual adaptation from experiment to experiment (Falk et al., 2019). The alternative manual definition of each region of interest (ROI), such as the cell cytoplasm, in all samples for each of the recorded time frames would not only be time consuming, but would also introduce the possibility of human error. In present study, hence a single ROI was defined, for which the mean fluorescence was extracted from all time frames. Changes in cell shape were taken into account as good as possible.

Therefore, it cannot be clearly concluded, whether the decline in ER Ca^{2+} concentrations is the direct cause or result of the cytosolic Ca^{2+} overload. After the initial decrease of ER Ca^{2+} a rise was detected, which peaked during the second half of the cytosolic Ca^{2+} rise, but did not exceed the resting ER Ca^{2+} concentration. The decrease followed by an increase in ER Ca^{2+} concentration points to a role of SOCE in *S. aureus*-induced Ca^{2+} cytosolic overload. During SOCE, release of Ca^{2+} from the ER triggers an influx of the ion from the extracellular space to refill the internal Ca^{2+} stores (Hogan and Rao, 2015).

To investigate a potential role of SOCE in *S. aureus*-induced perturbations of cellular Ca^{2+} and subsequent cell death, the inhibitor 2-APB was applied. This substance inhibits SOCE at higher concentrations ($\geq 10\text{-}50\ \mu\text{M}$), while potentiation occurs at lower concentrations ($1\text{-}5\ \mu\text{M}$) (Dellis et al., 2011; Prakriya and Lewis, 2001). Inhibition of SOCE with $30\ \mu\text{M}$ 2-APB led to strong reduction of *S. aureus* intracellular cytotoxicity (Figure 3.21A). While treatment with 2-APB did not affect *S. aureus* invasion and phagosomal escape, an effect on intracellular replication is likely (Figure 3.21B-E). *S. aureus* intracellular growth was attenuated upon inhibitor treatment. Likewise, *S. aureus* showed impaired growth *in vitro* in broth, when treated with 2-APB (Figure 3.21F). Thus, the inhibitory effect of 2-APB on *S. aureus*-induced host cell death may partly be attributed to bacterial growth attenuation. However, in the present study *S. aureus*-induced host cell death by staphopain A was replication-independent.

To minimize the inhibitory effect of 2-APB on *S. aureus* growth, infected epithelial cells were treated with the inhibitor only shortly before reaching intracellular Ca^{2+} overload (approx. 3 h p.i.), instead of 1 h before infection. Although intracellular replication of *S. aureus* was observed upon 2-APB treatment (Video 9), no effect of the SOCE inhibitor on *S. aureus*-induced cytosolic Ca^{2+} increase was detected (Figure 3.22). The efficacy of 2-APB should be examined and other SOCE inhibitors could be tested, since 2-APB lacks specificity (Hu et al., 2004; Maruyama et al., 1997; Missiaen et al., 2001; Trebak et al., 2002; Xu et al., 2005) and has a replication attenuating effect on *S. aureus*. However, most of the available inhibitors also

have drawbacks, such as poor specificity or high toxicity (Jairaman and Prakriya, 2013; Putney, 2010).

An attenuation of the cytosolic Ca^{2+} increase was observed, when extracellular Ca^{2+} was omitted from the cell culture medium (Figure 3.23B-D). This observation proves that intracellular *S. aureus* induces a Ca^{2+} influx from the extracellular space via the plasma membrane. Whether this is the initial cause for the cytosolic Ca^{2+} overload, cannot be answered, since the observed ER Ca^{2+} decrease may also be responsible for the cytosolic Ca^{2+} increase.

Treatment of *S. aureus*-infected cells with BAPTA-AM to chelate intracellular Ca^{2+} did not impair the cytosolic Ca^{2+} increase (Figure 3.24B-D). A test with the Ca^{2+} ionophore ionomycin showed that loading of HeLa cells with BAPTA-AM only shortly (seconds to minutes) delayed the cytosolic Ca^{2+} rise in a concentration-dependent manner (Figure 3.24A). Thus, the highly selective Ca^{2+} chelator is saturated rather fast even at high concentrations, which are cytotoxic at extended incubation times. At non-cytotoxic concentrations (5 μM), the Ca^{2+} -chelating effect of BAPTA-AM likely was too small to substantially interfere with *S. aureus*-induced cytosolic Ca^{2+} overload.

In conclusion, intracellular *S. aureus* triggers both an efflux of Ca^{2+} from the ER and Ca^{2+} influx from the extracellular space. Both events occur rather simultaneously or with a short delay in the range of only seconds to a few minutes. Inhibitor studies with 2-APB rather exclude an involvement of SOCE in this process. To conclude a possible mechanism for the *S. aureus*-induced cellular Ca^{2+} perturbations the timing of Ca^{2+} efflux from the ER and Ca^{2+} influx via the plasma membrane will have to be resolved.

4.5.4 *S. aureus* virulence factors and cytosolic Ca^{2+} overload

Secreted bacterial factors induce strong cytosolic Ca^{2+} elevations and oscillations in HeLa cells when added to the cell culture medium (Figure 3.34, Video 17). The morphology and Ca^{2+} rise in HeLa cells treated with *S. aureus* supernatant resembled that of intracellular *S. aureus* infection, in that the cytosolic Ca^{2+} elevation occurred after cell contraction but before the formation of plasma membrane blebs (compare Figure 3.17 and Figure 3.34). Thus, virulence factors secreted by *S. aureus* may also trigger Ca^{2+} flux(es) when secreted into the cytoplasm of the host cell by intracellular bacteria. Although the inner leaflet of the plasma membrane differs significantly from the outer leaflet in its composition of proteins and phospholipids, receptor-independent pore formation of *S. aureus* toxins, for instance, can possibly also occur from the inner side of the plasma membrane.

The pore-forming toxin α -hemolysin can nonspecifically integrate into the membrane at high concentrations (Hildebrand et al., 1991). Areas of specific lipid composition may be involved in receptor-independent attachment of α -toxin to the host cell plasma membrane (Galdiero and Gouaux, 2004; Tomita et al., 1992; Valeva et al., 2006; Watanabe et al., 1987; Ziesemer et al., 2019). *S. aureus* α -toxin was shown to induce cytosolic Ca^{2+} elevation in different types of cells at sublytic concentrations (Eichstaedt et al., 2009; Fink et al., 1989; Kwak et al., 2012; Rath et al., 2013; Suttorp et al., 1985; von Hoven et al., 2016) and calcium ions can enter the cells directly through α -toxin pores (Eiffler et al., 2016). Thus, it is conceivable that intracellular *S. aureus* secretes α -hemolysin in the cytoplasm of the host cell, where it forms Ca^{2+} -permissive pores in the plasma membrane and possibly also in membranes of host cell organelles, such as the ER, and consequently triggers cellular Ca^{2+} perturbations and host cell death. Yet, infection of epithelial cells with an α -toxin mutant did not significantly reduce the cytosolic Ca^{2+} overload (Figure 3.35). Only a small reduction of intracellular cytotoxicity of *S. aureus* Δhla was detected at 6 h p.i.. The same applies for a mutant in the virulence regulator gene *rsp*, which was previously shown to play a role in *S. aureus*-induced cytotoxicity and regulates α -toxin expression (Figure 3.35) (Das et al., 2016; Horn et al., 2018a).

Besides α -hemolysin, *S. aureus* leukotoxins can induce intracellular Ca^{2+} increase in leukocytes and neurons (Jover et al., 2013; Staali et al., 1998; Woodin and Wieneke, 1963; Yanai et al., 2014). Leukotoxin pores are likely not directly permeable to calcium ions, but mediate cellular Ca^{2+} rise indirectly by binding to a receptor linked to a divalent cation-selective channel or to the channel itself, which is activated subsequently. The bi-component γ -hemolysin was the most potent leukotoxin, initiating transient rises in intracellular Ca^{2+} concentration. However, a mutant in *hlgB* did not show reduced intracellular cytotoxicity in HeLa cells (Figure 3.36A). PSMs were shown to induce Ca^{2+} influx in human neutrophils, which can be blocked by an inhibitor for formyl peptide receptor 2 (FPR2) (Cheung et al., 2015; Kretschmer et al., 2010). Loss of function of PSM β or PSM γ (δ -toxin) did not affect *S. aureus*-induced host cell death, whereas a mutant in PSM α exhibited reduced cytotoxicity (Figure 3.36B). The reduced cytotoxicity of the PSM α mutant results, at least partly, from its ability to mediate phagosomal escape, which is a prerequisite for *S. aureus*-induced host cell death (Figure 3.1, Figure 3.43) (Blaettner et al., 2016; Grosz et al., 2014; Lam et al., 2010; Muenzenmayer et al., 2016).

It is conceivable that indirect Ca^{2+} influx, for instance, by activating or inhibiting a Ca^{2+} -permissive channel, is not only triggered by pore-forming toxins, but also by other *S. aureus* virulence factors, such as proteases or lipases. As mentioned above, mammalian calpain proteases were shown to cleave the mitochondrial $\text{Na}^+/\text{Ca}^{2+}$ exchanger (Kar et al., 2009).

Inactivation of the *S. aureus* cysteine protease staphopain A significantly reduced induction of host cell death (Figure 3.36A), but did not abolish cytosolic Ca^{2+} overload (Figure 3.40). Only the duration of the cytosolic Ca^{2+} rise seems to be shorter and Ca^{2+} oscillations were observed indicating that staphopain A might directly or indirectly interfere with *S. aureus*-induced Ca^{2+} overload. As inactivation of staphopain A did not abolish cellular Ca^{2+} perturbations and infection with the non-cytotoxic *S. aureus* strain RN4220 expressing staphopain A did not affect cytosolic Ca^{2+} concentrations (Figure 3.44D, Video 24), other factors are likely involved.

4.6 Staphopains in *S. aureus* intracellular cytotoxicity

4.6.1 A novel function for staphopain A

Staphopain A is one of two cysteine proteases secreted by *S. aureus*, which was first identified by Arvidson in 1973 (Arvidson et al., 1973). It was named after its structural similarity to the papaya protease papain, which founds the most abundant family of cysteine proteases, including human cathepsins and calpains. Early studies revealed that staphopain A possesses a rather broad substrate specificity, resembling the substrate preferences of cathepsins (Bjoerklind and Joernvall, 1974). The role of staphopain A in *S. aureus* virulence is not fully clear. Staphopain A can process elastin, collagen and fibrinogens found in connective tissues and extracellular matrix, which allows the conclusion that the protease is implicated in tissue invasion and destruction (Ohbayashi et al., 2011; Potempa et al., 1988). Staphopain A is also associated with biofilm dispersal, although aureolysin has a higher impact (Loughran et al., 2014; Mootz et al., 2013). Besides, staphopain A was shown to interfere with innate immunity by cleaving pulmonary surfactant protein A in the lung and the chemokine receptor CXCR2 on leukocytes (Kantyka et al., 2013; Laarman et al., 2012). Staphopain A promotes vascular leakage by activating the plasma kallikrein/kinin system, resulting in hypotension (Imamura et al., 2005).

In the present study, a novel function of staphopain A was elucidated. A *S. aureus* mutant in staphopain A as well as treatment of infected cells with the specific cysteine protease inhibitor E-64 showed significantly reduced cytotoxicity in epithelial cells (Figure 3.37). The morphology of the host cells infected with the staphopain A mutant further proved the involvement of this cysteine protease in the intracellular lifestyle of *S. aureus*. Infected cells showed no or less cell contraction when compared to infection with the wild type strain. Reintroduction of a functional staphopain A operon could reverse the attenuated cytotoxicity of the *scpA* mutant in a MRSA- and MSSA-strain background (Figure 3.38). In contrast, inactivation of the protease function of staphopain A by introduction of an active site mutation

did not restore *S. aureus* cytotoxicity. A role of the protease in other steps of *S. aureus* intracellular lifestyle was excluded. Staphopain A inactivation had no effect on *S. aureus* invasion and phagosomal escape in HeLa cells (Figure 3.39A-C). Intracellular replication was favored by knock-out of staphopain A at later time points of infection (8 h p.i., Figure 3.39D and E), but this effect was likely due to delayed induction of host cell death by the staphopain A mutant.

To clearly assign a cytotoxic role to staphopain A, the protease was overexpressed in an otherwise non-cytotoxic strain. *S. aureus* RN4220 exhibits altered expression of virulence factors, for instance this strain shows delayed expression of the virulence regulator *agr* with small amounts of its major effector RNAPIII and failure to translate α - and δ -toxin (Traber and Novick, 2006). This likely explains its non-cytotoxic phenotype of RN4220. Ectopic expression of δ -toxin allows RN4220 to translocate into the cytoplasm of the host cell, but no induction of host cell death was observed (Giese et al., 2011). However, additional expression of staphopain A led to plasma membrane permeabilization of the infected host cell (Figure 3.42). Expression of the inactive protease did not induce host cell death. Similarly, inhibition of cysteine proteases with E-64 reduced staphopain A-induced cytotoxicity. These findings prove the cytotoxic potential of this cysteine protease. Whether staphopain A acts alone or in combination with other bacterial factors, cannot be concluded with certainty, since *S. aureus* RN4220 may express other virulence factors involved.

4.6.2 The role of staphopain B in *S. aureus* cytotoxicity

Despite sharing limited primary sequence identity (46 %), ScpA and SspB share high structural similarity and the tertiary structure of both staphopains closely resembles the fold of papain (Filipek et al., 2005; Hofmann et al., 1993). Similarly to ScpA, staphopain B is implicated in biofilm dispersion and affects the host connective tissue and coagulation system (Loughran et al., 2014; Mootz et al., 2013; Ohbayashi et al., 2011; Potempa et al., 1988). However, staphopain B is reported to have a far more restricted specificity compared to staphopain A. It promotes bacterial survival by degradation of the antimicrobial peptide LL-37 and prevents phagocytosis and killing of the pathogen by host immune cells (Elmwall et al., 2017; Smagur et al., 2009a; Smagur et al., 2009b; Sonesson et al., 2017). Interestingly, treatment of human neutrophils and monocytes with purified staphopain B led to a mixed necrotic- and apoptotic-like cell death by reducing the expression of CD11b/CD18 integrins on the cell surface (Smagur et al., 2009b). In the present study no significant effect of staphopain B on *S. aureus*

intracellular cytotoxicity was detected (Figure 3.36A). A *sspB* mutant induced similar rates of host cell death in HeLa cells at 6 h p.i. when compared to the wild type.

To exclude that staphopain A possesses an extracellular cytotoxic activity similar to staphopain B, HeLa cells were treated with sterile supernatant from *S. aureus* RN4220 overexpressing staphopain A (Figure 3.43B and C). Supernatant, which contained the functional staphopain A, did not induce higher cell death rates compared to supernatant from RN4220 overexpressing non-functional staphopain A. Therefore, staphopain A possesses no extracellular cytotoxicity. Nevertheless, treatment with the RN4220 supernatant did induce a concentration-dependent cell lysis, but other factors besides staphopain A may account for this effect. For instance, δ -toxin, which is also highly expressed by this strain, has been shown to possess cytolytic properties (Verdon et al., 2009). Interestingly, it was found that staphopain A activity is inhibited in human plasma. The protease inhibitors α 2-macroglobulin, cystatins, serpins or other yet unidentified inhibitors may account for this effect (Kantyka et al., 2011a; Potempa et al., 1988; Takahashi et al., 1999). Staphopain B activity is affected by mouse serum, but not by human serum (Kantyka et al., 2011b). Additionally, no effective inhibitors of SspB in human plasma were found. These findings further strengthen an intracellular role of staphopain A in human cells.

4.6.3 Mechanism of staphopain A-induced cell death

Further evidence for an intracellular activity of staphopain A comes from the observation that cytotoxicity induced by staphopain A was only detected after translocation of *S. aureus* to the host cell cytosol (Figure 3.43A). This is in line with previous findings that induction of host cell death by intracellular *S. aureus* highly depends on phagosomal escape in non-phagocytic cells (Figure 3.1) (Blaettner et al., 2016; Grosz et al., 2014; Lam et al., 2010). Staphopain A may cleave protein(s) present in the phagosome, which only induce cell death upon entering the cytosol. Alternatively, the direct target substrate(s) of staphopain A may only have a cytoplasmic location.

Induction of cell death by staphopain A was rather fast. Host cell contraction was observed within minutes after phagosomal escape of *S. aureus* (Figure 3.43A, Video 23). Therefore, expression of SspA may already be induced during phagosomal residence of the bacterium. Intriguingly, *agr* expression, which induces synthesis of staphopain A (Bjoerklind and Arvidson, 1980), was found to be increased in phagolysosomes (Grosz et al., 2014; Qazi et al., 2001; Shompole et al., 2003). A comprehensive transcriptome study also showed that

staphopain A expression was increased during *S. aureus* intracellular residence in THP1 cells, however paradoxically not in the bronchial epithelial cell line S9 (Maeder et al., 2016).

Staphopain A expression is further dependent on the pleiotropic transcriptional regulator Rsp, which plays a role in *S. aureus* intracellular cytotoxicity in epithelial cells (Das et al., 2016). Infection of HeLa cells with the *rsp* mutant significantly reduced host cell death induced by intracellular *S. aureus* at 4 and 8 h p.i. in contrast to the wild type. This phenotype is reminiscent of the *scpA* mutant and may allow the conclusion that the attenuated cytotoxicity of the *rsp* mutant is the consequence of diminished staphopain A expression. However, *rsp* expression and *scpA* expression in the *rsp* mutant in intracellular *S. aureus* was not yet investigated.

Upon staphopain-induced host cell killing of HeLa cells, features of an apoptotic mode of cell death were detected. Infected cells first exposed phosphatidylserine on the cell surface indicated by annexin V staining, while at later time points loss of plasma membrane integrity shown by additional staining with 7AAD was detected (Figure 3.44), which is typical for apoptosis (Martin et al., 1995). Further, characteristic morphology of apoptotic cells, such as cell contraction, retraction of pseudopodia, plasma membrane blebbing and formation of extracellular vesicles, was observed (Kroemer et al., 2009, Lynch et al., 2017). Effector caspases were activated with the formation of membrane blebs (Video 24), but no elevations in cytosolic Ca^{2+} concentration were observed. The trypanosomal cysteine cathepsin cruzipain was shown to directly activate caspases 3/7 (Stoka et al., 2001). Since the activation of effector caspases upon staphopain A-induced cell death happened late, i.e. hours after phagosomal escape and cell contraction, and inactivation of staphopain A did not affect *S. aureus*-induced effector caspase activation (Figure 3.41, Video 22), a direct activation of caspases 3/7 by staphopain A is rather unlikely. Additionally, cytotoxicity of intracellular *S. aureus* RN4220 expressing staphopain A was attenuated after inhibition of caspases with Z-VAD-fmk (Figure 3.44). A potential inhibitory effect of Z-VAD-fmk on staphopain A has to be elucidated, as mentioned above. The fact that inhibition of caspases did not fully abolish staphopain A-induced cytotoxicity and permeabilization of the host cell plasma membrane was observed, suggests that other cell death pathways may be activated by staphopain A in parallel to apoptosis.

Interestingly, staphopains share the closest structural similarity with cathepsin B among the eukaryotic enzymes (Filipek et al., 2003; Hofmann et al., 1993) and the overall substrate preferences of human cathepsin H are most similar those of staphopains (Kalinska et al., 2012). This further underpins an intracellular role of staphopain A. Cytoplasmic location of cathepsins

upon lysosomal membrane rupture is associated with the induction of apoptosis via the cleavage of Bid and degradation of the anti-apoptotic BCL2 homologues BCL2, Bcl-xL and Mcl-1 (Cirman et al., 2004, Droga-Mazovec et al., 2008, Roberg et al., 2002, Stoka et al., 2001). A decrease in the protein amount of full-length Bid was detected in *S. aureus*-infected cells accompanied by the appearance of a slightly smaller protein, which possibly represents a degradation product of Bid (Figure 3.13A). The size of this degraded version of Bid is, however, larger (approx. 21-19 kDa) compared to truncated Bid (tBid, 15 kDa). tBid is generated by caspase 8-mediated Bid cleavage in so-called type II cells, which include HeLa cells, upon activation of extrinsic apoptosis and connects both apoptosis pathways by inducing cytochrome c release through the action of BAX or BAK (Borner, 2003). Bid is not only cleaved by caspase 8, but also by other caspases, granzyme B, calpains and cathepsins (Billen et al., 2008). Interestingly, JNK-dependent cleavage of Bid results in a larger degradation product, termed jBid, exhibiting approximately 21 kDa (Deng et al., 2003). The protease responsible for generation of jBid was not yet identified, but jBid translocates from the cytosol to mitochondria, where it induces MOMP. It is conceivable that staphopain A induces cleavage of Bid upon phagosomal escape of *S. aureus*, which results in jBid-mediated apoptosis. Staphopain A was also reported to liberate the activity of cathepsin B *in vitro* by proteolytic degradation of cystatin C, a natural inhibitor of cysteine proteases (Vincent et al., 2007). Accordingly, cathepsin-induced cell death may also represent a pathway of staphopain A-induced cytotoxicity.

4.6.4 *In vivo* effects of staphopain A

The *in vivo* relevance of *S. aureus* staphopain A is still under debate. Staphopain A had no effect on *S. aureus* virulence in a mouse abscess model (Shaw et al., 2004). However, *S. aureus* expression of staphopain A was enhanced during infection in a murine osteomyelitis model compared to *in vitro* exponential growth, similarly to other extracellular proteases of *S. aureus* (Szafranska et al., 2014). Moreover, antibodies specific to ScpA, SspB, SspA and Aur were detected in sera from *S. aureus*-infected mice (Calander et al., 2008). A *S. aureus* mutant lacking all ten major extracellular proteases, including staphopain A, exhibited higher mortality, but impairment during organ invasion and decreases in skin abscess formation in murine infection models (Kolar et al., 2013). The protease-null mutant also displayed increased bacterial numbers in professional phagocytes of whole human blood. This observation is in concordance with findings from the present study, where loss of staphopain A leads to higher numbers of intracellular bacteria at late time points of infection (8 h p.i.) (Figure 3.39D and E). However, the observed phenotype of the protease-null mutant cannot be clearly assigned to

staphopain A, since other extracellular proteases of *S. aureus* may also play a role. In the present study loss of staphopain A function led to less bacterial burden in the lung tissue of infected mice when compared to the wild type (Figure 3.45). This contrasts the above mentioned findings in a mouse abscess model (Shaw et al., 2004). These discrepancies may result from the use of different mouse models and bacterial strains. *S. aureus* 8325-4, which was used for infection in the latter study, was shown to be less cytotoxic in human cells compared to USA300 (Rasigade et al., 2013). Consequently, the intracellular cytotoxicity induced by staphopain A may not be as relevant for *in vivo* infection of *S. aureus* 8325-4 in contrast to USA300.

Quantification of intracellular *S. aureus* in HeLa cells revealed that loss of staphopain A function led to increased bacterial growth presumably due to prolonged intracellular residence of the pathogen (Figure 3.39D and E). Oppositely, staphopain A facilitated *S. aureus* colonization of the lung *in vivo*. However, these findings are not directly comparable, since strictly intracellular bacteria were quantified in the *in vitro* experiment with HeLa cells, whereas the bacterial location was not defined in the *in vivo* experiment. It is also not clear, whether the wild type was capable of colonizing the murine lung more efficiently due to increased bacterial replication or enhanced survival. Besides, other effects of staphopain A cannot be excluded, such as interference with innate immunity. For instance, staphopain A was shown degrade lung surfactant protein A (SP-A) (Kantyka et al., 2013).

4.7 Summary and perspectives

The fact that the mutation of staphopain A only delays, but does not prevent cytotoxicity induced by intracellular *S. aureus*, suggests that the pathogen possesses several mechanisms to kill the host cell. In the present study at least two independent mechanisms were detected, which were temporally separated (Figure 4.3). First, staphopain A causes a relatively rapid cell death. It induces host cell killing within minutes characterized by cell contraction, induction of an apoptosis-like cell death and subsequent cell lysis. Phagosomal escape was identified as a prerequisite for staphopain A-induced cell death. Intracellular replication was not required proving that *S. aureus*-induced host cell death is not solely the consequence of mechanical stress resulting from bacterial overload. The mechanism of staphopain A-induced cell death is not yet clear. The protease may induce cytotoxicity by cleaving a cytoplasmic target protein.

A pull-down experiment could be performed to identify the intracellular target of staphopain A. Ideally, staphopain A containing the active site mutation would be fused to an affinity tag, since this may result in a more stable interaction of the protease with its target(s). Bid may be a promising target substrate of staphopain A. Therefore, Bid cleavage upon infection with the

ScpA mutant should be tested. Further, it would be interesting to elucidate the expression and localization of staphopain A in the host cell. Regarding the *in vivo* role of *S. aureus* staphopain A, cytotoxicity of the protease in primary cells as well as immune cells should be studied. Investigation of the presence of intracellular *S. aureus* in the lung or other organs and its contribution to virulence of the pathogen *in vivo* is of high interest for the present study. 3D tissue culture models, *ex vivo*-models, organoids or mouse models could be used to mimic the human *in vivo* situation. Application of cell-impermeable antibiotics or the use of cells lines devoid of bacterial invasins may allow to study the impact of intracellularity of *S. aureus in vivo*.

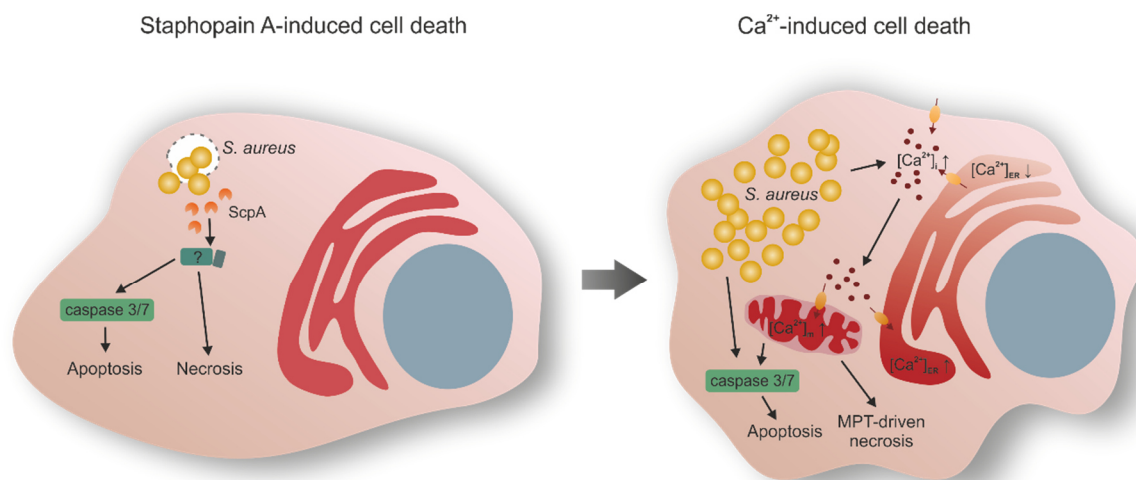


Figure 4.3: Potential mechanisms of *S. aureus* induced host cell death.

Upon phagosomal escape intracellular *S. aureus* employs its cysteine protease staphopain A to induce a mixed apoptotic and necrotic cell death. Staphopain A may cleave a yet unknown target substrate in the host cell cytosol, which results in cell contraction, activation of caspases 3/7 and plasma membrane permeabilization. This is followed by a Ca^{2+} -induced, staphopain A-independent cell death mechanisms. Intracellular *S. aureus* triggers cytosolic Ca^{2+} overload by release of Ca^{2+} from the ER and influx via the plasma membrane. High cytosolic Ca^{2+} concentrations induce a (re-)uptake of the ion into mitochondria and ER. Perturbations of mitochondrial Ca^{2+} homeostasis result in MPT-driven necrosis and/or apoptosis by activation of effector caspases 3/7.

Host cell death induced by bacteria lacking ScpA occurred at later stages of infection and is associated with the formation of membrane blebs, cellular Ca^{2+} perturbations, effector caspase activation, ROS generation and permeabilization of the plasma membrane. A bacterial virulence factor, which requires increased bacterial density or a certain critical concentration, in contrast to staphopain A, may account for this later cell death. Alternatively, physical forces imposed by the high number of intracellular bacteria occupying the host cell cytoplasm can trigger initial Ca^{2+} permeability of the plasma membrane, which culminates in cell lysis. *S. aureus*-induced Ca^{2+} perturbations in the host cell may lead to MPT-driven necrosis, which is initiated by mitochondrial Ca^{2+} overload. In parallel, apoptosis may be activated, which results in effector caspase activation.

The cytotoxicity of *S. aureus* double knock-out mutants in staphopain A and other virulence factors, for instance leukotoxins, PSMs, lipases or other extracellular proteases, can be tested to reveal, if additional bacterial factors are involved and if host cell death can be completely abrogated. Furthermore, inhibition of intracellular replication after phagosomal escape of the staphopain A mutant using, for instance, rifampicin can help to uncover, whether bacterial replication is necessary for staphopain A-independent host cell killing by *S. aureus*. Inhibition of cytosolic Ca^{2+} overload is difficult, as depletion of Ca^{2+} from the medium leads to detachment of cells and has cytotoxic effects. Nevertheless, reduced cytotoxicity of *S. aureus* under Ca^{2+} -depleted conditions would substantiate cytosolic Ca^{2+} overload as the trigger for staphopain A-independent cytotoxicity of *S. aureus*. To clearly assign MPT-driven necrosis to *S. aureus*-induced host cell death further experimentation needs to be performed. For instance, CYPD, a major mediator of MPT-driven necrosis, could be knocked-out or inhibited with cyclosporine A. Loss of the mitochondrial membrane potential may be investigated using MitoTracker (Chazotte, 2011). It would be also interesting to elucidate the role of calpain 10 in *S. aureus*-induced cytosolic and mitochondrial Ca^{2+} increase potentially leading to MPT-driven cell death. A role of caspases in *S. aureus*-induced cell death could not conclusively be proven. Using knock-out cell lines of caspases 3/7 may help to clarify, if these caspases are essential for *S. aureus*-induced cell death. Direct inhibition of staphopain A by Z-VAD-fmk may be tested *in vitro* to study potential unspecific inhibitory effects.

The activation of at least two independent cell death mechanisms by intracellular *S. aureus* might be the reason, why the haploid genetic screen resulted in very few and poorly enriched hits. Although the determined selective pressure applied by infection with cytotoxic *S. aureus* was sufficient for a successful haploid genetic screen, the identification of relevant genes was impeded by a high background noise. False-positives, which could not be eliminated, likely led to reduction of the selective pressure. Besides redundancy of *S. aureus*-activated cell death pathways, the heterogeneity in *S. aureus* intracellular infection may also be responsible. Nevertheless, a genetic screen could be performed with *S. aureus* wild type and staphopain A mutant infection to discriminate between the two cell death mechanisms. Moreover, other selection criteria for FACS may be used, such as the cytosolic location of the bacteria, since phagosomal escape is known to be a prerequisite for induction of host cell death in non-phagocytic cells (Blaettner et al., 2016; Strobel et al., 2016) and SCVs persist in phagosomes (Horn et al., 2018b).

5 References

- Abuaita, B.H., Schultz, T.L., and O'Riordan, M.X. (2018). Mitochondria-Derived Vesicles Deliver Antimicrobial Reactive Oxygen Species to Control Phagosome-Localized *Staphylococcus aureus*. *Cell Host Microbe* *24*, 625-636 e625.
- Aggarwal, B.B., Gupta, S.C., and Kim, J.H. (2012). Historical perspectives on tumor necrosis factor and its superfamily: 25 years later, a golden journey. *Blood* *119*, 651-665.
- Aguilar, H.I., Botla, R., Arora, A.S., Bronk, S.F., and Gores, G.J. (1996). Induction of the mitochondrial permeability transition by protease activity in rats: a mechanism of hepatocyte necrosis. *Gastroenterology* *110*, 558-566.
- Aguilar, J., Urday-Cornejo, V., Donabedian, S., Perri, M., Tibbetts, R., and Zervos, M. (2010). *Staphylococcus aureus* meningitis: case series and literature review. *Medicine (Baltimore)* *89*, 117-125.
- Aits, S., and Jaattela, M. (2013). Lysosomal cell death at a glance. *J Cell Sci* *126*, 1905-1912.
- Alexander, E.H., Bento, J.L., Hughes, F.M., Jr., Marriott, I., Hudson, M.C., and Bost, K.L. (2001). *Staphylococcus aureus* and *Salmonella enterica* serovar Dublin induce tumor necrosis factor-related apoptosis-inducing ligand expression by normal mouse and human osteoblasts. *Infect Immun* *69*, 1581-1586.
- Alexander, E.H., Rivera, F.A., Marriott, I., Anguita, J., Bost, K.L., and Hudson, M.C. (2003). *Staphylococcus aureus* - induced tumor necrosis factor - related apoptosis - inducing ligand expression mediates apoptosis and caspase-8 activation in infected osteoblasts. *BMC Microbiol* *3*, 5.
- Alonzo, F., 3rd, Benson, M.A., Chen, J., Novick, R.P., Shopsin, B., and Torres, V.J. (2012). *Staphylococcus aureus* leucocidin ED contributes to systemic infection by targeting neutrophils and promoting bacterial growth in vivo. *Mol Microbiol* *83*, 423-435.
- Alonzo, F., 3rd, Kozhaya, L., Rawlings, S.A., Reyes-Robles, T., DuMont, A.L., Myszkowski, D.G., Landau, N.R., Unutmaz, D., and Torres, V.J. (2013). CCR5 is a receptor for *Staphylococcus aureus* leukotoxin ED. *Nature* *493*, 51-55.
- Aman, M.J., Karauzum, H., Bowden, M.G., and Nguyen, T.L. (2010). Structural model of the pre-pore ring-like structure of Pantone-Valentine leukocidin: providing dimensionality to biophysical and mutational data. *J Biomol Struct Dyn* *28*, 1-12.
- Andersson, B.S., Collins, V.P., Kurzrock, R., Larkin, D.W., Childs, C., Ost, A., Cork, A., Trujillo, J.M., Freireich, E.J., Siciliano, M.J., *et al.* (1995). KBM-7, a human myeloid leukemia cell line with double Philadelphia chromosomes lacking normal c-ABL and BCR transcripts. *Leukemia* *9*, 2100-2108.
- Archer, N.K., Mazaitis, M.J., Costerton, J.W., Leid, J.G., Powers, M.E., and Shirtliff, M.E. (2011). *Staphylococcus aureus* biofilms: properties, regulation, and roles in human disease. *Virulence* *2*, 445-459.
- Arrington, D.D., Van Vleet, T.R., and Schnellmann, R.G. (2006). Calpain 10: a mitochondrial calpain and its role in calcium-induced mitochondrial dysfunction. *Am J Physiol Cell Physiol* *291*, C1159-1171.
- Arvidson, S., Holme, T., and Lindholm, B. (1973). Studies on extracellular proteolytic enzymes from *Staphylococcus aureus*. I. Purification and characterization of one neutral and one alkaline protease. *Biochim Biophys Acta* *302*, 135-148.

- Baba, T., Takeuchi, F., Kuroda, M., Yuzawa, H., Aoki, K., Oguchi, A., Nagai, Y., Iwama, N., Asano, K., Naimi, T., *et al.* (2002). Genome and virulence determinants of high virulence community-acquired MRSA. *Lancet* *359*, 1819-1827.
- Baggen, J., Thibaut, H.J., Staring, J., Jae, L.T., Liu, Y., Guo, H., Slager, J.J., de Bruin, J.W., van Vliet, A.L., Blomen, V.A., *et al.* (2016). Enterovirus D68 receptor requirements unveiled by haploid genetics. *Proc Natl Acad Sci U S A* *113*, 1399-1404.
- Baines, C.P., Kaiser, R.A., Purcell, N.H., Blair, N.S., Osinska, H., Hambleton, M.A., Brunskill, E.W., Sayen, M.R., Gottlieb, R.A., Dorn, G.W., *et al.* (2005). Loss of cyclophilin D reveals a critical role for mitochondrial permeability transition in cell death. *Nature* *434*, 658-662.
- Bantel, H., Sinha, B., Domschke, W., Peters, G., Schulze-Osthoff, K., and Janicke, R.U. (2001). alpha-Toxin is a mediator of *Staphylococcus aureus*-induced cell death and activates caspases via the intrinsic death pathway independently of death receptor signaling. *J Cell Biol* *155*, 637-648.
- Baran, J., Guzik, K., Hryniewicz, W., Ernst, M., Flad, H.D., and Pryjma, J. (1996). Apoptosis of monocytes and prolonged survival of granulocytes as a result of phagocytosis of bacteria. *Infect Immun* *64*, 4242-4248.
- Barnhart, B.C., Alappat, E.C., and Peter, M.E. (2003). The CD95 type I/type II model. *Semin Immunol* *15*, 185-193.
- Barrangou, R., Birmingham, A., Wiemann, S., Beijersbergen, R.L., Hornung, V., and Smith, A. (2015). Advances in CRISPR-Cas9 genome engineering: lessons learned from RNA interference. *Nucleic Acids Res* *43*, 3407-3419.
- Basso, E., Fante, L., Fowlkes, J., Petronilli, V., Forte, M.A., and Bernardi, P. (2005). Properties of the permeability transition pore in mitochondria devoid of Cyclophilin D. *J Biol Chem* *280*, 18558-18561.
- Bateman, B.T., Donegan, N.P., Jarry, T.M., Palma, M., and Cheung, A.L. (2001). Evaluation of a tetracycline-inducible promoter in *Staphylococcus aureus* in vitro and in vivo and its application in demonstrating the role of sigB in microcolony formation. *Infect Immun* *69*, 7851-7857.
- Battistoni, A., Ajello, M., Ammendola, S., Superti, F., Rotilio, G., and Valenti, P. (2004). Involvement of reactive oxygen species in bacterial killing within epithelial cells. *Int J Immunopathol Pharmacol* *17*, 71-76.
- Bayles, K.W., Wesson, C.A., Liou, L.E., Fox, L.K., Bohach, G.A., and Trumble, W.R. (1998). Intracellular *Staphylococcus aureus* escapes the endosome and induces apoptosis in epithelial cells. *Infect Immun* *66*, 336-342.
- Bedard, K., and Krause, K.H. (2007). The NOX family of ROS-generating NADPH oxidases: physiology and pathophysiology. *Physiol Rev* *87*, 245-313.
- Benfield, T., Espersen, F., Frimodt-Moller, N., Jensen, A.G., Larsen, A.R., Pallesen, L.V., Skov, R., Westh, H., and Skinhoj, P. (2007). Increasing incidence but decreasing in-hospital mortality of adult *Staphylococcus aureus* bacteraemia between 1981 and 2000. *Clin Microbiol Infect* *13*, 257-263.
- Berchtold, M.W., Brinkmeier, H., and Muntener, M. (2000). Calcium ion in skeletal muscle: its crucial role for muscle function, plasticity, and disease. *Physiol Rev* *80*, 1215-1265.
- Bergounioux, J., Elisee, R., Prunier, A.L., Donnadiou, F., Sperandio, B., Sansonetti, P., and Arbibe, L. (2012). Calpain activation by the *Shigella flexneri* effector VirA regulates key steps in the formation and life of the bacterium's epithelial niche. *Cell Host Microbe* *11*, 240-252.

- Bhosale, G., Sharpe, J.A., Sundier, S.Y., and Duchon, M.R. (2015). Calcium signaling as a mediator of cell energy demand and a trigger to cell death. *Ann N Y Acad Sci* 1350, 107-116.
- Biedenbach, D.J., Moet, G.J., and Jones, R.N. (2004). Occurrence and antimicrobial resistance pattern comparisons among bloodstream infection isolates from the SENTRY Antimicrobial Surveillance Program (1997-2002). *Diagn Microbiol Infect Dis* 50, 59-69.
- Bilan, D.S., Pase, L., Joosen, L., Gorokhovatsky, A.Y., Ermakova, Y.G., Gadella, T.W., Grabher, C., Schultz, C., Lukyanov, S., and Belousov, V.V. (2013). HyPer-3: a genetically encoded H₂O₂ probe with improved performance for ratiometric and fluorescence lifetime imaging. *ACS Chem Biol* 8, 535-542.
- Billen, L.P., Shamas-Din, A., and Andrews, D.W. (2008). Bid: a Bax-like BH3 protein. *Oncogene* 27 *Suppl 1*, S93-104.
- Birsoy, K., Wang, T., Possemato, R., Yilmaz, O.H., Koch, C.E., Chen, W.W., Hutchins, A.W., Gultekin, Y., Peterson, T.R., Carette, J.E., *et al.* (2013). MCT1-mediated transport of a toxic molecule is an effective strategy for targeting glycolytic tumors. *Nat Genet* 45, 104-108.
- Bischoff, M., Dunman, P., Kormanec, J., Macapagal, D., Murphy, E., Mounts, W., Berger-Bachi, B., and Projan, S. (2004). Microarray-based analysis of the *Staphylococcus aureus* sigmaB regulon. *J Bacteriol* 186, 4085-4099.
- Bizat, N., Hermel, J.M., Humbert, S., Jacquard, C., Creminon, C., Escartin, C., Saudou, F., Krajewski, S., Hantraye, P., and Brouillet, E. (2003). In vivo calpain/caspase cross-talk during 3-nitropropionic acid-induced striatal degeneration: implication of a calpain-mediated cleavage of active caspase-3. *J Biol Chem* 278, 43245-43253.
- Bjoerklind, A., and Arvidson, S. (1980). Mutants of *Staphylococcus Aureus* Affected in the Regulation of Exoprotein Synthesis. *FEMS Microbiology Letters* 7, 203-206.
- Bjoerklind, A., and Joernvall, H. (1974). Substrate specificity of three different extracellular proteolytic enzymes from *Staphylococcus aureus*. *Biochim Biophys Acta* 370, 524-529.
- Blaettner, S., Das, S., Paprotka, K., Eilers, U., Krischke, M., Kretschmer, D., Remmele, C.W., Dittrich, M., Muller, T., Schuelein-Voelk, C., *et al.* (2016). *Staphylococcus aureus* Exploits a Non-ribosomal Cyclic Dipeptide to Modulate Survival within Epithelial Cells and Phagocytes. *PLoS Pathog* 12, e1005857.
- Blomen, V.A., Majek, P., Jae, L.T., Bigenzahn, J.W., Nieuwenhuis, J., Staring, J., Sacco, R., van Diemen, F.R., Olk, N., Stukalov, A., *et al.* (2015). Gene essentiality and synthetic lethality in haploid human cells. *Science* 350, 1092-1096.
- Blomgren, K., Zhu, C., Wang, X., Karlsson, J.O., Leverin, A.L., Bahr, B.A., Mallard, C., and Hagberg, H. (2001). Synergistic activation of caspase-3 by m-calpain after neonatal hypoxia-ischemia: a mechanism of "pathological apoptosis"? *J Biol Chem* 276, 10191-10198.
- Boehme, L., and Rudel, T. (2009). Host cell death machinery as a target for bacterial pathogens. *Microbes Infect* 11, 1063-1070.
- Boehning, D., Patterson, R.L., Sedaghat, L., Glebova, N.O., Kurosaki, T., and Snyder, S.H. (2003). Cytochrome c binds to inositol (1,4,5) trisphosphate receptors, amplifying calcium-dependent apoptosis. *Nat Cell Biol* 5, 1051-1061.
- Bogaert, D., van Belkum, A., Sluijter, M., Luijendijk, A., de Groot, R., Rumke, H.C., Verbrugh, H.A., and Hermans, P.W. (2004). Colonisation by *Streptococcus pneumoniae* and *Staphylococcus aureus* in healthy children. *Lancet* 363, 1871-1872.

- Bohach, G.A., Fast, D.J., Nelson, R.D., and Schlievert, P.M. (1990). Staphylococcal and streptococcal pyrogenic toxins involved in toxic shock syndrome and related illnesses. *Crit Rev Microbiol* 17, 251-272.
- Bokarewa, M.I., Jin, T., and Tarkowski, A. (2006). Staphylococcus aureus: Staphylokinase. *Int J Biochem Cell Biol* 38, 504-509.
- Bonnet, M., and Tran Van Nhieu, G. (2016). How Shigella Utilizes Ca(2+) Jagged Edge Signals during Invasion of Epithelial Cells. *Front Cell Infect Microbiol* 6, 16.
- Borner, C. (2003). The Bcl-2 protein family: sensors and checkpoints for life-or-death decisions. *Mol Immunol* 39, 615-647.
- Bouillot, S., Reboud, E., and Huber, P. (2018). Functional Consequences of Calcium Influx Promoted by Bacterial Pore-Forming Toxins. *Toxins (Basel)* 10.
- Bouzakri, K., Ribaux, P., and Halban, P.A. (2009). Silencing mitogen-activated protein 4 kinase 4 (MAP4K4) protects beta cells from tumor necrosis factor-alpha-induced decrease of IRS-2 and inhibition of glucose-stimulated insulin secretion. *J Biol Chem* 284, 27892-27898.
- Boya, P., Gonzalez-Polo, R.A., Casares, N., Perfettini, J.L., Dessen, P., Larochette, N., Metivier, D., Meley, D., Souquere, S., Yoshimori, T., *et al.* (2005). Inhibition of macroautophagy triggers apoptosis. *Mol Cell Biol* 25, 1025-1040.
- Bradley, S.F. (2005). Staphylococcus aureus pneumonia: emergence of MRSA in the community. *Semin Respir Crit Care Med* 26, 643-649.
- Bravo-Santano, N., Ellis, J.K., Mateos, L.M., Calle, Y., Keun, H.C., Behrends, V., and Letek, M. (2018). Intracellular Staphylococcus aureus Modulates Host Central Carbon Metabolism To Activate Autophagy. *mSphere* 3.
- Brinkmann, V., and Zychlinsky, A. (2012). Neutrophil extracellular traps: is immunity the second function of chromatin? *J Cell Biol* 198, 773-783.
- Bukowski, M., Wladyka, B., and Dubin, G. (2010). Exfoliative toxins of Staphylococcus aureus. *Toxins (Basel)* 2, 1148-1165.
- Burian, M., Rautenberg, M., Kohler, T., Fritz, M., Krismer, B., Unger, C., Hoffmann, W.H., Peschel, A., Wolz, C., and Goerke, C. (2010a). Temporal expression of adhesion factors and activity of global regulators during establishment of Staphylococcus aureus nasal colonization. *J Infect Dis* 201, 1414-1421.
- Burian, M., Wolz, C., and Goerke, C. (2010b). Regulatory adaptation of Staphylococcus aureus during nasal colonization of humans. *Plos One* 5, e10040.
- Cai, Z., Jitkaew, S., Zhao, J., Chiang, H.C., Choksi, S., Liu, J., Ward, Y., Wu, L.G., and Liu, Z.G. (2014). Plasma membrane translocation of trimerized MLKL protein is required for TNF-induced necroptosis. *Nat Cell Biol* 16, 55-65.
- Calander, A.M., Dubin, G., Potempa, J., and Tarkowski, A. (2008). Staphylococcus aureus infection triggers production of neutralizing, V8 protease-specific antibodies. *FEMS Immunol Med Microbiol* 52, 267-272.
- Cao, J.Y., Poddar, A., Magtanong, L., Lumb, J.H., Mileur, T.R., Reid, M.A., Dovey, C.M., Wang, J., Locasale, J.W., Stone, E., *et al.* (2019). A Genome-wide Haploid Genetic Screen Identifies Regulators of Glutathione Abundance and Ferroptosis Sensitivity. *Cell Rep* 26, 1544-1556 e1548.

- Carette, J.E., Guimaraes, C.P., Varadarajan, M., Park, A.S., Wuethrich, I., Godarova, A., Kotecki, M., Cochran, B.H., Spooner, E., Ploegh, H.L., *et al.* (2009). Haploid genetic screens in human cells identify host factors used by pathogens. *Science* *326*, 1231-1235.
- Carette, J.E., Guimaraes, C.P., Wuethrich, I., Blomen, V.A., Varadarajan, M., Sun, C., Bell, G., Yuan, B., Muellner, M.K., Nijman, S.M., *et al.* (2011a). Global gene disruption in human cells to assign genes to phenotypes by deep sequencing. *Nat Biotechnol* *29*, 542-546.
- Carette, J.E., Raaben, M., Wong, A.C., Herbert, A.S., Obernosterer, G., Mulherkar, N., Kuehne, A.I., Kranzusch, P.J., Griffin, A.M., Ruthel, G., *et al.* (2011b). Ebola virus entry requires the cholesterol transporter Niemann-Pick C1. *Nature* *477*, 340-343.
- Carneiro, L.A., Travassos, L.H., Soares, F., Tattoli, I., Magalhaes, J.G., Bozza, M.T., Plotkowski, M.C., Sansonetti, P.J., Molkentin, J.D., Philpott, D.J., *et al.* (2009). Shigella induces mitochondrial dysfunction and cell death in nonmyeloid cells. *Cell Host Microbe* *5*, 123-136.
- Caro, A.A., and Cederbaum, A.I. (2007). Role of intracellular calcium and phospholipase A2 in arachidonic acid-induced toxicity in liver cells overexpressing CYP2E1. *Arch Biochem Biophys* *457*, 252-263.
- Celsi, F., Pizzo, P., Brini, M., Leo, S., Fotino, C., Pinton, P., and Rizzuto, R. (2009). Mitochondria, calcium and cell death: a deadly triad in neurodegeneration. *Biochim Biophys Acta* *1787*, 335-344.
- Centers for Disease, C., and Prevention (1999). Four pediatric deaths from community-acquired methicillin-resistant *Staphylococcus aureus* - Minnesota and North Dakota, 1997-1999. *MMWR Morb Mortal Wkly Rep* *48*, 707-710.
- Cerella, C., Diederich, M., and Ghibelli, L. (2010). The dual role of calcium as messenger and stressor in cell damage, death, and survival. *Int J Cell Biol* *2010*, 546163.
- Chaitanya, G.V., Steven, A.J., and Babu, P.P. (2010). PARP-1 cleavage fragments: signatures of cell-death proteases in neurodegeneration. *Cell Commun Signal* *8*, 31.
- Chavakis, T., Wiechmann, K., Preissner, K.T., and Herrmann, M. (2005). *Staphylococcus aureus* interactions with the endothelium: the role of bacterial "secretable expanded repertoire adhesive molecules" (SERAM) in disturbing host defense systems. *Thromb Haemost* *94*, 278-285.
- Chazotte, B. (2011). Labeling mitochondria with MitoTracker dyes. *Cold Spring Harb Protoc* *2011*, 990-992.
- Chen, M., He, H., Zhan, S., Krajewski, S., Reed, J.C., and Gottlieb, R.A. (2001). Bid is cleaved by calpain to an active fragment in vitro and during myocardial ischemia/reperfusion. *J Biol Chem* *276*, 30724-30728.
- Chen, Q., Paillard, M., Gomez, L., Ross, T., Hu, Y., Xu, A., and Lesnefsky, E.J. (2011). Activation of mitochondrial mu-calpain increases AIF cleavage in cardiac mitochondria during ischemia-reperfusion. *Biochem Biophys Res Commun* *415*, 533-538.
- Chen, X., Li, W., Ren, J., Huang, D., He, W.T., Song, Y., Yang, C., Li, W., Zheng, X., Chen, P., *et al.* (2014). Translocation of mixed lineage kinase domain-like protein to plasma membrane leads to necrotic cell death. *Cell Res* *24*, 105-121.
- Cheng, A.G., McAdow, M., Kim, H.K., Bae, T., Missiakas, D.M., and Schneewind, O. (2010). Contribution of coagulases towards *Staphylococcus aureus* disease and protective immunity. *PLoS Pathog* *6*, e1001036.

- Cheung, A.L., Bayer, A.S., Zhang, G., Gresham, H., and Xiong, Y.Q. (2004). Regulation of virulence determinants in vitro and in vivo in *Staphylococcus aureus*. *FEMS Immunol Med Microbiol* 40, 1-9.
- Cheung, G.Y., Yeh, A.J., Kretschmer, D., Duong, A.C., Tuffuor, K., Fu, C.L., Joo, H.S., Diep, B.A., Li, M., Nakamura, Y., *et al.* (2015). Functional characteristics of the *Staphylococcus aureus* delta-toxin allelic variant G10S. *Sci Rep* 5, 18023.
- Chi, C.Y., Lin, C.C., Liao, I.C., Yao, Y.C., Shen, F.C., Liu, C.C., and Lin, C.F. (2014). Panton-Valentine leukocidin facilitates the escape of *Staphylococcus aureus* from human keratinocyte endosomes and induces apoptosis. *J Infect Dis* 209, 224-235.
- Choi, C.S., Yin, C.S., Bakar, A.A., Sakewi, Z., Naing, N.N., Jamal, F., and Othman, N. (2006). Nasal carriage of *Staphylococcus aureus* among healthy adults. *J Microbiol Immunol Infect* 39, 458-464.
- Chong, J.X., Caputo, V., Phelps, I.G., Stella, L., Worgan, L., Dempsey, J.C., Nguyen, A., Leuzzi, V., Webster, R., Pizzuti, A., *et al.* (2016). Recessive Inactivating Mutations in TBCK, Encoding a Rab GTPase-Activating Protein, Cause Severe Infantile Syndromic Encephalopathy. *Am J Hum Genet* 98, 772-781.
- Chua, B.T., Guo, K., and Li, P. (2000). Direct cleavage by the calcium-activated protease calpain can lead to inactivation of caspases. *J Biol Chem* 275, 5131-5135.
- Clapham, D.E. (2007). Calcium signaling. *Cell* 131, 1047-1058.
- Clauditz, A., Resch, A., Wieland, K.P., Peschel, A., and Gotz, F. (2006). Staphyloxanthin plays a role in the fitness of *Staphylococcus aureus* and its ability to cope with oxidative stress. *Infect Immun* 74, 4950-4953.
- Clement, S., Vaudaux, P., Francois, P., Schrenzel, J., Huggler, E., Kampf, S., Chaponnier, C., Lew, D., and Lacroix, J.S. (2005). Evidence of an intracellular reservoir in the nasal mucosa of patients with recurrent *Staphylococcus aureus* rhinosinusitis. *J Infect Dis* 192, 1023-1028.
- Coleman, D.C., Arbuthnott, J.P., Pomeroy, H.M., and Birkbeck, T.H. (1986). Cloning and expression in *Escherichia coli* and *Staphylococcus aureus* of the beta-lysin determinant from *Staphylococcus aureus*: evidence that bacteriophage conversion of beta-lysin activity is caused by insertional inactivation of the beta-lysin determinant. *Microb Pathog* 1, 549-564.
- Cookson, B.T., and Brennan, M.A. (2001). Pro-inflammatory programmed cell death. *Trends Microbiol* 9, 113-114.
- Cosgrove, K., Coutts, G., Jonsson, I.M., Tarkowski, A., Kokai-Kun, J.F., Mond, J.J., and Foster, S.J. (2007). Catalase (KatA) and alkyl hydroperoxide reductase (AhpC) have compensatory roles in peroxide stress resistance and are required for survival, persistence, and nasal colonization in *Staphylococcus aureus*. *J Bacteriol* 189, 1025-1035.
- Crossley, K., Landesman, B., and Zaske, D. (1979). An outbreak of infections caused by strains of *Staphylococcus aureus* resistant to methicillin and aminoglycosides. II. Epidemiologic studies. *J Infect Dis* 139, 280-287.
- Dahlberg, C.L., and Juo, P. (2014). The WD40-repeat proteins WDR-20 and WDR-48 bind and activate the deubiquitinating enzyme USP-46 to promote the abundance of the glutamate receptor GLR-1 in the ventral nerve cord of *Caenorhabditis elegans*. *J Biol Chem* 289, 3444-3456.
- Das, S., Lindemann, C., Young, B.C., Muller, J., Osterreich, B., Ternette, N., Winkler, A.C., Paprotka, K., Reinhardt, R., Forstner, K.U., *et al.* (2016). Natural mutations in a *Staphylococcus aureus* virulence regulator attenuate cytotoxicity but permit bacteremia and abscess formation. *Proc Natl Acad Sci U S A* 113, E3101-3110.

- David, K.K., Andrabi, S.A., Dawson, T.M., and Dawson, V.L. (2009). Parthanatos, a messenger of death. *Front Biosci (Landmark Ed)* *14*, 1116-1128.
- de Duve, C. (1983). Lysosomes revisited. *Eur J Biochem* *137*, 391-397.
- de Haas, C.J., Veldkamp, K.E., Peschel, A., Weerkamp, F., Van Wamel, W.J., Heezius, E.C., Poppelier, M.J., Van Kessel, K.P., and van Strijp, J.A. (2004). Chemotaxis inhibitory protein of *Staphylococcus aureus*, a bacterial antiinflammatory agent. *J Exp Med* *199*, 687-695.
- Dellis, O., Mercier, P., and Chomienne, C. (2011). The boron-oxygen core of borinate esters is responsible for the store-operated calcium entry potentiation ability. *BMC Pharmacol* *11*, 1.
- Denecker, G., Vercammen, D., Declercq, W., and Vandenamee, P. (2001). Apoptotic and necrotic cell death induced by death domain receptors. *Cell Mol Life Sci* *58*, 356-370.
- Deng, Y., Ren, X., Yang, L., Lin, Y., and Wu, X. (2003). A JNK-dependent pathway is required for TNF α -induced apoptosis. *Cell* *115*, 61-70.
- Denton, D., Xu, T., and Kumar, S. (2015). Autophagy as a pro-death pathway. *Immunol Cell Biol* *93*, 35-42.
- Deplanche, M., Mouhali, N., Nguyen, M.T., Cauty, C., Ezan, F., Diot, A., Raulin, L., Dutertre, S., Langouet, S., Legembre, P., *et al.* (2019). *Staphylococcus aureus* induces DNA damage in host cell. *Sci Rep* *9*, 7694.
- Deszcz, L., Seipelt, J., Vassilieva, E., Roetzer, A., and Kuechler, E. (2004). Antiviral activity of caspase inhibitors: effect on picornaviral 2A proteinase. *FEBS Lett* *560*, 51-55.
- Dickens, L.S., Powley, I.R., Hughes, M.A., and MacFarlane, M. (2012). The 'complexities' of life and death: death receptor signalling platforms. *Exp Cell Res* *318*, 1269-1277.
- Dickinson, B.C., and Chang, C.J. (2011). Chemistry and biology of reactive oxygen species in signaling or stress responses. *Nat Chem Biol* *7*, 504-511.
- Dixon, S.J., Winter, G.E., Musavi, L.S., Lee, E.D., Snijder, B., Rebsamen, M., Superti-Furga, G., and Stockwell, B.R. (2015). Human Haploid Cell Genetics Reveals Roles for Lipid Metabolism Genes in Nonapoptotic Cell Death. *ACS Chem Biol* *10*, 1604-1609.
- Doery, H.M., Magnusson, B.J., Cheyne, I.M., and Sulasekharam, J. (1963). A phospholipase in staphylococcal toxin which hydrolyses sphingomyelin. *Nature* *198*, 1091-1092.
- Dolmetsch, R.E., Xu, K., and Lewis, R.S. (1998). Calcium oscillations increase the efficiency and specificity of gene expression. *Nature* *392*, 933-936.
- Dovey, C.M., Diep, J., Clarke, B.P., Hale, A.T., McNamara, D.E., Guo, H., Brown, N.W., Jr., Cao, J.Y., Grace, C.R., Gough, P.J., *et al.* (2018). MLKL Requires the Inositol Phosphate Code to Execute Necroptosis. *Mol Cell* *70*, 936-948 e937.
- Drapeau, G.R. (1978). Role of metalloprotease in activation of the precursor of staphylococcal protease. *J Bacteriol* *136*, 607-613.
- Du, C., Fang, M., Li, Y., Li, L., and Wang, X. (2000). Smac, a mitochondrial protein that promotes cytochrome c-dependent caspase activation by eliminating IAP inhibition. *Cell* *102*, 33-42.
- DuMont, A.L., Yoong, P., Day, C.J., Alonzo, F., 3rd, McDonald, W.H., Jennings, M.P., and Torres, V.J. (2013a). *Staphylococcus aureus* LukAB cytotoxin kills human neutrophils by targeting the CD11b subunit of the integrin Mac-1. *Proc Natl Acad Sci U S A* *110*, 10794-10799.

- DuMont, A.L., Yoong, P., Surewaard, B.G., Benson, M.A., Nijland, R., van Strijp, J.A., and Torres, V.J. (2013b). Staphylococcus aureus elaborates leukocidin AB to mediate escape from within human neutrophils. *Infect Immun* 81, 1830-1841.
- Dunai, Z.A., Imre, G., Barna, G., Korcsmaros, T., Petak, I., Bauer, P.I., and Mihalik, R. (2012). Staurosporine induces necroptotic cell death under caspase-compromised conditions in U937 cells. *PLoS One* 7, e41945.
- Dupont, N., Lacas-Gervais, S., Bertout, J., Paz, I., Freche, B., Van Nhieu, G.T., van der Goot, F.G., Sansonetti, P.J., and Lafont, F. (2009). Shigella phagocytic vacuolar membrane remnants participate in the cellular response to pathogen invasion and are regulated by autophagy. *Cell Host Microbe* 6, 137-149.
- Earnshaw, W.C., Martins, L.M., and Kaufmann, S.H. (1999). Mammalian caspases: structure, activation, substrates, and functions during apoptosis. *Annu Rev Biochem* 68, 383-424.
- Eichstaedt, S., Gabler, K., Below, S., Muller, C., Kohler, C., Engelmann, S., Hildebrandt, P., Volker, U., Hecker, M., and Hildebrandt, J.P. (2009). Effects of Staphylococcus aureus-hemolysin A on calcium signalling in immortalized human airway epithelial cells. *Cell Calcium* 45, 165-176.
- Eiffler, I., Behnke, J., Ziesemer, S., Muller, C., and Hildebrandt, J.P. (2016). Staphylococcus aureus alpha-toxin-mediated cation entry depolarizes membrane potential and activates p38 MAP kinase in airway epithelial cells. *Am J Physiol Lung Cell Mol Physiol* 311, L676-685.
- Eliseev, R.A., Filippov, G., Velos, J., VanWinkle, B., Goldman, A., Rosier, R.N., and Gunter, T.E. (2007). Role of cyclophilin D in the resistance of brain mitochondria to the permeability transition. *Neurobiol Aging* 28, 1532-1542.
- Elling, U., Taubenschmid, J., Wirnsberger, G., O'Malley, R., Demers, S.P., Vanhaelen, Q., Shukalyuk, A.I., Schmauss, G., Schramek, D., Schnuetgen, F., et al. (2011). Forward and reverse genetics through derivation of haploid mouse embryonic stem cells. *Cell Stem Cell* 9, 563-574.
- Elmwall, J., Kwiecinski, J., Na, M., Ali, A.A., Osla, V., Shaw, L.N., Wang, W., Savman, K., Josefsson, E., Bylund, J., et al. (2017). Galectin-3 Is a Target for Proteases Involved in the Virulence of Staphylococcus aureus. *Infect Immun* 85.
- Emonts, M., Uitterlinden, A.G., Nouwen, J.L., Kardys, I., Maat, M.P., Melles, D.C., Witteman, J., Jong, P.T., Verbrugh, H.A., Hofman, A., et al. (2008). Host polymorphisms in interleukin 4, complement factor H, and C-reactive protein associated with nasal carriage of Staphylococcus aureus and occurrence of boils. *J Infect Dis* 197, 1244-1253.
- Esen, M., Schreiner, B., Jendrossek, V., Lang, F., Fassbender, K., Grassme, H., and Gulbins, E. (2001). Mechanisms of Staphylococcus aureus induced apoptosis of human endothelial cells. *Apoptosis* 6, 431-439.
- Eskes, R., Desagher, S., Antonsson, B., and Martinou, J.C. (2000). Bid induces the oligomerization and insertion of Bax into the outer mitochondrial membrane. *Mol Cell Biol* 20, 929-935.
- Essletzbichler, P., Konopka, T., Santoro, F., Chen, D., Gapp, B.V., Kralovics, R., Brummelkamp, T.R., Nijman, S.M., and Burckstummer, T. (2014). Megabase-scale deletion using CRISPR/Cas9 to generate a fully haploid human cell line. *Genome Res* 24, 2059-2065.
- Falk, T., Mai, D., Bensch, R., Cicek, O., Abdulkadir, A., Marrakchi, Y., Bohm, A., Deubner, J., Jackel, Z., Seiwald, K., et al. (2019). U-Net: deep learning for cell counting, detection, and morphometry. *Nat Methods* 16, 67-70.

- Fatokun, A.A., Dawson, V.L., and Dawson, T.M. (2014). Parthanatos: mitochondrial-linked mechanisms and therapeutic opportunities. *Br J Pharmacol* *171*, 2000-2016.
- Fey, P.D., Endres, J.L., Yajjala, V.K., Widhelm, T.J., Boissy, R.J., Bose, J.L., and Bayles, K.W. (2013). A genetic resource for rapid and comprehensive phenotype screening of nonessential *Staphylococcus aureus* genes. *MBio* *4*, e00537-00512.
- Filipek, R., Potempa, J., and Bochtler, M. (2005). A comparison of staphostatin B with standard mechanism serine protease inhibitors. *J Biol Chem* *280*, 14669-14674.
- Filipek, R., Rzychon, M., Oleksy, A., Gruca, M., Dubin, A., Potempa, J., and Bochtler, M. (2003). The Staphostatin-staphopain complex: a forward binding inhibitor in complex with its target cysteine protease. *J Biol Chem* *278*, 40959-40966.
- Fink, D., Contreras, M.L., Lelkes, P.I., and Lazarovici, P. (1989). *Staphylococcus aureus* alpha-toxin activates phospholipases and induces a Ca²⁺ influx in PC12 cells. *Cell Signal* *1*, 387-393.
- Flanagan, R.S., Heit, B., and Heinrichs, D.E. (2016). Intracellular replication of *Staphylococcus aureus* in mature phagolysosomes in macrophages precedes host cell death, and bacterial escape and dissemination. *Cell Microbiol* *18*, 514-535.
- Flieger, A., Frischknecht, F., Hacker, G., Hornef, M.W., and Pradel, G. (2018). Pathways of host cell exit by intracellular pathogens. *Microb Cell* *5*, 525-544.
- Foster, T.J., Geoghegan, J.A., Ganesh, V.K., and Hook, M. (2014). Adhesion, invasion and evasion: the many functions of the surface proteins of *Staphylococcus aureus*. *Nat Rev Microbiol* *12*, 49-62.
- Fowler, V.G., Jr., Olsen, M.K., Corey, G.R., Woods, C.W., Cabell, C.H., Reller, L.B., Cheng, A.C., Dudley, T., and Oddone, E.Z. (2003). Clinical identifiers of complicated *Staphylococcus aureus* bacteremia. *Arch Intern Med* *163*, 2066-2072.
- Frank, D.N., Feazel, L.M., Bessesen, M.T., Price, C.S., Janoff, E.N., and Pace, N.R. (2010). The human nasal microbiota and *Staphylococcus aureus* carriage. *Plos One* *5*, e10598.
- Gafni, J., Cong, X., Chen, S.F., Gibson, B.W., and Ellerby, L.M. (2009). Calpain-1 cleaves and activates caspase-7. *J Biol Chem* *284*, 25441-25449.
- Galdiero, S., and Gouaux, E. (2004). High resolution crystallographic studies of alpha-hemolysin-phospholipid complexes define heptamer-lipid head group interactions: implication for understanding protein-lipid interactions. *Protein Sci* *13*, 1503-1511.
- Galluzzi, L., Bravo-San Pedro, J.M., Vitale, I., Aaronson, S.A., Abrams, J.M., Adam, D., Alnemri, E.S., Altucci, L., Andrews, D., Annicchiarico-Petruzzelli, M., *et al.* (2015). Essential versus accessory aspects of cell death: recommendations of the NCCD 2015. *Cell Death Differ* *22*, 58-73.
- Galluzzi, L., Kepp, O., and Kroemer, G. (2016). Mitochondrial regulation of cell death: a phylogenetically conserved control. *Microb Cell* *3*, 101-108.
- Galluzzi, L., Vitale, I., Aaronson, S.A., Abrams, J.M., Adam, D., Agostinis, P., Alnemri, E.S., Altucci, L., Amelio, I., Andrews, D.W., *et al.* (2018). Molecular mechanisms of cell death: recommendations of the Nomenclature Committee on Cell Death 2018. *Cell Death Differ* *25*, 486-541.
- Gao, G., and Dou, Q.P. (2000). N-terminal cleavage of bax by calpain generates a potent proapoptotic 18-kDa fragment that promotes bcl-2-independent cytochrome C release and apoptotic cell death. *J Cell Biochem* *80*, 53-72.

- Gao, T., Brognard, J., and Newton, A.C. (2008). The phosphatase PHLPP controls the cellular levels of protein kinase C. *J Biol Chem* 283, 6300-6311.
- Gao, T., Furnari, F., and Newton, A.C. (2005). PHLPP: a phosphatase that directly dephosphorylates Akt, promotes apoptosis, and suppresses tumor growth. *Mol Cell* 18, 13-24.
- Garzoni, C., and Kelley, W.L. (2009). *Staphylococcus aureus*: new evidence for intracellular persistence. *Trends Microbiol* 17, 59-65.
- Gibert, B., and Mehlen, P. (2015). Dependence Receptors and Cancer: Addiction to Trophic Ligands. *Cancer Res* 75, 5171-5175.
- Giese, B., Dittmann, S., Paprotka, K., Levin, K., Weltrowski, A., Biehler, D., Lam, T.T., Sinha, B., and Fraunholz, M.J. (2009). Staphylococcal alpha-toxin is not sufficient to mediate escape from phagolysosomes in upper-airway epithelial cells. *Infect Immun* 77, 3611-3625.
- Giese, B., Glowinski, F., Paprotka, K., Dittmann, S., Steiner, T., Sinha, B., and Fraunholz, M.J. (2011). Expression of delta-toxin by *Staphylococcus aureus* mediates escape from phago-endosomes of human epithelial and endothelial cells in the presence of beta-toxin. *Cell Microbiol* 13, 316-329.
- Gong, Y.N., Guy, C., Crawford, J.C., and Green, D.R. (2017). Biological events and molecular signaling following MLKL activation during necroptosis. *Cell Cycle* 16, 1748-1760.
- Gonzalez, D.J., Okumura, C.Y., Hollands, A., Kersten, R., Akong-Moore, K., Pence, M.A., Malone, C.L., Derieux, J., Moore, B.S., Horswill, A.R., *et al.* (2012). Novel phenol-soluble modulins identified through imaging mass spectrometry. *J Biol Chem* 287, 13889-13898.
- Gordon, R.J., and Lowy, F.D. (2008). Pathogenesis of methicillin-resistant *Staphylococcus aureus* infection. *Clin Infect Dis* 46 Suppl 5, S350-359.
- Gores, G.J., Miyoshi, H., Botla, R., Aguilar, H.I., and Bronk, S.F. (1998). Induction of the mitochondrial permeability transition as a mechanism of liver injury during cholestasis: a potential role for mitochondrial proteases. *Biochim Biophys Acta* 1366, 167-175.
- Gouaux, J.E., Braha, O., Hobaugh, M.R., Song, L., Cheley, S., Shustak, C., and Bayley, H. (1994). Subunit stoichiometry of staphylococcal alpha-hemolysin in crystals and on membranes: a heptameric transmembrane pore. *Proc Natl Acad Sci U S A* 91, 12828-12831.
- Green, D.R., Oguin, T.H., and Martinez, J. (2016). The clearance of dying cells: table for two. *Cell Death Differ* 23, 915-926.
- Greenberg, E.F., Lavik, A.R., and Distelhorst, C.W. (2014). Bcl-2 regulation of the inositol 1,4,5-trisphosphate receptor and calcium signaling in normal and malignant lymphocytes: potential new target for cancer treatment. *Biochim Biophys Acta* 1843, 2205-2210.
- Greenlee-Wacker, M.C., Kremserova, S., and Nauseef, W.M. (2017). Lysis of human neutrophils by community-associated methicillin-resistant *Staphylococcus aureus*. *Blood* 129, 3237-3244.
- Greenlee-Wacker, M.C., Rigby, K.M., Kobayashi, S.D., Porter, A.R., DeLeo, F.R., and Nauseef, W.M. (2014). Phagocytosis of *Staphylococcus aureus* by human neutrophils prevents macrophage efferocytosis and induces programmed necrosis. *J Immunol* 192, 4709-4717.
- Gresham, H.D., Lowrance, J.H., Caver, T.E., Wilson, B.S., Cheung, A.L., and Lindberg, F.P. (2000). Survival of *Staphylococcus aureus* inside neutrophils contributes to infection. *J Immunol* 164, 3713-3722.

- Groenendyk, J., Agellon, L.B., and Michalak, M. (2013). Coping with endoplasmic reticulum stress in the cardiovascular system. *Annu Rev Physiol* 75, 49-67.
- Grootjans, S., Vanden Berghe, T., and Vandenabeele, P. (2017). Initiation and execution mechanisms of necroptosis: an overview. *Cell Death Differ* 24, 1184-1195.
- Grosz, M., Kolter, J., Paprotka, K., Winkler, A.C., Schafer, D., Chatterjee, S.S., Geiger, T., Wolz, C., Ohlsen, K., Otto, M., *et al.* (2014). Cytoplasmic replication of *Staphylococcus aureus* upon phagosomal escape triggered by phenol-soluble modulins. *Cell Microbiol* 16, 451-465.
- Guimaraes, C.P., Carette, J.E., Varadarajan, M., Antos, J., Popp, M.W., Spooner, E., Brummelkamp, T.R., and Ploegh, H.L. (2011). Identification of host cell factors required for intoxication through use of modified cholera toxin. *J Cell Biol* 195, 751-764.
- Guinan, M.E., Dan, B.B., Guidotti, R.J., Reingold, A.L., Schmid, G.P., Bettoli, E.J., Lossick, J.G., Shands, K.N., Kramer, M.A., Hargrett, N.T., *et al.* (1982). Vaginal colonization with *Staphylococcus aureus* in healthy women: a review of four studies. *Ann Intern Med* 96, 944-947.
- Gurumurthy, S., Goswami, A., Vasudevan, K.M., and Rangnekar, V.M. (2005). Phosphorylation of Par-4 by protein kinase A is critical for apoptosis. *Mol Cell Biol* 25, 1146-1161.
- Halliwell, B. (2011). Free radicals and antioxidants - quo vadis? *Trends Pharmacol Sci* 32, 125-130.
- Hamill, R.J., Vann, J.M., and Proctor, R.A. (1986). Phagocytosis of *Staphylococcus aureus* by cultured bovine aortic endothelial cells: model for postadherence events in endovascular infections. *Infect Immun* 54, 833-836.
- Hammer, N.D., and Skaar, E.P. (2011). Molecular mechanisms of *Staphylococcus aureus* iron acquisition. *Annu Rev Microbiol* 65, 129-147.
- Han, S., Nam, J., Li, Y., Kim, S., Cho, S.H., Cho, Y.S., Choi, S.Y., Choi, J., Han, K., Kim, Y., *et al.* (2010). Regulation of dendritic spines, spatial memory, and embryonic development by the TANC family of PSD-95-interacting proteins. *J Neurosci* 30, 15102-15112.
- Hanson, C.J., Bootman, M.D., Distelhorst, C.W., Wojcikiewicz, R.J., and Roderick, H.L. (2008). Bcl-2 suppresses Ca²⁺ release through inositol 1,4,5-trisphosphate receptors and inhibits Ca²⁺ uptake by mitochondria without affecting ER calcium store content. *Cell Calcium* 44, 324-338.
- Hanssen, A.M., Kindlund, B., Stenklev, N.C., Furberg, A.S., Fismen, S., Olsen, R.S., Johannessen, M., and Sollid, J.U. (2017). Localization of *Staphylococcus aureus* in tissue from the nasal vestibule in healthy carriers. *BMC Microbiol* 17, 89.
- Harraghy, N., Hussain, M., Hagggar, A., Chavakis, T., Sinha, B., Herrmann, M., and Flock, J.I. (2003). The adhesive and immunomodulating properties of the multifunctional *Staphylococcus aureus* protein Eap. *Microbiology* 149, 2701-2707.
- Haslinger-Loeffler, B., Kahl, B.C., Grundmeier, M., Strangfeld, K., Wagner, B., Fischer, U., Cheung, A.L., Peters, G., Schulze-Osthoff, K., and Sinha, B. (2005). Multiple virulence factors are required for *Staphylococcus aureus*-induced apoptosis in endothelial cells. *Cell Microbiol* 7, 1087-1097.
- Haslinger-Loeffler, B., Wagner, B., Bruck, M., Strangfeld, K., Grundmeier, M., Fischer, U., Volker, W., Peters, G., Schulze-Osthoff, K., and Sinha, B. (2006). *Staphylococcus aureus* induces caspase-independent cell death in human peritoneal mesothelial cells. *Kidney Int* 70, 1089-1098.
- Hassoun, A., Linden, P.K., and Friedman, B. (2017). Incidence, prevalence, and management of MRSA bacteremia across patient populations-a review of recent developments in MRSA management and treatment. *Crit Care* 21, 211.

- Hayes, S.M., Howlin, R., Johnston, D.A., Webb, J.S., Clarke, S.C., Stoodley, P., Harries, P.G., Wilson, S.J., Pender, S.L., Faust, S.N., *et al.* (2015). Intracellular residency of *Staphylococcus aureus* within mast cells in nasal polyps: A novel observation. *J Allergy Clin Immunol* *135*, 1648-1651.
- Hebbar, N., Wang, C., and Rangnekar, V.M. (2012). Mechanisms of apoptosis by the tumor suppressor Par-4. *J Cell Physiol* *227*, 3715-3721.
- Henderson, M.J., Baldwin, H.A., Werley, C.A., Boccardo, S., Whitaker, L.R., Yan, X., Holt, G.T., Schreiter, E.R., Looger, L.L., Cohen, A.E., *et al.* (2015). A Low Affinity GCaMP3 Variant (GCaMPer) for Imaging the Endoplasmic Reticulum Calcium Store. *Plos One* *10*, e0139273.
- Hennekinne, J.A., De Buyser, M.L., and Dragacci, S. (2012). *Staphylococcus aureus* and its food poisoning toxins: characterization and outbreak investigation. *FEMS Microbiol Rev* *36*, 815-836.
- Herold, B.C., Immergluck, L.C., Maranan, M.C., Lauderdale, D.S., Gaskin, R.E., Boyle-Vavra, S., Leitch, C.D., and Daum, R.S. (1998). Community-acquired methicillin-resistant *Staphylococcus aureus* in children with no identified predisposing risk. *JAMA* *279*, 593-598.
- Hidron, A.I., Edwards, J.R., Patel, J., Horan, T.C., Sievert, D.M., Pollock, D.A., Fridkin, S.K., National Healthcare Safety Network, T., and Participating National Healthcare Safety Network, F. (2008). NHSN annual update: antimicrobial-resistant pathogens associated with healthcare-associated infections: annual summary of data reported to the National Healthcare Safety Network at the Centers for Disease Control and Prevention, 2006-2007. *Infect Control Hosp Epidemiol* *29*, 996-1011.
- Hildebrand, A., Pohl, M., and Bhakdi, S. (1991). *Staphylococcus aureus* alpha-toxin. Dual mechanism of binding to target cells. *J Biol Chem* *266*, 17195-17200.
- Hiramatsu, K., Aritaka, N., Hanaki, H., Kawasaki, S., Hosoda, Y., Hori, S., Fukuchi, Y., and Kobayashi, I. (1997). Dissemination in Japanese hospitals of strains of *Staphylococcus aureus* heterogeneously resistant to vancomycin. *Lancet* *350*, 1670-1673.
- Hirota, J., Furuichi, T., and Mikoshiba, K. (1999). Inositol 1,4,5-trisphosphate receptor type 1 is a substrate for caspase-3 and is cleaved during apoptosis in a caspase-3-dependent manner. *J Biol Chem* *274*, 34433-34437.
- Hirschhausen, N., Schlesier, T., Schmidt, M.A., Gotz, F., Peters, G., and Heilmann, C. (2010). A novel staphylococcal internalization mechanism involves the major autolysin Atl and heat shock cognate protein Hsc70 as host cell receptor. *Cell Microbiol* *12*, 1746-1764.
- Hoffmann, H.H., Schneider, W.M., Blomen, V.A., Scull, M.A., Hovnanian, A., Brummelkamp, T.R., and Rice, C.M. (2017). Diverse Viruses Require the Calcium Transporter SPCA1 for Maturation and Spread. *Cell Host Microbe* *22*, 460-470 e465.
- Hofmann, B., Schomburg, D., and Hecht, H.J. (1993). Crystal structure of a thiol proteinase from *Staphylococcus aureus* V-8 in the E-64 inhibitor complex. *Acta Crystallographica* *49 (Supplement)*, 102.
- Hogan, P.G., and Rao, A. (2015). Store-operated calcium entry: Mechanisms and modulation. *Biochem Biophys Res Commun* *460*, 40-49.
- Holtfreter, S., and Broker, B.M. (2005). Staphylococcal superantigens: do they play a role in sepsis? *Arch Immunol Ther Exp (Warsz)* *53*, 13-27.
- Horn, J., Klepsch, M., Manger, M., Wolz, C., Rudel, T., and Fraunholz, M. (2018a). Long Noncoding RNA SSR42 Controls *Staphylococcus aureus* Alpha-Toxin Transcription in Response to Environmental Stimuli. *J Bacteriol* *200*.

- Horn, J., Stelzner, K., Rudel, T., and Fraunholz, M. (2018b). Inside job: *Staphylococcus aureus* host-pathogen interactions. *Int J Med Microbiol* 308, 607-624.
- Hsu, Y.T., Wolter, K.G., and Youle, R.J. (1997). Cytosol-to-membrane redistribution of Bax and Bcl-X(L) during apoptosis. *Proc Natl Acad Sci U S A* 94, 3668-3672.
- Hu, H.Z., Gu, Q., Wang, C., Colton, C.K., Tang, J., Kinoshita-Kawada, M., Lee, L.Y., Wood, J.D., and Zhu, M.X. (2004). 2-aminoethoxydiphenyl borate is a common activator of TRPV1, TRPV2, and TRPV3. *J Biol Chem* 279, 35741-35748.
- Huang, X., Liu, F., Zhu, C., Cai, J., Wang, H., Wang, X., He, S., Liu, C., Yao, L., Ding, Z., *et al.* (2014). Suppression of KIF3B expression inhibits human hepatocellular carcinoma proliferation. *Dig Dis Sci* 59, 795-806.
- Hutchison, M., Berman, K.S., and Cobb, M.H. (1998). Isolation of TAO1, a protein kinase that activates MEKs in stress-activated protein kinase cascades. *J Biol Chem* 273, 28625-28632.
- Imamura, T., Tanase, S., Szmyd, G., Kozik, A., Travis, J., and Potempa, J. (2005). Induction of vascular leakage through release of bradykinin and a novel kinin by cysteine proteinases from *Staphylococcus aureus*. *J Exp Med* 201, 1669-1676.
- Inoshima, I., Inoshima, N., Wilke, G.A., Powers, M.E., Frank, K.M., Wang, Y., and Bubeck Wardenburg, J. (2011). A *Staphylococcus aureus* pore-forming toxin subverts the activity of ADAM10 to cause lethal infection in mice. *Nat Med* 17, 1310-1314.
- Iurlaro, R., and Munoz-Pinedo, C. (2016). Cell death induced by endoplasmic reticulum stress. *FEBS J* 283, 2640-2652.
- Izzo, V., Bravo-San Pedro, J.M., Sica, V., Kroemer, G., and Galluzzi, L. (2016). Mitochondrial Permeability Transition: New Findings and Persisting Uncertainties. *Trends Cell Biol* 26, 655-667.
- Jacobson, L.S., Lima, H., Jr., Goldberg, M.F., Gocheva, V., Tshiperson, V., Sutterwala, F.S., Joyce, J.A., Gapp, B.V., Blomen, V.A., Chandran, K., *et al.* (2013). Cathepsin-mediated necrosis controls the adaptive immune response by Th2 (T helper type 2)-associated adjuvants. *J Biol Chem* 288, 7481-7491.
- Jae, L.T., Raaben, M., Herbert, A.S., Kuehne, A.I., Wirchnianski, A.S., Soh, T.K., Stubbs, S.H., Janssen, H., Damme, M., Saftig, P., *et al.* (2014). Virus entry. Lassa virus entry requires a trigger-induced receptor switch. *Science* 344, 1506-1510.
- Jae, L.T., Raaben, M., Riemersma, M., van Beusekom, E., Blomen, V.A., Velds, A., Kerkhoven, R.M., Carette, J.E., Topaloglu, H., Meinecke, P., *et al.* (2013). Deciphering the glycosylome of dystroglycanopathies using haploid screens for lassa virus entry. *Science* 340, 479-483.
- Jairaman, A., and Prakriya, M. (2013). Molecular pharmacology of store-operated CRAC channels. *Channels (Austin)* 7, 402-414.
- Jarry, T.M., Memmi, G., and Cheung, A.L. (2008). The expression of alpha-haemolysin is required for *Staphylococcus aureus* phagosomal escape after internalization in CFT-1 cells. *Cell Microbiol* 10, 1801-1814.
- Jin, T., Zhu, Y.L., Li, J., Shi, J., He, X.Q., Ding, J., and Xu, Y.Q. (2013). Staphylococcal protein A, Panton-Valentine leukocidin and coagulase aggravate the bone loss and bone destruction in osteomyelitis. *Cell Physiol Biochem* 32, 322-333.
- Johannessen, M., Sollid, J.E., and Hanssen, A.M. (2012). Host- and microbe determinants that may influence the success of *S. aureus* colonization. *Front Cell Infect Microbiol* 2, 56.

- Jonas, D., Walev, I., Berger, T., Liebetrau, M., Palmer, M., and Bhakdi, S. (1994). Novel path to apoptosis: small transmembrane pores created by staphylococcal alpha-toxin in T lymphocytes evoke internucleosomal DNA degradation. *Infect Immun* *62*, 1304-1312.
- Jover, E., Tawk, M.Y., Laventie, B.J., Poulain, B., and Prevost, G. (2013). Staphylococcal leukotoxins trigger free intracellular Ca²⁺ rise in neurones, signalling through acidic stores and activation of store-operated channels. *Cell Microbiol* *15*, 742-758.
- Jubrail, J., Morris, P., Bewley, M.A., Stoneham, S., Johnston, S.A., Foster, S.J., Peden, A.A., Read, R.C., Marriott, H.M., and Dockrell, D.H. (2016). Inability to sustain intraphagolysosomal killing of *Staphylococcus aureus* predisposes to bacterial persistence in macrophages. *Cell Microbiol* *18*, 80-96.
- Kabir, J., Lobo, M., and Zachary, I. (2002). Staurosporine induces endothelial cell apoptosis via focal adhesion kinase dephosphorylation and focal adhesion disassembly independent of focal adhesion kinase proteolysis. *Biochem J* *367*, 145-155.
- Kaesler, P.S., and Regehr, W.G. (2014). Molecular mechanisms for synchronous, asynchronous, and spontaneous neurotransmitter release. *Annu Rev Physiol* *76*, 333-363.
- Kahl, B.C. (2010). Impact of *Staphylococcus aureus* on the pathogenesis of chronic cystic fibrosis lung disease. *Int J Med Microbiol* *300*, 514-519.
- Kahl, B.C., Goulian, M., van Wamel, W., Herrmann, M., Simon, S.M., Kaplan, G., Peters, G., and Cheung, A.L. (2000). *Staphylococcus aureus* RN6390 replicates and induces apoptosis in a pulmonary epithelial cell line. *Infect Immun* *68*, 5385-5392.
- Kantyka, T., Plaza, K., Koziel, J., Florczyk, D., Stennicke, H.R., Thogersen, I.B., Enghild, J.J., Silverman, G.A., Pak, S.C., and Potempa, J. (2011a). Inhibition of *Staphylococcus aureus* cysteine proteases by human serpin potentially limits staphylococcal virulence. *Biol Chem* *392*, 483-489.
- Kantyka, T., Pyrc, K., Gruca, M., Smagur, J., Plaza, K., Guzik, K., Zeglen, S., Ochman, M., and Potempa, J. (2013). *Staphylococcus aureus* proteases degrade lung surfactant protein A potentially impairing innate immunity of the lung. *J Innate Immun* *5*, 251-260.
- Kantyka, T., Shaw, L.N., and Potempa, J. (2011b). Papain-like proteases of *Staphylococcus aureus*. *Adv Exp Med Biol* *712*, 1-14.
- Kar, P., Chakraborti, T., Roy, S., Choudhury, R., and Chakraborti, S. (2007). Identification of calpastatin and mu-calpain and studies of their association in pulmonary smooth muscle mitochondria. *Arch Biochem Biophys* *466*, 290-299.
- Kar, P., Chakraborti, T., Samanta, K., and Chakraborti, S. (2009). mu-Calpain mediated cleavage of the Na⁺/Ca²⁺ exchanger in isolated mitochondria under A23187 induced Ca²⁺ stimulation. *Arch Biochem Biophys* *482*, 66-76.
- Karavolos, M.H., Horsburgh, M.J., Ingham, E., and Foster, S.J. (2003). Role and regulation of the superoxide dismutases of *Staphylococcus aureus*. *Microbiology* *149*, 2749-2758.
- Karlsson, A., Saravia-Otten, P., Tegmark, K., Morfeldt, E., and Arvidson, S. (2001). Decreased amounts of cell wall-associated protein A and fibronectin-binding proteins in *Staphylococcus aureus* sarA mutants due to up-regulation of extracellular proteases. *Infect Immun* *69*, 4742-4748.
- Kayagaki, N., Stowe, I.B., Lee, B.L., O'Rourke, K., Anderson, K., Warming, S., Cuellar, T., Haley, B., Roose-Girma, M., Phung, Q.T., *et al.* (2015). Caspase-11 cleaves gasdermin D for non-canonical inflammasome signalling. *Nature* *526*, 666-671.

- Kee, Y., Yang, K., Cohn, M.A., Haas, W., Gygi, S.P., and D'Andrea, A.D. (2010). WDR20 regulates activity of the USP12 x UAF1 deubiquitinating enzyme complex. *J Biol Chem* *285*, 11252-11257.
- Kim, H., Tu, H.C., Ren, D., Takeuchi, O., Jeffers, J.R., Zambetti, G.P., Hsieh, J.J., and Cheng, E.H. (2009). Stepwise activation of BAX and BAK by tBID, BIM, and PUMA initiates mitochondrial apoptosis. *Mol Cell* *36*, 487-499.
- Kim, H.J., Koo, S.Y., Ahn, B.H., Park, O., Park, D.H., Seo, D.O., Won, J.H., Yim, H.J., Kwak, H.S., Park, H.S., *et al.* (2010). NecroX as a novel class of mitochondrial reactive oxygen species and ONOO(-) scavenger. *Arch Pharm Res* *33*, 1813-1823.
- King, M.D., Humphrey, B.J., Wang, Y.F., Kourbatova, E.V., Ray, S.M., and Blumberg, H.M. (2006). Emergence of community-acquired methicillin-resistant *Staphylococcus aureus* USA 300 clone as the predominant cause of skin and soft-tissue infections. *Ann Intern Med* *144*, 309-317.
- Kinnally, K.W., Peixoto, P.M., Ryu, S.Y., and Dejean, L.M. (2011). Is mPTP the gatekeeper for necrosis, apoptosis, or both? *Biochim Biophys Acta* *1813*, 616-622.
- Kitur, K., Parker, D., Nieto, P., Ahn, D.S., Cohen, T.S., Chung, S., Wachtel, S., Bueno, S., and Prince, A. (2015). Toxin-induced necroptosis is a major mechanism of *Staphylococcus aureus* lung damage. *PLoS Pathog* *11*, e1004820.
- Kitur, K., Wachtel, S., Brown, A., Wickersham, M., Paulino, F., Penaloza, H.F., Soong, G., Bueno, S., Parker, D., and Prince, A. (2016). Necroptosis Promotes *Staphylococcus aureus* Clearance by Inhibiting Excessive Inflammatory Signaling. *Cell Rep* *16*, 2219-2230.
- Kluytmans, J., van Belkum, A., and Verbrugh, H. (1997). Nasal carriage of *Staphylococcus aureus*: epidemiology, underlying mechanisms, and associated risks. *Clin Microbiol Rev* *10*, 505-520.
- Kobayashi, S.D., Braughton, K.R., Palazzolo-Ballance, A.M., Kennedy, A.D., Sampaio, E., Kristosturyan, E., Whitney, A.R., Sturdevant, D.E., Dorward, D.W., Holland, S.M., *et al.* (2010). Rapid neutrophil destruction following phagocytosis of *Staphylococcus aureus*. *J Innate Immun* *2*, 560-575.
- Kolar, S.L., Ibarra, J.A., Rivera, F.E., Mootz, J.M., Davenport, J.E., Stevens, S.M., Horswill, A.R., and Shaw, L.N. (2013). Extracellular proteases are key mediators of *Staphylococcus aureus* virulence via the global modulation of virulence-determinant stability. *Microbiologyopen* *2*, 18-34.
- Kollef, M.H., Shorr, A., Tabak, Y.P., Gupta, V., Liu, L.Z., and Johannes, R.S. (2005). Epidemiology and outcomes of health-care-associated pneumonia: results from a large US database of culture-positive pneumonia. *Chest* *128*, 3854-3862.
- Kotecki, M., Reddy, P.S., and Cochran, B.H. (1999). Isolation and characterization of a near-haploid human cell line. *Exp Cell Res* *252*, 273-280.
- Krebs, J., Groenendyk, J., and Michalak, M. (2011). Ca²⁺-signaling, alternative splicing and endoplasmic reticulum stress responses. *Neurochem Res* *36*, 1198-1211.
- Kreiswirth, B.N., Lofdahl, S., Betley, M.J., O'Reilly, M., Schlievert, P.M., Bergdoll, M.S., and Novick, R.P. (1983). The toxic shock syndrome exotoxin structural gene is not detectably transmitted by a prophage. *Nature* *305*, 709-712.
- Kretschmer, D., Gleske, A.K., Rautenberg, M., Wang, R., Koberle, M., Bohn, E., Schoneberg, T., Rabet, M.J., Boulay, F., Klebanoff, S.J., *et al.* (2010). Human formyl peptide receptor 2 senses highly pathogenic *Staphylococcus aureus*. *Cell Host Microbe* *7*, 463-473.
- Kristian, T., and Siesjo, B.K. (1998). Calcium in ischemic cell death. *Stroke* *29*, 705-718.

- Kroemer, G., Galluzzi, L., Vandenabeele, P., Abrams, J., Alnemri, E.S., Baehrecke, E.H., Blagosklonny, M.V., El-Deiry, W.S., Golstein, P., Green, D.R., *et al.* (2009). Classification of cell death: recommendations of the Nomenclature Committee on Cell Death 2009. *Cell Death Differ* 16, 3-11.
- Krut, O., Sommer, H., and Kronke, M. (2004). Antibiotic-induced persistence of cytotoxic *Staphylococcus aureus* in non-phagocytic cells. *J Antimicrob Chemother* 53, 167-173.
- Krut, O., Utermohlen, O., Schloscherr, X., and Kronke, M. (2003). Strain-specific association of cytotoxic activity and virulence of clinical *Staphylococcus aureus* isolates. *Infect Immun* 71, 2716-2723.
- Kubica, M., Guzik, K., Koziel, J., Zarebski, M., Richter, W., Gajkowska, B., Golda, A., Maciag-Gudowska, A., Brix, K., Shaw, L., *et al.* (2008a). A potential new pathway for *Staphylococcus aureus* dissemination: the silent survival of *S. aureus* phagocytosed by human monocyte-derived macrophages. *Plos One* 3, e1409.
- Kubica, M., Guzik, K., Koziel, J., Zarebski, M., Richter, W., Gajkowska, B., Golda, A., Maciag-Gudowska, A., Brix, K., Shaw, L., *et al.* (2008b). A Potential New Pathway for *Staphylococcus aureus* Dissemination: The Silent Survival of *S. aureus* Phagocytosed by Human Monocyte-Derived Macrophages. *Plos One* 3.
- Kuhn, M.L., Prachi, P., Minasov, G., Shuvalova, L., Ruan, J., Dubrovskaya, I., Winsor, J., Giraldo, M., Biagini, M., Liberatori, S., *et al.* (2014). Structure and protective efficacy of the *Staphylococcus aureus* autocleaving protease EpiP. *Faseb J* 28, 1780-1793.
- Kuo, I.Y., and Ehrlich, B.E. (2015). Signaling in muscle contraction. *Cold Spring Harb Perspect Biol* 7, a06023.
- Kwak, Y.K., Vikstrom, E., Magnusson, K.E., Vecsey-Semjen, B., Colque-Navarro, P., and Mollby, R. (2012). The *Staphylococcus aureus* alpha-toxin perturbs the barrier function in Caco-2 epithelial cell monolayers by altering junctional integrity. *Infect Immun* 80, 1670-1680.
- Laarman, A.J., Mijnheer, G., Mootz, J.M., van Rooijen, W.J., Ruyken, M., Malone, C.L., Heezius, E.C., Ward, R., Milligan, G., van Strijp, J.A., *et al.* (2012). *Staphylococcus aureus* Staphopain A inhibits CXCR2-dependent neutrophil activation and chemotaxis. *EMBO J* 31, 3607-3619.
- LaFave, M.C., Varshney, G.K., Gildea, D.E., Wolfsberg, T.G., Baxevanis, A.D., and Burgess, S.M. (2014). MLV integration site selection is driven by strong enhancers and active promoters. *Nucleic Acids Res* 42, 4257-4269.
- Lam, M., Dubyak, G., Chen, L., Nunez, G., Miesfeld, R.L., and Distelhorst, C.W. (1994). Evidence that BCL-2 represses apoptosis by regulating endoplasmic reticulum-associated Ca²⁺ fluxes. *Proc Natl Acad Sci U S A* 91, 6569-6573.
- Lam, T.T., Giese, B., Chikkaballi, D., Kuhn, A., Wolber, W., Pane-Farre, J., Schafer, D., Engelmann, S., Fraunholz, M., and Sinha, B. (2010). Phagolysosomal integrity is generally maintained after *Staphylococcus aureus* invasion of nonprofessional phagocytes but is modulated by strain 6850. *Infect Immun* 78, 3392-3403.
- Leeb, M., and Wutz, A. (2013). Haploid genomes illustrate epigenetic constraints and gene dosage effects in mammals. *Epigenetics Chromatin* 6, 41.
- Lehar, S.M., Pillow, T., Xu, M., Staben, L., Kajihara, K.K., Vandlen, R., DePalatis, L., Raab, H., Hazenbos, W.L., Morisaki, J.H., *et al.* (2015). Novel antibody-antibiotic conjugate eliminates intracellular *S. aureus*. *Nature* 527, 323-328.

- Lemasters, J.J., Qian, T., Bradham, C.A., Brenner, D.A., Cascio, W.E., Trost, L.C., Nishimura, Y., Nieminen, A.L., and Herman, B. (1999). Mitochondrial dysfunction in the pathogenesis of necrotic and apoptotic cell death. *J Bioenerg Biomembr* *31*, 305-319.
- Leyden, J.J., Marples, R.R., and Kligman, A.M. (1974). Staphylococcus aureus in the lesions of atopic dermatitis. *Br J Dermatol* *90*, 525-530.
- Li, H., Zhu, H., Xu, C.J., and Yuan, J. (1998). Cleavage of BID by caspase 8 mediates the mitochondrial damage in the Fas pathway of apoptosis. *Cell* *94*, 491-501.
- Li, M., Diep, B.A., Villaruz, A.E., Braughton, K.R., Jiang, X., DeLeo, F.R., Chambers, H.F., Lu, Y., and Otto, M. (2009). Evolution of virulence in epidemic community-associated methicillin-resistant Staphylococcus aureus. *Proc Natl Acad Sci U S A* *106*, 5883-5888.
- Li, X., Stevens, P.D., Yang, H., Gulhati, P., Wang, W., Evers, B.M., and Gao, T. (2013). The deubiquitination enzyme USP46 functions as a tumor suppressor by controlling PHLPP-dependent attenuation of Akt signaling in colon cancer. *Oncogene* *32*, 471-478.
- Lina, G., Bohach, G.A., Nair, S.P., Hiramatsu, K., Jouvin-Marche, E., Mariuzza, R., and International Nomenclature Committee for Staphylococcal, S. (2004). Standard nomenclature for the superantigens expressed by Staphylococcus. *J Infect Dis* *189*, 2334-2336.
- Lina, G., Boutite, F., Tristan, A., Bes, M., Etienne, J., and Vandenesch, F. (2003). Bacterial competition for human nasal cavity colonization: role of Staphylococcal agr alleles. *Appl Environ Microbiol* *69*, 18-23.
- Lindqvist, L.M., Vikstrom, I., Chambers, J.M., McArthur, K., Ann Anderson, M., Henley, K.J., Hoppo, L., Cluse, L., Johnstone, R.W., Roberts, A.W., *et al.* (2012). Translation inhibitors induce cell death by multiple mechanisms and Mcl-1 reduction is only a minor contributor. *Cell Death Dis* *3*, e409.
- Linkermann, A., and Green, D.R. (2014). Necroptosis. *N Engl J Med* *370*, 455-465.
- Linkermann, A., Stockwell, B.R., Krautwald, S., and Anders, H.J. (2014). Regulated cell death and inflammation: an auto-amplification loop causes organ failure. *Nat Rev Immunol* *14*, 759-767.
- Liu, J., Weiss, H.L., Rychahou, P., Jackson, L.N., Evers, B.M., and Gao, T. (2009). Loss of PHLPP expression in colon cancer: role in proliferation and tumorigenesis. *Oncogene* *28*, 994-1004.
- Liu, Y., Yan, X., and Zhou, T. (2013). TBCK influences cell proliferation, cell size and mTOR signaling pathway. *Plos One* *8*, e71349.
- Livak, K.J., and Schmittgen, T.D. (2001). Analysis of relative gene expression data using real-time quantitative PCR and the 2(-Delta Delta C(T)) Method. *Methods* *25*, 402-408.
- Loeffler, B., Hussain, M., Grundmeier, M., Bruck, M., Holzinger, D., Varga, G., Roth, J., Kahl, B.C., Proctor, R.A., and Peters, G. (2010). Staphylococcus aureus panton-valentine leukocidin is a very potent cytotoxic factor for human neutrophils. *PLoS Pathog* *6*, e1000715.
- Loeffler, M., Daugas, E., Susin, S.A., Zamzami, N., Metivier, D., Nieminen, A.L., Brothers, G., Penninger, J.M., and Kroemer, G. (2001). Dominant cell death induction by extramitochondrially targeted apoptosis-inducing factor. *Faseb J* *15*, 758-767.
- Lopatniuk, P., and Witkowski, J.M. (2011). Conventional calpains and programmed cell death. *Acta Biochim Pol* *58*, 287-296.

- Loughran, A.J., Atwood, D.N., Anthony, A.C., Harik, N.S., Spencer, H.J., Beenken, K.E., and Smeltzer, M.S. (2014). Impact of individual extracellular proteases on *Staphylococcus aureus* biofilm formation in diverse clinical isolates and their isogenic *sarA* mutants. *Microbiologyopen* 3, 897-909.
- Lowy, F.D. (1998). *Staphylococcus aureus* infections. *N Engl J Med* 339, 520-532.
- Lowy, F.D., Fant, J., Higgins, L.L., Ogawa, S.K., and Hatcher, V.B. (1988). *Staphylococcus aureus*--human endothelial cell interactions. *J Ultrastruct Mol Struct Res* 98, 137-146.
- Luo, X., Budihardjo, I., Zou, H., Slaughter, C., and Wang, X. (1998). Bid, a Bcl2 interacting protein, mediates cytochrome c release from mitochondria in response to activation of cell surface death receptors. *Cell* 94, 481-490.
- Lyytikäinen, O., Ruotsalainen, E., Jarvinen, A., Valtonen, V., and Ruutu, P. (2005). Trends and outcome of nosocomial and community-acquired bloodstream infections due to *Staphylococcus aureus* in Finland, 1995-2001. *Eur J Clin Microbiol Infect Dis* 24, 399-404.
- Machaca, K. (2010). Ca²⁺ signaling, genes and the cell cycle. *Cell Calcium* 48, 243-250.
- Maeder, U., Nicolas, P., Depke, M., Pane-Farre, J., Debarbouille, M., van der Kooi-Pol, M.M., Guerin, C., Derozier, S., Hiron, A., Jarmer, H., *et al.* (2016). *Staphylococcus aureus* Transcriptome Architecture: From Laboratory to Infection-Mimicking Conditions. *PLoS Genet* 12, e1005962.
- Mahmood, S.F., Gruel, N., Chapeaublanc, E., Lescure, A., Jones, T., Reyat, F., Vincent-Salomon, A., Raynal, V., Pierron, G., Perez, F., *et al.* (2014). A siRNA screen identifies RAD21, EIF3H, CHRAC1 and TANC2 as driver genes within the 8q23, 8q24.3 and 17q23 amplicons in breast cancer with effects on cell growth, survival and transformation. *Carcinogenesis* 35, 670-682.
- Majno, G., and Joris, I. (1995). Apoptosis, oncosis, and necrosis. An overview of cell death. *Am J Pathol* 146, 3-15.
- Malachowa, N., Kobayashi, S.D., Braughton, K.R., Whitney, A.R., Parnell, M.J., Gardner, D.J., and Deleo, F.R. (2012). *Staphylococcus aureus* leukotoxin GH promotes inflammation. *J Infect Dis* 206, 1185-1193.
- Mandal, M., Crusio, K.M., Meng, F., Liu, S., Kinsella, M., Clark, M.R., Takeuchi, O., and Aifantis, I. (2008). Regulation of lymphocyte progenitor survival by the proapoptotic activities of Bim and Bid. *Proc Natl Acad Sci U S A* 105, 20840-20845.
- Mandal, M., Maggirwar, S.B., Sharma, N., Kaufmann, S.H., Sun, S.C., and Kumar, R. (1996). Bcl-2 prevents CD95 (Fas/APO-1)-induced degradation of lamin B and poly(ADP-ribose) polymerase and restores the NF-kappaB signaling pathway. *J Biol Chem* 271, 30354-30359.
- Mandal, P., Berger, S.B., Pillay, S., Moriwaki, K., Huang, C., Guo, H., Lich, J.D., Finger, J., Kasparcova, V., Votta, B., *et al.* (2014). RIP3 induces apoptosis independent of pronecrotic kinase activity. *Mol Cell* 56, 481-495.
- Mandic, A., Viktorsson, K., Strandberg, L., Heiden, T., Hansson, J., Linder, S., and Shoshan, M.C. (2002). Calpain-mediated Bid cleavage and calpain-independent Bak modulation: two separate pathways in cisplatin-induced apoptosis. *Mol Cell Biol* 22, 3003-3013.
- Maree, C.L., Daum, R.S., Boyle-Vavra, S., Matayoshi, K., and Miller, L.G. (2007). Community-associated methicillin-resistant *Staphylococcus aureus* isolates causing healthcare-associated infections. *Emerg Infect Dis* 13, 236-242.
- Martin, G.S., Mannino, D.M., Eaton, S., and Moss, M. (2003). The epidemiology of sepsis in the United States from 1979 through 2000. *N Engl J Med* 348, 1546-1554.

- Martins, L.M., Iaccarino, I., Tenev, T., Gschmeissner, S., Totty, N.F., Lemoine, N.R., Savopoulos, J., Gray, C.W., Creasy, C.L., Dingwall, C., *et al.* (2002). The serine protease Omi/HtrA2 regulates apoptosis by binding XIAP through a reaper-like motif. *J Biol Chem* *277*, 439-444.
- Maruyama, T., Kanaji, T., Nakade, S., Kanno, T., and Mikoshiba, K. (1997). 2APB, 2-aminoethoxydiphenyl borate, a membrane-penetrable modulator of Ins(1,4,5)P₃-induced Ca²⁺ release. *J Biochem* *122*, 498-505.
- Masini, M., Lupi, R., Bugliani, M., Boggi, U., Filipponi, F., Masiello, P., and Marchetti, P. (2009). A role for autophagy in beta-cell life and death. *Islets* *1*, 157-159.
- Massimi, I., Park, E., Rice, K., Muller-Esterl, W., Sauder, D., and McGavin, M.J. (2002). Identification of a novel maturation mechanism and restricted substrate specificity for the SspB cysteine protease of *Staphylococcus aureus*. *J Biol Chem* *277*, 41770-41777.
- Matsch, I. (2018). Untersuchungen zum Einfluss der Gene TAOK1, TBCK, PAWR und TANC im Hinblick auf den *Staphylococcus* induzierten Wirtszelltod (Master Thesis, University Würzburg).
- Maurer, K., Reyes-Robles, T., Alonzo, F., 3rd, Durbin, J., Torres, V.J., and Cadwell, K. (2015). Autophagy mediates tolerance to *Staphylococcus aureus* alpha-toxin. *Cell Host Microbe* *17*, 429-440.
- Mauthe, M., Yu, W., Krut, O., Kronke, M., Gotz, F., Robenek, H., and Proikas-Cezanne, T. (2012). WIPI-1 Positive Autophagosome-Like Vesicles Entrap Pathogenic *Staphylococcus aureus* for Lysosomal Degradation. *Int J Cell Biol* *2012*, 179207.
- McAleese, F.M., Walsh, E.J., Sieprawska, M., Potempa, J., and Foster, T.J. (2001). Loss of clumping factor B fibrinogen binding activity by *Staphylococcus aureus* involves cessation of transcription, shedding and cleavage by metalloprotease. *J Biol Chem* *276*, 29969-29978.
- McCarthy, A.J., and Lindsay, J.A. (2010). Genetic variation in *Staphylococcus aureus* surface and immune evasion genes is lineage associated: implications for vaccine design and host-pathogen interactions. *BMC Microbiol* *10*, 173.
- McConkey, D.J., Hartzell, P., Nicotera, P., and Orrenius, S. (1989). Calcium-activated DNA fragmentation kills immature thymocytes. *Faseb J* *3*, 1843-1849.
- McDonald, M.C., Mota-Filipe, H., Paul, A., Cuzzocrea, S., Abdelrahman, M., Harwood, S., Plevin, R., Chatterjee, P.K., Yaqoob, M.M., and Thiernemann, C. (2001). Calpain inhibitor I reduces the activation of nuclear factor-kappaB and organ injury/dysfunction in hemorrhagic shock. *Faseb J* *15*, 171-186.
- McGavin, M.J., Zahradka, C., Rice, K., and Scott, J.E. (1997). Modification of the *Staphylococcus aureus* fibronectin binding phenotype by V8 protease. *Infect Immun* *65*, 2621-2628.
- McNamara, P.J., and Iandolo, J.J. (1998). Genetic instability of the global regulator agr explains the phenotype of the xpr mutation in *Staphylococcus aureus* KSI9051. *J Bacteriol* *180*, 2609-2615.
- Mehlen, P., and Bredesen, D.E. (2011). Dependence receptors: from basic research to drug development. *Sci Signal* *4*, mr2.
- Mehlin, C., Headley, C.M., and Klebanoff, S.J. (1999). An inflammatory polypeptide complex from *Staphylococcus epidermidis*: isolation and characterization. *J Exp Med* *189*, 907-918.
- Melehani, J.H., James, D.B., DuMont, A.L., Torres, V.J., and Duncan, J.A. (2015). *Staphylococcus aureus* Leukocidin A/B (LukAB) Kills Human Monocytes via Host NLRP3 and ASC when Extracellular, but Not Intracellular. *PLoS Pathog* *11*, e1004970.

- Melloni, E., Salamino, F., and Sparatore, B. (1992). The calpain-calpastatin system in mammalian cells: properties and possible functions. *Biochimie* 74, 217-223.
- Melly, M.A., Thomison, J.B., and Rogers, D.E. (1960). Fate of staphylococci within human leukocytes. *J Exp Med* 112, 1121-1130.
- Menzies, B.E., and Kourteva, I. (1998). Internalization of *Staphylococcus aureus* by endothelial cells induces apoptosis. *Infect Immun* 66, 5994-5998.
- Menzies, B.E., and Kourteva, I. (2000). *Staphylococcus aureus* alpha-toxin induces apoptosis in endothelial cells. *FEMS Immunol Med Microbiol* 29, 39-45.
- Mertz, D., Frei, R., Jaussi, B., Tietz, A., Stebler, C., Fluckiger, U., and Widmer, A.F. (2007). Throat swabs are necessary to reliably detect carriers of *Staphylococcus aureus*. *Clin Infect Dis* 45, 475-477.
- Messaritakis, I., Samonis, G., Dimopoulou, D., Maraki, S., Papadakis, J.A., Daraki, V., Fragaki, M., Choulaki, C., Andrianaki, A.M., and Kofteridis, D.P. (2014). *Staphylococcus aureus* nasal carriage might be associated with vitamin D receptor polymorphisms in type 2 diabetes. *Clin Microbiol Infect* 20, 920-925.
- Mestre, M.B., Fader, C.M., Sola, C., and Colombo, M.I. (2010). Alpha-hemolysin is required for the activation of the autophagic pathway in *Staphylococcus aureus*-infected cells. *Autophagy* 6, 110-125.
- Miled, C., Pontoglio, M., Garbay, S., Yaniv, M., and Weitzman, J.B. (2005). A genomic map of p53 binding sites identifies novel p53 targets involved in an apoptotic network. *Cancer Res* 65, 5096-5104.
- Miller, L.G., and Diep, B.A. (2008). Clinical practice: colonization, fomites, and virulence: rethinking the pathogenesis of community-associated methicillin-resistant *Staphylococcus aureus* infection. *Clin Infect Dis* 46, 752-760.
- Miller, L.G., Perdreau-Remington, F., Rieg, G., Mehdi, S., Perthroth, J., Bayer, A.S., Tang, A.W., Phung, T.O., and Spellberg, B. (2005). Necrotizing fasciitis caused by community-associated methicillin-resistant *Staphylococcus aureus* in Los Angeles. *N Engl J Med* 352, 1445-1453.
- Misaghi, S., Korbel, G.A., Kessler, B., Spooner, E., and Ploegh, H.L. (2006). z-VAD-fmk inhibits peptide:N-glycanase and may result in ER stress. *Cell Death Differ* 13, 163-165.
- Misaghi, S., Pacold, M.E., Blom, D., Ploegh, H.L., and Korbel, G.A. (2004). Using a small molecule inhibitor of peptide: N-glycanase to probe its role in glycoprotein turnover. *Chem Biol* 11, 1677-1687.
- Mishra, A.K., Yadav, P., and Mishra, A. (2016). A Systemic Review on Staphylococcal Scalded Skin Syndrome (SSSS): A Rare and Critical Disease of Neonates. *Open Microbiol J* 10, 150-159.
- Missiaen, L., Callewaert, G., De Smedt, H., and Parys, J.B. (2001). 2-Aminoethoxydiphenyl borate affects the inositol 1,4,5-trisphosphate receptor, the intracellular Ca²⁺ pump and the non-specific Ca²⁺ leak from the non-mitochondrial Ca²⁺ stores in permeabilized A7r5 cells. *Cell Calcium* 29, 111-116.
- Mitsopoulos, C., Zihni, C., Garg, R., Ridley, A.J., and Morris, J.D. (2003). The prostate-derived sterile 20-like kinase (PSK) regulates microtubule organization and stability. *J Biol Chem* 278, 18085-18091.
- Moffat, J., Grueneberg, D.A., Yang, X., Kim, S.Y., Kloepfer, A.M., Hinkle, G., Piqani, B., Eisenhaure, T.M., Luo, B., Grenier, J.K., *et al.* (2006). A lentiviral RNAi library for human and mouse genes applied to an arrayed viral high-content screen. *Cell* 124, 1283-1298.
- Mohamed, W., Domann, E., Chakraborty, T., Mannala, G., Lips, K.S., Heiss, C., Schnettler, R., and Alt, V. (2016). TLR9 mediates *S. aureus* killing inside osteoblasts via induction of oxidative stress. *BMC Microbiol* 16, 230.

- Moisan, H., Brouillette, E., Jacob, C.L., Langlois-Begin, P., Michaud, S., and Malouin, F. (2006). Transcription of virulence factors in *Staphylococcus aureus* small-colony variants isolated from cystic fibrosis patients is influenced by SigB. *J Bacteriol* *188*, 64-76.
- Moldovan, A., and Fraunholz, M.J. (2018). In or out: phagosomal escape of *Staphylococcus aureus*. *Cell Microbiol*, e12997.
- Moore, T.M., Garg, R., Johnson, C., Coptcoat, M.J., Ridley, A.J., and Morris, J.D. (2000). PSK, a novel STE20-like kinase derived from prostatic carcinoma that activates the c-Jun N-terminal kinase mitogen-activated protein kinase pathway and regulates actin cytoskeletal organization. *J Biol Chem* *275*, 4311-4322.
- Mootz, J.M., Malone, C.L., Shaw, L.N., and Horswill, A.R. (2013). Staphopains modulate *Staphylococcus aureus* biofilm integrity. *Infect Immun* *81*, 3227-3238.
- Morinaga, N., Kaihou, Y., and Noda, M. (2003). Purification, cloning and characterization of variant LukE-LukD with strong leukocidal activity of staphylococcal bi-component leukotoxin family. *Microbiol Immunol* *47*, 81-90.
- Moujalled, D.M., Cook, W.D., Okamoto, T., Murphy, J., Lawlor, K.E., Vince, J.E., and Vaux, D.L. (2013). TNF can activate RIPK3 and cause programmed necrosis in the absence of RIPK1. *Cell Death Dis* *4*, e465.
- Mrschtk, M., O'Prey, J., Lao, L.Y., Long, J.S., Beaumatin, F., Strachan, D., O'Prey, M., Skommer, J., and Ryan, K.M. (2015). DRAM-3 modulates autophagy and promotes cell survival in the absence of glucose. *Cell Death Differ* *22*, 1714-1726.
- Muenzenmayer, L., Geiger, T., Daiber, E., Schulte, B., Autenrieth, S.E., Fraunholz, M., and Wolz, C. (2016). Influence of Sae-regulated and Agr-regulated factors on the escape of *Staphylococcus aureus* from human macrophages. *Cell Microbiol* *18*, 1172-1183.
- Murphy, M.P. (2009). How mitochondria produce reactive oxygen species. *Biochem J* *417*, 1-13.
- Nakagawa, M., Mammoto, T., Hazama, A., Kita, T., Akamatsu, T., Kambara, N., Sakai, T., and Kishi, Y. (2000). Midazolam premedication reduces propofol requirements for sedation during regional anesthesia. *Can J Anaesth* *47*, 47-49.
- Nakagawa, T., Shimizu, S., Watanabe, T., Yamaguchi, O., Otsu, K., Yamagata, H., Inohara, H., Kubo, T., and Tsujimoto, Y. (2005). Cyclophilin D-dependent mitochondrial permeability transition regulates some necrotic but not apoptotic cell death. *Nature* *434*, 652-658.
- Nakagawa, T., and Yuan, J. (2000). Cross-talk between two cysteine protease families. Activation of caspase-12 by calpain in apoptosis. *J Cell Biol* *150*, 887-894.
- Nakatsuji, T., Chen, T.H., Two, A.M., Chun, K.A., Narala, S., Geha, R.S., Hata, T.R., and Gallo, R.L. (2016). *Staphylococcus aureus* Exploits Epidermal Barrier Defects in Atopic Dermatitis to Trigger Cytokine Expression. *J Invest Dermatol* *136*, 2192-2200.
- Neumann, Y., Bruns, S.A., Rohde, M., Prajsnar, T.K., Foster, S.J., and Schmitz, I. (2016). Intracellular *Staphylococcus aureus* eludes selective autophagy by activating a host cell kinase. *Autophagy* *12*, 2069-2084.
- Nickerson, N., Ip, J., Passos, D.T., and McGavin, M.J. (2010). Comparison of Staphopain A (ScpA) and B (SspB) precursor activation mechanisms reveals unique secretion kinetics of proSspB (Staphopain B), and a different interaction with its cognate Staphostatin, SspC. *Mol Microbiol* *75*, 161-177.

- Nickerson, N.N., Joag, V., and McGavin, M.J. (2008). Rapid autocatalytic activation of the M4 metalloprotease aureolysin is controlled by a conserved N-terminal fungalysin-thermolysin-propeptide domain. *Mol Microbiol* 69, 1530-1543.
- Noda, T., and Ohsumi, Y. (1998). Tor, a phosphatidylinositol kinase homologue, controls autophagy in yeast. *J Biol Chem* 273, 3963-3966.
- Norberg, E., Gogvadze, V., Ott, M., Horn, M., Uhlen, P., Orrenius, S., and Zhivotovsky, B. (2008). An increase in intracellular Ca²⁺ is required for the activation of mitochondrial calpain to release AIF during cell death. *Cell Death Differ* 15, 1857-1864.
- Novick, R.P. (2003). Autoinduction and signal transduction in the regulation of staphylococcal virulence. *Mol Microbiol* 48, 1429-1449.
- Nutt, L.K., Chandra, J., Pataer, A., Fang, B., Roth, J.A., Swisher, S.G., O'Neil, R.G., and McConkey, D.J. (2002a). Bax-mediated Ca²⁺ mobilization promotes cytochrome c release during apoptosis. *J Biol Chem* 277, 20301-20308.
- Nutt, L.K., Pataer, A., Pahler, J., Fang, B., Roth, J., McConkey, D.J., and Swisher, S.G. (2002b). Bax and Bak promote apoptosis by modulating endoplasmic reticular and mitochondrial Ca²⁺ stores. *J Biol Chem* 277, 9219-9225.
- Nuzzo, I., Sanges, M.R., Folgore, A., and Carratelli, C.R. (2000). Apoptosis of human keratinocytes after bacterial invasion. *FEMS Immunol Med Microbiol* 27, 235-240.
- O'Keeffe, K.M., Wilk, M.M., Leech, J.M., Murphy, A.G., Laabei, M., Monk, I.R., Massey, R.C., Lindsay, J.A., Foster, T.J., Geoghegan, J.A., *et al.* (2015). Manipulation of Autophagy in Phagocytes Facilitates Staphylococcus aureus Bloodstream Infection. *Infect Immun* 83, 3445-3457.
- Ofengeim, D., and Yuan, J. (2013). Regulation of RIP1 kinase signalling at the crossroads of inflammation and cell death. *Nat Rev Mol Cell Biol* 14, 727-736.
- Ogston, A. (1882). Micrococcus Poisoning. *J Anat Physiol* 17, 24-58.
- Ohbayashi, T., Irie, A., Murakami, Y., Nowak, M., Potempa, J., Nishimura, Y., Shinohara, M., and Imamura, T. (2011). Degradation of fibrinogen and collagen by staphopains, cysteine proteases released from Staphylococcus aureus. *Microbiology* 157, 786-792.
- Oliveira, D., Borges, A., and Simoes, M. (2018). Staphylococcus aureus Toxins and Their Molecular Activity in Infectious Diseases. *Toxins (Basel)* 10.
- Olsen, K., Falch, B.M., Danielsen, K., Johannessen, M., Ericson Sollid, J.U., Thune, I., Grimnes, G., Jorde, R., Simonsen, G.S., and Furberg, A.S. (2012). Staphylococcus aureus nasal carriage is associated with serum 25-hydroxyvitamin D levels, gender and smoking status. The Tromso Staph and Skin Study. *Eur J Clin Microbiol Infect Dis* 31, 465-473.
- Ono, Y., Saido, T.C., and Sorimachi, H. (2016). Calpain research for drug discovery: challenges and potential. *Nat Rev Drug Discov* 15, 854-876.
- Ono, Y., and Sorimachi, H. (2012). Calpains: an elaborate proteolytic system. *Biochim Biophys Acta* 1824, 224-236.
- Orrenius, S., Gogvadze, V., and Zhivotovsky, B. (2015). Calcium and mitochondria in the regulation of cell death. *Biochem Biophys Res Commun* 460, 72-81.
- Otto, M. (2014). Staphylococcus aureus toxins. *Curr Opin Microbiol* 17, 32-37.

- Ou, J., Drilling, A., Singhal, D., Tan, N.C., Wallis-Hill, D., Vreugde, S., Psaltis, A.J., and Wormald, P.J. (2016). Association of intracellular *Staphylococcus aureus* with prognosis in chronic rhinosinusitis. *Int Forum Allergy Rhinol* 6, 792-799.
- Ousingsawat, J., Cabrita, I., Wanitchakool, P., Sirianant, L., Krautwald, S., Linkermann, A., Schreiber, R., and Kunzelmann, K. (2017). Ca²⁺ signals, cell membrane disintegration, and activation of TMEM16F during necroptosis. *Cell Mol Life Sci* 74, 173-181.
- Oyama, T., Harigaya, K., Sasaki, N., Okamura, Y., Kokubo, H., Saga, Y., Hozumi, K., Suganami, A., Tamura, Y., Nagase, T., *et al.* (2011). Mastermind-like 1 (MamL1) and mastermind-like 3 (MamL3) are essential for Notch signaling in vivo. *Development* 138, 5235-5246.
- Ozaki, T., Yamashita, T., and Ishiguro, S. (2008). ERp57-associated mitochondrial mu-calpain truncates apoptosis-inducing factor. *Biochim Biophys Acta* 1783, 1955-1963.
- Ozaki, T., Yamashita, T., and Ishiguro, S. (2009). Mitochondrial m-calpain plays a role in the release of truncated apoptosis-inducing factor from the mitochondria. *Biochim Biophys Acta* 1793, 1848-1859.
- Paharik, A.E., Salgado-Pabon, W., Meyerholz, D.K., White, M.J., Schlievert, P.M., and Horswill, A.R. (2016). The Spl Serine Proteases Modulate *Staphylococcus aureus* Protein Production and Virulence in a Rabbit Model of Pneumonia. *mSphere* 1.
- Painter, K.L., Strange, E., Parkhill, J., Bamford, K.B., Armstrong-James, D., and Edwards, A.M. (2015). *Staphylococcus aureus* adapts to oxidative stress by producing H₂O₂-resistant small-colony variants via the SOS response. *Infect Immun* 83, 1830-1844.
- Pajak, B., Gajkowska, B., and Orzechowski, A. (2005). Cycloheximide-mediated sensitization to TNF- α -induced apoptosis in human colorectal cancer cell line COLO 205; role of FLIP and metabolic inhibitors. *J Physiol Pharmacol* 56 Suppl 3, 101-118.
- Palma Medina, L.M., Becker, A.K., Michalik, S., Yedavally, H., Raineri, E.J.M., Hildebrandt, P., Gesell Salazar, M., Surmann, K., Pfortner, H., Mekonnen, S.A., *et al.* (2019). Metabolic Cross-talk Between Human Bronchial Epithelial Cells and Internalized *Staphylococcus aureus* as a Driver for Infection. *Mol Cell Proteomics* 18, 892-908.
- Pan, Z., Bhat, M.B., Nieminen, A.L., and Ma, J. (2001). Synergistic movements of Ca²⁺ and Bax in cells undergoing apoptosis. *J Biol Chem* 276, 32257-32263.
- Panaretakis, T., Pokrovskaja, K., Shoshan, M.C., and Grandier, D. (2002). Activation of Bak, Bax, and BH3-only proteins in the apoptotic response to doxorubicin. *J Biol Chem* 277, 44317-44326.
- Pannaraj, P.S., Hulten, K.G., Gonzalez, B.E., Mason, E.O., Jr., and Kaplan, S.L. (2006). Infective pyomyositis and myositis in children in the era of community-acquired, methicillin-resistant *Staphylococcus aureus* infection. *Clin Infect Dis* 43, 953-960.
- Paoli, P., Giannoni, E., and Chiarugi, P. (2013). Anoikis molecular pathways and its role in cancer progression. *Biochim Biophys Acta* 1833, 3481-3498.
- Papatheodorou, P., Carette, J.E., Bell, G.W., Schwan, C., Guttenberg, G., Brummelkamp, T.R., and Aktories, K. (2011). Lipolysis-stimulated lipoprotein receptor (LSR) is the host receptor for the binary toxin *Clostridium difficile* transferase (CDT). *Proc Natl Acad Sci U S A* 108, 16422-16427.
- Paprotka, K., Giese, B., and Fraunholz, M.J. (2010). Codon-improved fluorescent proteins in investigation of *Staphylococcus aureus* host pathogen interactions. *J Microbiol Methods* 83, 82-86.

- Park, C.Y., Hoover, P.J., Mullins, F.M., Bachhawat, P., Covington, E.D., Raunser, S., Walz, T., Garcia, K.C., Dolmetsch, R.E., and Lewis, R.S. (2009). STIM1 clusters and activates CRAC channels via direct binding of a cytosolic domain to Orai1. *Cell* 136, 876-890.
- Peacock, J.E., Jr., Marsik, F.J., and Wenzel, R.P. (1980). Methicillin-resistant *Staphylococcus aureus*: introduction and spread within a hospital. *Ann Intern Med* 93, 526-532.
- Pecci, A., Ma, X., Savoia, A., and Adelstein, R.S. (2018). MYH9: Structure, functions and role of non-muscle myosin IIA in human disease. *Gene* 664, 152-167.
- Periasamy, S., Joo, H.S., Duong, A.C., Bach, T.H., Tan, V.Y., Chatterjee, S.S., Cheung, G.Y., and Otto, M. (2012). How *Staphylococcus aureus* biofilms develop their characteristic structure. *Proc Natl Acad Sci U S A* 109, 1281-1286.
- Peschel, A., and Otto, M. (2013). Phenol-soluble modulins and staphylococcal infection. *Nat Rev Microbiol* 11, 667-673.
- Pettitt, S.J., Rehman, F.L., Bajrami, I., Brough, R., Wallberg, F., Kozarewa, I., Fenwick, K., Assiotis, I., Chen, L., Campbell, J., *et al.* (2013). A genetic screen using the PiggyBac transposon in haploid cells identifies Parp1 as a mediator of olaparib toxicity. *Plos One* 8, e61520.
- Planells-Cases, R., Lutter, D., Guyader, C., Gerhards, N.M., Ullrich, F., Elger, D.A., Kucukosmanoglu, A., Xu, G., Voss, F.K., Reincke, S.M., *et al.* (2015). Subunit composition of VRAC channels determines substrate specificity and cellular resistance to Pt-based anti-cancer drugs. *EMBO J* 34, 2993-3008.
- Plouin-Gaudon, I., Clement, S., Huggler, E., Chaponnier, C., Francois, P., Lew, D., Schrenzel, J., Vaudaux, P., and Lacroix, J.S. (2006). Intracellular residency is frequently associated with recurrent *Staphylococcus aureus* rhinosinusitis. *Rhinology* 44, 249-254.
- Polster, B.M., Basanez, G., Etxebarria, A., Hardwick, J.M., and Nicholls, D.G. (2005). Calpain I induces cleavage and release of apoptosis-inducing factor from isolated mitochondria. *J Biol Chem* 280, 6447-6454.
- Popov, L.M., Marceau, C.D., Starkl, P.M., Lumb, J.H., Shah, J., Guerrero, D., Cooper, R.L., Merakou, C., Bouley, D.M., Meng, W., *et al.* (2015). The adherens junctions control susceptibility to *Staphylococcus aureus* alpha-toxin. *Proc Natl Acad Sci U S A* 112, 14337-14342.
- Potempa, J., Dubin, A., Korzus, G., and Travis, J. (1988). Degradation of elastin by a cysteine proteinase from *Staphylococcus aureus*. *J Biol Chem* 263, 2664-2667.
- Prahallad, A., Sun, C., Huang, S., Di Nicolantonio, F., Salazar, R., Zecchin, D., Beijersbergen, R.L., Bardelli, A., and Bernards, R. (2012). Unresponsiveness of colon cancer to BRAF(V600E) inhibition through feedback activation of EGFR. *Nature* 483, 100-103.
- Prakriya, M., Feske, S., Gwack, Y., Srikanth, S., Rao, A., and Hogan, P.G. (2006). Orai1 is an essential pore subunit of the CRAC channel. *Nature* 443, 230-233.
- Prakriya, M., and Lewis, R.S. (2001). Potentiation and inhibition of Ca(2+) release-activated Ca(2+) channels by 2-aminoethyldiphenyl borate (2-APB) occurs independently of IP(3) receptors. *J Physiol* 536, 3-19.
- Prat, C., Bestebroer, J., de Haas, C.J., van Strijp, J.A., and van Kessel, K.P. (2006). A new staphylococcal anti-inflammatory protein that antagonizes the formyl peptide receptor-like 1. *J Immunol* 177, 8017-8026.

- Prat, C., Haas, P.J., Bestebroer, J., de Haas, C.J., van Strijp, J.A., and van Kessel, K.P. (2009). A homolog of formyl peptide receptor-like 1 (FPRL1) inhibitor from *Staphylococcus aureus* (FPRL1 inhibitory protein) that inhibits FPRL1 and FPR. *J Immunol* *183*, 6569-6578.
- Proctor, R.A., Balwit, J.M., and Vesga, O. (1994). Variant subpopulations of *Staphylococcus aureus* as cause of persistent and recurrent infections. *Infect Agents Dis* *3*, 302-312.
- Purcell, K., and Fergie, J. (2005). Epidemic of community-acquired methicillin-resistant *Staphylococcus aureus* infections: a 14-year study at Driscoll Children's Hospital. *Arch Pediatr Adolesc Med* *159*, 980-985.
- Putney, J.W. (2010). Pharmacology of store-operated calcium channels. *Mol Interv* *10*, 209-218.
- Qazi, S.N., Counil, E., Morrissey, J., Rees, C.E., Cockayne, A., Winzer, K., Chan, W.C., Williams, P., and Hill, P.J. (2001). *agr* expression precedes escape of internalized *Staphylococcus aureus* from the host endosome. *Infect Immun* *69*, 7074-7082.
- Qiu, S., Liu, J., and Xing, F. (2017). 'Hints' in the killer protein gasdermin D: unveiling the secrets of gasdermins driving cell death. *Cell Death Differ* *24*, 588-596.
- Rajesh, M., Samundeeswari, M., and Archana, B. (2017). Isolation of Biosurfactant Producing Bacteria from Garbage Soil. *Journal of Applied & Environmental Microbiology* *5*, 74-78.
- Raman, M., Earnest, S., Zhang, K., Zhao, Y., and Cobb, M.H. (2007). TAO kinases mediate activation of p38 in response to DNA damage. *EMBO J* *26*, 2005-2014.
- Ran, F.A., Hsu, P.D., Wright, J., Agarwala, V., Scott, D.A., and Zhang, F. (2013). Genome engineering using the CRISPR-Cas9 system. *Nat Protoc* *8*, 2281-2308.
- Randolph, A.G., Vaughn, F., Sullivan, R., Rubinson, L., Thompson, B.T., Yoon, G., Smoot, E., Rice, T.W., Loftis, L.L., Helfaer, M., *et al.* (2011). Critically ill children during the 2009-2010 influenza pandemic in the United States. *Pediatrics* *128*, e1450-1458.
- Rasigade, J.P., Trouillet-Assant, S., Ferry, T., Diep, B.A., Sapin, A., Lhoste, Y., Ranfaing, J., Badiou, C., Benito, Y., Bes, M., *et al.* (2013). PSMs of hypervirulent *Staphylococcus aureus* act as intracellular toxins that kill infected osteoblasts. *Plos One* *8*, e63176.
- Rath, S., Ziesemer, S., Witte, A., Konkel, A., Muller, C., Hildebrandt, P., Volker, U., and Hildebrandt, J.P. (2013). *S. aureus* haemolysin A-induced IL-8 and IL-6 release from human airway epithelial cells is mediated by activation of p38- and Erk-MAP kinases and additional, cell type-specific signalling mechanisms. *Cell Microbiol* *15*, 1253-1265.
- Redza-Dutordoir, M., and Averill-Bates, D.A. (2016). Activation of apoptosis signalling pathways by reactive oxygen species. *Biochim Biophys Acta* *1863*, 2977-2992.
- Reed, S.B., Wesson, C.A., Liou, L.E., Trumble, W.R., Schlievert, P.M., Bohach, G.A., and Bayles, K.W. (2001). Molecular characterization of a novel *Staphylococcus aureus* serine protease operon. *Infect Immun* *69*, 1521-1527.
- Reiling, J.H., Olive, A.J., Sanyal, S., Carette, J.E., Brummelkamp, T.R., Ploegh, H.L., Starnbach, M.N., and Sabatini, D.M. (2013). A CREB3-ARF4 signalling pathway mediates the response to Golgi stress and susceptibility to pathogens. *Nat Cell Biol* *15*, 1473-1485.
- Riblett, A.M., Blomen, V.A., Jae, L.T., Altamura, L.A., Doms, R.W., Brummelkamp, T.R., and Wojcechowskyj, J.A. (2016). A Haploid Genetic Screen Identifies Heparan Sulfate Proteoglycans Supporting Rift Valley Fever Virus Infection. *J Virol* *90*, 1414-1423.

- Richter, E., Harms, M., Venz, K., Nolker, R., Fraunholz, M.J., Mostertz, J., and Hochgrafe, F. (2016). Quantitative Proteomics Reveals the Dynamics of Protein Phosphorylation in Human Bronchial Epithelial Cells during Internalization, Phagosomal Escape, and Intracellular Replication of *Staphylococcus aureus*. *J Proteome Res* *15*, 4369-4386.
- Riedl, S.J., and Salvesen, G.S. (2007). The apoptosome: signalling platform of cell death. *Nat Rev Mol Cell Biol* *8*, 405-413.
- Rieg, S., Peyerl-Hoffmann, G., de With, K., Theilacker, C., Wagner, D., Hubner, J., Dettenkofer, M., Kaasch, A., Seifert, H., Schneider, C., *et al.* (2009). Mortality of *S. aureus* bacteremia and infectious diseases specialist consultation--a study of 521 patients in Germany. *J Infect* *59*, 232-239.
- Ringberg, H., Cathrine Petersson, A., Walder, M., and Hugo Johansson, P.J. (2006). The throat: an important site for MRSA colonization. *Scand J Infect Dis* *38*, 888-893.
- Rollin, G., Tan, X., Tros, F., Dupuis, M., Nassif, X., Charbit, A., and Coureuil, M. (2017). Intracellular Survival of *Staphylococcus aureus* in Endothelial Cells: A Matter of Growth or Persistence. *Front Microbiol* *8*, 1354.
- Rooijackers, S.H., Ruyken, M., Roos, A., Daha, M.R., Presanis, J.S., Sim, R.B., van Wamel, W.J., van Kessel, K.P., and van Strijp, J.A. (2005). Immune evasion by a staphylococcal complement inhibitor that acts on C3 convertases. *Nat Immunol* *6*, 920-927.
- Rosenbach, F.J. (1884). *Mikro-Organismen bei den Wund-Infektions-Krankheiten des Menschen* (Wiesbaden J.F. Bergmann).
- Rosmarin, D.M., Carette, J.E., Olive, A.J., Starnbach, M.N., Brummelkamp, T.R., and Ploegh, H.L. (2012). Attachment of *Chlamydia trachomatis* L2 to host cells requires sulfation. *Proc Natl Acad Sci U S A* *109*, 10059-10064.
- Rozman-Pungercar, J., Kopitar-Jerala, N., Bogyo, M., Turk, D., Vasiljeva, O., Stefe, I., Vandenabeele, P., Bromme, D., Puizdar, V., Fonovic, M., *et al.* (2003). Inhibition of papain-like cysteine proteases and legumain by caspase-specific inhibitors: when reaction mechanism is more important than specificity. *Cell Death Differ* *10*, 881-888.
- Ruiz-Vela, A., Gonzalez de Buitrago, G., and Martinez, A.C. (1999). Implication of calpain in caspase activation during B cell clonal deletion. *EMBO J* *18*, 4988-4998.
- Rzychon, M., Sabat, A., Kosowska, K., Potempa, J., and Dubin, A. (2003). Staphostatins: an expanding new group of proteinase inhibitors with a unique specificity for the regulation of staphopains, *Staphylococcus* spp. cysteine proteinases. *Mol Microbiol* *49*, 1051-1066.
- Saleh, T., Cuttino, L., and Gewirtz, D.A. (2016). Autophagy is not uniformly cytoprotective: a personalized medicine approach for autophagy inhibition as a therapeutic strategy in non-small cell lung cancer. *Biochim Biophys Acta* *1860*, 2130-2136.
- Sasaki, T., Kishi, M., Saito, M., Tanaka, T., Higuchi, N., Kominami, E., Katunuma, N., and Murachi, T. (1990). Inhibitory effect of di- and tripeptidyl aldehydes on calpains and cathepsins. *J Enzyme Inhib* *3*, 195-201.
- Sause, W.E., Buckley, P.T., Strohl, W.R., Lynch, A.S., and Torres, V.J. (2016). Antibody-Based Biologics and Their Promise to Combat *Staphylococcus aureus* Infections. *Trends Pharmacol Sci* *37*, 231-241.
- Sax, J.K., Fei, P., Murphy, M.E., Bernhard, E., Korsmeyer, S.J., and El-Deiry, W.S. (2002). BID regulation by p53 contributes to chemosensitivity. *Nat Cell Biol* *4*, 842-849.

- Schindelin, J., Arganda-Carreras, I., Frise, E., Kaynig, V., Longair, M., Pietzsch, T., Preibisch, S., Rueden, C., Saalfeld, S., Schmid, B., *et al.* (2012). Fiji: an open-source platform for biological-image analysis. *Nat Methods* *9*, 676-682.
- Schinzel, A.C., Takeuchi, O., Huang, Z., Fisher, J.K., Zhou, Z., Rubens, J., Hetz, C., Danial, N.N., Moskowicz, M.A., and Korsmeyer, S.J. (2005). Cyclophilin D is a component of mitochondrial permeability transition and mediates neuronal cell death after focal cerebral ischemia. *Proc Natl Acad Sci U S A* *102*, 12005-12010.
- Schmidt, A., Benard, S., and Cyr, S. (2015). Hospital Cost of Staphylococcal Infection after Cardiothoracic or Orthopedic Operations in France: A Retrospective Database Analysis. *Surg Infect (Larchmt)* *16*, 428-435.
- Schnaith, A., Kashkar, H., Leggio, S.A., Addicks, K., Kronke, M., and Krut, O. (2007). Staphylococcus aureus subvert autophagy for induction of caspase-independent host cell death. *J Biol Chem* *282*, 2695-2706.
- Schotte, P., Declercq, W., Van Huffel, S., Vandenaabeele, P., and Beyaert, R. (1999). Non-specific effects of methyl ketone peptide inhibitors of caspases. *FEBS Lett* *442*, 117-121.
- Schwab, B.L., Guerini, D., Didszun, C., Bano, D., Ferrando-May, E., Fava, E., Tam, J., Xu, D., Xanthoudakis, S., Nicholson, D.W., *et al.* (2002). Cleavage of plasma membrane calcium pumps by caspases: a link between apoptosis and necrosis. *Cell Death Differ* *9*, 818-831.
- Senn, L., Basset, P., Nahimana, I., Zanetti, G., and Blanc, D.S. (2012). Which anatomical sites should be sampled for screening of methicillin-resistant Staphylococcus aureus carriage by culture or by rapid PCR test? *Clin Microbiol Infect* *18*, E31-33.
- Shalem, O., Sanjana, N.E., Hartenian, E., Shi, X., Scott, D.A., Mikkelsen, T., Heckl, D., Ebert, B.L., Root, D.E., Doench, J.G., *et al.* (2014). Genome-scale CRISPR-Cas9 knockout screening in human cells. *Science* *343*, 84-87.
- Sharma, K., Le, N., Alotaibi, M., and Gewirtz, D.A. (2014). Cytotoxic autophagy in cancer therapy. *Int J Mol Sci* *15*, 10034-10051.
- Shaw, L., Golonka, E., Potempa, J., and Foster, S.J. (2004). The role and regulation of the extracellular proteases of Staphylococcus aureus. *Microbiology* *150*, 217-228.
- Shen, Z., Jiang, H., Hsu, H.T., Qian, L., Fu, Q., Shen, M., Chen, S., and Yang, T. (2019). MicroRNA-127 inhibits cell proliferation via targeting Kif3b in pancreatic beta cells. *Aging (Albany NY)*.
- Shi, J., Zhao, Y., Wang, K., Shi, X., Wang, Y., Huang, H., Zhuang, Y., Cai, T., Wang, F., and Shao, F. (2015). Cleavage of GSDMD by inflammatory caspases determines pyroptotic cell death. *Nature* *526*, 660-665.
- Shi, J., Zhao, Y., Wang, Y., Gao, W., Ding, J., Li, P., Hu, L., and Shao, F. (2014). Inflammatory caspases are innate immune receptors for intracellular LPS. *Nature* *514*, 187-192.
- Shompole, S., Henon, K.T., Liou, L.E., Dziewanowska, K., Bohach, G.A., and Bayles, K.W. (2003). Biphasic intracellular expression of Staphylococcus aureus virulence factors and evidence for Agr-mediated diffusion sensing. *Mol Microbiol* *49*, 919-927.
- Sieprawska-Lupa, M., Mydel, P., Krawczyk, K., Wojcik, K., Puklo, M., Lupa, B., Suder, P., Silberring, J., Reed, M., Pohl, J., *et al.* (2004). Degradation of human antimicrobial peptide LL-37 by Staphylococcus aureus-derived proteinases. *Antimicrob Agents Chemother* *48*, 4673-4679.

- Silva, M.T. (2010). Secondary necrosis: the natural outcome of the complete apoptotic program. *FEBS Lett* 584, 4491-4499.
- Simenc, J., and Lipnik-Stangelj, M. (2012). Staurosporine induces different cell death forms in cultured rat astrocytes. *Radiol Oncol* 46, 312-320.
- Sinha, B., Francois, P., Que, Y.A., Hussain, M., Heilmann, C., Moreillon, P., Lew, D., Krause, K.H., Peters, G., and Herrmann, M. (2000). Heterologously expressed *Staphylococcus aureus* fibronectin-binding proteins are sufficient for invasion of host cells. *Infect Immun* 68, 6871-6878.
- Smagur, J., Guzik, K., Bzowska, M., Kuzak, M., Zarebski, M., Kantyka, T., Walski, M., Gajkowska, B., and Potempa, J. (2009a). Staphylococcal cysteine protease staphopain B (SspB) induces rapid engulfment of human neutrophils and monocytes by macrophages. *Biol Chem* 390, 361-371.
- Smagur, J., Guzik, K., Magiera, L., Bzowska, M., Gruca, M., Thogersen, I.B., Enghild, J.J., and Potempa, J. (2009b). A new pathway of staphylococcal pathogenesis: apoptosis-like death induced by Staphopain B in human neutrophils and monocytes. *J Innate Immun* 1, 98-108.
- Sollid, J.U., Furberg, A.S., Hanssen, A.M., and Johannessen, M. (2014). *Staphylococcus aureus*: determinants of human carriage. *Infect Genet Evol* 21, 531-541.
- Somerville, G.A., Beres, S.B., Fitzgerald, J.R., DeLeo, F.R., Cole, R.L., Hoff, J.S., and Musser, J.M. (2002). In vitro serial passage of *Staphylococcus aureus*: changes in physiology, virulence factor production, and agr nucleotide sequence. *J Bacteriol* 184, 1430-1437.
- Sonesson, A., Przybyszewska, K., Eriksson, S., Morgelin, M., Kjellstrom, S., Davies, J., Potempa, J., and Schmidtchen, A. (2017). Identification of bacterial biofilm and the *Staphylococcus aureus* derived protease, staphopain, on the skin surface of patients with atopic dermatitis. *Sci Rep* 7, 8689.
- Song, G., Chen, G.G., Yun, J.P., and Lai, P.B. (2009). Association of p53 with Bid induces cell death in response to etoposide treatment in hepatocellular carcinoma. *Curr Cancer Drug Targets* 9, 871-880.
- Song, L., Hobaugh, M.R., Shustak, C., Cheley, S., Bayley, H., and Gouaux, J.E. (1996). Structure of staphylococcal alpha-hemolysin, a heptameric transmembrane pore. *Science* 274, 1859-1866.
- Staali, L., Monteil, H., and Colin, D.A. (1998). The staphylococcal pore-forming leukotoxins open Ca²⁺ channels in the membrane of human polymorphonuclear neutrophils. *J Membr Biol* 162, 209-216.
- Staring, J., von Castelmur, E., Blomen, V.A., van den Hengel, L.G., Brockmann, M., Baggen, J., Thibaut, H.J., Nieuwenhuis, J., Janssen, H., van Kuppeveld, F.J., *et al.* (2017). PLA2G16 represents a switch between entry and clearance of Picornaviridae. *Nature* 541, 412-416.
- Stefani, S., Chung, D.R., Lindsay, J.A., Friedrich, A.W., Kearns, A.M., Westh, H., and Mackenzie, F.M. (2012). Methicillin-resistant *Staphylococcus aureus* (MRSA): global epidemiology and harmonisation of typing methods. *Int J Antimicrob Agents* 39, 273-282.
- Stone, A., and Saiman, L. (2007). Update on the epidemiology and management of *Staphylococcus aureus*, including methicillin-resistant *Staphylococcus aureus*, in patients with cystic fibrosis. *Curr Opin Pulm Med* 13, 515-521.
- Strobel, M., Pfortner, H., Tuchscher, L., Volker, U., Schmidt, F., Kramko, N., Schnittler, H.J., Fraunholz, M.J., Löffler, B., Peters, G., *et al.* (2016). Post-invasion events after infection with *Staphylococcus aureus* are strongly dependent on both the host cell type and the infecting *S. aureus* strain. *Clin Microbiol Infect* 22, 799-809.

- Sun, C., Hobor, S., Bertotti, A., Zecchin, D., Huang, S., Galimi, F., Cottino, F., Prahallad, A., Grenrum, W., Tzani, A., *et al.* (2014). Intrinsic resistance to MEK inhibition in KRAS mutant lung and colon cancer through transcriptional induction of ERBB3. *Cell Rep* 7, 86-93.
- Sun, C.H., Wacquier, B., Aguilar, D.I., Carayol, N., Denis, K., Boucherie, S., Valencia-Gallardo, C., Simsek, C., Erneux, C., Lehman, A., *et al.* (2017). The Shigella type III effector IpgD recodes Ca(2+) signals during invasion of epithelial cells. *EMBO J* 36, 2567-2580.
- Sun, L., Wang, H., Wang, Z., He, S., Chen, S., Liao, D., Wang, L., Yan, J., Liu, W., Lei, X., *et al.* (2012). Mixed lineage kinase domain-like protein mediates necrosis signaling downstream of RIP3 kinase. *Cell* 148, 213-227.
- Surewaard, B.G., de Haas, C.J., Vervoort, F., Rigby, K.M., DeLeo, F.R., Otto, M., van Strijp, J.A., and Nijland, R. (2013). Staphylococcal alpha-phenol soluble modulins contribute to neutrophil lysis after phagocytosis. *Cell Microbiol* 15, 1427-1437.
- Susin, S.A., Lorenzo, H.K., Zamzami, N., Marzo, I., Snow, B.E., Brothers, G.M., Mangion, J., Jacotot, E., Costantini, P., Loeffler, M., *et al.* (1999). Molecular characterization of mitochondrial apoptosis-inducing factor. *Nature* 397, 441-446.
- Suttorp, N., Seeger, W., Dewein, E., Bhakdi, S., and Roka, L. (1985). Staphylococcal alpha-toxin-induced PG12 production in endothelial cells: role of calcium. *Am J Physiol* 248, C127-134.
- Suzuki, J., Kanemaru, K., Ishii, K., Ohkura, M., Okubo, Y., and Iino, M. (2014). Imaging intraorganellar Ca2+ at subcellular resolution using CEPIA. *Nat Commun* 5, 4153.
- Suzuki, K., and Sorimachi, H. (1998). A novel aspect of calpain activation. *FEBS Lett* 433, 1-4.
- Szafranska, A.K., Oxley, A.P., Chaves-Moreno, D., Horst, S.A., Rosslenbroich, S., Peters, G., Goldmann, O., Rohde, M., Sinha, B., Pieper, D.H., *et al.* (2014). High-resolution transcriptomic analysis of the adaptive response of *Staphylococcus aureus* during acute and chronic phases of osteomyelitis. *MBio* 5.
- Szalai, G., Krishnamurthy, R., and Hajnoczky, G. (1999). Apoptosis driven by IP(3)-linked mitochondrial calcium signals. *EMBO J* 18, 6349-6361.
- Szklarczyk, D., Franceschini, A., Wyder, S., Forslund, K., Heller, D., Huerta-Cepas, J., Simonovic, M., Roth, A., Santos, A., Tsafou, K.P., *et al.* (2015). STRING v10: protein-protein interaction networks, integrated over the tree of life. *Nucleic Acids Res* 43, D447-452.
- Tait, S.W., and Green, D.R. (2010). Mitochondria and cell death: outer membrane permeabilization and beyond. *Nat Rev Mol Cell Biol* 11, 621-632.
- Takahashi, M., Tezuka, T., Korant, B., and Katunuma, N. (1999). Inhibition of cysteine protease and growth of *Staphylococcus aureus* V8 and poliovirus by phosphorylated cystatin alpha conjugate of skin. *Biofactors* 10, 339-345.
- Talbot, J.C., Thiaudiere, E., Vincent, M., Gallay, J., Siffert, O., and Dufourcq, J. (2001). Dynamics and orientation of amphipathic peptides in solution and bound to membranes: a steady-state and time-resolved fluorescence study of staphylococcal delta-toxin and its synthetic analogues. *Eur Biophys J* 30, 147-161.
- Tang, D.G., Chen, Y.Q., and Honn, K.V. (1996). Arachidonate lipoxygenases as essential regulators of cell survival and apoptosis. *Proc Natl Acad Sci U S A* 93, 5241-5246.
- Tavares, A., and Duque-Magalhaes, M.C. (1991). Demonstration of three calpains in the matrix of rat liver mitochondria. *Biomed Biochim Acta* 50, 523-529.

- Taylor, C.W., and Machaca, K. (2019). IP3 receptors and store-operated Ca(2+) entry: a license to fill. *Curr Opin Cell Biol* 57, 1-7.
- Taylor, C.W., and Tovey, S.C. (2010). IP(3) receptors: toward understanding their activation. *Cold Spring Harb Perspect Biol* 2, a004010.
- Tesz, G.J., Guilherme, A., Guntur, K.V., Hubbard, A.C., Tang, X., Chawla, A., and Czech, M.P. (2007). Tumor necrosis factor alpha (TNFalpha) stimulates Map4k4 expression through TNFalpha receptor 1 signaling to c-Jun and activating transcription factor 2. *J Biol Chem* 282, 19302-19312.
- Tewari, M., Quan, L.T., O'Rourke, K., Desnoyers, S., Zeng, Z., Beidler, D.R., Poirier, G.G., Salvesen, G.S., and Dixit, V.M. (1995). Yama/ CPP32 beta, a mammalian homolog of CED-3, is a CrmA-inhibitable protease that cleaves the death substrate poly(ADP-ribose) polymerase. *Cell* 81, 801-809.
- Thor, H., Hartzell, P., and Orrenius, S. (1984). Potentiation of oxidative cell injury in hepatocytes which have accumulated Ca2+. *J Biol Chem* 259, 6612-6615.
- Thu, V.T., Kim, H.K., Long le, T., Lee, S.R., Hanh, T.M., Ko, T.H., Heo, H.J., Kim, N., Kim, S.H., Ko, K.S., *et al.* (2012). NecroX-5 prevents hypoxia/reoxygenation injury by inhibiting the mitochondrial calcium uniporter. *Cardiovasc Res* 94, 342-350.
- Thwaites, G.E., and Gant, V. (2011). Are bloodstream leukocytes Trojan Horses for the metastasis of *Staphylococcus aureus*? *Nat Rev Microbiol* 9, 215-222.
- Tomita, T., Watanabe, M., and Yasuda, T. (1992). Influence of membrane fluidity on the assembly of *Staphylococcus aureus* alpha-toxin, a channel-forming protein, in liposome membrane. *J Biol Chem* 267, 13391-13397.
- Tong, S.Y., Davis, J.S., Eichenberger, E., Holland, T.L., and Fowler, V.G., Jr. (2015). *Staphylococcus aureus* infections: epidemiology, pathophysiology, clinical manifestations, and management. *Clin Microbiol Rev* 28, 603-661.
- Traber, K., and Novick, R. (2006). A slipped-mispairing mutation in *AgrA* of laboratory strains and clinical isolates results in delayed activation of *agr* and failure to translate delta- and alpha-haemolysins. *Mol Microbiol* 59, 1519-1530.
- Traber, K.E., Lee, E., Benson, S., Corrigan, R., Cantera, M., Shopsin, B., and Novick, R.P. (2008). *agr* function in clinical *Staphylococcus aureus* isolates. *Microbiology* 154, 2265-2274.
- Tran Van Nhieu, G., Clair, C., Bruzzone, R., Mesnil, M., Sansonetti, P., and Combettes, L. (2003). Connexin-dependent inter-cellular communication increases invasion and dissemination of *Shigella* in epithelial cells. *Nat Cell Biol* 5, 720-726.
- Tran Van Nhieu, G., Kai Liu, B., Zhang, J., Pierre, F., Prigent, S., Sansonetti, P., Erneux, C., Kuk Kim, J., Suh, P.G., Dupont, G., *et al.* (2013). Actin-based confinement of calcium responses during *Shigella* invasion. *Nat Commun* 4, 1567.
- Tranchemontagne, Z.R., Camire, R.B., O'Donnell, V.J., Baugh, J., and Burkholder, K.M. (2016). *Staphylococcus aureus* Strain USA300 Perturbs Acquisition of Lysosomal Enzymes and Requires Phagosomal Acidification for Survival inside Macrophages. *Infect Immun* 84, 241-253.
- Trebak, M., Bird, G.S., McKay, R.R., and Putney, J.W., Jr. (2002). Comparison of human TRPC3 channels in receptor-activated and store-operated modes. Differential sensitivity to channel blockers suggests fundamental differences in channel composition. *J Biol Chem* 277, 21617-21623.

- Tuscherr, L., Bischoff, M., Lattar, S.M., Noto Llana, M., Pfortner, H., Niemann, S., Geraci, J., Van de Vyver, H., Fraunholz, M.J., Cheung, A.L., *et al.* (2015). Sigma Factor SigB Is Crucial to Mediate Staphylococcus aureus Adaptation during Chronic Infections. *PLoS Pathog* *11*, e1004870.
- Tuscherr, L., Medina, E., Hussain, M., Volker, W., Heitmann, V., Niemann, S., Holzinger, D., Roth, J., Proctor, R.A., Becker, K., *et al.* (2011). Staphylococcus aureus phenotype switching: an effective bacterial strategy to escape host immune response and establish a chronic infection. *EMBO Mol Med* *3*, 129-141.
- Tucker, K.A., Reilly, S.S., Leslie, C.S., and Hudson, M.C. (2000). Intracellular Staphylococcus aureus induces apoptosis in mouse osteoblasts. *FEMS Microbiol Lett* *186*, 151-156.
- Udo, E.E., Pearman, J.W., and Grubb, W.B. (1993). Genetic analysis of community isolates of methicillin-resistant Staphylococcus aureus in Western Australia. *J Hosp Infect* *25*, 97-108.
- Uehara, Y., Nakama, H., Agematsu, K., Uchida, M., Kawakami, Y., Abdul Fattah, A.S., and Maruchi, N. (2000). Bacterial interference among nasal inhabitants: eradication of Staphylococcus aureus from nasal cavities by artificial implantation of Corynebacterium sp. *J Hosp Infect* *44*, 127-133.
- Upton, J.W., Kaiser, W.J., and Mocarski, E.S. (2010). Virus inhibition of RIP3-dependent necrosis. *Cell Host Microbe* *7*, 302-313.
- Urrea, H., Dufey, E., Lisbona, F., Rojas-Rivera, D., and Hetz, C. (2013). When ER stress reaches a dead end. *Biochim Biophys Acta* *1833*, 3507-3517.
- Valeva, A., Hellmann, N., Walev, I., Strand, D., Plate, M., Boukhallouk, F., Brack, A., Hanada, K., Decker, H., and Bhakdi, S. (2006). Evidence that clustered phosphocholine head groups serve as sites for binding and assembly of an oligomeric protein pore. *J Biol Chem* *281*, 26014-26021.
- van Belkum, A., Verkaik, N.J., de Vogel, C.P., Boelens, H.A., Verveer, J., Nouwen, J.L., Verbrugh, H.A., and Wertheim, H.F. (2009). Reclassification of Staphylococcus aureus nasal carriage types. *J Infect Dis* *199*, 1820-1826.
- van den Akker, E.L., Nouwen, J.L., Melles, D.C., van Rossum, E.F., Koper, J.W., Uitterlinden, A.G., Hofman, A., Verbrugh, H.A., Pols, H.A., Lamberts, S.W., *et al.* (2006). Staphylococcus aureus nasal carriage is associated with glucocorticoid receptor gene polymorphisms. *J Infect Dis* *194*, 814-818.
- Vanden Berghe, T., Vanlangenakker, N., Parthoens, E., Deckers, W., Devos, M., Festjens, N., Guerin, C.J., Brunk, U.T., Declercq, W., and Vandenabeele, P. (2010). Necroptosis, necrosis and secondary necrosis converge on similar cellular disintegration features. *Cell Death Differ* *17*, 922-930.
- Vandenabeele, P., Galluzzi, L., Vanden Berghe, T., and Kroemer, G. (2010). Molecular mechanisms of necroptosis: an ordered cellular explosion. *Nat Rev Mol Cell Biol* *11*, 700-714.
- Vandenesch, F., Naimi, T., Enright, M.C., Lina, G., Nimmo, G.R., Heffernan, H., Liassine, N., Bes, M., Greenland, T., Reverdy, M.E., *et al.* (2003). Community-acquired methicillin-resistant Staphylococcus aureus carrying Panton-Valentine leukocidin genes: worldwide emergence. *Emerg Infect Dis* *9*, 978-984.
- Vann, J.M., and Proctor, R.A. (1987). Ingestion of Staphylococcus aureus by bovine endothelial cells results in time- and inoculum-dependent damage to endothelial cell monolayers. *Infect Immun* *55*, 2155-2163.
- Ventura, C.L., Malachowa, N., Hammer, C.H., Nardone, G.A., Robinson, M.A., Kobayashi, S.D., and DeLeo, F.R. (2010). Identification of a novel Staphylococcus aureus two-component leukotoxin using cell surface proteomics. *Plos One* *5*, e11634.

- Vesga, O., Groeschel, M.C., Otten, M.F., Brar, D.W., Vann, J.M., and Proctor, R.A. (1996). Staphylococcus aureus small colony variants are induced by the endothelial cell intracellular milieu. *J Infect Dis* 173, 739-742.
- Virag, L., Robaszekiewicz, A., Rodriguez-Vargas, J.M., and Oliver, F.J. (2013). Poly(ADP-ribose) signaling in cell death. *Mol Aspects Med* 34, 1153-1167.
- von Eiff, C., Becker, K., Machka, K., Stammer, H., and Peters, G. (2001). Nasal carriage as a source of Staphylococcus aureus bacteremia. Study Group. *N Engl J Med* 344, 11-16.
- von Hoven, G., Rivas, A.J., Neukirch, C., Klein, S., Hamm, C., Qin, Q., Meyenburg, M., Fuser, S., Saftig, P., Hellmann, N., *et al.* (2016). Dissecting the role of ADAM10 as a mediator of Staphylococcus aureus alpha-toxin action. *Biochem J* 473, 1929-1940.
- von Karstedt, S., Montinaro, A., and Walczak, H. (2017). Exploring the TRAILs less travelled: TRAIL in cancer biology and therapy. *Nat Rev Cancer* 17, 352-366.
- Voyich, J.M., Braughton, K.R., Sturdevant, D.E., Whitney, A.R., Said-Salim, B., Porcella, S.F., Long, R.D., Dorward, D.W., Gardner, D.J., Kreiswirth, B.N., *et al.* (2005). Insights into mechanisms used by Staphylococcus aureus to avoid destruction by human neutrophils. *J Immunol* 175, 3907-3919.
- Vuononvirta, J., Toivonen, L., Grondahl-Yli-Hannuksela, K., Barkoff, A.M., Lindholm, L., Mertsola, J., Peltola, V., and He, Q. (2011). Nasopharyngeal bacterial colonization and gene polymorphisms of mannose-binding lectin and toll-like receptors 2 and 4 in infants. *Plos One* 6, e26198.
- Wajant, H. (2002). The Fas signaling pathway: more than a paradigm. *Science* 296, 1635-1636.
- Wang, R., Braughton, K.R., Kretschmer, D., Bach, T.H., Queck, S.Y., Li, M., Kennedy, A.D., Dorward, D.W., Klebanoff, S.J., Peschel, A., *et al.* (2007). Identification of novel cytolytic peptides as key virulence determinants for community-associated MRSA. *Nat Med* 13, 1510-1514.
- Wang, T., Wei, J.J., Sabatini, D.M., and Lander, E.S. (2014). Genetic screens in human cells using the CRISPR-Cas9 system. *Science* 343, 80-84.
- Wang, Y., An, R., Umanah, G.K., Park, H., Nambiar, K., Eacker, S.M., Kim, B., Bao, L., Harraz, M.M., Chang, C., *et al.* (2016). A nuclease that mediates cell death induced by DNA damage and poly(ADP-ribose) polymerase-1. *Science* 354.
- Wang, Y., Kim, N.S., Haince, J.F., Kang, H.C., David, K.K., Andrabi, S.A., Poirier, G.G., Dawson, V.L., and Dawson, T.M. (2011). Poly(ADP-ribose) (PAR) binding to apoptosis-inducing factor is critical for PAR polymerase-1-dependent cell death (parthanatos). *Sci Signal* 4, ra20.
- Watanabe, M., Tomita, T., and Yasuda, T. (1987). Membrane-damaging action of staphylococcal alpha-toxin on phospholipid-cholesterol liposomes. *Biochim Biophys Acta* 898, 257-265.
- Waterhouse, N.J., Finucane, D.M., Green, D.R., Elce, J.S., Kumar, S., Alnemri, E.S., Litwack, G., Khanna, K., Lavin, M.F., and Watters, D.J. (1998). Calpain activation is upstream of caspases in radiation-induced apoptosis. *Cell Death Differ* 5, 1051-1061.
- Weglarczyk, K., Baran, J., Zembala, M., and Pryjma, J. (2004). Caspase-8 activation precedes alterations of mitochondrial membrane potential during monocyte apoptosis induced by phagocytosis and killing of Staphylococcus aureus. *Infect Immun* 72, 2590-2597.
- Wei, M.C., Lindsten, T., Mootha, V.K., Weiler, S., Gross, A., Ashiya, M., Thompson, C.B., and Korsmeyer, S.J. (2000). tBID, a membrane-targeted death ligand, oligomerizes BAK to release cytochrome c. *Genes Dev* 14, 2060-2071.

- Weigel, L.M., Clewell, D.B., Gill, S.R., Clark, N.C., McDougal, L.K., Flannagan, S.E., Kolonay, J.F., Shetty, J., Killgore, G.E., and Tenover, F.C. (2003). Genetic analysis of a high-level vancomycin-resistant isolate of *Staphylococcus aureus*. *Science* *302*, 1569-1571.
- Weinrick, B., Dunman, P.M., McAleese, F., Murphy, E., Projan, S.J., Fang, Y., and Novick, R.P. (2004). Effect of mild acid on gene expression in *Staphylococcus aureus*. *J Bacteriol* *186*, 8407-8423.
- Wertheim, H.F., Vos, M.C., Ott, A., van Belkum, A., Voss, A., Kluytmans, J.A., van Keulen, P.H., Vandenbroucke-Grauls, C.M., Meester, M.H., and Verbrugh, H.A. (2004). Risk and outcome of nosocomial *Staphylococcus aureus* bacteraemia in nasal carriers versus non-carriers. *Lancet* *364*, 703-705.
- Wesson, C.A., Deringer, J., Liou, L.E., Bayles, K.W., Bohach, G.A., and Trumble, W.R. (2000). Apoptosis induced by *Staphylococcus aureus* in epithelial cells utilizes a mechanism involving caspases 8 and 3. *Infect Immun* *68*, 2998-3001.
- Wijdeven, R.H., Pang, B., van der Zanden, S.Y., Qiao, X., Blomen, V., Hoogstraat, M., Lips, E.H., Janssen, L., Wessels, L., Brummelkamp, T.R., *et al.* (2015). Genome-Wide Identification and Characterization of Novel Factors Conferring Resistance to Topoisomerase II Poisons in Cancer. *Cancer Res* *75*, 4176-4187.
- Wilke, G.A., and Bubeck Wardenburg, J. (2010). Role of a disintegrin and metalloprotease 10 in *Staphylococcus aureus* alpha-hemolysin-mediated cellular injury. *Proc Natl Acad Sci U S A* *107*, 13473-13478.
- Williams, R.E. (1963). Healthy carriage of *Staphylococcus aureus*: its prevalence and importance. *Bacteriol Rev* *27*, 56-71.
- Wingrave, J.M., Schaecher, K.E., Sribnick, E.A., Wilford, G.G., Ray, S.K., Hazen-Martin, D.J., Hogan, E.L., and Banik, N.L. (2003). Early induction of secondary injury factors causing activation of calpain and mitochondria-mediated neuronal apoptosis following spinal cord injury in rats. *J Neurosci Res* *73*, 95-104.
- Winkler, A.C. (2015). Identification of human host cell factors involved in *Staphylococcus aureus* 6850 infection (Dissertation, University Würzburg).
- Winkler, K.C., de Waart, J., and Grooten, C. (1965). Lysogenic conversion of staphylococci to loss of beta-toxin. *J Gen Microbiol* *39*, 321-333.
- Winnepenninckx, B., Debacker, K., Ramsay, J., Smeets, D., Smits, A., FitzPatrick, D.R., and Kooy, R.F. (2007). CGG-repeat expansion in the DIP2B gene is associated with the fragile site FRA12A on chromosome 12q13.1. *Am J Hum Genet* *80*, 221-231.
- Winstel, V., Missiakas, D., and Schneewind, O. (2018). *Staphylococcus aureus* targets the purine salvage pathway to kill phagocytes. *Proc Natl Acad Sci U S A* *115*, 6846-6851.
- Winter, G.E., Radic, B., Mayor-Ruiz, C., Blomen, V.A., Trefzer, C., Kandasamy, R.K., Huber, K.V.M., Gridling, M., Chen, D., Klampfl, T., *et al.* (2014). The solute carrier SLC35F2 enables YM155-mediated DNA damage toxicity. *Nat Chem Biol* *10*, 768-773.
- Wolf, B.B., Goldstein, J.C., Stennicke, H.R., Beere, H., Amarante-Mendes, G.P., Salvesen, G.S., and Green, D.R. (1999). Calpain functions in a caspase-independent manner to promote apoptosis-like events during platelet activation. *Blood* *94*, 1683-1692.
- Wood, D.E., Thomas, A., Devi, L.A., Berman, Y., Beavis, R.C., Reed, J.C., and Newcomb, E.W. (1998). Bax cleavage is mediated by calpain during drug-induced apoptosis. *Oncogene* *17*, 1069-1078.

- Woodin, A.M., and Wieneke, A.A. (1963). The accumulation of calcium by the polymorphonuclear leucocyte treated with staphylococcal leucocidin and its significance in the extrusion of protein. *Biochem J* *87*, 487-495.
- Wu, J., Li, Q., Li, Y., Lin, J., Yang, D., Zhu, G., Wang, L., He, D., Lu, G., and Zeng, C. (2014a). A long type of TBCK is a novel cytoplasmic and mitotic apparatus-associated protein likely suppressing cell proliferation. *J Genet Genomics* *41*, 69-72.
- Wu, J., Prole, D.L., Shen, Y., Lin, Z., Gnanasekaran, A., Liu, Y., Chen, L., Zhou, H., Chen, S.R., Usachev, Y.M., *et al.* (2014b). Red fluorescent genetically encoded Ca²⁺ indicators for use in mitochondria and endoplasmic reticulum. *Biochem J* *464*, 13-22.
- Xia, G., Kohler, T., and Peschel, A. (2010). The wall teichoic acid and lipoteichoic acid polymers of *Staphylococcus aureus*. *Int J Med Microbiol* *300*, 148-154.
- Xu, S.Z., Zeng, F., Boulay, G., Grimm, C., Harteneck, C., and Beech, D.J. (2005). Block of TRPC5 channels by 2-aminoethoxydiphenyl borate: a differential, extracellular and voltage-dependent effect. *Br J Pharmacol* *145*, 405-414.
- Yamashita, K., Kawai, Y., Tanaka, Y., Hirano, N., Kaneko, J., Tomita, N., Ohta, M., Kamio, Y., Yao, M., and Tanaka, I. (2011). Crystal structure of the octameric pore of staphylococcal gamma-hemolysin reveals the beta-barrel pore formation mechanism by two components. *Proc Natl Acad Sci U S A* *108*, 17314-17319.
- Yamazaki, H., Nakata, T., Okada, Y., and Hirokawa, N. (1995). KIF3A/B: a heterodimeric kinesin superfamily protein that works as a microtubule plus end-directed motor for membrane organelle transport. *J Cell Biol* *130*, 1387-1399.
- Yanai, M., Rocha, M.A., Matolek, A.Z., Chintalacheruvu, A., Taira, Y., Chintalacheruvu, K., and Beenhouwer, D.O. (2014). Separately or combined, LukG/LukH is functionally unique compared to other staphylococcal bicomponent leukotoxins. *Plos One* *9*, e89308.
- Yao, Z., Zhou, G., Wang, X.S., Brown, A., Diener, K., Gan, H., and Tan, T.H. (1999). A novel human STE20-related protein kinase, HGK, that specifically activates the c-Jun N-terminal kinase signaling pathway. *J Biol Chem* *274*, 2118-2125.
- Yasuhara, N., Sahara, S., Kamada, S., Eguchi, Y., and Tsujimoto, Y. (1997). Evidence against a functional site for Bcl-2 downstream of caspase cascade in preventing apoptosis. *Oncogene* *15*, 1921-1928.
- Yoong, P., and Torres, V.J. (2013). The effects of *Staphylococcus aureus* leukotoxins on the host: cell lysis and beyond. *Curr Opin Microbiol* *16*, 63-69.
- Young, A.B., Cooley, I.D., Chauhan, V.S., and Marriott, I. (2011). Causative agents of osteomyelitis induce death domain-containing TNF-related apoptosis-inducing ligand receptor expression on osteoblasts. *Bone* *48*, 857-863.
- Yousefi, S., Perozzo, R., Schmid, I., Ziemiecki, A., Schaffner, T., Scapozza, L., Brunner, T., and Simon, H.U. (2006). Calpain-mediated cleavage of Atg5 switches autophagy to apoptosis. *Nat Cell Biol* *8*, 1124-1132.
- Yu, S.W., Andrabi, S.A., Wang, H., Kim, N.S., Poirier, G.G., Dawson, T.M., and Dawson, V.L. (2006). Apoptosis-inducing factor mediates poly(ADP-ribose) (PAR) polymer-induced cell death. *Proc Natl Acad Sci U S A* *103*, 18314-18319.

- Zautner, A.E., Krause, M., Stropahl, G., Holtfreter, S., Frickmann, H., Maletzki, C., Kreikemeyer, B., Pau, H.W., and Podbielski, A. (2010). Intracellular persisting *Staphylococcus aureus* is the major pathogen in recurrent tonsillitis. *Plos One* 5, e9452.
- Zhang, J., Yang, Y., He, W., and Sun, L. (2016). Necrosome core machinery: MLKL. *Cell Mol Life Sci* 73, 2153-2163.
- Zhang, S.L., Yu, Y., Roos, J., Kozak, J.A., Deerinck, T.J., Ellisman, M.H., Stauderman, K.A., and Cahalan, M.D. (2005). STIM1 is a Ca²⁺ sensor that activates CRAC channels and migrates from the Ca²⁺ store to the plasma membrane. *Nature* 437, 902-905.
- Zhang, Z., Larner, S.F., Liu, M.C., Zheng, W., Hayes, R.L., and Wang, K.K. (2009). Multiple alphaII-spectrin breakdown products distinguish calpain and caspase dominated necrotic and apoptotic cell death pathways. *Apoptosis* 14, 1289-1298.
- Zhivotovsky, B., and Orrenius, S. (2011). Calcium and cell death mechanisms: a perspective from the cell death community. *Cell Calcium* 50, 211-221.
- Zhuo, Y., Solntsev, K.M., Reddish, F., Tang, S., and Yang, J.J. (2015). Effect of Ca(2)(+) on the steady-state and time-resolved emission properties of the genetically encoded fluorescent sensor CatchER. *J Phys Chem B* 119, 2103-2111.
- Zielinska, A.K., Beenken, K.E., Joo, H.S., Mrak, L.N., Griffin, L.M., Luong, T.T., Lee, C.Y., Otto, M., Shaw, L.N., and Smeltzer, M.S. (2011). Defining the strain-dependent impact of the *Staphylococcal* accessory regulator (*sarA*) on the alpha-toxin phenotype of *Staphylococcus aureus*. *J Bacteriol* 193, 2948-2958.
- Ziesemer, S., Moller, N., Nitsch, A., Muller, C., Beule, A.G., and Hildebrandt, J.P. (2019). Sphingomyelin Depletion from Plasma Membranes of Human Airway Epithelial Cells Completely Abrogates the Deleterious Actions of *S. aureus* Alpha-Toxin. *Toxins (Basel)* 11.
- Zihni, C., Mitsopoulos, C., Tavares, I.A., Baum, B., Ridley, A.J., and Morris, J.D. (2007). Prostate-derived sterile 20-like kinase 1-alpha induces apoptosis. JNK- and caspase-dependent nuclear localization is a requirement for membrane blebbing. *J Biol Chem* 282, 6484-6493.
- Zipperer, A., Konnerth, M.C., Laux, C., Berscheid, A., Janek, D., Weidenmaier, C., Burian, M., Schilling, N.A., Slavetinsky, C., Marschal, M., *et al.* (2016). Human commensals producing a novel antibiotic impair pathogen colonization. *Nature* 535, 511-516.
- Zong, W.X., Li, C., Hatzivassiliou, G., Lindsten, T., Yu, Q.C., Yuan, J., and Thompson, C.B. (2003). Bax and Bak can localize to the endoplasmic reticulum to initiate apoptosis. *J Cell Biol* 162, 59-69.

6 Appendix

6.1 Electronical supplement

Videos and Table 6.1 are available in the electronical supplement attached to this thesis. The respective video and table captions are found below.

Video 1: Phagosomal escape of *S. aureus* in epithelial cells.

HeLa YFP-cwt cells were infected with *S. aureus* 6850 mRFP and live cell imaging was performed to visualize translocation of intracellular bacteria from the phagosome into the cytosol of the host cell (yellow: YFP-cwt, red: *S. aureus*, gray: BF).

Video 2: Phagosomal escape of *S. aureus* upon inhibition of caspases.

Pre-treatment of HeLa YFP-cwt cells with 80 μ M Z-VAD-fmk or DMSO as solvent control and subsequent infection with *S. aureus* 6850 mRFP was performed to visualize phagosomal escape of *S. aureus* by live cell imaging (yellow: YFP-cwt, red: *S. aureus*, gray: BF).

Video 3: Activation of effector caspases by intracellular *S. aureus*.

HeLa cells were infected with *S. aureus* 6850 mRFP after pre-treatment of cells with 80 μ M Z-VAD-fmk or DMSO. CellEvent™ Caspase 3/7 detection reagent was added prior to live cell imaging (green: CellEvent, red: *S. aureus*, gray: BF).

Video 4: Visualization of host cell plasma membrane permeabilization induced by intracellular *S. aureus*.

HeLa cells were infected with *S. aureus* 6850 GFP and Alexa Fluor 633 hydrazide (AF633) was added prior to live cell imaging (magenta: AF633, green: *S. aureus*, gray: BF).

Video 5: *S. aureus* increases cellular H₂O₂ concentration during intracellular infection.

HeLa HyPer-3 cells were infected with *S. aureus* 6850 mRFP and live cell imaging was performed to measure the relative amount of intracellular H₂O₂ during infection (red: *S. aureus*, green: HyPer-3 (ratio ex. 496/405 nm), gray: BF).

Video 6: Intracellular *S. aureus* induces a rise in cytosolic Ca²⁺.

HeLa R-Geco cells were infected with *S. aureus* 6850 GFP and live cell imaging was performed to visualize cytosolic Ca²⁺ concentrations during infection (green: *S. aureus*, red: R-Geco, gray: BF).

Video 7: *S. aureus*-induced cytosolic Ca²⁺ overload is followed by a mitochondrial Ca²⁺ rise.

HeLa Mito-LAR-Geco G-Geco cells were infected with *S. aureus* 6850 Cerulean and live cell imaging was performed to visualize cytosolic and mitochondrial Ca²⁺ concentrations during infection (cyan: *S. aureus*, green: G-Geco, red: Mito-LAR-Geco, gray: BF).

Video 8: Cytosolic and ER Ca²⁺ concentration during *S. aureus* infection.

HeLa ER-LAR-Geco G-Geco cells were infected with *S. aureus* 6850 Cerulean and live cell imaging was performed to visualize cytosolic and ER Ca²⁺ concentrations during infection (cyan: *S. aureus*, green: G-Geco, red: ER-LAR-Geco, gray: BF).

Video 9: The cytosolic Ca²⁺ rise induced by intracellular *S. aureus* is not affected by 2-APB treatment.

HeLa R-Geco cells were infected with *S. aureus* 6850 GFP and during live cell imaging 30 μ M 2-APB or DMSO were added. Cytosolic Ca²⁺ concentrations were recorded over the time course of infection (green: *S. aureus*, red: R-Geco, gray: BF).

Video 10: Visualization of *S. aureus*-induced cytosolic Ca²⁺ overload in Ca²⁺ depleted medium.

HeLa R-Geco cells were infected with *S. aureus* 6850 GFP and prior to live cell imaging medium was replaced by DMEM with 1.8 mM CaCl₂, DMEM without CaCl₂ or DMEM without CaCl₂ and 0.2 mM BAPTA. Cytosolic Ca²⁺ concentrations were recorded over the time course of infection (green: *S. aureus*, red: R-Geco, gray: BF).

Video 11: Visualization of *S. aureus*-induced cytosolic Ca²⁺ overload in Ca²⁺ depleted medium.

HeLa R-Geco cells were infected with *S. aureus* 6850 GFP and prior to live cell imaging 5 μ M BAPTA-AM or DMSO were added. Cytosolic Ca²⁺ concentrations were recorded over the time course of infection (green: *S. aureus*, red: R-Geco, gray: BF).

Video 12: Cytosolic Ca²⁺ overload precedes activation of effector caspases in *S. aureus*-infected cells.

HeLa R-Geco cells were infected with *S. aureus* 6850 Cerulean or Cowan I Cerulean and CellEvent™ Caspase 3/7 detection reagent was added prior to live cell imaging (green: CellEvent, red: R-Geco, cyan: *S. aureus*, gray: BF).

Video 13: *S. aureus*-induced cytosolic Ca²⁺ rise upon inhibition of caspases.

Pre-treatment of HeLa G-Geco cells with 80 μM Z-VAD-fmk or DMSO as solvent control and subsequent infection with *S. aureus* 6850 mRFP was performed to visualize cytosolic Ca²⁺ concentrations by live cell imaging (green: G-Geco, red: *S. aureus*, gray: BF).

Video 14: *S. aureus*-induced cytosolic Ca²⁺ overload is followed by plasma membrane permeabilization.

HeLa R-Geco cells were infected with *S. aureus* 6850 GFP and Alexa Fluor 633 hydrazide (AF633) was added prior to live cell imaging (red: R-Geco, magenta: AF633, green: *S. aureus*, gray: BF).

Video 15: Cytosolic Ca²⁺ signaling upon apoptosis-inducing agents.

HeLa R-Geco cells remained untreated, were treated with 5 μg/ml CHX and 5 ng/ml TNFα, 50 μg/ml blasticidin or 10 μM staurosporine (STS) or infected with *S. aureus* GFP. Live cell imaging was performed to monitor cytoplasmic Ca²⁺ concentrations (red: R-Geco, green: *S. aureus*, gray: BF).

Video 16: Activation of effector caspases by intracellular *S. aureus* in calpain 4 knock-out cells.

HAP1 wild type cells (WT) or calpain 4 knock-out clone 10 (CAPN4 KO cl.10) were infected with *S. aureus* 6850 mRFP and CellEvent™ Caspase 3/7 detection reagent was added prior to live cell imaging (green: CellEvent, red: *S. aureus*, gray: BF).

Video 17: *S. aureus* secreted factors induce cytosolic Ca²⁺ signaling and overload.

HeLa R-Geco were treated with 10 % sterile supernatant from a *S. aureus* 6850 overnight culture. Live cell imaging was performed to monitor cytoplasmic Ca²⁺ fluxes (red: R-Geco, gray: BF).

Video 18: α-toxin and *rsp* do not affect *S. aureus*-induced cytosolic Ca²⁺ rise.

HeLa R-Geco cells were infected with *S. aureus* 6850 GFP, 6850 Δ*hla* GFP or 6850 Δ*rsp* GFP and live cell imaging was performed to visualize cytosolic Ca²⁺ concentrations during infection (green: *S. aureus*, red: R-Geco, gray: BF).

Video 19: Phagosomal escape of *S. aureus* JE2 and JE2 *scpA*.

HeLa YFP-cwt cells were infected with *S. aureus* JE2 mRFP or JE2 *scpA* mRFP and live cell imaging was performed to visualize translocation of intracellular bacteria from the phagosome into the cytosol of the host cell (yellow: YFP-cwt, red: *S. aureus*, gray: BF) (Stelzner et al. (2019) submitted).

Video 20: Intracellular replication of *S. aureus* JE2 and JE2 *scpA*.

HeLa cells were infected with *S. aureus* JE2 GFP or JE2 *scpA* GFP and live cell imaging was performed to visualize intracellular replication (green: *S. aureus*, gray: BF) (Stelzner et al. (2019) submitted).

Video 21: Staphopain A does not interfere with *S. aureus*-induced cytosolic Ca²⁺ rise.

HeLa R-Geco cells were infected with *S. aureus* JE2 GFP or JE2 *scpA* GFP and cytosolic Ca²⁺ concentrations were measured during infection by time-lapse imaging (green: *S. aureus*, red: R-Geco, gray: BF).

Video 22: Loss of function of staphopain A does not prevent activation of effector caspases by intracellular *S. aureus*.

HeLa cells were infected with *S. aureus* JE2 mRFP or JE2 *scpA* mRFP and CellEvent™ Caspase 3/7 detection reagent was added prior to live cell imaging (green: CellEvent, red: *S. aureus*, gray: BF).

Video 23: Phagosomal escape of *S. aureus* RN4220 *phld-scpAB* and RN4220 *phld-scpA*(C238A)B.

HeLa YFP-cwt cells were infected with *S. aureus* RN4220 *phld-scpAB* or RN4220 *phld-scpA*(C238A)B after AHT treatment (200 ng/ml) and live cell imaging was performed to visualize translocation of intracellular bacteria from the phagosome into the cytosol of the host cell (yellow: YFP-cwt, cyan: *S. aureus*, gray: BF) (Stelzner et al. (2019) submitted).

Video 24: Ca²⁺ signaling and activation of effector caspase in *S. aureus* RN4220 *phld-scpAB*-infected cells.

HeLa R-Geco cells were infected with *S. aureus* RN4220 *phld-scpAB* after AHT treatment (200 ng/ml) and CellEvent™ Caspase 3/7 detection reagent was added prior to live cell imaging. Cytoplasmic Ca²⁺ concentrations and activation of effector caspases were monitored over the time course of infection (red: R-Geco, green: CellEvent, cyan: *S. aureus*, gray: BF) (Stelzner et al. (2019) submitted).

Table 6.1: HAP1 screen sequencing data table

6.2 Abbreviations

A	ampere	et al.	et alii (and others)
AF633	Alexa fluor 633	EtOH	ethanol
AFU	arbitrary fluorescence units	FBS	fetal bovine serum
Agr	accessory gene regulator	FSC	forward scatter
AHT	anhydrotetracycline	fwd	forward
AIF	apoptosis inducing factor	g	gram
Amp/Amp ^R	ampicillin/ampicillin resistance	GFP	green fluorescent protein
APC	Allophycocyanin	h	hour
ATP	adenosine triphosphate	H	height
AU	arbitrary units	HA	hospital acquired
BF	brightfield	HRP	horseradish peroxidase
Bid	BH3 interacting-domain death agonist	H ₂ O ₂	hydrogen peroxide
bp	base pairs	IMDM	Iscove's Modified Dulbecco's Media
BSA	bovine serum albumin	i.e.	id est (that is)
c	centi (10 ⁻²)	k	kilo (10 ³)
CA	community acquired	kb	kilo bases
Ca ²⁺	calcium ion	KCl	potassium chloride
CaCl ₂	calcium chloride	KO	knock-out
cDNA	complementary DNA	l	Liter
CFU	colony forming unit	LB	Luria Bertani
CHX	cycloheximide	LDH	lactate dehydrogenase
Cm/Cm ^R	chloramphenicol/ chloramphenicol resistance	m	meter, milli (10 ⁻³)
CO ₂	carbon dioxide	M	Molar
cwt	cell wall targeting	μ	Micro (10 ⁻⁶)
°C	degree Celsius	MEM	minimal essential medium
Da	dalton	MFI	mean fluorescence intensity
dH ₂ O	distilled water	MgCl ₂	magnesium chloride
DMEM	Dulbecco's Modified Eagle's Medium	min	minute
DMSO	dimethyl sulfoxide	MOI	multiplicity of infection
DNA	deoxyribonucleic acid	MOMP	mitochondrial outer membrane permeabilization
DNase	deoxyribonuclease	MPT	mitochondrial permeability transition
dNTPs	deoxyribonucleoside-triphosphate	mRFP	monomeric red fluorescent protein
DPBS	Dulbecco's phosphate buffered saline	mRNA	messenger RNA
ECL	enhanced chemiluminescence	MRSA	methicillin-resistant <i>S. aureus</i>
<i>E. coli</i>	<i>Escherichia coli</i>	n	nano (10 ⁻⁹)
EDTA	ethylenediaminetetraacetate	NA	numerical aperture
EGTA	triethylene glycol diamine tetraacetic acid	NaCl	sodium chloride
e.g.	exempli gratia (for example)	ncRNA	non-coding RNA
ER	endoplasmic reticulum	n.i.	not infected
Erm/Erm ^R	erythromycin/erythromycin resistance	ns	not significant
		OD	optical density
		ONC	Overnight culture
		<i>P</i>	probability value

PAGE	polyacrylamide gel electrophoresis
PC	phase contrast
PCR	Polymerase Chain Reaction
PEI	polyethyleneimine
pH	pH value
p.i.	post infection
p.t.	post treatment
PVDF	polyvinylidene difluoride
rev	reverse
RFU	relative fluorescence units
Rif/Rif ^R	rifampicin/rifampicin resistance
RNA	ribonucleic acid
RNase	ribonuclease
ROI	region of interest
rpm	rounds per minute
RPMI	Roswell park memorial institute
RT	room temperature; reverse transcription
<i>S. aureus</i>	<i>Staphylococcus aureus</i>
ScpA	Staphopain A
SD	standard deviation
SDS	sodium dodecyl sulfate
sec	second
sgRNA	single guide RNA
shRNA	small hairpin RNA
siRNA	small interfering RNA
SNT	supernatant
SOC	super optimal broth
SOCE	store-operated channel entry
SSC	side scatter
SspB	Staphopain B
STS	staurosporine
TAE	tris-acetate-EDTA
TCA	trichloroacetic acid
TEMED	tetramethylethylenediamine
T _m	melting temperature
Tris	tris(hydroxymethyl)amino-methane
U	unit
UV	ultraviolet
V	volt; volume
v/v	volume per volume
W	width
wt	wild type
w/v	weight per volume
YFP	yellow fluorescent protein

6.3 List of Figures

Figure 1.1: Microscopic and macroscopic characteristics of <i>S. aureus</i>	9
Figure 1.2: Overview of <i>S. aureus</i> major virulence factors.....	13
Figure 1.3: <i>S. aureus</i> extracellular protease genes and proteolytic activation.....	16
Figure 1.4: The intracellular lifestyle of <i>S. aureus</i>	18
Figure 1.5: Major pathways of regulated cell death in mammalian cells.....	22
Figure 1.6: Calcium signaling in non-excitable cells.....	28
Figure 1.7: The role of Ca ²⁺ signaling in cell survival and death upon cell damage.....	30
Figure 1.8: Genetic screens with human haploid cells.....	32
Figure 3.1: Intracellular lifestyle of <i>S. aureus</i> in epithelial cells.....	60
Figure 3.2: Kinetics of intracellular cytotoxicity of <i>S. aureus</i>	61
Figure 3.3: <i>S. aureus</i> intracellular lifestyle in HAP1 and HeLa cells.....	63
Figure 3.4: Timing of <i>S. aureus</i> 6850 induced cell death in HAP1 cells.....	64
Figure 3.5: Optimization of screening conditions.....	65
Figure 3.6: Simplified illustration of the experimental setup for the haploid genetic screen.....	68
Figure 3.7: Protein-protein interaction analysis of significantly enriched genes in the haploid genetic screen using STRING.....	71
Figure 3.8: Inhibition of caspases reduces <i>S. aureus</i> induced host cell death.....	72
Figure 3.9: Invasion, phagosomal escape and replication of <i>S. aureus</i> 6850 upon caspase inhibition.....	73
Figure 3.10: Caspase activation by intracellular <i>S. aureus</i>	75
Figure 3.11: Effector caspase activation in <i>S. aureus</i> infected cells cannot be inhibited with Z-VAD-fmk.....	76
Figure 3.12: Nuclear fragmentation in <i>S. aureus</i> 6850 infected cells.....	77
Figure 3.13: Immunoblot analyses of apoptosis-related proteins during infection with <i>S. aureus</i>	78
Figure 3.14: Immunoblot analyses of AIF truncation during HeLa infection with <i>S. aureus</i>	78
Figure 3.15: Cytotoxic <i>S. aureus</i> induces host cell lysis.....	79
Figure 3.16: Intracellular <i>S. aureus</i> induces production of reactive oxygen species.....	80
Figure 3.17: Infection with <i>S. aureus</i> leads to a massive cytosolic Ca ²⁺ increase in epithelial cells.....	82
Figure 3.18: The <i>S. aureus</i> triggered cytosolic Ca ²⁺ increase in epithelial cells leads to a rise of mitochondrial Ca ²⁺ concentration.....	83
Figure 3.19: Intracellular <i>S. aureus</i> modulates ER Ca ²⁺ concentration.....	84
Figure 3.20: Validation of the Ca ²⁺ indicator cell lines.....	85
Figure 3.21: 2-APB reduces <i>S. aureus</i> induced cytotoxicity, but also attenuates bacterial replication.....	86
Figure 3.22: 2-APB treatment does not abolish <i>S. aureus</i> induced cytosolic Ca ²⁺ increase.....	88
Figure 3.23: Removal of extracellular Ca ²⁺ during <i>S. aureus</i> intracellular infection in epithelial cells.....	89
Figure 3.24: Chelation of intracellular Ca ²⁺ during <i>S. aureus</i> infection of epithelial cells.....	90
Figure 3.25: Activation of effector caspase follows cytosolic Ca ²⁺ increase in <i>S. aureus</i> infected cells.....	92

Figure 3.26: Z-VAD-fmk treatment does not prevent cytosolic Ca ²⁺ overload in <i>S. aureus</i> infected cells.....	93
Figure 3.27: The cytosolic Ca ²⁺ increase in <i>S. aureus</i> infected cells is followed by cell lysis.....	94
Figure 3.28: Ca ²⁺ signaling in different types of cell death.....	95
Figure 3.29: Calpain activation in <i>S. aureus</i> infected cells.....	97
Figure 3.30: Calpain inhibitors attenuate <i>S. aureus</i> growth.....	98
Figure 3.31: Knock-down of calpains 1, 2 or 4 has no significant effect on <i>S. aureus</i> intracellular lifestyle.....	99
Figure 3.32: Knock-out of calpain 1 or 4 in HAP1 cells has no impact on <i>S. aureus</i> -induced cytotoxicity.....	100
Figure 3.33: Effector caspase activation in <i>S. aureus</i> infected Calpain 4 knock-out cells.....	101
Figure 3.34: Effects of <i>S. aureus</i> secreted factors on cellular Ca ²⁺ signaling.....	102
Figure 3.35: Ca ²⁺ signaling and cytotoxicity in epithelial cells infected with <i>S. aureus</i> 6850 Δhla or 6850 Δrsp	103
Figure 3.36: Cytotoxicity of different <i>S. aureus</i> mutants in epithelial cells.....	104
Figure 3.37: Inactivation or inhibition of staphopain A leads to less cell death induced by intracellular <i>S. aureus</i>	105
Figure 3.38: Complementation with <i>scpAB</i> , but not with <i>pscpA</i> _(C238) B, restores the cytotoxicity of the staphopain A mutant.....	106
Figure 3.39: Loss of staphopain A function has no effect on <i>S. aureus</i> invasion or phagosomal escape, but leads to prolonged intracellular replication.....	108
Figure 3.40: <i>S. aureus</i> JE2 <i>scpA</i> triggers cytosolic Ca ²⁺ overload in epithelial cells.....	109
Figure 3.41: <i>S. aureus</i> JE2 <i>scpA</i> triggers activation of effector caspases.....	110
Figure 3.42: Ectopic expression of staphopain A in a non-cytotoxic <i>S. aureus</i> strain leads to host cell death.....	111
Figure 3.43: Staphopain A leads to cell death after phagosomal escape.....	113
Figure 3.44: Staphopain A-induced cell death shows features of apoptosis.....	114
Figure 3.45: Staphopain A promotes <i>S. aureus</i> colonization of the lung.....	115
Figure 4.1: Activation of p38 during <i>S. aureus</i> infection is dependent on TAOK1.....	120
Figure 4.2: The role of TAOK1, TBCK, PAWR and TANC2 in <i>S. aureus</i> cytotoxicity.....	121
Figure 4.3: Potential mechanisms of <i>S. aureus</i> induced host cell death.....	140

6.4 List of Tables

Table 2.1: Laboratory instruments used in this study.....	34
Table 2.2: Consumables and glassware used in this study.....	35
Table 2.3: Chemicals and enzymes used in this study	36
Table 2.4: Kits used in this study	39
Table 2.5: Composition of bacterial media	39
Table 2.6: Used antibiotics.....	40
Table 2.7: Composition of cell culture media and solutions.....	40
Table 2.8: Buffers and solutions used in this study.....	41
Table 2.9: Primary antibodies.....	43
Table 2.10: Secondary antibodies.....	43
Table 2.11: Used cell lines	43
Table 2.12: Bacterial strains used in this study	44
Table 2.13: Plasmids used in this study.....	45
Table 2.14: DNA oligonucleotides used in this study.....	46
Table 2.15: siRNA oligonucleotides used in this study.....	46
Table 2.16: sgRNA oligonucleotides used in this study.....	47
Table 3.1: Composition of tested sort buffers	66
Table 3.2: Survival rates of HAP1 cells after infection with <i>S. aureus</i> 6850.....	67
Table 3.3: Sort performance and selection stringency of the HAP1 screen.....	69
Table 3.4: Significantly enriched genes in mutagenized HAP1 cells surviving infection by intracellular	69
Table 3.5: Function of significantly enriched genes in mutagenized HAP1 cells surviving infection by intracellular <i>S. aureus</i> 6850	70
Table 4.1: Morphological and biochemical changes of different modes of cell death detected in <i>S. aureus</i> -infected epithelial cells.....	123
Table 6.1: HAP1 screen sequencing data table	178

6.5 List of Videos

- Video 1: Phagosomal escape of *S. aureus* in epithelial cells.
- Video 2: Phagosomal escape of *S. aureus* upon inhibition of caspases.
- Video 3: Activation of effector caspases by intracellular *S. aureus*.
- Video 4: Visualization of host cell plasma membrane permeabilization induced by intracellular *S. aureus*.
- Video 5: *S. aureus* increases cellular H₂O₂ concentration during intracellular infection.
- Video 6: Intracellular *S. aureus* induces a rise in cytosolic Ca²⁺.
- Video 7: *S. aureus*-induced cytosolic Ca²⁺ overload is followed by a mitochondrial Ca²⁺ rise.
- Video 8: Cytosolic and ER Ca²⁺ concentration during *S. aureus* infection.
- Video 9: The cytosolic Ca²⁺ rise induced by intracellular *S. aureus* is not affected by 2-APB treatment.
- Video 10: Visualization of *S. aureus*-induced cytosolic Ca²⁺ overload in Ca²⁺ depleted medium.
- Video 11: Visualization of *S. aureus*-induced cytosolic Ca²⁺ overload in Ca²⁺ depleted medium.
- Video 12: Cytosolic Ca²⁺ overload precedes activation of effector caspases in *S. aureus*-infected cells.
- Video 13: *S. aureus*-induced cytosolic Ca²⁺ rise upon inhibition of caspases.
- Video 14: *S. aureus*-induced cytosolic Ca²⁺ overload is followed by plasma membrane permeabilization.
- Video 15: Cytosolic Ca²⁺ signaling upon apoptosis-inducing agents.
- Video 16: Activation of effector caspases by intracellular *S. aureus* in calpain 4 knock-out cells.
- Video 17: *S. aureus* secreted factors induce cytosolic Ca²⁺ signaling and overload.
- Video 18: α -toxin and *rsp* do not affect *S. aureus*-induced cytosolic Ca²⁺ rise.
- Video 19: Phagosomal escape of *S. aureus* JE2 and JE2 *scpA*.
- Video 20: Intracellular replication of *S. aureus* JE2 and JE2 *scpA*.
- Video 21: Staphopain A does not interfere with *S. aureus*-induced cytosolic Ca²⁺ rise.
- Video 22: Loss of function of staphopain A does not prevent activation of effector caspases by intracellular *S. aureus*.
- Video 23: Phagosomal escape of *S. aureus* RN4220 *phld-scpAB* and RN4220 *phld-scpA*_(C238A)B.
- Video 24: Ca²⁺ signaling and activation of effector caspase in *S. aureus* RN4220 *phld-scpAB*-infected cells.

Danksagung

Ich bedanke mich herzlich bei Prof. Dr. Thomas Rudel als Erstgutachter und Betreuer dieser Arbeit für die Möglichkeit meine Doktorarbeit am Lehrstuhl für Mikrobiologie anfertigen zu können. Vielen Dank, dass du dir immer Zeit genommen hast, um meine Fragen zu beantworten und Ergebnisse und Ideen mit mir zu diskutieren

Bei Herrn Dr. Knut Ohlsen möchte ich mich herzlich für die Übernahme des Zweitgutachtens bedanken. Außerdem bedanke ich mich bei ihm und Tobias Hertlein für die produktive und freundliche Zusammenarbeit.

Ein besonderer Dank gilt Dr. Martin Fraunholz für seine stetige Hilfs- und Diskussionsbereitschaft zu allen Staphylococcus-Themen oder auch sonstigen Fragen. Danke, dass deine Tür immer für mich offen war.

Weiterhin bedanke ich mich bei Lucas Jae für die Kooperation beim HAP1 screen, besonders für die Beantwortung all meiner Fragen.

Ein großer Dank gilt auch der Staph-Gruppe Jessica, Adriana, Michaela, Kerstin, David, Sudip und Sebastian. Danke für die schöne Zeit im Labor, gegenseitige Unterstützung im „we-lab“ und gute Diskussionen. Danke an Isabel und Helene für eure tolle Arbeit. Es war mir eine Freude euch zu betreuen. Außerdem danke ich allen Mitarbeitern am Lehrstuhl für Mikrobiologie für die nette Arbeitsatmosphäre und Hilfsbereitschaft.

Besonders danke ich Dani, Anastasija, Franzi & Franzi, Jessica und Max für die lustigen Kaffeerunden in der Küche und nach Feierabend, für seelische und moralische Unterstützung sowie Hilfe im Labor. Danke für die tolle, gemeinsame Zeit! Vor allem danke ich Dani für stets aufbauende Worte und ihre Freundschaft.

Bei allen Mitgliedern des Mibi-Running Clubs bedanke ich mich für gemeinsames Schwitzen, Stressabbau und Spaß beim wöchentlichen Training und diversen Wettkämpfen.

Außerdem danke ich meinen Eltern und meiner Schwester Kristin für ihre Liebe, Unterstützung und Aufmunterung. Danke, dass ihr immer für mich da seid! Ich danke Chris für seinen Beistand in allen Hochs und Tiefs dieser Arbeit. Danke, dass du mir immer zugehört, mich motiviert und unterstützt hast. Danke für alles!

Selbstständigkeitserklärung

Eidesstattliche Erklärungen nach §7 Abs. 2 Satz 3, 4, 5 der Promotionsordnung der Fakultät für Biologie

Eidesstattliche Erklärung

Hiermit erkläre ich an Eides statt, die Dissertation: „Identifizierung von Faktoren, die am *Staphylococcus aureus*-induzierten Wirtszelltod beteiligt sind“, eigenständig, d. h. insbesondere selbständig und ohne Hilfe eines kommerziellen Promotionsberaters, angefertigt und keine anderen, als die von mir angegebenen Quellen und Hilfsmittel verwendet zu haben.

Ich erkläre außerdem, dass die Dissertation weder in gleicher noch in ähnlicher Form bereits in einem anderen Prüfungsverfahren vorgelegen hat.

Weiterhin erkläre ich, dass bei allen Abbildungen und Texten bei denen die Verwertungsrechte (Copyright) nicht bei mir liegen, diese von den Rechtsinhabern eingeholt wurden und die Textstellen bzw. Abbildungen entsprechend den rechtlichen Vorgaben gekennzeichnet sind sowie bei Abbildungen, die dem Internet entnommen wurden, der entsprechende Hypertextlink angegeben wurde.

Affidavit

I hereby declare that my thesis entitled: „Identification of factors involved in *Staphylococcus aureus*-induced host cell death” is the result of my own work. I did not receive any help or support from commercial consultants. All sources and / or materials applied are listed and specified in the thesis.

Furthermore I verify that the thesis has not been submitted as part of another examination process neither in identical nor in similar form.

Besides I declare that if I do not hold the copyright for figures and paragraphs, I obtained it from the rights holder and that paragraphs and figures have been marked according to law or for figures taken from the internet the hyperlink has been added accordingly.

Würzburg, den